Theoretical Studies of Positronium Formation in Low Energy Positron-Helium Collisions

Peter G. Van Reeth

ProQuest Number: 10046029
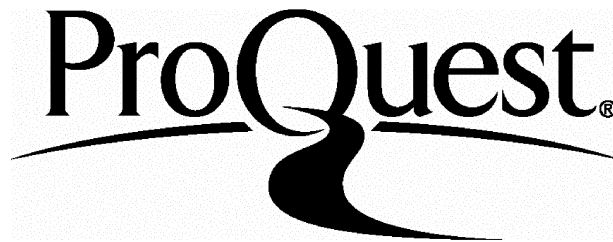
ProQuest 10046029

Abstract

Theoretical investigations of the collisions of low energy positrons with helium atoms have been made in the energy region where only the elastic scattering and the positronium formation channels are open.

We have used the two channel Kohn variational method and new accurate numerical procedures have been developed to perform the many six dimensional integrations. The effect of the inexactness of the target wavefunction on the final results has been investigated and consequently we have used very elaborate helium wavefunctions in our calculations.

The s-wave positronium formation cross section has been calculated using trial functions containing 502 short-range terms and is found to be very small. The s-wave elastic scattering cross section is found to be the main contributor to the total elastic cross section and a detailed investigation of the behaviour of the cross section at the positronium formation threshold reveals a 'rounded step' feature which is predicted by Wigner's threshold theory. The positronium formation cross sections for p- and d-wave scattering have been calculated, and we find the d-wave component to be dominant for energies greater than 1eV above threshold. The total positronium formation cross section is evaluated using the s-, p- and d-wave results of this work and the first Born approximation for the higher partial waves. A difference is found between theory and experiment which is attributed to the uncertainty in the absolute values of the experimental data and the convergence of the theoretical results. The p- and d-wave elastic scattering cross sections have been calculated and are found to be $\approx$30% of the total elastic scattering cross section for energies above the positronium formation threshold.

We have also investigated the annihilition of positrons with the electrons in the helium atom at energies corresponding to room temperature. The angular correlation function has been calculated and is found to agree very well with the latest experimental measurements.

Acknowlegements

Contents

Chapter 1

Introduction

The prediction in 1928 by P. A. M. Dirac of the existence of anti-particles can be considered as one of the main theoretical achievements of 20th century physics and also as a great success of both the quantum theory of matter and the theory of special relativity which had been developed in the previous 20 years. The intrinsic nature of anti-particles could not have been inferred using the classical theory of matter, and it was only after modifying the quantum theory of Schrödinger so as to include particles with kinetic energies comparable to their rest mass, that Dirac was able to make his prediction.

Dirac started by considering the Schrödinger equation,

$$i\hbar \frac{\partial}{\partial t}\Psi = H\Psi, \tag{1.1}$$

where H is the total Hamiltonian. This equation is of first order in t, and as in special relativity the spatial and time coordinates must be on the same footing, i.e. we define points in space-time by $(x_1, x_2, x_3, x_4 = ict)$, Dirac proposed that a wave equation which would hold for relativistic velocities should be of first order both in t and space, and therefore linear in both the energy and the momentum operator. For a free particle, for instance an electron, Dirac's equation is

$$i\hbar \frac{\partial}{\partial t}\Psi = -i\hbar \sum_{k=1}^{3} \alpha_k \frac{\partial}{\partial x_k}\Psi + \beta mc^2 \Psi, \tag{1.2}$$

where m is the mass of the electron and α and β are constants which must be (4×4)

matrices for there to be any solution to the equation. Therefore, the wavefunction, Ψ, needs to have four components and Dirac proposed to associate the first two with the two spin 1/2 states (spin up and spin down) of the electron, and the other two components with the two spin states of a new spin 1/2 particle, with opposite electric charge to the electron but with identical mass, the positron.

Dirac's theory predicted that the allowed values of the total relativistic energy E for a free electron would be

$$E = \pm\sqrt{c^2p^2 + (m_0c^2)^2}. \tag{1.3}$$

The positive values of E are those for the relativistic free electron, represented by the first two components of the wavefunction, and Dirac understood that the negative values of E did have physical significance and corresponded to electrons with negative energies. This led him to propose a theory in which the vacuum is considered as a sea of electrons with fully occupied negative energy levels which are separated from the positive energy levels by at least $\Delta E = 2m_0c^2$. The creation from the vacuum of an electron-positron pair could then be explained by considering an electron in a negative energy level as having been excited by a photon, with energy greater than $2m_0c^2$. to a positive energy level (the electron cannot be excited to another negative state as these states are considered to be fully occupied). The result of such a transition would be to create an electron with positive energy and to leave one of the negative energy levels unoccupied. This hole in the sea of negative energy electrons would have all the mechanical and electrical properties of the positron. Both the existence of the positron and the possibility of pair production were confirmed experimentally by Anderson in 1932 in his studies of cosmic rays, and by Blackett and Occhialini in 1933. Although Dirac's theory predicted correctly the existence of anti-particles, it did not fully explain the whole phenomenon, and it is only with the introduction of quantum field theory that a complete theory for particle - anti-particle interactions was developed.

Since the nineteen thirties positrons have been a very important topic of modern physics and have been studied extensively. At first, the fundamental properties of positrons were investigated to verify the new theories of anti-matter, but more

recently, positrons have been used as probes in atomic and solid states physics. The study of the interaction of positrons with atoms and molecules was undertaken not only because of the interest in the new phenomena associated with this type of collision, but also because it provided a testing ground for collision theories which had been developed for electron-atom and electron-molecule scattering. As emphasized by Massey in his review article (Massey 1976), applying the approximation methods developed for the study of electron-atom scattering to the investigation of positron-atom collisions, involves mainly a reversing of the sign of the projectile electric charge and also the removal of the exchange between the incoming projectile and the target electrons. This can provide a severe test of the quality of the approximation used and it is found that in general positron scattering calculations are more sensitive to the level of approximation than is the case for electron-atom scattering. In addition. this change of the electric charge of the incoming projectile means that the physical interaction between the target and the projectile will be very different for electron and positron scattering and, therefore, the comparison of the cross sections for both types of collision can give useful information on these projectile-atom interactions.

There are three main components to the interaction between an electron or positron projectile and the atomic target, which are important in the low energy collisions in which we are mainly interested in this work. First, we have the component which arises from the interaction between the projectile and the undistorted target (i.e. the static interaction) and second, we have the polarization interaction between the projectile and the distorted charge distribution of the target atom. The third component is the exchange interaction which is present if the projectile is identical with the electrons in the target. The static interaction affects electron-atom and positron-atom scattering at all energies, but it is repulsive for positron scattering and attractive for electron scattering. On the other hand, the polarization interaction is attractive for both types of collision, but it is effective only at very low energies, for which the interaction time between the projectile and the target is such that the electron cloud has time to be polarized. The exchange interaction only affects electron scattering, the positron being distinguishable from

	Type of Projectile	
Interaction	e^+	e^-
Static	Repulsive	Attractive
Polarization	Attractive	Attractive
Exchange	No	Yes
Positronium formation	Yes	No
Annihilation	Yes	No

Table 1.1: The differences between the interactions in electron-atom and positron-atom scattering.

the target electrons, and it will be mainly effective when the electron projectile and the target electrons have similar kinetic energies. (See Kaupilla and Stein 1990 for a comparative review on positron and electron scattering.)

In table 1.1 we sumarize the interactions for electron and positron scattering, and one can see that a major difference between the two types of collision is the cancellation of the static and the polarization interactions in positron-atom scattering which usually leads to smaller cross sections at low energy as compared to those for electron-atom scattering. At sufficiently high energies, above a few hundred eV, both the polarization and exchange interactions become negligible, so that only the static interaction is effective and the total cross section for electron-atom and positron-atom scattering merge in this energy region (see figure 1.1). This merging of the total cross section occurs at a much lower energy than the merging of the individual partial cross sections (Kauppila and Stein 1982 and Stein *et al.* 1990) and this can be explained (Humberston 1994) by considering the optical theorem,

$$\sigma_{tot} = \frac{4}{k} Im f_{el}(0) \tag{1.4}$$

where $f_{el}(0)$ is the forward elastic scattering amplitude.

If we take a Born expansion of $f_{el}(0)$,

$$f_{el}(0) = \sum_{n=1}^{\infty} f_{el}^{B(n)}(0) \tag{1.5}$$

10
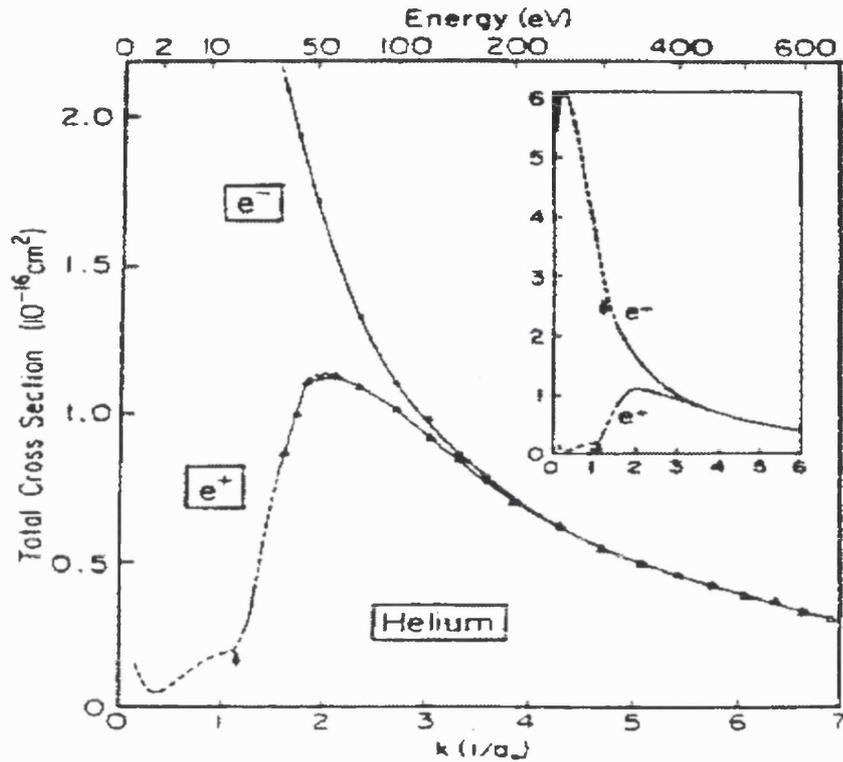
Figure 1.1: Total cross section for electron- and positron-helium scattering showing the merging of the cross section at high energies, taken from Kauppila *et al* (1981).

we find that the first term is real and therefore the first non-zero term in σ_{tot} is from the second Born amplititude. If exchange is neglected, we find that this term, being quadratic in the projectile - atom potential, is the same for electrons and positrons and this will also be the case for all even n terms in the Born expansion. Hence, only the odd orders of the Born expansion, with $n \geq 3$, will contribute to make the total cross section for electrons and positrons different, and these terms are presumably very small at energies much lower then those where the first Born approximation for the individual cross section is valid.

There are two new types of processes which occur in positron-atom scattering but cannot take place in electron-atom collisions. The first one, positron-electron annihilation, is due to the intrinsic nature of the positron, i.e. it is the anti-particle of the electron. The cross section for this process is very small as compared to those for the other processes which are allowed in the energy range we are considering, ex-

11

cept in the limit of zero incoming positrons energy where it is infinite. Nevertheless, it is still of great interest, as the angular distribution of the two γ-rays emitted in the annihilation can give important information about the momentum distribution of the annihilating electron-positron pair. The second process specific to positron scattering is the formation of a bound state of the positron and one of the target electrons, called positronium, Ps. This atom is hydrogenic, with a reduced mass of half that of hydrogen, and it has allowed energies (excluding the fine structure effects) which have half the values of the corresponding ones for hydrogen, with a ground state energy of -6.8 eV. The positronium atom can be either in a triplet (S=1) spin state or in a singlet (S=0) spin state, called orthopositronium and para-positronium respectively, and both types of positronium are unstable and decay by the annihilation of the positron with the electron. The lifetime for parapositronium, which decays predominantly into two γ-rays, is $\tau_{pa}=1.25 \times 10^{-10}$ seconds, while that for orthopositronium, which decays predominantly into three γ-rays, is $\tau_{or}=1.41 \times 10^{-7}$ seconds. One should note that the interaction time, i.e. the time it takes for the positronium atom to leave the interaction region, is of the order of $10^{-14} - 10^{-16}$ seconds, much shorter than its lifetime, and therefore the positronium atom can escape from the interaction region and be detected.

The threshold energy for positronium formation is defined as $E_{Th} = E_I - E_{Ps}$, where E_I is the ionization energy of the target atom and $E_{Ps}= 6.8$eV is the binding energy of the positronium. The next threshold, E_{Ex}, is usually the first excitation state of the target atom, which is not always the same as that for electron-atom scattering, because excitations involving a spin-flip cannot be initiated by positron impact. The energy region between the E_{Th} and E_{Ex} is referred to as the Ore gap (Ore 1949) within which only two scattering processes may occur; elastic scattering and positronium formation, or schematically

$$e^+ + \text{He} \rightarrow e^+ + \text{He} \quad (\text{ elastic scattering})$$
$$\rightarrow \text{Ps} + \text{He}^+ \quad (\text{ positronium formation})$$
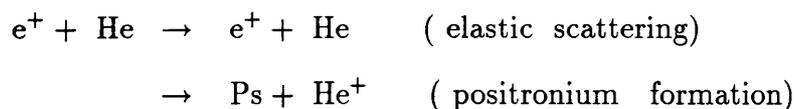
It is important to differentiate between positronium formation and ionization processes, although in both cases a singly ionized target atom is produced. The main dif-

ference is that in positronium formation, the fragments consist of a neutral positronium atom and a positive ion, while in ionization the final state consists of the free e^- and e^+ and the ion, and therefore the interactions between the fragments will be very different in each case.

In this work, we will consider only positrons scattering on helium atoms and restrict ourselves to positron energies less then E_{Ex}. The scattering of positrons on helium is an important topic in positron physics for both theoretical and experimental reasons. Theoretically, the positron-helium system is of interest because, although it is a four body problem and therefore involves a much more complicated calculation than is the case for positron-hydrogen scattering, it is still possible, for low positron energies. to do *ab initio* calculations which are not feasible for scattering processes on atoms with $Z > 2$. These *ab initio* calculations can then be used to verify the validity of more approximate methods employed in positron-helium scattering at higher energies or in positron scattering from heavier atoms.

One of the ironies of positron-atom scattering is that the collision which is the simplest to treat theoretically, i.e. positron-hydrogen, is very difficult to investigate experimentally. On the other hand, helium gas is much easier to manipulate and recent developments in positron beam techniques have made it possible to make very accurate experimental studies of positron-helium scattering, and detailed comparisons between theory and experiment for this type of collision can now be made. In figure 1.2 the cross section for positronium formation in helium is plotted for positron energies between E_{Th} and 300 eV. The details of each experiment are discussed in the review of Charlton and Laricchia (1990), but we see that all experiments reveal a similar energy dependence of the cross section, with a rapid rise from threshold and a maximum at 50 eV of 0.5 - 0.6 πa_0^2. In figure 1.3, the experimental results obtained in the Ore gap by Fornari *et al.* (1983) and the more recent data of Sueoka *et al.* (1994) and Moxon *et al.* (1994) are presented, and one sees that there is reasonable agreement between all experiments. Furthermore, a good enough energy resolution has been achieved to make detailed comparisons with theoretical investigations interesting.

13
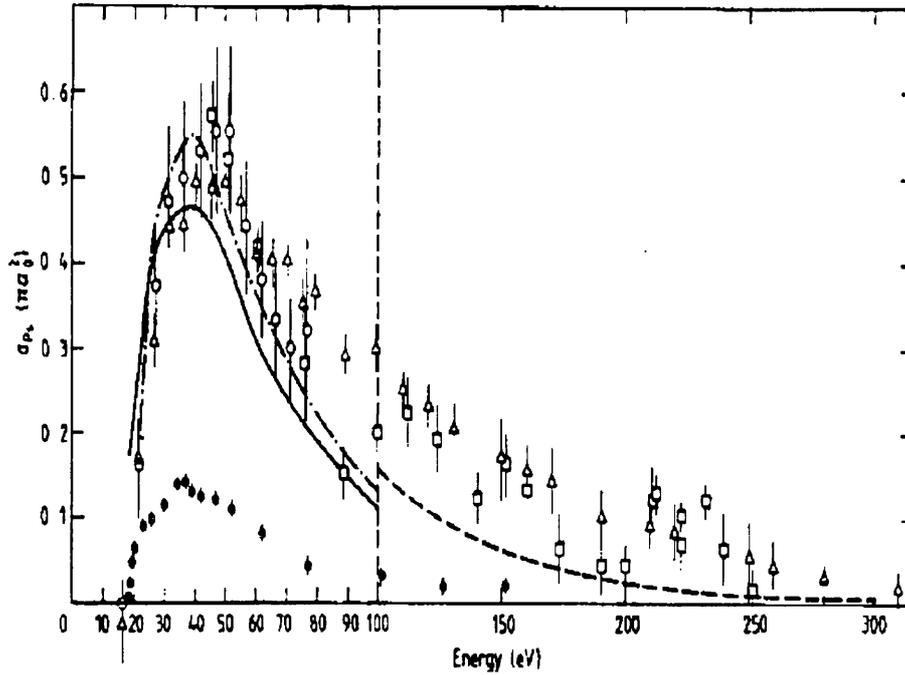
Figure 1.2: Positronium formation cross section for positron-helium scattering, taken from Charlton and Laricchia (1990).

The first calculation of positronium formation in positron-helium scattering was performed by Massey and Moussa (1960), using the first Born approximation which gave results much too large compared to experimental data at low energies. Since then, various more elaborate approximation methods have been employed to study this problem. The main interest of these works was to investigate the scattering process over a wide energy range where elastic scattering, positronium formation, excitation of the positronium atom and excitation or ionization of the helium target can all occur. The close coupling calculations of Hewitt *et al.* (1992) and McAlinden and Walters (1992) agree well with experiment at high energies, but these authors did not investigate positron collisions at energies within the Ore gap. The only calculations which included energies within the Ore gap are those of Mandal *et al.* (1979), who used the distorted wave approximation, and the polarized orbital calculations of Kahn and Ghosh (1983). These methods are not expected to give very

14
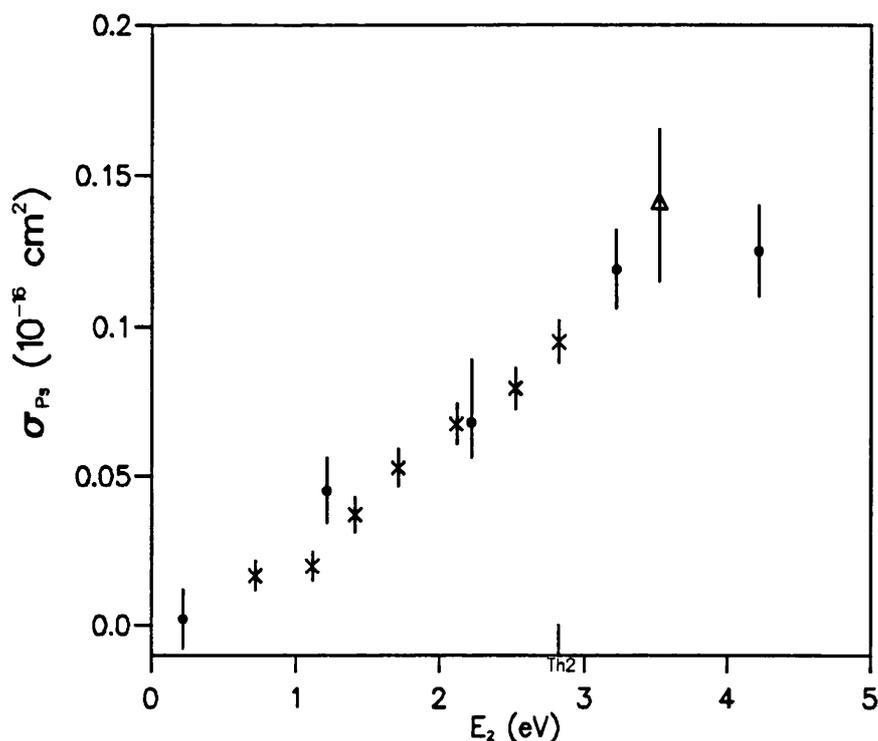
Figure 1.3: Positronium cross section for positron-helium scattering. $\times$ Moxom *et al.*, o Sueoka *et al.* and $\triangle$ Fornari *et al.*. E_2 is the excess energy of the positron, i.e. $E_2 = E_{e+} - E_{Th}$.

reliable results at very low energies and, therefore, these authors did not undertake a very detailed investigation of the positronium formation cross section in the Ore gap. On the other hand, as one can see from figure 1.2, these calculations are in reasonable agreement with experiment at the higher energies, describing relatively well the energy dependence of the positronium formation cross section above 40 eV. In chapter 6 and 7 these theoretical results and the experimental data will be compared with the cross sections obtained in this work using an *ab initio* variational calculation and we will also consider the recent first Born approximation results of McAlinden (1996).

The elastic scattering cross section below the positronium formation threshold has been studied in great detail both theoretically (Drachman 1968, McEachran *et al.* 1977, Humberston 1973 and Campeanu and Humberston 1977) and experi-

15

mentally (Canter *et al.* 1973, Burciaga *et al.* 1977 and Stein *et al.* 1978). Above the threshold, this cross section has been calculated mainly for the higher energies using the various approximations methods described for positronium, for instance by McAlinden and Walters (1992) and also by McEachran *et al.* (1996) who have extended their polarized-orbital calculations to above threshold energies, but have not included the positronium formation channel.

As can be seen from the above description of the experimental and theoretical work on positron-helium scattering, there is a real need for reliable theoretical results to be obtained within the Ore gap. These results will become even more important when the increase in beam resolution is such that very detailed measurements of the threshold behaviour of the positronium formation and elastic cross sections become possible. In this work we will undertake *ab initio* calculations of the elastic scattering and positronium formation cross sections for positron-helium scattering at energies below the first excitation threshold, using the Kohn variational formalism. This method has been successfully used in similar studies of positron-hydrogen and positron-lithium scattering (Humberston 1982, Brown and Humberston 1985, Watts and Humberston 1992) and also for the evaluation of the elastic phase shifts below the positronium threshold in positron-helium scattering (Humberston 1973, Campeanu and Humberston 1977).

An outline of the variational principle on which the Kohn method is based will be given in chapter 2 in which we will also derive the Kohn method for the two channel scattering process, based on a partial wave analysis in terms of the K-matrix formalism. The variational principle can also be applied to bound state problems, and the well-known Raleigh-Ritz method for the evaluation of binding energies is derived in chapter 2. A major difference between positron-hydrogen and positron-helium scattering is the fact that in the latter case, the target wavefunction is not known exactly, i.e. it is not an exact eigenfunction of the target Hamiltonian. The difficulties which arise in variational calculations because of this inexactness of the target wavefunction are well known and we have investigated this problem very thoroughly. In chapter 3, we present several very elaborate new helium target

functions and also an empirical method which we believe can be used to verify that the scattering results we have obtained are not affected by the inexactness of the target function.

In theory, the partial wave analysis of a scattering process requires us to evaluate the partial cross sections for an infinite number of partial waves. But it has been shown in previous calculations of similar types of scattering that at the low energies which we are considering, the main contribution to the total cross section can be expected to come from the first three partial waves, s, p and d, and that the higher partial waves contributions can be estimated with a reasonable accuracy by using various simple approximation methods. In chapter 4, we will derive the precise formalism for the two channel s-wave positron-helium scattering and, in chapter 5, the new numerical and computational methods which have been developed for this work will be described. The s-wave elastic and positronium formation cross sections will be presented, analyzed and compared to previous calculations in chapter 6, and the inclusion of a virtual positronium term in the elastic scattering wavefunction below the positronium formation threshold will be discussed with specific emphasis on the threshold behaviour of the elastic scattering cross section. The p- and d-wave formalism and results will be presented in chapter 7, together with a detailed comparison of the theoretical and experimental cross section sections.

As mentioned above, although the annihilation cross section for a free electron-positron pair is negligible as compared to that for the other allowed processes, this phenomenon is in itself of great interest. In chapter 8, we have reinvestigated low energy positron annihilation in helium and calculated the temperature dependence of Z_{eff}, which is directly related to the positron-electron annihilation rate. Also, we have calculated the annihilation γ-ray spectrum from which information on the momentum distribution of the electron-positron pair can be found, and excellent agreement with the latest experimental data has been achieved.

Chapter 2

Two channel scattering theory and the variational method

2.1   Introduction

The aim of this work is to investigate elastic scattering and positronium formation in low energy positron-helium collisions, and we will restrict our analysis to incoming positron energies within the Ore gap, which for helium is defined as the energy region between the positronium formation threshold (17.78 eV) and the $2\,^1S$ excitation threshold of helium (20.58 eV). As mentioned in chapter 1, there is a difference in this case between electron and positron scattering : because spin interactions are ignored and no exchange can take place between the positron and the target electron, the $2\,^3S$ excitation of helium, with a lower threshold energy (19.79 eV), is not possible for positron scattering. Strictly, there is also the possibility of direct electron-positron annihilation, but the cross section for this process is very small, and negligible compared to that for elastic scattering and positronium formation. However, we must recognise that the system we will describe should also allow for two other processes to occur. These are positronium scattering elastically on a helium plus ion target and helium formation by positronium impact due to its electron becoming bound to the positive ion. We could associate these processes

with a kind of time reversal of the two original processes, and it is imperative that our solution to the scattering problem describes them as well.
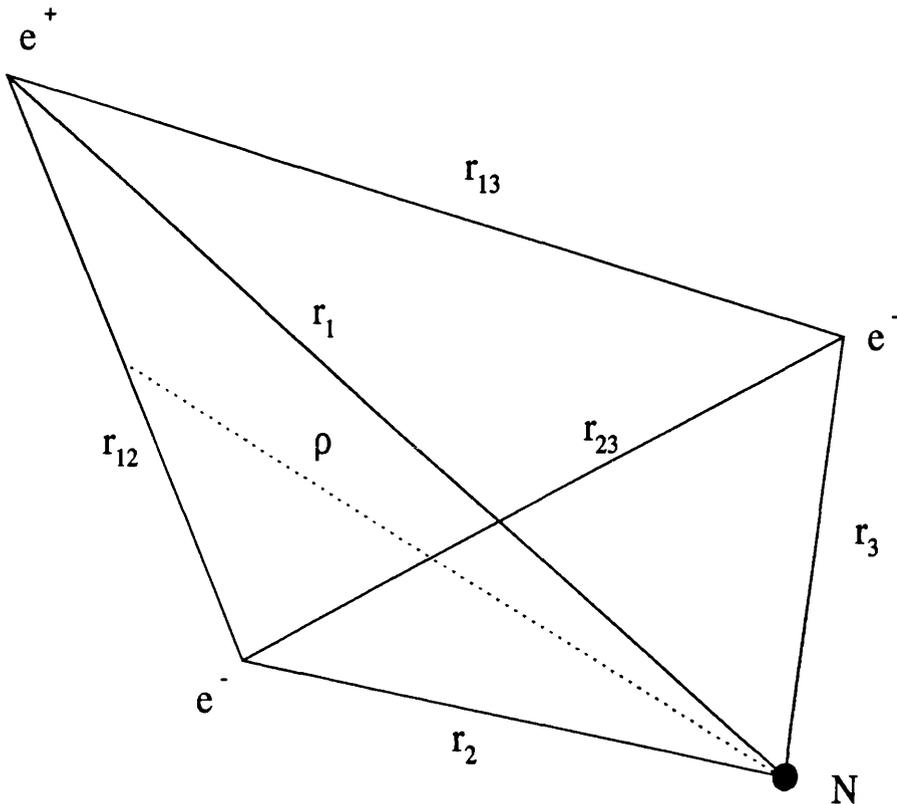
Figure 2.1: The positron-helium atom coordinate system.

The configuration of the total system is shown in figure 2.1. We define the variable ρ as the vector between the nucleus and the center of mass of the positronium atom. So if electron 2, with position vector r_2, is detached from the helium atom and forms positronium, we have

$$\rho = \frac{1}{2}(r_1 + r_2). \tag{2.1}$$

As mentioned before, in positron-helium scattering there is no exchange between the incoming projectile and the target electrons, and therefore the interactions are very different from those found in electron scattering. Nevertheless, the exchange between the target electrons must be included, which complicates the calculation compared to that for positron-hydrogen scattering. This is obvious in the case of positronium formation, as the incoming positron can pick up either of the two electrons. Thus

we also need to consider the variable

$$\rho' = \frac{1}{2}(r_1 + r_3) \qquad (2.2)$$

which is done by introducing an exchange operator, P_{23}, in the scattering wavefunction. However, for the general formulation of the scattering problem and of the variational method it will be clearer, especially in the notation, to consider only one case, i.e. that with electron 2 being involved in the positronium formation. The exchange operator will then be introduced explicitly when we consider the actual wavefunction used in the calculation.

We now need to establish the general form of the scattering wavefunctions, which will satisfy all the boundary conditions and which describe the two channel processes we are interested in.

2.2 The two channel scattering formalism

In order to relate the scattering wavefunctions and the theoretical values calculated in this work to the experimental measurements, it is important to determine from the experimental set-up the general form we require the wavefunction to take, i.e. a form which, implicitly at least, contains information about the measurements experimentalists make. The experimental set up can be described schematically as in figure 2.2.

The radial dimension of the beam is always much larger than the dimension of the target atom. Therefore, the uncertainty in the momentum of the incident projectile is negligible and a plane wave representation for the incoming positron far away from the target is very suitable. Also, the mass of the positron is much less than that of the helium atom (and the same is true for the mass of the positronium versus that of He^+), so we can take the nucleus as being of infinite mass at the origin of coordinates of the system.
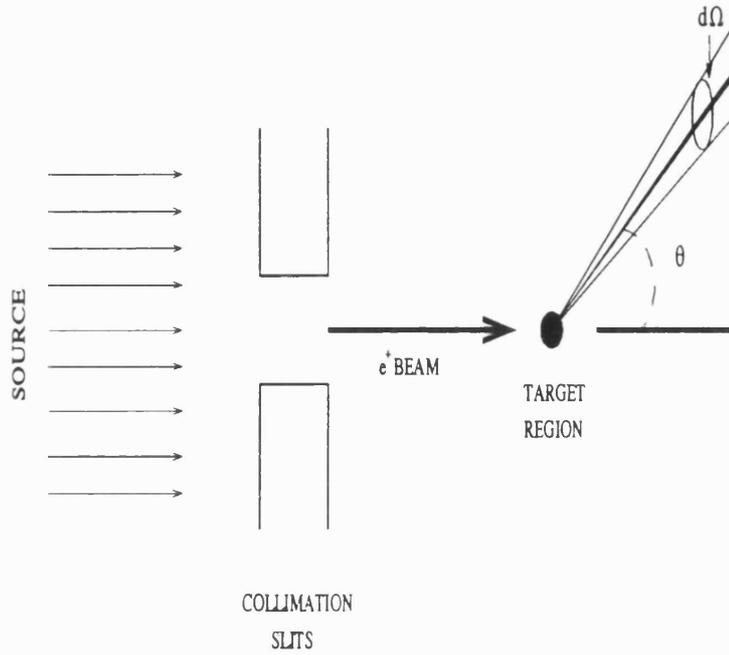
Figure 2.2: Schematic diagram of a scattering experiment.

The time-independent Schrödinger equation is. in atomic units,

$$H_T \Psi(\boldsymbol{r_1}, \boldsymbol{r_2}, \boldsymbol{r_3}) = E_T \Psi(\boldsymbol{r_1}, \boldsymbol{r_2}, \boldsymbol{r_3}), \tag{2.3}$$

where H_T is the total Hamiltonian of the system and is given by

$$H_T = -\frac{1}{2}\boldsymbol{\nabla}_{r_1}^2 - \frac{1}{2}\boldsymbol{\nabla}_{r_2}^2 - \frac{1}{2}\boldsymbol{\nabla}_{r_3}^2 + \frac{2}{r_1} - \frac{2}{r_2} - \frac{2}{r_3} - \frac{1}{r_{12}} - \frac{1}{r_{13}} + \frac{1}{r_{23}} \tag{2.4}$$

and E_T is the total energy of the system.

In the case of positron-helium elastic scattering we can write for large r_1 :

$$\Psi(\boldsymbol{r_1}, \boldsymbol{r_2}, \boldsymbol{r_3}) \underset{r_1 \to \infty}{\sim} \Phi_{He}(\boldsymbol{r_2}, \boldsymbol{r_3})\psi_{sc}(\boldsymbol{r_1}), \tag{2.5}$$

where $\psi_{sc}(\boldsymbol{r_1})$ is the scattering wavefunction and $\Phi_{He}(\boldsymbol{r_2}, \boldsymbol{r_3})$ is the helium target ground state eigenfunction such that

$$H_{He}\Phi_{He}(\boldsymbol{r_2}, \boldsymbol{r_3}) = E_{He}\Phi_{He}(\boldsymbol{r_2}, \boldsymbol{r_3}), \tag{2.6}$$

with

$$H_{He} = -\frac{1}{2}\boldsymbol{\nabla}_{r_2}^2 - \frac{1}{2}\boldsymbol{\nabla}_{r_3}^2 - \frac{2}{r_2} - \frac{2}{r_3} + \frac{1}{r_{23}} \tag{2.7}$$

21

and

$$E_T = E_{He} + \frac{1}{2}k^2 \qquad (2.8)$$

where k is the positron wavenumber.

Therefore for large values of r_1 equation 2.3 becomes

$$-\frac{1}{2}\nabla^2_{r_1}\Phi_{He}(r_2, r_3)\psi_{sc}(r_1) = \frac{1}{2}k^2\Phi_{He}(r_2, r_3)\psi_{sc}(r_1) \qquad (2.9)$$

as the potential term. $\frac{2}{r_1} - \frac{1}{r_{12}} - \frac{1}{r_{13}}, \to 0$ as $r_1 \to \infty$. The complexity of the positron-helium system prevents us from using a simple description of the scattering wavefunction when the projectile is close to the target, but it is possible to describe it in the asymptotic region, $r_1 \to \infty$, both before and after the scattering has taken place. As mentioned above, before the collision, the particles in the beam can be represented by an incoming plane wave. This can also be seen by solving the free particle equation in 2.9. After the collision, the particles will be deviated from the beam direction by angle θ (see fig. 2.2), and will be represented by a spherical outgoing wave. Hence the scattering wavefunction for elastic scattering can be written as

$$\psi_{sc}(r_1) \underset{r_1 \to \infty}{\sim} e^{ik.r_1} + f_{el}(\theta_1)\frac{e^{ikr_1}}{r_1} \qquad (2.10)$$

where θ_1 is the angle between the incident beam direction and the vector r_1 and $f_{el}(\theta_1)$ is called the scattering amplitude for elastic scattering which will modulate the outgoing spherical wave.

In the case of positronium formation the form we use for the total Hamiltonian is

$$H_T = -\frac{1}{4}\nabla^2_\rho - \frac{1}{2}\nabla^2_{r_3} - \nabla^2_{r_{12}} + \frac{2}{r_1} - \frac{2}{r_2} - \frac{2}{r_3} - \frac{1}{r_{12}} - \frac{1}{r_{13}} + \frac{1}{r_{23}}. \qquad (2.11)$$

In this rearrangement process, for large values of ρ, the total wavefunction will be a product of a scattering wavefunction, and the ground state eigenfunctions of the helium ion, $\Phi_{He^+}(r_3)$, and the positronium atom, $\Phi_{Ps}(r_{12})$, such that

$$\left(-\frac{1}{2}\nabla^2_{r_3} - \frac{2}{r_3}\right)\Phi_{He^+}(r_3) = E_{He^+}\Phi_{He^+}(r_3) \qquad (2.12)$$

and

$$\left(-\nabla^2_{r_{12}} - \frac{1}{r_{12}}\right)\Phi_{Ps}(r_{12}) = E_{Ps}\Phi_{Ps}(r_{12}) \qquad (2.13)$$

22

where E_{He^+} and E_{Ps} are the ground state energies of the helium ion and the positronium atom respectively. By conservation of energy we have

$$E_T = E_{He} + \frac{1}{2}k^2 = \frac{1}{4}\kappa^2 + E_{He^+} + E_{Ps} = \frac{1}{4}\kappa^2 - 2.25 \qquad (2.14)$$

where κ is the wavenumber of the positronium atom. So we have for large ρ,

$$\Psi(r_1, r_2, r_3) \underset{\rho \to \infty}{\sim} \Phi_{He^+}(r_3)\Phi_{Ps}(r_{12})\psi_{sc}(\rho). \qquad (2.15)$$

In this case there is no incoming plane wave and the general form of the scattering wavefunction is

$$\psi_{sc}(\rho) \underset{\rho \to \infty}{\sim} f_{Ps}(\theta_\rho)\frac{e^{i\kappa\rho}}{\rho}. \qquad (2.16)$$

Here θ_ρ is the angle between the incident beam direction and the vector ρ, and $f_{Ps}(\theta_\rho)$ is the scattering amplitude for positronium formation. So if we choose the z axis along the direction of the vector k we can write the wave function for both processes as

$$\Psi_{sc,1} \underset{r_1 \to \infty}{\sim} e^{i k \cdot r_1} + f_{11}(\theta_1)\frac{e^{ikr_1}}{r_1}$$

$$\underset{\rho \to \infty}{\sim} f_{12}(\theta_\rho)\frac{e^{i\kappa\rho}}{\rho}. \qquad (2.17)$$

We have introduced here a numerical subscript of the scattering amplitudes to indicate between which channels the process is occurring. The positron-helium channel is labelled 1 and the positronium-helium plus channel is labelled 2. So for positronium formation we start in channel 1 and end up in channel 2, and we use $f_{12}(\theta_\rho)$ (thus $f_{11} \equiv f_{el}$ and $f_{12} \equiv f_{Ps}$).

A similar analysis shows that for the time reversed processes, i.e. for positronium elastic scattering on the helium ion with the possibility of helium formation, we have

$$\Psi_{sc,2} \underset{\rho \to \infty}{\sim} e^{i\kappa \cdot \rho} + f_{22}(\theta_\rho)\frac{e^{i\kappa\rho}}{\rho}$$

$$\underset{r_1 \to \infty}{\sim} f_{21}(\theta_1)\frac{e^{ikr_1}}{r_1}. \qquad (2.18)$$

The scattering amplitudes f_{mi} are related to the measured differential cross sections by

$$\frac{d\sigma_{mi}(\theta_i)}{d\Omega} = \frac{k_m}{k_i}|f_{mi}(\theta_i)|^2 \qquad m, i = 1, 2 \qquad (2.19)$$

23

where $k_1 = k$, $k_2 = \kappa$ and $\theta_1 = \theta_1$, $\theta_2 = \theta_\rho$.

We now need to relate the descriptive forms of the scattering wavefunctions given by equations 2.17 and 2.18 to those which will be used in the variational method. In a numerical calculation of the scattering process, it is easier to use real wavefunctions which contain the matrix elements of the reactance matrix K, as these are real quantities. The asymptotic form of the radial solution to Schrödinger equations for the system which takes into account the coupling between the channels is (see Bransden 1983), for the l th partial wave,

$$g_1^l(r_1, \rho) \underset{r_1 \to \infty}{\sim} Y_{l,0}(\theta_1, \phi_1)\sqrt{k} \left[j_l(kr_1) - K_{11}^l n_l(kr_1) \right] X_1(x_1)$$

$$\underset{\rho \to \infty}{\sim} -Y_{l,0}(\theta_\rho, \phi_\rho)\sqrt{2\kappa} K_{12}^l X_2(x_2) n_l(\kappa\rho) \tag{2.20}$$

$$g_2^l(r_1, \rho) \underset{\rho \to \infty}{\sim} Y_{l,0}(\theta_\rho, \phi_\rho)\sqrt{2\kappa} \left[j_l(\kappa\rho) - K_{22}^l n_l(\kappa\rho) \right] X_2(x_2)$$

$$\underset{r_1 \to \infty}{\sim} -Y_{l,0}(\theta_1, \phi_1)\sqrt{k} K_{21}^l X_1(x_1) n_l(kr_1) \tag{2.21}$$

where the factor 2 in $\sqrt{2\kappa}$ is due to the positronium mass being double that of the positron, and $X_1(x_1) = \Phi_{He}(r_2, r_3)$, $X_2(x_2) = \Phi_{He^+}(r_3)\Phi_{Ps}(r_{12})$. The constants K_{mi}^l are the elements of the reactance matrix, K, and $j_l(kr)$ and $n_l(kr)$ are the Bessel and Neumann functions respectively. To relate the K matrix elements to the cross sections for each process we can write

$$f_{mi}(\theta_i) = \sqrt{\frac{k_m}{k_i}} \sum_{l=0}^{\infty} \frac{(2l+1)}{k_m} T_{mi}^l P_l(\cos\theta_i) \tag{2.22}$$

where $P_l(\cos\theta_i)$ are the Legendre polynomials and T_{mi}^l are the partial wave scattering amplitudes which form the T matrix, and which, for single channel elastic scattering, are related to the phase shift by

$$T^l = e^{i\eta_l} \sin\eta_l. \tag{2.23}$$

The relation between the T and the K matrix elements, which can be found by comparing the asymptotic forms of the wavefunctions as in equations 2.17, 2.18, 2.20 and 2.21 , is given by

$$T^l = \frac{K^l}{I - iK^l}. \tag{2.24}$$

24

Now replacing T^l_{mi} in eq. 2.22 with this relation and using eq. 2.19 we find that the partial wave cross sections for each process can be calculated from the values of the K matrix elements using

$$\sigma_{mi} = \frac{4(2l+1)}{k_m^2} \left| \left(\frac{K}{I - iK} \right)_{mi} \right|^2.$$ (2.25)

2.3 Variational methods

We have shown that in order to calculate the cross sections for the various processes occurring in low energy positron-helium scattering we need to evaluate the K matrix elements in the formal scattering wavefunctions which describe these processes. The complexity of the system, a four body problem, makes it impossible for exact scattering wavefunctions to be determined and we will need to use an approximation method. In this work, the Kohn variational method is used to solve the scattering problem and to find numerical values for the K matrix elements which are approximations to the exact values. The variational principle on which the Kohn method is based is similar to the Rayleigh-Ritz method used for the determination of the energy levels of bound states and we have made extensive use of it in the calculation of the wavefunction and properties of the helium target. The complexity of the two channel scattering problem makes the derivation of the Kohn method much more complicated than that of the bound state problem . Therefore, we have derived the latter first so that the essence of the method is made clear before we concentrate on the Kohn method.

The variational principle

$$\delta I = 0$$ (2.26)

states that the functional I, which is a function of a function characteristic of the system under consideration, is stationary with respect to variations in the latter function away from its exact form. If the functions which make up the functional I are not known exactly, we use instead trial functions which depend on a finite set of parameters, $(\alpha_1, \alpha_2, \ldots, \alpha_n)$, called the variational parameters. The stationary

properties of I then lead to a set of equations :

$$\frac{\partial I}{\partial \alpha_i} = 0 \qquad i = 1, 2, \ldots, n \qquad (2.27)$$

which can be solved to determine the optimum values of the parameters $\alpha_1^0, \alpha_2^0, \ldots, \alpha_n^0$.

The variational value of the functional $I^0 = I(\alpha_1^0, \alpha_2^0, \ldots, \alpha_n^0)$ is then correct to first order in the error in the trial function, the error in I^0 being of second order.

2.3.1 The Rayleigh-Ritz variational method

The aim of this method is to calculate the energy levels and variational wavefunctions of atoms for which we do not know the exact eigenfunctions and can only consider trial functions which describe the physical system under consideration as well as possible.

The expectation value of the ground state energy for the chosen trial function is

$$E_0^t = \frac{< \Phi^t \mid H \mid \Phi^t >}{< \Phi^t \mid \Phi^t >}, \qquad (2.28)$$

where H is the Hamiltonian of the atomic system. If we now consider variations in the expectation value of E due to small variations in the trial function, we have

$$
\begin{aligned}
\delta E_0^t &= \delta \left[\frac{< \Phi^t \mid H \mid \Phi^t >}{< \Phi^t \mid \Phi^t >} \right] \\
&= \frac{\delta[< \Phi^t \mid H \mid \Phi^t >] < \Phi^t \mid \Phi^t > -\delta[< \Phi^t \mid \Phi^t >] < \Phi^t \mid H \mid \Phi^t >}{< \Phi^t \mid \Phi^t >^2} \\
&= \frac{\delta < \Phi^t \mid H - E_0^t \mid \Phi^t >}{< \Phi^t \mid \Phi^t >}.
\end{aligned}
\qquad (2.29)
$$

We can also evaluate the variation of E_0 by considering $\delta E_0^t = E_0^t - E_0$, and using 2.28 with $\Phi^t = \Phi + \delta\Phi$ we have

$$
\begin{aligned}
E_0^t &= \frac{< \Phi + \delta\phi \mid H \mid \Phi + \delta\Phi >}{< \Phi + \delta\Phi \mid \Phi + \delta\Phi >} \\
&= \frac{E_0 < \Phi \mid \Phi > +2E_0 < \delta\Phi \mid \Phi > + < \delta\Phi \mid H \mid \delta\Phi >}{< \Phi \mid \Phi > +2 < \delta\Phi \mid \Phi > + < \delta\Phi \mid \delta\Phi >},
\end{aligned}
\qquad (2.30)
$$

where we have used $H\Phi = E_0\Phi$ and the Hermiciticity of H. Therefore,

$$
\begin{aligned}
\delta E_0^t &= E_0^t - E_0 \\
&= \frac{< \delta\Phi \mid H \mid \delta\Phi > -E_0 < \delta\Phi \mid \delta\Phi >}{< \Phi \mid \Phi > +2 < \delta\Phi \mid \Phi > + < \delta\Phi \mid \delta\Phi >},
\end{aligned}
\qquad (2.31)
$$

so that to first order in $\delta\Phi$ we have $\delta E_0^t = 0$ and from 2.29 we have

$$
\delta < \Phi^t \mid H - E_0^t \mid \Phi^t >= 0.
\qquad (2.32)
$$

Therefore, the functional

$$
I = < \Phi^t \mid H - E_0^t \mid \Phi^t >
\qquad (2.33)
$$

is stationary and can be used to find a variational value for the ground state energy E_0^v, the error in which will be of second order in the error in the trial function.

One of the characteristics of the Rayleigh-Ritz method is that it provides a rigorous upper bound on the ground state energy E_0 of the system. To show this, we first expand the normalizable trial function in terms of a complete set of orthonormal eigenfunctions, Φ_i, of H, i.e.

$$
\Phi_n^t = \sum_{i=0}^{N} c_i \Phi_i.
\qquad (2.34)
$$

Therefore, using $H\Phi_i = E_i\Phi_i$ and equation 2.28 we have

$$
E_n^t = \frac{\sum_{i,j=0}^{N} c_i^* c_j E_j < \Phi_i \mid \Phi_j >}{\sum_{i,j=0}^{N} c_i^* c_j < \Phi_i \mid \Phi_j >},
\qquad (2.35)
$$

which as Φ_n^t forms an orthonormal set, reduces to

$$
E_n^t = \frac{\sum_{j=0}^{N} \mid c_j \mid^2 E_j}{\sum_{j=0}^{N} \mid c_j \mid^2}
\qquad (2.36)
$$

and

$$
E_n^t - E_0 = \frac{\sum_{j=0}^{N} \mid c_j \mid^2 [E_j - E_0]}{\sum_{j=0}^{N} \mid c_j \mid^2}.
\qquad (2.37)
$$

Now E_j is an eigenvalue of H, hence it is always more positive than, or equal to, the ground state energy E_0, and we find that $E_n^t \geq E_0$.

To calculate the ground state energy of a given system, we choose a form for the trial function which is representative of the physical situation and contains a number of variational parameters. This trial function is then inserted into the functional,

and the set of equations which follows from (2.27) is then solved. A more detailed description of actual Rayleigh-Ritz calculations used in this work will be given in chapter 3 where we discuss the helium atom target wavefunction in detail.

2.3.2 The two channel Kohn variational method

In contrast to the case for bound state calculations, the determination of scattering data requires us to use trial functions which are not normalizable, but whose radial asymptotic behaviour we know is given by 2.20 and 2.21.

In the Kohn variational method (Kohn 1948) we will consider a functional somewhat similar to that used in the Rayleigh -Ritz method, given by

$$I_{mn}^t = I = < \Psi_m^t \mid L \mid \Psi_n^t > \qquad (2.38)$$

where $L = 2(H - E)$ and Ψ_m^t is a trial function.

Thus,

$$\Psi_m = \Psi_m^t - \delta\psi_m, \qquad (2.39)$$

where Ψ_m is the exact eigenfunction of H, the total Hamiltonian of the system, and E is the total energy which is assumed to be known exactly. The variation in the functional, $\delta I_{mn} = I_{mn}^t - I_{mn}$, can be written as

$$
\begin{aligned}
\delta I_{mn} &= < \Psi_m + \delta\psi_m \mid L \mid \Psi_n + \delta\psi_n > - < \Psi_m \mid L \mid \Psi_n > \\
&= < \delta\psi_m \mid L \mid \Psi_n > + < \Psi_m \mid L \mid \delta\psi_n > + < \delta\psi_m \mid L \mid \delta\psi_n > .(2.40)
\end{aligned}
$$

As $L\Psi_n = 0$ and $L\Psi_m = 0$, we can write

$$< \delta\psi_m \mid L \mid \Psi_n >= - < \delta\psi_n \mid L \mid \Psi_m >= 0 \qquad (2.41)$$

and

$$\delta I_{mn} =< \Psi_m \mid L \mid \delta\psi_n > - < \delta\psi_n \mid L \mid \Psi_m > + < \delta\psi_m \mid L \mid \delta\psi_n > . \qquad (2.42)$$

Now considering the first two terms on the right hand side , we can rewrite them as

$$\delta I_{mn}' = 2 < \Psi_m \mid H - E \mid \delta\psi_n > -2 < \delta\psi_n \mid H - E \mid \Psi_m > \qquad (2.43)$$

In the case of positron-helium scattering the total Hamiltonian H can be written as

$$H = -\frac{1}{2}\nabla^2_{r_1} - \frac{1}{2}\nabla^2_{r_2} - \frac{1}{2}\nabla^2_{r_3} + \frac{2}{r_1} - \frac{2}{r_2} - \frac{2}{r_3} - \frac{1}{r_{12}} - \frac{1}{r_{13}} + \frac{1}{r_{23}} \qquad (2.44)$$

or

$$H = -\frac{1}{4}\nabla^2_{\rho} - \frac{1}{2}\nabla^2_{r_3} - \nabla^2_{r_{12}} + \frac{2}{r_1} - \frac{2}{r_2} - \frac{2}{r_3} - \frac{1}{r_{12}} - \frac{1}{r_{13}} + \frac{1}{r_{23}}, \qquad (2.45)$$

depending on which function we need to operate on.

Using equations 2.20 and 2.21 we know that the asymptotic forms of the two components of the wavefunction,

$$\Psi = \left[\begin{array}{c} \Psi_1 \\ \Psi_2 \end{array} \right]$$

can be written as

$$\Psi_1 \underset{r_1 \to \infty}{\sim} Y_{l,0}(\theta_1, \phi_1)\sqrt{k}X_1(\boldsymbol{x_1})\left[j_l(kr_1) - K_{11}n_l(kr_1)\right]$$

$$\underset{\rho \to \infty}{\sim} -Y_{l,0}(\theta_\rho, \phi_\rho)\sqrt{2\kappa}X_2(\boldsymbol{x_2})K_{21}n_l(\kappa\rho) \qquad (2.46)$$

$$\Psi_2 \underset{\rho \to \infty}{\sim} Y_{l,0}(\theta_\rho, \phi_\rho)\sqrt{2\kappa}X_2(\boldsymbol{x_2})\left[j_l(\kappa\rho) - K_{22}n_l(\kappa\rho)\right]$$

$$\underset{r_1 \to \infty}{\sim} -Y_{l,0}(\theta_1, \phi_1)\sqrt{k}X_1(\boldsymbol{x_1})K_{12}n_l(kr_1). \qquad (2.47)$$

We can see that in the equations above the labelling of the K matrix elements is different to that in 2.20 and 2.21. This is because, had the same labelling been kept, we would have arrived at a variational solution for the transpose of the K matrix. This occurs because the subscript on the K matrix elements as defined by 2.25 corresponds to the transition from one channel into another. But the labelling of the functional 2.38 does not have the same meaning, it refers to the two components of the total wavefunction, each of which contains information about both channels. The choice we have made in (2.46) and (2.47) is the same as in the literature, and the cross section can still be calculated with (2.25) because the exact K matrix is symmetric, i.e. $K_{12} = K_{21}$, and we will show that this will also be true for the variational K matrix.

The variation in the asymptotic form of the wavefunction is only in the K matrix elements and therefore we have

$$\delta\psi_1 \underset{r_1 \to \infty}{\sim} Y_{l,0}(\theta_1, \phi_1)\sqrt{k}X_1(\boldsymbol{x}_1)\left[K_{11}^t - K_{11}\right]n_l(kr_1)$$

$$\underset{\rho \to \infty}{\sim} -Y_{l,0}(\theta_\rho, \phi_\rho)\sqrt{2\kappa}X_2(\boldsymbol{x}_2)\left[K_{21}^t - K_{21}\right]n_l(\kappa\rho) \qquad (2.48)$$

$$\delta\psi_2 \underset{\rho \to \infty}{\sim} Y_{l,0}(\theta_\rho, \phi_\rho)\sqrt{2\kappa}X_2(\boldsymbol{x}_2)\left[K_{22}^t - K_{22}\right]n_l(\kappa\rho)$$

$$\underset{r_1 \to \infty}{\sim} -Y_{l,0}(\theta_1, \phi_1)\sqrt{k}X_1(\boldsymbol{x}_1)\left[K_{12}^t - K_{12}\right]n_l(kr_1). \qquad (2.49)$$

Now we can write the total Hamiltonian H given by 2.44 and 2.45 as

$$H_{r_1} = -\frac{1}{2}\boldsymbol{\nabla}_{r_1}^2 + \frac{2}{r_1} - \frac{1}{r_{12}} - \frac{1}{r_{13}} + H_{He} \qquad (2.50)$$

or

$$H_\rho = -\frac{1}{4}\boldsymbol{\nabla}_\rho^2 + \frac{2}{r_1} - \frac{2}{r_2} - \frac{1}{r_{13}} + \frac{1}{r_{23}} + H_{Ps} + H_{He^+} \qquad (2.51)$$

where H_{He}, H_{Ps} and H_{He^+} are given by eqs. 2.7, 2.12 and 2.13 respectively.

Using Green's theorem

$$\int_{V_1}\int_{V_2}\left[u\boldsymbol{\nabla}_1^2v - v\boldsymbol{\nabla}_1^2u\right]d\tau_1 d\tau_2 = \int_{S_1}\int_{V_2}\left[u\boldsymbol{\nabla}_1 v - v\boldsymbol{\nabla}_1 u\right]d\sigma_1 d\tau_2, \qquad (2.52)$$

we can write

$$\begin{aligned}
\delta I'_{mn} = &-\int_{S_1}\int_{V_A}\left[\Psi_m\boldsymbol{\nabla}_{r_1}\delta\psi_n - \delta\psi_n\boldsymbol{\nabla}_{r_1}\Psi_m\right].d\sigma_1 d\tau_A \\
&+ \int\left\{2\Psi_m(H_{He} - E + \frac{2}{r_1} - \frac{1}{r_{12}} - \frac{1}{r_{13}})\delta\psi_n\right. \\
&\left. - 2\delta\psi_n(H_{He} - E + \frac{2}{r_1} - \frac{1}{r_{12}} - \frac{1}{r_{13}})\Psi_m\right\}d\tau \qquad (2.53)
\end{aligned}$$

or

$$\begin{aligned}
\delta I'_{mn} = &-\int_{S_2}\int_{V_B}\left[\Psi_m\frac{\boldsymbol{\nabla}_\rho}{2}\delta\psi_n - \delta\psi_n\frac{\boldsymbol{\nabla}_\rho}{2}\Psi_m\right].d\sigma_2 d\tau_B \\
&+ \int\left\{2\Psi_m(H_{Ps} + H_{He^+} - E + \frac{2}{r_1} - \frac{2}{r_2} - \frac{1}{r_{13}} + \frac{1}{r_{23}})\delta\psi_n\right. \\
&\left. - 2\delta\psi_n(H_{Ps} + H_{He^+} - E + \frac{2}{r_1} - \frac{2}{r_2} - \frac{1}{r_{13}} + \frac{1}{r_{23}})\Psi_m\right\}d\tau, \qquad (2.54)
\end{aligned}$$

where S_1 is the surface at $r_1 \to \infty$ and S_2 is the surface at $\rho \to \infty$ and we have

$$d\sigma_1 = r_1^2 \sin\theta_1 d\theta_1 d\phi_1 \hat{\boldsymbol{r}}_1 \qquad (2.55)$$

$$d\sigma_2 = \rho^2 \sin\theta_\rho d\theta_\rho d\phi_\rho \hat{\boldsymbol{\rho}}. \qquad (2.56)$$

30

As the target and fragment functions are normalized. the volume elements, $d\tau_A$ and $d\tau_B$. which depend on the target or fragment variables, are such that with $d\tau_A = d\tau_1$ and $d\tau_B = d\tau_2$, we have

$$\int_{V_i} X_i^2(\boldsymbol{x}_i)d\tau_i = 1. \qquad (2.57)$$

On the surface $r_1 \to \infty$. we know that the wavefunction has the product form given by 2.5 and on the surface $\rho \to \infty$ it takes the form given by 2.15 and because of the exponential fall-off in the target and fragments functions the last two terms in the integrand of 2.53 and 2.54 cancel trivially.

Using the following notation.

$$J_1 = Y_{l,0}(\theta_1, \phi_1)\sqrt{k}X_1(\boldsymbol{x}_1)j_l(kr_1) \qquad (2.58)$$

$$N_1 = -Y_{l,0}(\theta_1, \phi_1)\sqrt{k}X_1(\boldsymbol{x}_1)n_l(kr_1) \qquad (2.59)$$

$$J_2 = Y_{l,0}(\theta_\rho, \phi_\rho)\sqrt{2\kappa}X_2(\boldsymbol{x}_2)j_l(\kappa\rho) \qquad (2.60)$$

$$N_2 = -Y_{l,0}(\theta_\rho, \phi_\rho)\sqrt{2\kappa}X_2(\boldsymbol{x}_2)n_l(\kappa\rho), \qquad (2.61)$$

$$\qquad (2.62)$$

we write

$$\Psi_m \underset{r_1,\rho\to\infty}{\sim} J_m + K_{1m}N_1 + K_{2m}N_2 \qquad (2.63)$$

$$\delta\psi_m \underset{r_1,\rho\to\infty}{\sim} \left[K_{1m}^t - K_{1m}\right]N_1 + \left[K_{2m}^t - K_{2m}\right]N_2. \qquad (2.64)$$

As we are considering surface elements which are perpendicular to $\boldsymbol{r_1}$ or $\boldsymbol{\rho}$, the dot product of the the angular operators in ∇_{r_1} and ∇_ρ with those of the surface elements will be zero. and (2.53 and 2.54) become

$$\begin{aligned}
\delta I'_{mn} = &-\int_{\sigma_i}\int_{V_i} \{[J_m + K_{1m}N_1 + K_{2m}N_2] \\
&\times\nabla_{R_i}\left[\left(K_{1n}^t - K_{1n}\right)N_1 + \left(K_{2n}^t - K_{2n}\right)N_2\right] \\
&-\left[\left(K_{1n}^t - K_{1n}\right)N_1 + \left(K_{2n}^t - K_{2n}\right)N_2\right] \\
&\times\nabla_{R_i}\left[J_m + K_{1m}N_1 + K_{2m}N_2\right]\} R_i^2 \sin\Theta_i d\Theta_i d\Phi_i d\tau_i, \qquad (2.65)
\end{aligned}$$

where $i = 1$ refers to $r_1 \to \infty$ and $i = 2$ to $\rho \to \infty$, . i.e. $(R_1 = r_1, R_2 = \rho, \Theta_1 = \theta_1, \Theta_2 = \theta_\rho$, etc). We note that from the definition of the Neumann and Bessel

functions we have

$$\nabla_{R_i} N_i(k_i R_i) = -k_i J_i(k_i R_i) \tag{2.66}$$

$$\nabla_{R_i} J_i(k_i R_i) = k_i N_i(k_i R_i), \tag{2.67}$$

with $k_1 = k$ and $k_2 = \kappa$. All the terms which will be of the form $N_i N_j$, $J_i N_j$ and $J_i J_j$ with $i \neq j$ will involve products of the target function and of the fragments functions $X_1(x_1)X_2(x_2)$, which have the explicit form

$$X_1(x_1)X_2(x_2) = \Phi_{He}(r_2, r_3)\Phi_{Ps}(r_{12})\Phi_{He^+}(r_3) \tag{2.68}$$

and whose exponential fall-off will be of the form $\exp(-\gamma(r_2+r_3))\exp(-\frac{r_{12}}{2})\exp(-2r_3)$ where γ is a constant. As on the surface $r_1 \to \infty$, for fixed values of r_2, we have $r_{12} \to \infty$, and on the surface $\rho \to \infty$, for fixed values of r_{12}, we have $r_2 \to \infty$, all terms with exponential fall-off will go to zero on both surfaces at infinity that we are considering. Further, after operating with ∇_{R_i} and multiplying out, all the terms involving quadratics in K or with KK^t will cancel out, so that

$$\begin{aligned}
\delta I'_{mn} = \int_{\sigma_i} \int_{V_i} & \left\{ J_m \left(K_{1n}^t - K_{1n} \right) k_i J_1 \right. \\
& + J_m \left(K_{2n}^t - K_{2n} \right) k_i J_2 + N_1 \left(K_{1n}^t - K_{1n} \right) k_i N_m \\
& \left. + N_2 \left(K_{2n}^t - K_{2n} \right) k_i N_m \right\} R_i^2 \sin \Theta_i d\Theta_i d\Phi_i d\tau_i.
\end{aligned} \tag{2.69}$$

Again for all values of m and n, we have terms of the form $J_1 J_2$ and $N_1 N_2$ which will vanish on both surfaces $r_1 \to \infty$ and $\rho \to \infty$. If we now consider a specific case, i.e. $m = 1$, $n = 1$, we have

$$\begin{aligned}
\delta I'_{11} = \int_{\sigma_i} \int_{V_i} & \left\{ J_1 \left(K_{11}^t - K_{11} \right) k J_1 \right. \\
& \left. + N_1 \left(K_{11}^t - K_{11} \right) k N_1 \right\} r_1^2 \sin \theta_1 d\theta_1 d\phi_1 d\tau_A.
\end{aligned} \tag{2.70}$$

The asymptotic form of J_1 and that of N_1 are

$$J_1 \underset{r_1 \to \infty}{\sim} = Y_{l,0}(\theta_1, \phi_1)\frac{1}{\sqrt{k}}\frac{\sin\left(kr_1 - \frac{l\pi}{2}\right)}{r_1}\Phi_{He}(r_2, r_3) \tag{2.71}$$

$$N_1 \underset{r_1 \to \infty}{\sim} = -Y_{l,0}(\theta_1, \phi_1)\frac{1}{\sqrt{k}}\frac{\cos\left(kr_1 - \frac{l\pi}{2}\right)}{r_1}\Phi_{He}(r_2, r_3). \tag{2.72}$$

Therefore,

$$\delta I'_{11} = \int_{\sigma_i} \int_{V_i} \left\{ \left(K^t_{11} - K_{11} \right) Y^2_{l,0}(\theta_1, \phi_1) \Phi^2_{He}(r_2, r_3) \right.$$
$$\left. \times \left[\frac{\sin^2 \left(kr_1 - \frac{l\pi}{2} \right)}{r_1^2} + \frac{\cos^2 \left(kr_1 - \frac{l\pi}{2} \right)}{r_1^2} \right] \right\} r_1^2 \sin \theta_1 d\theta_1 d\phi_1 d\tau_A \quad (2.73)$$

which, using the normalization properties of the spherical harmonics and the helium wavefunction given by (2.57), gives

$$\delta I'_{11} = K^t_{11} - K_{11}. \quad (2.74)$$

In a similar manner, we find

$$\delta I'_{12} = K^t_{12} - K_{12} \quad (2.75)$$

$$\delta I'_{21} = K^t_{21} - K_{21} \quad (2.76)$$

$$\delta I'_{22} = K^t_{22} - K_{22}, \quad (2.77)$$

or in matrix notation

$$\delta I'_{mn} = K^t_{mn} - K_{mn}, \quad (2.78)$$

and the full Kato identity can be written as

$$\delta I_{mn} = K^t_{mn} - K_{mn} + < \delta \psi_m \mid L \mid \delta \psi_n > = I^t_{mn} - I_{mn}. \quad (2.79)$$

The exact functional being zero, i.e. $I_{mn} = 0$, if we neglect the term of second order in $\delta \phi$ and replace the exact K matrix by the variational one K^v, we have

$$K^v = K^t - I^t. \quad (2.80)$$

or more explicitely

$$\begin{bmatrix} K^v_{11} & K^v_{12} \\ K^v_{21} & K^v_{22} \end{bmatrix} = \begin{bmatrix} K^t_{11} & K^t_{12} \\ K^t_{21} & K^t_{22} \end{bmatrix} - \begin{bmatrix} (\Psi_1, L\Psi_1) & (\Psi_1, L\Psi_2) \\ (\Psi_2, L\Psi_1) & (\Psi_2, L\Psi_2) \end{bmatrix} \quad (2.81)$$

The symmetry of the variational K matrix can be shown by considering

$$K^v_{12} - K^v_{21} = K^t_{12} - K^t_{21} - [< \Psi_1 \mid L \mid \Psi_2 > - < \Psi_2 \mid L \mid \Psi_1 >]. \quad (2.82)$$

We can note the similarity of the last bracket on the R.H.S. with that of 2.43 (replacing Ψ_m by Ψ_1 and $\delta \Psi_n$ by Ψ_2). So, using Green's theorem and the asymptotic

33

forms of Ψ_1 and Ψ_2 in a similar manner as above, we find that

$$[< \Psi_1 \mid L \mid \Psi_2 > - < \Psi_2 \mid L \mid \Psi_1 >] =$$

$$\int_{\sigma_1} \int_{V_A} \left\{ J_1 K_{12}^{\prime t} k J_1 + N_1 K_{12}^{\prime t} k N_1 \right\} r_i^2 \sin \theta_1 d\theta_1 d\phi_1 d\tau_A$$

$$- \int_{\sigma_2} \int_{V_B} \left\{ J_2 K_{21}^{\prime t} \kappa J_2 + N_2 K_{21}^{\prime t} \kappa N_2 \right\} \rho_i^2 \sin \theta_\rho d\theta_\rho d\phi_\rho d\tau_B, \qquad (2.83)$$

which, after integrating as in (2.70), is equal to

$$\left[K_{12}^t - K_{21}^t \right]. \qquad (2.84)$$

Therefore, we find that

$$K_{12}^{\prime v} = K_{21}^{\prime v}, \qquad (2.85)$$

which shows that (2.25) can indeed be used with the choice of labelling we have taken for the scattering wavefunction.

In the derivation for the Kato identity we only needed to consider the asymptotic form of the wavefunction. To describe the processes within the interaction region, we will need to include terms which deal specifically with that region of space. This can be done in various ways, for instance by a close coupling expansion in terms of the open and closed channel states or by an expansion in terms of square integrable analytical functions depending on all the variables of the system. In this work, the latter way has been chosen, and the form taken is that of a Hylleraas-type expansion

$$\Phi = \sum_{i=1}^{N} c_i \phi_i, \qquad (2.86)$$

where $\phi_i = \exp\left(-(\alpha r_1 + \beta r_2 + \beta r_3)\right) \left(r_1^{k_i} r_2^{l_i} r_{12}^{m_i} r_3^{n_i} r_{13}^{p_i} r_{23}^{q_i} \right)$ and the c_i are extra variational parameters. The value of N is such that all terms with

$$k_i + l_i + m_i + n_i + p_i + q_i \leq \omega \qquad (2.87)$$

are included in the summation (these quantities being non-negative integers). The exponential fall-off in r_1, r_2 and r_3 ensures that these functions have a short-range behaviour, and do not affect the asymptotic form of the wavefunction. The choice of the constants α and β will be discussed in detail later, but one of the principal criteria will be that they must ensure a sufficiently short-range character for the ϕ_is.

34

The wavefunction must be finite as $r_1 \to 0$, or $\rho \to 0$, and we see that this will not be the case if we include the N_1 and N_2 functions as defined in (2.59 and 2.61), as they are singular at $r_1 = 0$ and $\rho = 0$ respectively. For these functions to be finite at their respective origins, we remove the singularities by multiplying them by shielding functions $f^1_{sh}(r_1)$ or $f^2_{sh}(\rho)$. The precise form of these functions will depend on which partial wave is being considered, and will be described more explicitly in the discussion of each partial wave calculation.

We now write the two components of the trial wavefunction, as

$$\Psi_1 = S_1 + K^t_{11}C_1 + K^t_{21}C_2 + \sum_{i=1}^{N} c_i\phi_i \qquad (2.88)$$

$$\Psi_2 = S_2 + K^t_{22}C_2 + K^t_{12}C_1 + \sum_{j=1}^{N} d_j\phi_j, \qquad (2.89)$$

using the following notation

$$S_1 = Y_{l,0}(\theta_1, \phi_1)\Phi_{He}(r_2, r_3)\sqrt{k}j_l(kr_1) \qquad (2.90)$$

$$C_1 = -Y_{l,0}(\theta_1, \phi_1)\Phi_{He}(r_2, r_3)\sqrt{k}n_l(kr_1) \qquad (2.91)$$

$$S_2 = Y_{l,0}(\theta_\rho, \phi_\rho)\Phi_{He^+}(r_3)\Phi_{ps}(r_{12})\sqrt{2\kappa}j_l(\kappa\rho) \qquad (2.92)$$

$$C_2 = -Y_{l,0}(\theta_\rho, o_\rho)\Phi_{He^+}(r_3)\Phi_{ps}(r_{12})\sqrt{2\kappa}n_l(\kappa\rho). \qquad (2.93)$$

Expressing the variational K matrix in terms of these equations, using (2.80) and expanding out I^t, we find that

$$K^v = -DFD^T, \qquad (2.94)$$

where

$$D = \begin{bmatrix} K^t_{11} & K^t_{21} & c_1 & c_2 & \ldots & c_n & 1 & 0 \\ K^t_{12} & K^t_{22} & d_1 & d_2 & \ldots & d_n & 0 & 1 \end{bmatrix} \qquad (2.95)$$

and

$$F = \begin{bmatrix} CLC & CL\Phi & CLS \\ \Phi LC & \Phi L\Phi & \Phi LS \\ CLS & SL\Phi & SLS \end{bmatrix}. \qquad (2.96)$$

35

The 2×2 matrices CLC, CLS and SLS contain the matrix elements which involve only the asymptotic, or long range, part of the wave function. For example we have

$$CLC = \begin{bmatrix} (C_1, LC_1) & (C_1, LC_2) \\ (C_2, LC_1) & (C_2, LC_2) \end{bmatrix}.$$ (2.97)

The brackets in the matrix element representation mean an integration over the whole space of the system. To express the variational K matrix in this concise matrix form we have used the relation $(C_i, LS_i) = (S_i, LC_i) + \delta_{ij}$, which can be shown by using Green's theorem in a similar manner as before (see appendix A). This also explains how the reference to the trial K matrix as in 2.80 was eliminated from equation 2.94.

The $2 \times N$ matrices ΦLS, ΦLC, $SL\Phi$ and $CL\Phi$ contain the long-range – short-range cross terms, and have the form

$$CL\Phi = \begin{bmatrix} (C_1, L\phi_1) & (C_1, L\phi_2) & \ldots & (C_1, L\phi_N) \\ (C_2, L\phi_1) & (C_2, L\phi_2) & \ldots & (C_2, L\phi_N) \end{bmatrix}.$$ (2.98)

The $N \times N$ matrix $\Phi L\Phi$ contains all the short-range – short-range terms

$$\Phi L\Phi = (\phi_i, L\phi_j). \qquad i,j, = 1, 2, \ldots, N$$ (2.99)

From 2.94 we find that the dependency of the variational K matrix elements variational parameters is as follows :

$$
\begin{aligned}
K_{11}^v &= f(K_{11}^t, K_{21}^t, c_i) \\
K_{12}^v &= f(K_{11}^t, K_{12}^t, K_{21}^t, K_{22}^t, c_i, d_i) \\
K_{21}^v &= f(K_{11}^t, K_{12}^t, K_{21}^t, K_{22}^t, c_i, d_i) \\
K_{22}^v &= f(K_{22}^t, K_{12}^t, d_i).
\end{aligned}
$$ (2.100)

The variational principle requires

$$\frac{\partial I}{\partial \alpha_i} = 0, \qquad i = 1, 2, \ldots, n$$ (2.101)

where the α_is are the variational parameters. Therefore, we need to differentiate each variational K matrix element with respect to the variational parameters indicated

36

in 2.100. This will lead , as can be seen from 2.100, to a set of $6N + 12$ equations, of which only $2N + 4$ are independent, and these can be expressed in a matrix form as

$$
\begin{bmatrix}
(C_1, LC_1) & (C_1, LC_2) & \dots & (C_1, L\phi_j) & \dots \\
(C_2, LC_1) & (C_2, LC_2) & \dots & (C_2, L\phi_j) & \dots \\
\vdots & \vdots & & \vdots & \\
(\phi_i, LC_1) & (\phi_i, LC_2) & \dots & (\phi_i, L\phi_j) & \dots \\
\vdots & \vdots & & \vdots &
\end{bmatrix}
\begin{bmatrix}
K_{11}^t & K_{12}^t \\
K_{21}^t & K_{22}^t \\
\vdots & \vdots \\
c_i & d_i \\
\vdots & \vdots
\end{bmatrix}
= -
\begin{bmatrix}
(C_1, LS_1) & (C_1, LS_2) \\
(C_2, LS_1) & (C_2, LS_2) \\
\vdots & \vdots \\
(\phi_i, LS_1) & (\phi_i, LS_2) \\
\vdots & \vdots
\end{bmatrix}
$$

$$(2.102)$$

or more concisely as

$$\boldsymbol{AX} = -\boldsymbol{B}. \qquad (2.103)$$

Using this notation we can write 2.94 as

$$
\boldsymbol{K^v} = - \begin{bmatrix} \boldsymbol{X}^T & 1 \end{bmatrix}
\begin{bmatrix} \boldsymbol{A} & \boldsymbol{B} \\ \boldsymbol{B}^T & \boldsymbol{SLS} \end{bmatrix}
\begin{bmatrix} \boldsymbol{X} \\ 1 \end{bmatrix}, \qquad (2.104)
$$

which, using 2.103, gives

$$\boldsymbol{K^v} = -\boldsymbol{B}^T \boldsymbol{X} - \boldsymbol{SLS} \qquad (2.105)$$

$$= -\boldsymbol{\Psi}^{t,0} \boldsymbol{LS}, \qquad (2.106)$$

where $-\boldsymbol{\Psi}^{t,0}\boldsymbol{LS}$ is a 2×2 matrix with elements $-(\Psi_i^{t,0}LS_j)$ and $\Psi^{t,0}$ is the trial wavefunction with the optimum values of the variational parameters given by 2.103.

2.4   The inverse Kohn method

The choice of the asymptotic form of the wavefunction as in eqs 2.20 and 2.21 is to some extent arbitrary, and we could have considered any form for which the boundary conditions are obeyed. Therefore various forms of the Kohn method can be derived, each based on a specific choice of wavefunction and each in principal giving the same final variational result. This can readily be seen from the one

channel case in which the general form of the asymptotic part of the wavefunction is

$$\Psi(r_1) = Y_{l,0}(\theta_1, o_1)\sqrt{k}\left[Dj_l(kr_1) - Fn_l(kr_1)\right]\Phi_{He}(r_2, r_3). \tag{2.107}$$

The coefficients D and F which are energy dependent are related to the elastic phase shift η by

$$\frac{F}{D} = \tan\eta_l. \tag{2.108}$$

The generalized Kohn functional is then (see Armour and Humberston 1991)

$$\tan(\eta_v - \tau) = \tan(\eta_t - \tau) - (\Psi_t, L\Psi_t) \tag{2.109}$$

where τ is a phase parameter. When $\tau = 0$, we have the normal Kohn functional and in the trial function $D_t = 1$ and $F_t = \tan\eta_l$. Any other choice of values for D_t and F_t can be made as long as the relation 2.108 is satisfied, so that the case $D_t = \cot\eta_l$ and $F_t = 1$, is also a correct choice. This will lead to the functional 2.109 with $\tau = \pi/2$, and is called the inverse Kohn method. When used with very flexible trial wavefunctions both the Kohn and the inverse Kohn method will give very similar result for η_l^v, with the main difference being due to the numerical precision of the calculation. Because the evaluation of the variational phase shift with either the Kohn or the inverse Kohn method involves the use of a different ordering of the long-range – long-range and short-range – long-range matrix elements in the one channel equivalent to 2.103. the agreement within the numerical precision of the results for both methods is a good test of the accuracy of the evaluation of these types of matrix elements.

In the two channel case. the coupling between the channels, which is implied in the use of the K matrix elements, makes the relations between the Kohn and inverse Kohn methods more complex to derive. The inverse Kohn wavefunction is, using the same notation as in 2.88 and 2.89,

$$\Psi_1 = \overline{K}_{11}^t S_1 + \overline{K}_{21}^t S_2 + C_1 + \sum_{i=1}^{N} c_i \phi_i \tag{2.110}$$

$$\Psi_2 = \overline{K}_{12}^t S_1 + \overline{K}_{22}^t S_2 + C_2 + \sum_{j=1}^{N} d_j \phi_j, \tag{2.111}$$

where

$$\overline{K} = K^{-1} \tag{2.112}$$

is the inverse Kohn K matrix. The formulation of the variational method can be carried out as before, leading to a set of simultaneous equations similar to that in equation 2.102 but where all the Ss and Cs have been interchanged and K_{mn} replaced by $\overline{K}_{mn}$. From this new matrix relation we find that

$$\overline{K}^v = -\Psi^{t,0}LC, \qquad (2.113)$$

where $-\Psi^{t,0}LC$ is a 2×2 matrix with elements $-(\Psi_i^{t,0}LC_j)$ and $\Psi^{t,0}$ is the trial wavefunction with the optimum values of the variational parameters. We have used both the Kohn and the inverse Kohn methods as a check on the accuracy and the general consistency of our calculation and to identify the cases where non physical resonance features occur as discussed in the next section.

2.5 Schwartz singularities

Although the Kohn variational method only yields a rigorous upper bound on the scattering length of positron-helium scattering (Spruch and Rosenberg 1962) and not for the phase shift, there is an empirical lower bound on the phase shift, i.e. it usually becomes more positive as the trial function is improved. The early calculations of the scattering data using the Kohn variational method indicated that the behaviour of the variational results could, under certain conditions, become very unpredictable because of the presence of non-physical resonance features which clearly do not respect the empirical bound.

Schwartz (1961) provided the first numerical analysis of this phenomenon in his calculation of the s-wave phase shifts for both electron and positron-hydrogen scattering. He noted that he obtained results which were very dependent on the value of a non-linear parameter in the trial function. By repeating his calculation for a given set of short range terms and a given energy, but varying the non linear parameter, κ, he showed that the tangent of the phase shift, $\tan \eta$, became singular for some values of κ (see figure 2.3. Note that κ used in the work of Schwartz is different from the positronium wavenumber, κ, we have used in this work). He
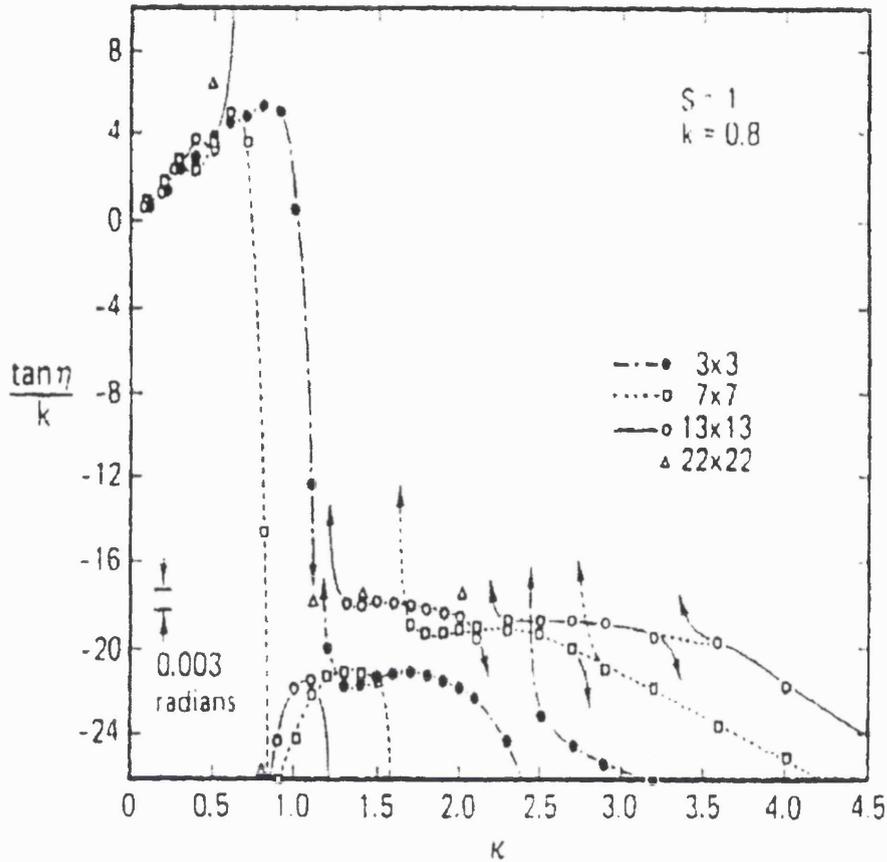
Figure 2.3: Variations of $\tan \eta^v/k$ with respect to a non-linear parameter, κ, in the trial function for s-wave $e^- - H$ scattering where $k = 0.8$. The different lines correspond to different sets of short-range terms. Taken from Schwartz (1961a).

repeated the calculation for trial functions containing more short range terms and found that more of these singularities appeared at different values of κ but that they became more narrow. This means that, as the the trial function is improved, the region of the values of κ over which $\tan \eta$ is well behaved becomes larger and the results become more reliable. These singularities also appear when the energy of the incoming particle is varied for a given value of κ.

The analysis of the Schwartz singularities and the various modifications to the variational method to eliminate them have been the subject of many studies (see Nesbet 1980, Callaway 1978 and Truhlar *et al.* 1974 for reviews). The variational method used in these studies is different from the one used in this work as they first solved the set of linear equations resulting from the variational principle for

the short-range parameters, i.e. $\partial I/\partial c_i = 0$, and use the resulting values of c_i, which for the one channel case are then a function of $\tan\eta$, to solve $\partial I/\partial\tan\eta = 0$. Using this method, Schwartz proposed that the singularities in $\tan\eta$ originated in the inversion of the matrix $\boldsymbol{\Phi L\Phi}$. This matrix will have N eigenvalues of the operator $L = 2(H - E)$ and these eigenvalues will vary continuously as the value of the non-linear parameter or the energy is changed. Therefore the operator L has a continuous set of eigenvalues which will pass through zero and in theory the matrix will be singular when one of these eigenvalues is exactly zero as its inverse will be ill-defined. In a numerical calculation it is sufficient for the eigenvalue to be numerically close to zero for the matrix to become ill-conditioned and therefore the variational values of the $\boldsymbol{K}$ matrix elements may lie anywhere between $-\infty$ to $+\infty$. When more short-range terms are added to the trial wavefunction the density of eigenvalues close to zero increases, because the matrix $\boldsymbol{\Phi L\Phi}$ becomes larger, and therefore the probability of ill-conditioning increases. Nesbet (1980) showed that the singularities in $\tan\eta$ did not come from the singularities of the matrix $\boldsymbol{\Phi L\Phi}$ on its own, but from a combination of this matrix with the various short-range - long-range and long-range – long-range matrix elements. A series of variations of the Kohn method have been developed to overcome the problems with these singularities (the Harris method, the Optimized Minimum Norm method, the Optimized Anomaly Free method, etc... all discussed in the reviews cited above) but they are all based on the two stage solution of the set of linear equations, 2.103.

In the method used in this work, we see that the matrix $\boldsymbol{A}$ also has eigenvalues which must pass through zero, as the Hamiltonian of the system, H, has a continuous spectrum in which the total energy is embedded. Therefore the matrix $\boldsymbol{A}$ may have eigenvalues close to zero and its inverse is then ill-conditioned. Again, as the number of short-range terms increases, the probability for a singularity to occur increases too but we now have a very narrow resonance-type feature, and reliable results can be found from the data which are not affected. The various methods to eliminate these singularities to which we have referred above have not been applied to the version of the Kohn method we have used in this work. Instead, we have used a comparison method, where the agreement of the results obtained with the

Kohn and the inverse Kohn method is taken as the criterion of the reliability of the calculation. As the problem arises in the inversion of the matrix A, the change in the form of this matrix when using either the Kohn or the inverse Kohn method is such that it is very improbable for it to be ill-conditioned in both cases at the same values of the non linear parameters and at the same energy. We have found this criterion to be very reliable and in general have not encountered many Schwartz singularities in our calculations. If the contrary had been the case and if the Kohn - inverse Kohn criterion had not been found to be reliable, the method developed by Armour (Armour and Humberston 1991), in which the generalized form of the Kohn functional 2.109 can be used. The method consists in considering a set of values for the phase parameters τ , between 0 and π, rejecting those for whom $det\,A$ is very close to zero and taking the average of the ones left.

Chapter 3

The use of inexact target wavefunctions

3.1 Introduction

Both the general theory of atomic scattering and the Kohn variational method we have described in the previous chapter assume that the wavefunction of the target atom is known exactly, i.e. that it is an eigenfunction of the target Hamiltonian which is itself part of the total Hamiltonian of the system.

This condition can only be satisfied if the target is a hydrogen atom or is of a hydrogenic form (Ps, He^+, etc), but for any other atom we must introduce an approximate wavefunction based either on a simplified model representation of the complex atom, for instance a hydrogenic model for the lithium atom, or on a variational calculation when possible. The use of these approximations will introduce into the scattering formalism a certain number of inconsistencies which may affect the final result dramatically. Variational calculations of scattering data have sometimes been found to be very sensitive to the quality of the approximate target wavefunction and various authors have investigated this for very low energy elastic scattering (Peterkop and Rabik 1971, Houston 1973, Page 1975). In the case of positron-atom

scattering, where the projectile is distinguishable from the target electrons, Drach-man (1972) showed that these difficulties could be avoided by using the method of models. In this method, the exact target Hamiltonian is implicitly replaced by a model Hamiltonian of which the approximate target wavefunction is assumed to be an eigenfunction. This leads to more consistency in the scattering formalism and has shown to give excellent results in positron-helium elastic scattering below the positronium formation threshold (Humberston 1973, Campeanu and Humberston 1975 & 1977). In the case of a rearrangement process, such as positronium forma-tion, the method of models cannot be used consistently and the exact Hamiltonian must be used throughout the calculation.

We have therefore investigated the effect of the quality of the helium wavefunc-tion on our results by comparing the phase shifts obtained with and without the method of models for elastic scattering below the positronium threshold where both methods can be used. For this we have created a set of helium target wavefunctions which can be used in the Kohn variational method and which give good results for the helium ground state energy and polarizability.

In this chapter we will show how the various helium wavefunctions have been calculated, expand on the method of models and its limitation in positronium forma-tion calculations, and make an empirical analysis of the effect of the use of inexact target wavefunctions on the calculation of the elastic scattering phase shifts which will be used as a reference for the main calculation of this work, i.e. positronium formation.

3.2 The helium target wavefunctions

Hydrogen is the only stable atom for which the wavefunction is known exactly and the analytical form for the various states of hydrogen can be found in any text book on atomic physics. Although helium is the next atom in terms of complexity, there are no exact solutions to the Schrödinger equation which describes the nucleus-two

electron system. This lack of a formal solution has meant that many approximation methods have been developed to evaluate inexact wavefunctions for atoms, other than hydrogen, which could be used to calculate their physical properties.

One of the most important of these properties is the ground state energy, and the first quantum mechanical calculation of this quantity for the helium atom was done by Unsöld (1927) using first order perturbation theory. He used a simple wavefunction based on the product of two one-electron wavefunctions and found $E_o = -5.50(\text{Ryd.})$, which is only 5% more positive than the experimental value. A more elaborate wavefunction was developed by Hylleraas (1930) and, using a Rayleigh-Ritz variational method, he found a value of $E_o = -5.80648$ (Ryd.), which is only 0.01% more positive than the most accurate value of $E_o = -5.807448752$ (Ryd.) found by Bishop and Lam (1988). Because of its complexity, their wave-
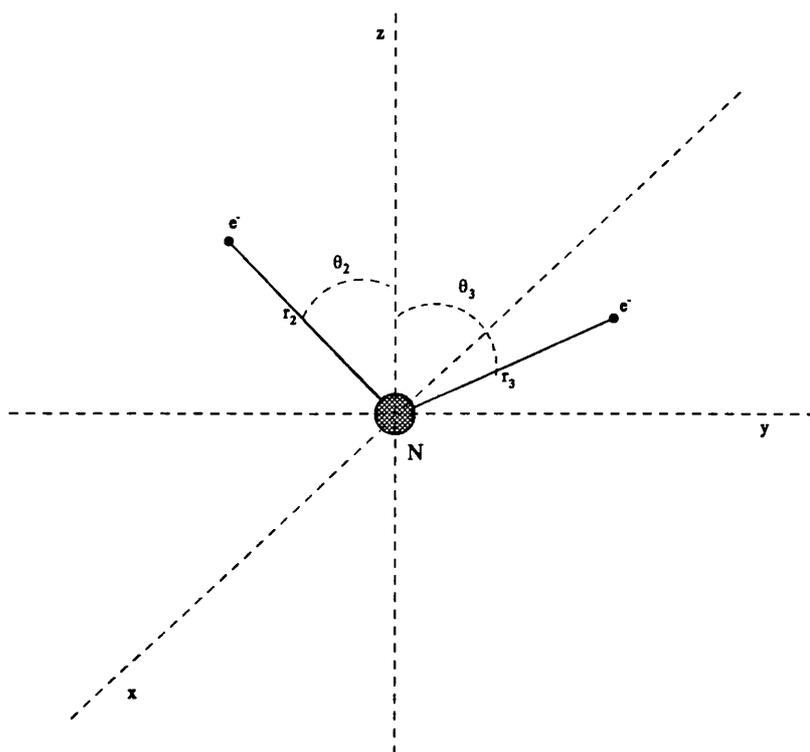
Figure 3.1: The helium atom coordinate system.

function cannot be used in a scattering calculation, but their result shows that the use of a Hylleraas type of wavefunction (even with a lower number of terms in the expansion) and the Rayleigh-Ritz method does give good helium target functions

45

which can be used effectively in the scattering problem, and we have taken the same approach for this work.

The helium atom system we are considering is a three body system where we assume the nucleus to be infinitely heavy and placed at the origin of our coordinate system (see figure 3.1). For the $1\,^1S$ ground state, the spatial wavefunction is spherically symmetric and does not depend on any of the Euler angles. Therefore, the helium target function will only depend on r_2, r_3 and $r_{23} = \mid \boldsymbol{r_2} - \boldsymbol{r_3} \mid$. A more convenient choice of variables is

$$s = r_2 + r_3$$
$$t = r_2 - r_3$$
$$u = r_{23}, \tag{3.1}$$

and the Hylleraas form of trial target function is

$$\Phi(\boldsymbol{r_2}, \boldsymbol{r_3}) = e^{-\gamma s} \sum_{j=1}^{n} b_j s^{K_j} t^{M_j} u^{N_j}. \tag{3.2}$$

The summation includes all terms with $K_j + M_j + N_j \leq \omega_{He}$ and because the ground state of helium is a para-state, i.e. space symmetric, we must take M_j as even only, in order to ensure the symmetry in r_2 and r_3. In previous Kohn variational calculations of positron-helium elastic scattering below the positronium formation threshold (Humberston 1973, Campeanu and Humberston 1975 & 1977, Campeanu 1977), the powers of r_{23}, i.e. N_j, were restricted to be even only. This restriction was due to the difficulty in the numerical integration of that variable in the scattering calculation, which will be explained in detail in chapter 5. In this work we have not made this restriction, and have evaluated helium wavefunctions containing both even and odd powers of r_{23}. As expected, the quality of the target wavefunction when containing odd powers of r_{23} was greatly improved, as this configuration represents much better the electron correlation within the atom. This improvement is mainly due to the linear r_{23} terms which are needed to represent the cusp in the wavefunction at $r_{23} = 0$.

The Rayleigh-Ritz variational method, as described in chapter 2, was used to determine the optimum value of the linear parameters b_j in equation 3.2.

The Hamiltonian for the helium system is

$$H_{He} = -\frac{1}{2}\nabla^2_{r_2} - \frac{1}{2}\nabla^2_{r_3} - \frac{2}{r_2} - \frac{2}{r_3} + \frac{1}{r_{23}} \qquad (3.3)$$

and using the Rayleigh-Ritz functional 2.33 we have

$$E^v_o = \frac{\int \Phi^t_{He}(r_2, r_3)H_{He}\Phi^t_{He}(r_2, r_3)dr_2dr_3}{\int \Phi^t_{He}(r_2, r_3)\Phi^t_{He}(r_2, r_3)dr_2dr_3}, \qquad (3.4)$$

where E^v_o is the variational approximation to the exact ground state energy, which was shown in chapter 2 to be always more positive than the exact ground state energy E_o. The method therefore consists of choosing the number of terms in the sum of 3.2, calculating the optimum values of the linear parameters, b_j, and then using these to evaluate E^v_0 for the corresponding trial function. This procedure is then repeated for a set of values for the non-linear parameter γ, and the trial function which gives the most negative value for the ground state energy is then taken as the optimum trial function for the given value of ω_{He} (see figure 3.2). Because these
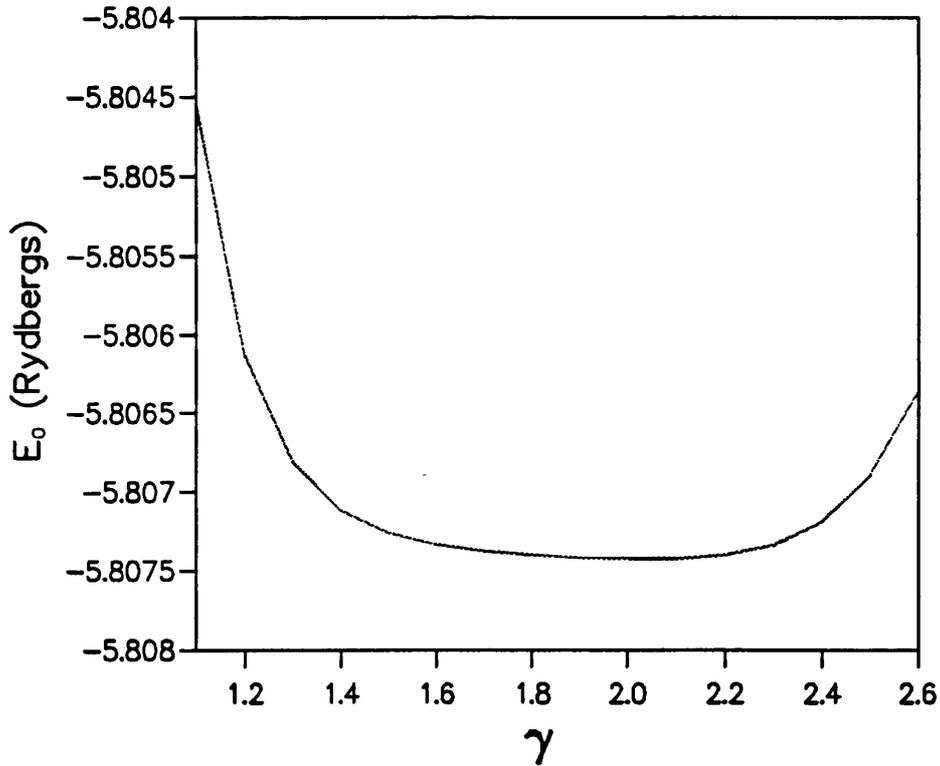

Figure 3.2: The variation of E_0 with γ for helium model H22.

target wavefunctions will be used in a scattering calculation, we wish not only that

47

the variational ground state energy agrees well with the 'exact' value, but even more we require that the dipole polarizability calculated with the target function is also in good agreement with the best experimental value. The dipole polarizability, α_d, determines how much the atom is distorted by the incoming projectile and it will therefore play an important role both in the elastic scattering and the positronium formation channels, even in helium where the electrons are tightly bound to the nucleus and α_d is relatively small. The dipole polarizability is evaluated by considering the perturbation of the energy of the helium atom placed in a small uniform electric field, (Thomas and Humberston 1972), which we can choose to be along the z-axis.

The Hamiltonian for the helium atom in this uniform field is then

$$H_{Pol} = -\frac{1}{2}\nabla_{r_2}^2 - \frac{1}{2}\nabla_{r_3}^2 - \frac{2}{r_2} - \frac{2}{r_3} + \frac{1}{r_{23}} - \epsilon(r_2 \cos\theta_2 + r_3 \cos\theta_3), \qquad (3.5)$$

where ϵ is the field strength, and $\cos\theta_2$ and $\cos\theta_3$ are the angles between the z-axis and the vectors r_2 and r_3 respectively. The change in energy (ΔE) of the helium ground state can be shown from perturbation theory to be quadratic in ϵ, and to be always negative.

The dipole polarizability is defined by

$$\alpha_d = \frac{-2\Delta E}{\epsilon^2}. \qquad (3.6)$$

The evaluation of ΔE is carried out using a Rayleigh-Ritz calculation of the perturbed ground state energy, but because the presence of the electric field has destroyed the spherical symmetry of the system, a new form of trial wavefunction needs to be considered. This trial function now includes a p-state character angular dependence and can be written as

$$\begin{aligned}
\Psi(r_2, r_3) &= \Phi_{He}(r_2, r_3) \\
&\times \left[1 + \sum_{k=1}^{m} \left(r_2 \cos\theta_2 + (-1)^{Q_k} r_3 \cos\theta_3 \right)(r_2 + r_3)^{P_k}(r_2 - r_3)^{Q_k} r_{23}^{S_k} \right]
\end{aligned} \qquad (3.7)$$

where $\Phi_{He}(r_2, r_3)$ is defined as in equations 3.2 and the summation is such that $P_k + Q_k + S_k \leq \omega_k$. To determine the dipole polarizability of a given helium wavefunction, we first need to choose values of ϵ for which the perturbation approach holds, i.e. we want ϵ to be very small and such that variations in it do not affect the final results

for α_d. We then calculate the perturbed ground state energy for different values of ω_k by increasing the number of terms in the perturbation wavefunction 3.7. The values of α_d are found using equation 3.6 and the most converged result is chosen. One must note that there is no bound on α_d in this calculation, and therefore the optimum value of γ for α_d is taken as that which gives a value of α_d closest to the best theoretical result $\alpha_d = 1.38319$ a_0^3 (Bishop and Lam 1988) (see figure 3.3).

The choice of non-linear parameter γ in the helium target wavefunction. Φ_{He}, affects the value of α_d, and the optimized value of γ for the ground state energy does not always correspond to that for the dipole polarizability. The value of γ was chosen so that it gave the best compromise between E_0^v and α_d, favouring the polarizability if required. We have also found that, as the number of terms in the helium wavefunction is increased, the optimum value of E_0 is less sensitive to the value of γ (see figure 3.4) and it was therefore easier to get a good compromise between the values of E_0 and of α_d for the more elaborate wavefunctions.
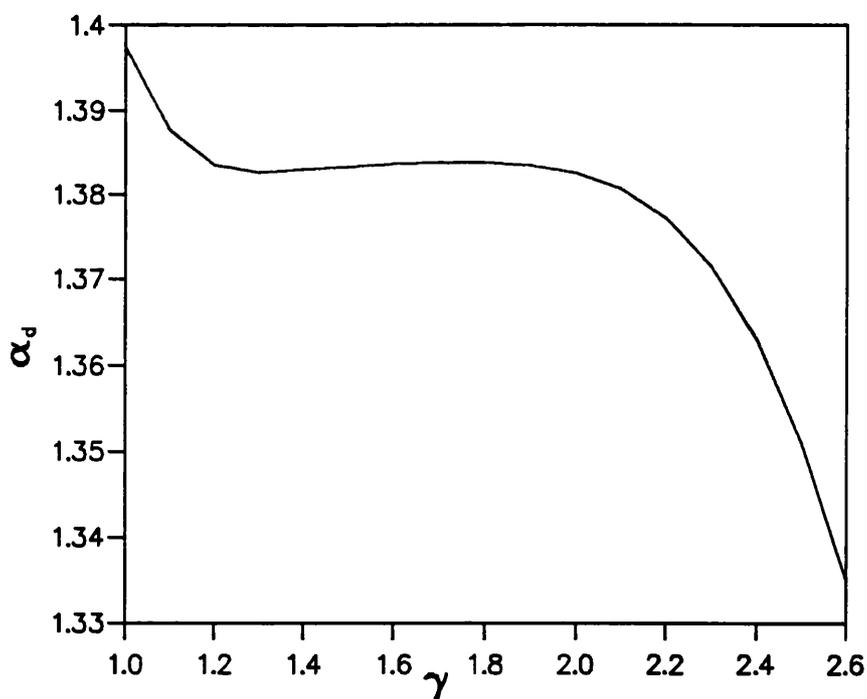
Figure 3.3: The variation of α_d (a_0^3) with γ for helium model H22.

Table 3.1 gives the values of E_0^v, α_d and γ for the various helium wavefunctions we
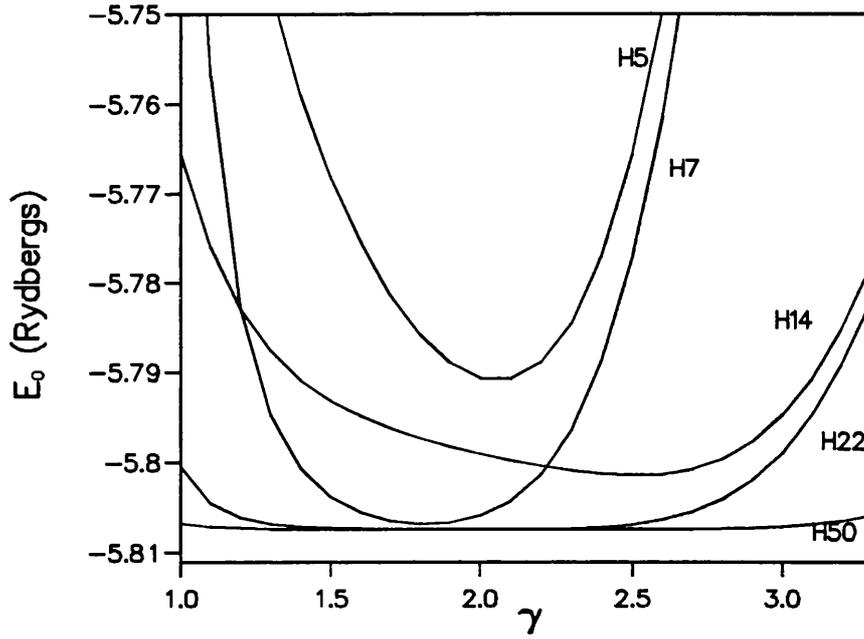
Figure 3.4: The variation of E_0 with γ for different helium wavefunctions.

have investigated. The models H5 and H14 are those used by Campeanu and Humberston in their investigations of elastic scattering below the positronium threshold, and both contain only even powers of r_{23}. The models H7, H22 and H50 have been generated for this work, and one can see how the inclusion of the odd powers of r_{23} has improved the values of E_0^v giving 99.9% of the correlation energy, which is the difference between the exact energy and the value found using the Hartree method of self consistent fields (Hartree 1928) with a product form helium wavefunction.

	H5	H14	H7	H22	H50	exact*
$\omega_{He}(n)$	2(5)	4(14)	2(7)	4(22)	6(50)	
γ	1.90	2.24	1.80	1.80	2.00	
Energy/Ryd.	-5.78890	-5.80060	-5.80684	-5.80740	-5.80745	-5.80745
Polarisability/a_0^3	1.39527	1.38823	1.37768	1.38376	1.38322	1.38319

Table 3.1: Properties of the helium wave functions. The 'exact' results are those of Bishop and Lam (1988)

3.3 The use of inexact target functions and the method of models

The effects of the inconsistencies introduced in the general formulation of the scattering problem by the use of an inexact target wavefunction have been known since the first variational calculations of scattering processes were made. With the advent of more computational power in the late 1960s, it became possible to undertake variational calculations with greater numbers of short range correlation terms than was previously envisaged, and several authors (Peterkop and Rabik 1971, Houston 1973 and Page 1975) found that the sensitivity of the results to the choice of target function became a major factor in the quality of the calculation. These authors investigated this problem, for both electron- and positron-atom scattering, mainly by considering the calculation of the scattering length for which there is a rigorous upper bound when using the Kohn variational method with exact target wavefunctions (Spruch and Rosenberg 1960). They used either an inexact helium wavefunction or an approximation to the hydrogen wavefunction of the form

$$\phi_H = \sqrt{\frac{\lambda^3}{\pi}} e^{-\lambda r_1} \tag{3.8}$$

from which the exact hydrogen wavefunction is obtained with $\lambda = 1$. Typical results can be seen in figure 3.5 taken from the work of Page (1975), which shows how the scattering length for positron-hydrogen scattering varies with the variation of a non-linear parameter η in the scattering wavefunction. One sees that for $\lambda = 1$ (i.e. the exact ϕ_H), the scattering length versus η curve shows a local minimum which is a consequence of the upper bound on the scattering length. One sees that for small changes in λ there is still a local minimum, but for values of λ only one percent less or greater then 1, there is no local minimum present and the bound on the scattering length is violated. The results of figure 3.5 correspond to 4 terms in the Hylleraas expansion in the scattering wavefunction, and it was found that when the number of terms was increased, the value of λ for which no local minimum could be found became closer to one (see Page 1975). The same phenomenon was observed for positron-helium scattering, for which there is no exact target function which can be
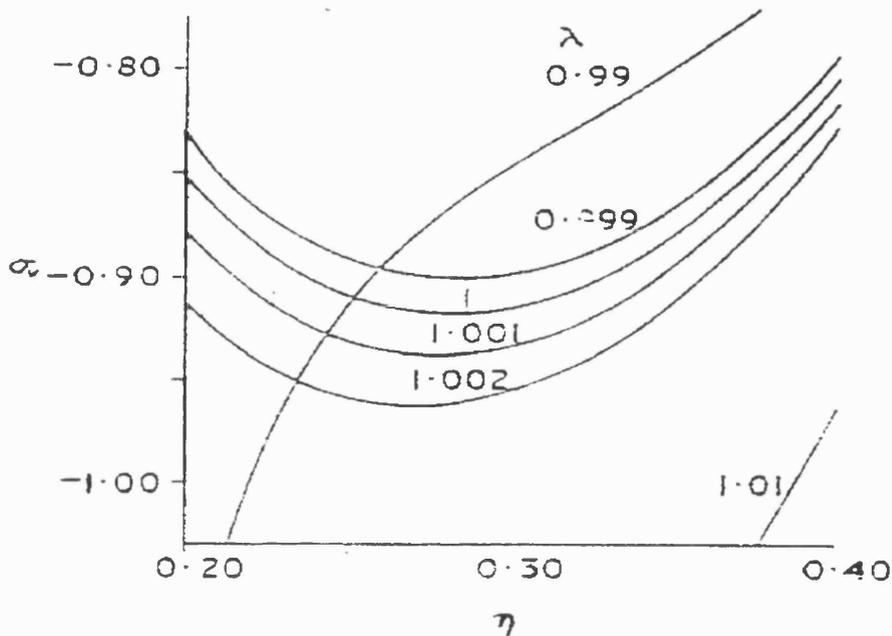
Figure 3.5: The variation of scattering length with respect to the non-linear parameter η for positron-hydrogen scattering taken from Page (1975).

modified in a systematic manner and instead various approximations for the helium wavefunction were used, for instance Hylleraas types in the work of Page (1975) and the Hartree-Fock approximation in that of Houston (1973).

To remedy this problem Drachman (1972) proposed the use of the so-called method of models. In this method the target Hamiltonian, H_{He}, is replaced by a approximate Hamiltonian, H_m, of which the approximate target wavefunction, ϕ_{He}, is an eigenfunction, and we have

$$H_m = -\frac{1}{2}\nabla_{r_2}^2 - \frac{1}{2}\nabla_{r_3}^2 + V_m \tag{3.9}$$

and

$$H_m\phi_{He} = E_m\phi_{He}, \tag{3.10}$$

where V_m and E_m are the model potential and the model ground state energy respectively.

The total Hamiltonian of the scattering problem becomes

$$H_T = -\frac{1}{2}\nabla^2_{r_1} + H_m + \frac{2}{r_1} - \frac{1}{r_{12}} - \frac{1}{r_{13}} = -\frac{1}{2}\nabla^2_{r_1} + H_m + V_{int}, \qquad (3.11)$$

and the total energy is given by

$$E_T = \frac{1}{2}k^2 + E_m. \qquad (3.12)$$

Both V_m and E_m can be evaluated explicitly, but only easily for fairly simple target functions, as can be seen from the following example. Consider, for instance, the helium model H1 (see Humberston 1973),

$$\phi_{He} = e^{-\alpha(r_2+r_3)} \qquad (\alpha = 1.5992) \qquad (3.13)$$

From equation 3.10 we have

$$\left(-\frac{1}{2}\nabla^2_{r_2} - \frac{1}{2}\nabla^2_{r_3} + V_m\right)e^{-\alpha(r_2+r_3)} = E_m e^{-\alpha(r_2+r_3)} \qquad (3.14)$$

and using $\nabla^2_{r_i}e^{-\alpha r_i} = (\alpha^2 - 2\alpha/r_i)e^{-\alpha r_i}$ we have

$$\left(\frac{\alpha}{r_2} + \frac{\alpha}{r_3} - \alpha^2 + V_m\right)e^{-\alpha(r_2+r_3)} = E_m e^{-\alpha(r_2+r_3)} \qquad (3.15)$$

As we require V_m to vanish for large values of r_2 and r_3 we have

$$\begin{aligned} E_m &= -\alpha^2 \\ V_m &= -\frac{\alpha}{r_2} - \frac{\alpha}{r_3} \end{aligned} \qquad (3.16)$$

As expected, because there is no electron correlation term in ϕ_{He}, the model potential does not have a r_{23} term either. One can see that the evaluation of V_m and E_m for more elaborate target functions will be complicated. Fortunately, however, if a suitable choice of total wavefunction for the scattering problem is used one does not need to evaluate V_m and E_m.

In the case of elastic scattering below the positronium formation threshold, we can take the total wavefunction to be of the form

$$\Psi_T = \phi_{He}\Psi_{sc}, \qquad (3.17)$$

where Ψ_{sc} is the scattering wavefunction. This product form of wavefunction is no restriction on the total wavefunction if the target wavefunction is nodeless, as is the case for helium. We now operate with $(H_T - E_T)$ on Ψ_T,

$$
\begin{aligned}
(H_T - E_T)\,\Psi_T &= \left[\sum_{i=1}^{3} -\frac{\nabla_{r_i}^2}{2} + V_{int} + V_m - \frac{k^2}{2} - E_m \right] \phi_{He} \Psi_{sc} \\
&= \phi_{He} \left[\sum_{i=1}^{3} -\frac{\nabla_{r_i}^2}{2} + V_{int} - \frac{k^2}{2} \right] \Psi_{sc} \\
&\qquad - \sum_{i=2}^{3} \nabla_{r_i} \Psi_{sc} \nabla_{r_i} \phi_{He} + \Psi_{sc} \left[H_m - E_m \right] \phi_{He} \\
&= \phi_{He} \left[\sum_{i=1}^{3} -\frac{\nabla_{r_i}^2}{2} + V_{int} - \frac{k^2}{2} \right] \Psi_{sc} - \sum_{i=2}^{3} \nabla_{r_i} \Psi_{sc} \nabla_{r_i} \phi_{He}. \quad (3.18)
\end{aligned}
$$

We note that there is no reference in this expression to either the model potential or the energy eigenvalue of the model Hamiltonian and that, as ϕ_{He} is now an exact eigenfunction of the model Hamiltonian, we have eliminated the formal inconsistencies introduced in the scattering formalism when inexact target functions are used. This method can be used in positron scattering calculations as there is no exchange between the projectile and the target electrons, whereas it cannot be used consistently for electron scattering as the model Hamiltonian is not symmetric under the interchange of all electrons.

The method of models has been employed successfully in many variational calculations of low energy positron atom scattering, for both the evaluation of the scattering length and the elastic phase shifts below the Ore gap (for instance Campeanu and Humberston (1977) for positron-helium scattering). The difficulty in a variational calculation of the positronium formation cross section in positron-atom collisions is that the product form for the total wavefunction cannot satisfy the boundary conditions for the rearrangement channel. As the main aim of this work is the evaluation of the various cross sections of positron-helium scattering within the Ore gap, we have had to abandon the method of models and accept that the inexactness of our target wavefunctions will affect our results. We have therefore investigated first the reliability of the elastic scattering phase shifts found without the method of models by comparing them with the results obtained with the method. The conclusion of this analysis was then used as an empirical criterion to

k	0.1	0.3	0.5	0.7	0.9
η_1	0.031	0.029	−0.023	−.093	−0.163
η_2	0.0300	0.0278	−0.0239	−.0927	−0.162
η_3	0.0300	0.0278	−0.0239	−.0927	−0.162

Table 3.2: η_1 : s-wave phase shifts for H5. ω= 4 (Humberston 1973); η_2 : s-wave phase shifts for H5 this work. ω= 4 with only even powers of r_{23}; η_3 : s-wave phase shifts for H5 this work. ω= 4 with even and odd powers of r_{23}

assess the reliability of the scattering data for which the method of models cannot be used. As the investigations of Peterkop and Rabik (1971), Houston (1973) and Page (1975) have shown, both the quality of the target wavefunction and the number of short-range terms in the scattering function have an effect on the reliability of the results obtained with inexact target functions and we have therefore investigated these effects in our calculations.

The results obtained with the method of models are known to be reliable and not affected by the inexactness of the target function, and we have evaluated the s-wave elastic phase shifts for positron-helium scattering using the various helium models we have generated. The models H5 and H14, which do not contain odd powers of r_{23}, were those used in the previous calculation of Humberston (1973) and Campeanu and Humberston (1977). We have repeated their calculations with the method of models to check the new numerical procedures we have introduced in this work and which are discussed in chapter 5.

In table 3.2 we compare the results for model H5 with $\omega = 4$ in the scattering wavefunction. We believe that there is a reasonable agreement and that the slight differences can be explained by the greater accuracy in the results of this work. The values of Humberston were obtained with a trial function containing no r_{23} terms at all in the scattering function, while the results of this work have been calculated with powers of r_{23} included. One can notice that the inclusion of odd powers of r_{23} does not affect the results, which is consistent with the findings of

Humberston (1973) who showed that the total removal of the r_{23} variable did not change the results significantly. In the work of Humberston (1973) and Campeanu and Humberston (1977) the results showed a monotonic convergence of the phase shift with increasing values of ω, and the same pattern was observed in the results obtained with the method of models in this work. This convergence is a feature of the Kohn method when used in conjunction with a Hylleraas expansion to represent the closed channels (instead of a pseudo-state type of representation, for instance) and, if a high enough value of ω is reached, an extrapolation procedure can be used to estimate the $\omega = \infty$ results (Armour and Humberston 1991).

These s-wave phase shifts have been recalculated without the method of models for both H5 and H14 using a scattering function containing Hylleraas type short-range terms in which the power of the variable r_{23} is either even only or both even and odd. For H5, we noticed that there was a rapid breakdown in the convergence of the phase shifts with respect to ω. The same phenomenon occurred for H14, and in both cases the breakdown was more pronounced when the scattering wavefunction contained even and odd powers of r_{23}. The type of breakdown is shown dramatically in figure 3.6 where we have plotted the values of the phase shifts, for $\omega = 2$ to $\omega = 5$, versus positron energy for the helium model H14.

Also plotted there are the best converged phase shifts calculated using the method of models and one can see that the results obtained without the method of models, with even and odd powers of r_{23} in the scattering wavefunction, do not converge to them. As mentioned earlier, the only established rigourous bound in positron-atom variational calculations using the Kohn variational method is that for the scattering length (Spruch and Rosenberg 1960), but it had been noticed in studies of positron-hydrogen scattering, and also in positron-helium scattering using the method of models, that an empirical bound could be observed on the phase shifts if one took care to identify and avoid the Schwartz singularities which may occur. From figure 3.6 it is clear that when the method of models is not used, this empirical bound principle is violated. It is true that the results obtained without the method of models do not need to correspond to those calculated with the
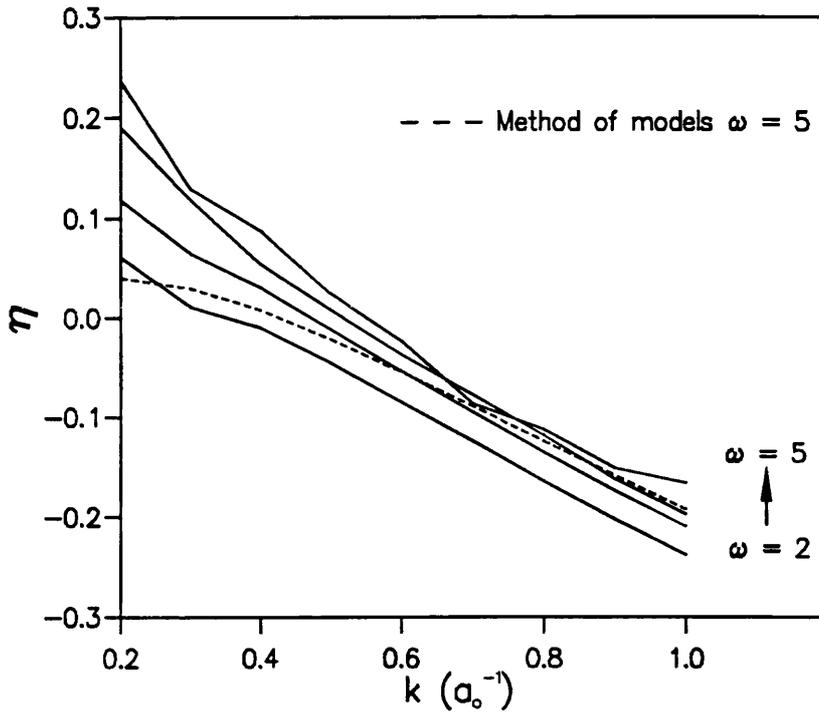
Figure 3.6: The breakdown of the convergence of the phase shift when not using the method of models for helium function H14. The scattering wavefunction contains both even and odd powers of r_{23}. The results for $k = 0.1$ are not plotted because the breakdown is so severe that they would distort the graph.

method for the same value of ω. but one does require the phase shifts in both cases to converge in a monotonic manner towards a best or exact value. As the results with the method of models are known to converge, one can assume that the phase shifts obtained with a high value of ω are very close to the exact results for the particular model being used. and they can be taken as reference values. The phase shifts obtained without the method of models are seen not to converge towards these reference values; they even seem to diverge, overshooting them by an amount which clearly indicates that there is a fundamental breakdown in the calculation. This phenomenon is not related to the presence of Schwartz singularities, as there is a smooth variation of η with k, i.e. there is no resonance type feature as found when a Schwartz singularity is encountered and, more importantly, the breakdown occurs when both the Kohn and the inverse Kohn methods are used. The fact that the breakdown is more pronounced for the lower energy region is probably due to the

importance of the polarization of the target in collisions with very slow incoming projectiles and also because the non-linear variational parameters in the trial function are better optimized for the lower energy region. This is an important feature, as it shows that the breakdown occurs because of a fundamental aspect of the trial wavefunction and not just because of the number of short range terms it contains. It has not been possible to determine exactly what this aspect is, but it is clear that the breakdown occurs with scattering wavefunctions which, when used with exact target functions (or when used with the method of models), give good results, and that it is more dramatic the better the scattering trial function becomes. One can therefore associate the breakdown in convergence of the final results with the quality of the scattering trial wavefunction, where quality is taken to describe how good the results obtained with the wavefunction would be in an ideal case with no breakdown. The quality of the wavefunctions we use in the Kohn calculation is determined by the optimization of the non linear parameters and by ω, which gives the number of short range correlation terms. The exclusion of odd powers of r_{23} in the scattering function makes the breakdown occur at higher values of ω, which indicates that these terms affect the quality of the scattering wavefunction in a much more important manner when the method of models is not used than when it is used.

The same analysis as the one presented above for model H14 was undertaken for model H5 and we have found that the results show a similar pattern as those for H14, but in a more dramatic way, i.e. that the breakdown occurs for very low values of ω when even and odd powers of r_{23} are included in the scattering trial function and also when only even powers are included (see figure 3.7).

This shows how the quality of the target function also affects the final results and highlights the limitation of both models H5 and H14 when used without the method of models. It is clear that no reliable data can be found with these helium wavefunctions using elaborate scattering trial functions without the method of models, and that it is not possible to use the convergence pattern, which is seen before the breakdown occurs, to extrapolate the results to infinite ω. As the variable r_{23}
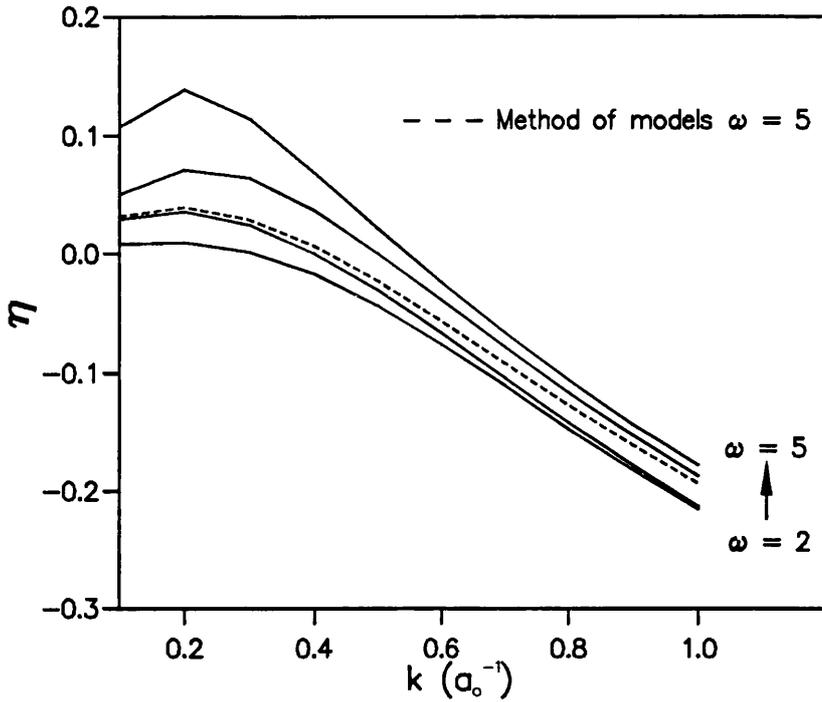
Figure 3.7: The breakdown of the convergence of the phase shift when not using the method of models with helium function H5. Only the results with r_{23} in the scattering wavefunction restricted to even powers are plotted.

will not be restricted in this work to have only even powers, we have created three new helium wavefunctions, H7, H22 and H50, containing even and odd powers of r_{23} (see table 3.2). Both the ground state energy and the polarizability of these two models are in much better agreement with the experimental data, which shows the importance of the linear electron-electron correlation terms in the helium target wavefunction. We have recalculated the phase shifts for these models with and without the method of models using the same two types of scattering wavefunctions as in the phase shifts calculations for model H5 and H14. The phase shifts evaluated with the method of models all increase monotonically with increasing ω and appear to converge. Therefore, we have chosen the results for model H22 with $\omega = 5$ (256 terms in Ψ_t) as our reference value.

This is because, although there is little difference with the same results for H14 and H7, the quality of the H22 helium wavefunction is such that we believe the phase

0.04

0.03

0.02

0.01

$\Delta\eta$ 0.0

-0.01

-0.02

-0.03

$\omega = 5$

$\omega = 2$

H14   H7   H22

$(\omega_{lb} = 4,$ even r_3) $(\omega_{lb} = 2)$ $(\omega_{lb} = 4)$
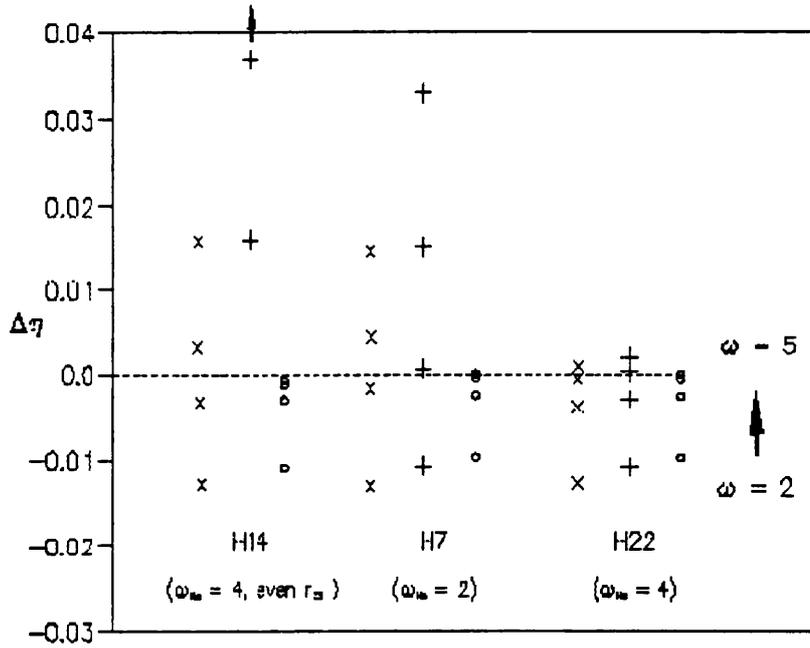
Figure 3.8: Differences between the most accurate s-wave phase shift at $k = 0.1a_0^{-1}$ for the helium function H22 ($\eta = 0.03246$) and the results for helium functions H7, H14, H22, obtained both with and without the method of models for $\omega = 2(1)5$: o, with the method of models and including both even and odd powers of r_{23} in the trial function :$\times$. without the method of models, and with only even powers of r_{23} in the trial function : +, without the method of models and with both even and odd powers of r_{23} in the trial function. (Note : for H14 the results for $\omega \geq 3$ are off scale)

shifts for H22 will be very close to the hypothetical exact ones. The results for H14, H7 and H22 for two positron energies are shown in figures 3.8 and 3.9 in which, for clarity, we have chosen to plot, for each value of k, the difference between a given result and the reference value of H22 with $\omega = 5$ (the dotted line). We have chosen to optimize the non-linear parameters in the trial function for the given value of k, so that the quality of the scattering function depends mainly on the value of ω. We can again notice in figure 3.8, for $k = 0.1$ (a_0^{-1}), that the inclusion of odd powers of r_{23} in the trial scattering function for the H14 calculation has provoked the breakdown at $\omega = 2$ while without the odd powers it occurred at $\omega = 4$. This highlights the

60

importance of the correlation between the target and the scattering wavefunctions, which is the main cause of the breakdown in convergence. The results for H7 also show a clear breakdown of the convergence pattern but it occurs at a higher value of ω than in the H14 case. The fact that the results for a given ω with and without odd powers of r_{23} in the scattering wavefunction are not as dramatically different as was the case for model H14, indicates that the inclusion of the odd powers of r_{23} in the target function makes it much more compatible with the more flexible scattering wavefunctions. The phase shifts calculated with the H22 target function show a clear convergence pattern for all types of scattering trial functions. The results obtained without the method of models up to $\omega = 4$ converge towards the best phase shift obtained with the same target function using the method of models. The $\omega = 5$ results are slightly more positive than the best result and they may be estimated to be just at the breakdown of the convergence pattern.

In figure 3.9 the s-wave phase shifts for a higher positron momentum ($k = 0.7(a_0^{-1})$) show a somewhat similar behaviour to that we have just discussed. The breakdown in convergence when using the H14 target function is again observed but it occurs at larger values of ω than was the case when $k = 0.1$ (a_0^{-1}). The results with only even powers of r_{23} in the scattering wavefunction, up to $\omega = 4$, could even be considered to converge monotonically to a slightly higher value than the most accurate one obtained with the H22 target function and with the method of models. For the helium models H7 and H22, without the method of models, one sees that there is a convergence pattern with increasing values of ω for both types of scattering wavefunctions. One can note that the results for H7 with the method of models, calculated only up to $\omega = 4$, are always a little more positive than those for H22. This is because the non-linear parameters in the scattering wavefunction are the same for all models, and they are seen to be slightly better optimized for H7 than for H22. Within the method of models there is no lower bound principle on the phase shift with respect to the target function used, as can be seen from the more positive phase shifts for model H1 than for model H5 found in the earlier work of Humberston (1973), and one must assume that the results obtained with the most accurate model will be the most reliable. Furthermore, the very small difference
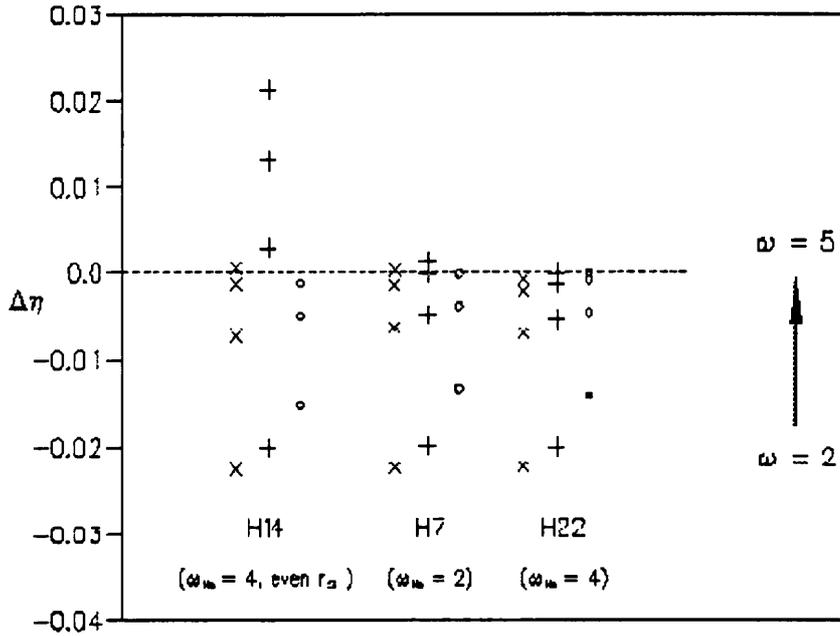
Figure 3.9: Similar to fig. 3.8 but at $k = 0.7a_0^{-1}$, where the most accurate phase shift for helium function H22 is $\eta = -0.08920$. (Note: for helium functions H14 and H7 with the method of models, the results are for $\omega = 2(1)4$ only)

between the values for $\omega = 4$ and $\omega = 5$ indicates that the latter is very close to the fully converged result. The phase shifts obtained with both types of scattering wavefunctions without the method of models for the H22 target function converge monotonically , and the $\omega = 5$ result with both even and odd powers of r_{23} in the trial function can be considered the most accurate phase shift calculated without using the method of models. The improvement in the quality of the convergence pattern, and in the case of H22 the total removal of the breakdown, is due to the fact that at higher positron energies the distortion of the target atom is much less important than at lower energies. This has been shown in earlier work on the scattering length, where the inclusion of polarization terms in the wavefunction was needed to improve the convergence of the results (Humberston 1973). As the incoming positron energy increases, the interaction time between the projectile and the target is reduced, and the helium atom does not have the time to be distorted as would have been the case if the positron were moving very slowly in its vicinity. Therefore, the positron can

be considered as distorting the target less for higher values of k than for lower ones, and this means that the correlation between the target function and the scattering wavefunction quality will be less important at the higher energies. This feature is important because it indicates that as no breakdown has occurred for H22 at $k = 0.7$ we can rely on the results obtained with the same model at higher energies. We have therefore taken model H22 as our standard model to investigate both the elastic scattering and the positronium formation cross sections at energies within the Ore gap. The results for H5 and H14 again highlight the relatively poor quality of these target functions as they do not agree at all with those for the more elaborate H22 helium function.

We have also investigated the effect of the use of inexact target functions in p-wave positron-helium elastic scattering and figure 3.10 shows the comparison of the p-wave phase shifts at $k = 0.8$ for all the models we have considered. We see that models H7,H22 and H50 all agree well and that model H5 does not give very good results. The relatively good quality of the H14 results can be explained by the fact that the scattering function used here contains only even powers of r_{23}.

The dependence on the target functions of the two channel results, which constitute the main interest of this work, has been investigated, but as the method of models cannot be used above the positronium formation threshold there is no accurate reference value as in the case of the phase shifts calculations. Also, there is no rigorous bound principle on the K matrix elements of a two channel variational calculation and therefore there are no bounds on the cross sections. Only the diagonal K matrix elements, K_{11} and K_{22}, obey an empirical lower bound principle and one may expect the variational elastic cross section, σ_{11}, to converge monotonically towards the exact value. Previous work on positron-hydrogen using the Kohn variational method (Brown and Humberston 1984) has shown that the positronium formation cross section is seen to converge in an oscillatory manner which makes extrapolation to $\omega = \infty$ very difficult. We have therefore chosen to examine the quality of our results not by considering their convergence with increasing values of ω towards a given value, but by comparing the most converged results for different
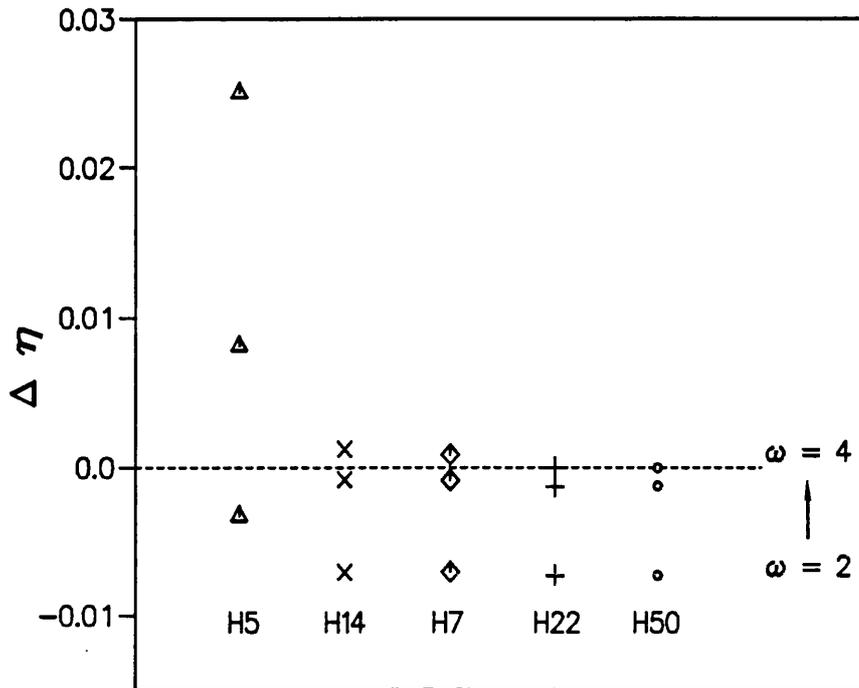
Figure 3.10: Differences between the most accurate p-wave phase shift at $k = 0.8a_0^{-1}$ for the helium function H22 ($\eta = 0.03246$) and the results for helium functions H5, H7, H14, H22, and H50 obtained without the method of models for $\omega = 2(1)4$ in both symmetries (see chapter 7). The power of r_{23} is even only in the scattering wave function.

models with each other.

In fig 3.11 we have plotted, in a similar manner as in the phase shift analysis, the s-wave elastic cross section, at a given energy above the positronium formation threshold, for 5 different models with the scattering trial function containing both even and odd powers of r_{23}, taking the H22 ($\omega = 5$) results as reference. One can see from the H7, H22 and H50 results that there is still a convergence pattern and that all $\omega = 5$ cross sections agree very well. We have included the H50 model as a check on our H22 results, because if these were in error this would show up immediately as a disagreement with the results for the more elaborate helium target function H50. As the helium target function needs to be evaluated and operated on within the six dimensional integration, the H50 calculations take much longer than those
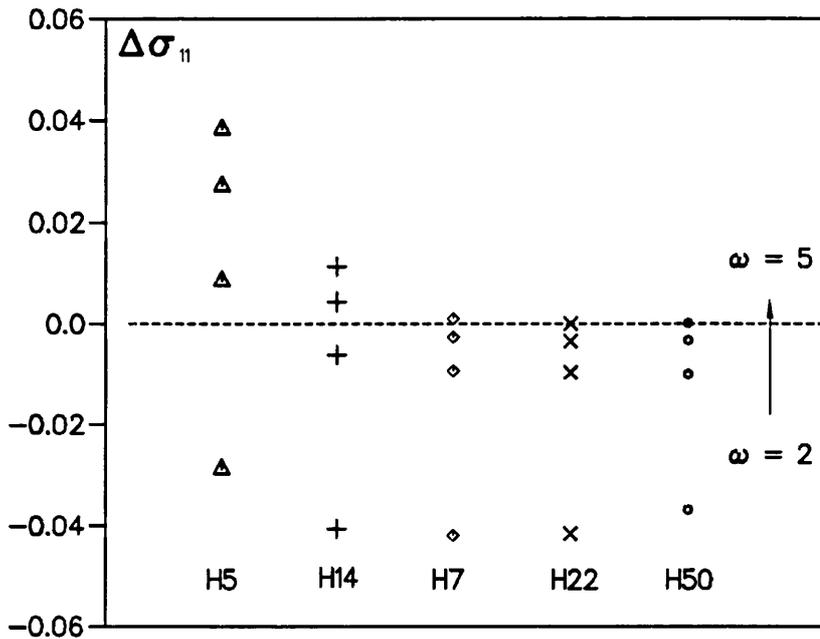
Figure 3.11: Differences between the most accurate s-wave elastic cross sections (in πa_0^2) at $k = 1.154 a_0^{-1}$ for the helium function H22 ($\sigma_{11} = 0.16070$) and the results for helium functions H5, H7, H14, H22,and H50 obtained without the method of models for $\omega = 2(1)5$

for model H22, and they could only be performed as a check on the H22 results for a few positron energies. The $\omega = 5$ cross sections for H5 and H14 are seen to disagree with those for the more accurate target functions and although there is not a breakdown as such in the convergence pattern, it is clear that the higher ω results do overshoot the exact cross sections.

The s-wave positronium formation cross sections are plotted in figure 3.12, and they show a similar behaviour. As expected, there is not as such a clear convergence pattern, even for models H7, H22 and H50, although here the cross sections increases monotonically with increasing ω. Again the $\omega = 5$ for all these models agree very well, and one can consider the cross sections for H22 to be very reliable.
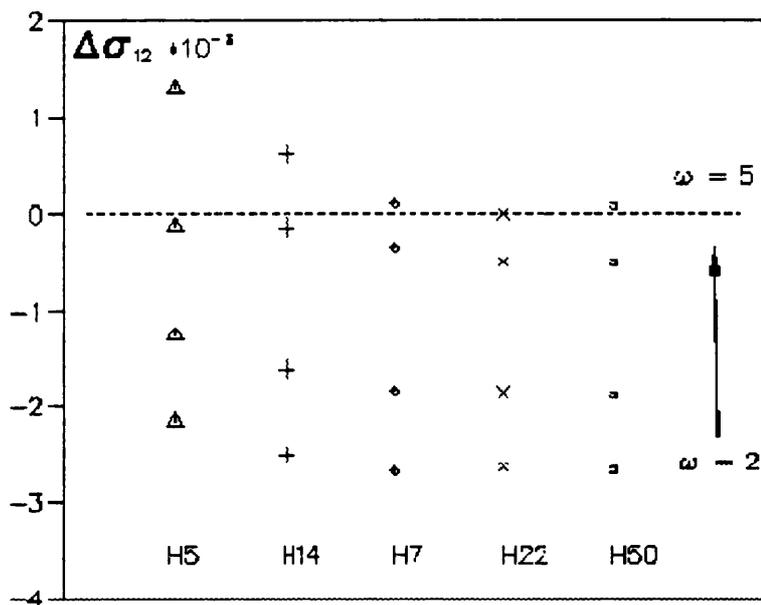
Figure 3.12: Differences between the most accurate s-wave positronium formation cross sections at $k = 1.154a_0^{-1}$ for the helium function H22 ($\sigma_{12} = 0.0037025$) and the results for helium functions H5, H7, H14, H22.and H50 obtained without the method of models for $\omega = 2(1)5$.

3.4 Conclusion

The analysis presented in this chapter clearly shows that the use of inexact target functions in a Kohn variational calculation, for both one and two channel cases, can lead to very erroneous results if the quality of the target function is relatively poor as compared with that of the scattering wavefunction. It was not possible within the scope of this work to investigate why this occurs. A detailed derivation of the scattering formulation and the Kohn variational method including the inexactness of the target wavefunction would have to be undertaken to know where the formulation breaks down and if a formal remedy can be found. A more empirical approach has been taken and it was found that reliable results could be obtained without the method of models if the helium model H22 was used and if the cross sections found agreed well with those for the more elaborate target function H50.

Chapter 4

Positron-helium s-wave scattering

4.1 Introduction

The partial wave analysis of the scattering process as described in chapter 2 requires us, in theory, to calculate the various cross sections we are investigating for an infinite number of partial waves. However, previous two channel variational calculations of positron-hydrogen scattering by Humberston (1982), and Brown and Humberston (1985) and of positron-lithium scattering by Watts and Humberston (1992), and the calculation of the phase shifts for positron-helium scattering (Campeanu and Humberston 1977), have shown that the main contributions to the total cross section at low positron energies ($\leq 20\epsilon V$) come from the first three partial waves (s,p,d). For higher partial waves ($l \geq 3$), the elastic scattering below the positronium formation threshold is dominated by the polarization potential $V_p = -\frac{\alpha}{2r^4}$, where α is the polarizability of the helium atom, and the phase shifts can then be calculated using the formula

$$\eta_l = \frac{\pi \alpha k^2}{(2l-1)(2l+1)(2l+3)} \tag{4.1}$$

given by O'Malley et al (1962). (Note that this formula also gives a good approximation for l=2 phase shifts.)

In the two channel case, the higher partial waves cross sections can be evaluated

quite accurately using the first Born approximation, as the increasing influence of the centrifugal term, $\frac{l(l+1)}{r^2}$, keeps the positron away from the region where the short-range correlation terms are effective. The use of these more approximate methods for the evaluation of the cross sections for partial waves higher than $l = 2$ is justified by their small contribution to the total cross sections.

Because we are not using the method of models in this work, as was done in the calculations cited above, various new numerical, computational and formal problems have occurred and these will be described in detail for s-wave only, on which the next two chapters will concentrate.

4.2 The s-wave trial function

The general form of the two channel trial function derived in chapter 2 is given by 2.88 and 2.89, and for s-wave calculation this becomes

$$
\begin{aligned}
\Psi_1 = {}& Y_{0,0}(\theta_1, \phi_1)\Phi_{He}(\boldsymbol{r_2}, \boldsymbol{r_3})\sqrt{k}\left\{j_0(kr_1) - K_{11}^t n_0(kr_1)\left[1 - \exp(-\lambda r_1)\right]\right\} \\
& - \frac{1}{\sqrt{2}}Y_{0,0}(\theta_\rho, \phi_\rho)\left[1 + P_{23}\right]\Phi_{Ps}(r_{12})\Phi_{He^+}(r_3) \\
& \times \sqrt{2\kappa}K_{21}^t\left\{n_0(\kappa\rho)\left[1 - \exp(-\mu\rho)(1 + \frac{\mu}{2}\rho)\right]\right\} \\
& + \left[1 + P_{23}\right]\exp\left(-(\alpha r_1 + \beta r_2 + \beta r_3)\right)\sum_{i=1}^{N} c_i r_1^{k_i} r_2^{l_i} r_{12}^{m_i} r_3^{n_i} r_{13}^{p_i} r_{23}^{q_i} \qquad (4.2)
\end{aligned}
$$

$$
\begin{aligned}
\Psi_2 = {}& \frac{1}{\sqrt{2}}Y_{0,0}(\theta_\rho, \phi_\rho)\left[1 + P_{23}\right]\Phi_{Ps}(r_{12})\Phi_{He^+}(r_3) \\
& \times \sqrt{2\kappa}\{j_0(\kappa\rho) - K_{22}^t n_0(\kappa\rho)\left[1 - \exp(-\mu\rho)(1 + \frac{\mu}{2}\rho)\right]\} \\
& - Y_{0,0}(\theta_1, \phi_1)\Phi_{He}(\boldsymbol{r_2}, \boldsymbol{r_3})\sqrt{k}K_{12}^t n_0(kr_1)\left[1 - \exp(-\lambda r_1)\right] \\
& + \left[1 + P_{23}\right]\exp\left(-(\alpha r_1 + \beta r_2 + \beta r_3)\right)\sum_{j=1}^{N} d_j r_1^{k_j} r_2^{l_j} r_{12}^{m_j} r_3^{n_j} r_{13}^{p_j} r_{23}^{q_j}, \qquad (4.3)
\end{aligned}
$$

where

$$
Y_{0,0}(\theta, \phi) = \frac{1}{\sqrt{4\pi}}. \qquad (4.4)
$$

We introduce the exchange operator P_{23}, which permutes the variable $\boldsymbol{r_2}$ into $\boldsymbol{r_3}$, but does not affect $\boldsymbol{r_1}$. The factor $\frac{1}{\sqrt{2}}$ ensures conservation of flux between channels

ω	1	2	3	4	5	6
N	5	18	50	120	256	502

Table 4.1: Relation between ω and the number of the short-range terms.

1 and 2. In the case of the short range terms we have chosen to absorb both the $\frac{1}{\sqrt{2}}$ factor and the spherical harmonic $Y_{0,0}(\theta, \phi) = 1/(\sqrt{4\pi})$ into the linear parameters c_i and d_j.

As explained in chapter 2, these short-range terms in the trial wavefunction represent the effect of the interaction between the projectile and the atom when the positron is close to the helium atom. Therefore, they will describe the distortion and the short-range polarization of the target in the elastic channel, and the polarization of the positronium atom and the helium formation in the positronium channel. The choice of the form for these correlation functions, i.e. Hylleraas functions, was dictated by the need to have flexible analytical functions which could be expanded in a systematic manner. This makes it then possible to investigate the convergence of the results with respect to the improvement of the trial wavefunctions by increasing the number of terms in the short range functions expansion. All terms with $k_i + l_i + m_i + n_i + p_i + q_i \leq \omega$ (these quantities being non-negative integers) are included in the summations of eqs 4.2 and 4.3. In order not to generate the same short range correlation term twice by the action of the exchange operator P_{23}, we must impose the constraints that $n_i \geq l_i$, but if $l_i = n_i$ then $p_i \geq m_i$. We have removed the constraint on q imposed in the calculation by Humberston (1973), Campeanu and Humberston (1975 & 1977) and Campeanu (1977), and in this work q_i can be either even or odd. The numerical consequence of this will be discussed in the next chapter. The relation between ω and the number of terms in the short-range expansion is given in table 4.1.

The long-range terms in the trial function correspond to the asymptotic forms discussed in chapter 2, and for s-wave scattering, the Bessel and Neumann functions

are

$$j_0(kr) = \frac{\sin(kr)}{kr} \qquad (4.5)$$

$$n_0(kr) = -\frac{\cos(kr)}{kr}. \qquad (4.6)$$

Also, at the origin we require the behaviour of the total wavefunction to be

$$\Psi \underset{r_1 \to 0}{\sim} r_1^l \qquad (4.7)$$

$$\Psi \underset{\rho \to 0}{\sim} \rho^l. \qquad (4.8)$$

As was indicated earlier, the Neumann function has a singularity at the origin, and a shielding factor, f_{sh}, needs to be introduced to remove it. The form of this function is arbitrary as long as it removes the singularity in $n_0(kr)$ and makes the total wavefunction finite as required by 4.7 and 4.8. We have chosen the shielding factor so that $n_0(kr)f_{sh}(kr)$ behaves as $j_0(kr)$ when $r \to 0$, i.e. the first few terms in the expansions around $x = 0$ are similar. This has given

$$f_{sh}(kr_1) = (1 - \exp(-\lambda r_1)) \qquad (4.9)$$

for the Neumann function , $n_0(kr_1)$, associated with channel one.

For $n_o(\kappa\rho)$, when $\rho \to 0$, the center of mass of the positronium atom lies at the origin. This imposes a second constraint:

$$\nabla^2_\rho \left(n_0(\kappa\rho) f_{sh}(\kappa\rho) \right) \underset{\rho \to 0}{\sim} \rho^l \qquad (4.10)$$

(see Brown 1986). We have taken

$$f_{sh}(\kappa\rho) = \left[1 - \exp(-\mu\rho)(1 + \frac{\mu\rho}{2}) \right], \qquad (4.11)$$

which ensures the correct behaviour at $\rho \to 0$, as can be seen by taking a Taylor expansion about $\rho = 0$. The choice of the non-linear parameters, λ and μ, will be discussed later, but the two main criteria are that the values of λ and μ make the shielding functions effective and optimize the final results.

We can now. using a notation similar to that in eqs. 2.91 to 2.93, write the long-range terms as

$$S_1 = Y_{0,0}(\theta_1.o_1)\Phi_{He}(\mathbf{r_2}.\mathbf{r_3})\sqrt{k}j_l(kr_1) \tag{4.12}$$

$$S_2 = Y_{0,0}(\theta_\rho.o_\rho)\Phi_{He^+}(\mathbf{r_3})\Phi_{ps}(\mathbf{r_{12}})\sqrt{2\kappa}j_l(\kappa\rho) \tag{4.13}$$

$$C_1 = -Y_{0,0}(\theta_1.o_1)\Phi_{He}(\mathbf{r_2},\mathbf{r_3})\sqrt{k}n_l(kr_1)\left[1-\exp(-\lambda r_1)\right] \tag{4.14}$$

$$C_2 = -Y_{0,0}(\theta_\rho.o_\rho)\Phi_{He^+}(\mathbf{r_3})\Phi_{ps}(\mathbf{r_{12}})\sqrt{2\kappa}n_l(\kappa\rho) \tag{4.15}$$

$$\times \left[1-\exp(-\mu\rho)(1+\frac{\mu}{2}\rho)\right].$$

The short range terms are written as

$$\phi_i = \exp\left(-(\alpha r_1+\beta r_2+\beta r_3)\right)r_1^{k_j}r_2^{l_j}r_{12}^{m_j}r_3^{n_j}r_{13}^{p_j}r_{23}^{q_j}. \tag{4.16}$$

We can therefore write the two component wavefunction including exchange as

$$\Psi_1^t = S_1+K_{11}^t C_1+K_{21}^t\frac{(1+P_{23})}{\sqrt{2}}C_2+\sum_{i=1}^{N}(1+P_{23})c_i\phi_i \tag{4.17}$$

$$\Psi_2^t = \frac{(1+P_{23})}{\sqrt{2}}S_2+K_{22}^t\frac{(1+P_{23})}{\sqrt{2}}C_2+K_{12}^t C_1+\sum_{j=1}^{N}(1+P_{23})d_j\phi_j. \tag{4.18}$$

In the next section we investigate the explicit form of the various matrix elements of $(\Psi^t, L\Psi^t)$.

4.3 The s-wave matrix elements

The matrix elements of $(\Psi^t, L\Psi^t)$ which appear in the matrices A and B (see equation 2.103) and their equivalent for the inverse Kohn formulation, can be divided into three sets. The first one contains all the matrix elements which involve only the long-range terms of the trial function. These are $(S_k, LS_l), (S_k, LC_l), (C_k, LS_l)$ and (C_k, LC_l) for $l, k = 1, 2$. The second set contains the elements which are the cross terms in $(\Psi^t, L\Psi^t)$ between the long-range terms and the short-range correlation terms. These are $(\phi_i, LS_k), (\phi_i, LC_k), (S_k, L\phi_i)$ and $(C_k, L\phi_i)$ for $i = 1, 2, \ldots, N$ and $k = 1, 2$. The matrix elements which involve only the short-range correlations terms, i.e. $(\phi_i, L\phi_j)$, form the third set. The formal and numerical evaluation of the matrix

elements is different for each set and will have to be done in a specific manner for each.

The number of elements of the long-range – long-range set which need to be evaluated can be reduced in a significant manner when considering the following relationships (see Appendix A):

$$(S_1, L\overline{S_2}) = (\overline{S_2}, LS_1)$$
$$(C_1, L\overline{S_2}) = (\overline{S_2}, LC_1)$$
$$(S_1, L\overline{C_2}) = (\overline{C_2}, LS_1)$$
$$(C_1, L\overline{C_2}) = (\overline{C_2}, LC_1) \tag{4.19}$$

and

$$(S_1, LC_1) = (C_1, LS_1) + 1$$
$$(\overline{S_2}, L\overline{C_2}) = (\overline{C_2}, L\overline{S_2}) + 1 \tag{4.20}$$

where $\overline{S_2} = \frac{(1+P_{23})}{\sqrt{2}} S_2$ and $\overline{C_2} = \frac{(1+P_{23})}{\sqrt{2}} C_2$.

The terms which involve only channel 1 functions are evaluated in a similar manner as that used in the purely elastic calculation of Campeanu (1977), except that we do not use the method of models and this introduces some fundamental differences.

For instance, for (S_1, LS_1) we have,

$$
\begin{aligned}
S_1 L S_1 &= \frac{1}{\sqrt{4\pi}} \Phi_{He}(\boldsymbol{r_2}, \boldsymbol{r_3}) \sqrt{k} \frac{\sin kr_1}{kr_1} \\
&\quad \left(-\nabla_{r_1}^2 - \nabla_{r_2}^2 - \nabla_{r_3}^2 + \frac{4}{r_1} - \frac{4}{r_2} - \frac{4}{r_3} - \frac{2}{r_{12}} - \frac{2}{r_{13}} + \frac{2}{r_{23}} - 2E_{He} - k^2 \right) \\
&\quad \times \frac{1}{\sqrt{4\pi}} \Phi_{He}(\boldsymbol{r_2}, \boldsymbol{r_3}) \sqrt{k} \frac{\sin kr_1}{kr_1}. \tag{4.21}
\end{aligned}
$$

If instead of using the method of models, we replace E_{He} by the expectation value of $\Phi_{He}(\boldsymbol{r_2}, \boldsymbol{r_3})$, we have

$$
S_1 L S_1 = \frac{1}{4\pi} \Phi_{He}^2(\boldsymbol{r_2}, \boldsymbol{r_3}) k \frac{\sin kr_1}{kr_1} \left(-\nabla_{r_1}^2 + \frac{4}{r_1} - \frac{2}{r_{12}} - \frac{2}{r_{13}} - k^2 \right) \frac{\sin kr_1}{kr_1} \tag{4.22}
$$

and as $\sin(kr_1)/(kr_1)$ is an eigenfunction of $-\nabla^2_{r_1}$, with eigenvalue k^2, equation 4.21 reduces to

$$S_1 L S_1 = \frac{1}{4\pi}\Phi^2_{He}(\boldsymbol{r_2},\boldsymbol{r_3})k\frac{\sin^2 kr_1}{k^2 r_1^2}\left(\frac{4}{r_1} - \frac{2}{r_{12}} - \frac{2}{r_{13}}\right). \qquad (4.23)$$

Similarly, we find

$$C_1 L S_1 = \frac{1}{4\pi}\Phi^2_{He}(\boldsymbol{r_2},\boldsymbol{r_3})k\frac{\sin kr_1}{kr_1}$$
$$\times \frac{\cos kr_1}{kr_1}\left(1 - e^{-\lambda r_1}\right)\left(\frac{4}{r_1} - \frac{2}{r_{12}} - \frac{2}{r_{13}}\right). \qquad (4.24)$$

For the element (S_1, LC_1) we use the relation $(S_1, LC_1) = (C_1, LS_1) + 1$. A similar analysis can be applied to LC_1, as $\cos(kr_1)/(kr_1)$ is also an eigenfunction of $-\nabla^2_{r_1}$, with eigenvalue k^2, but we need to take into account the action of $-\nabla^2_{r_1}$ on the shielding function. This leads to

$$C_1 L C_1 = \frac{1}{4\pi}\Phi^2_{He}(\boldsymbol{r_2},\boldsymbol{r_3})k\frac{\cos kr_1}{kr_1}\left(1 - e^{-\lambda r_1}\right)$$
$$\times \left[\frac{e^{-\lambda r_1}}{kr_1}\left(2k\lambda \sin kr_1 + \lambda^2 \cos kr_1\right)\right.$$
$$\left. + \left(\frac{4}{r_1} - \frac{2}{r_{12}} - \frac{2}{r_{13}}\right)\frac{\cos kr_1}{kr_1}\left(1 - e^{-\lambda r_1}\right)\right]. \qquad (4.25)$$

We now consider $L\overline{S}_2$, by first evaluating LS_2:

$$LS_2 = \left[-\frac{1}{2}\nabla^2_\rho - \nabla^2_{r_3} - 2\nabla^2_{r_{12}} + \frac{4}{r_1} - \frac{4}{r_2} - \frac{4}{r_3}\right.$$
$$\left. - \frac{2}{r_{12}} - \frac{2}{r_{13}} + \frac{2}{r_{23}} - 2E_{He^+} - 2E_{Ps} - \frac{\kappa^2}{2}\right]$$
$$\times \frac{1}{\sqrt{4\pi}}\Phi_{He^+}(r_3)\Phi_{Ps}(r_{12})\sqrt{2\kappa}\frac{\sin \kappa\rho}{\kappa\rho} \qquad (4.26)$$

Using the fact that $\Phi_{He^+}(r_3)$ and $\Phi_{Ps}(r_{12})$ are both eigenfunctions of H_{He^+} and H_{Ps} as given by eqs. 2.12 and 2.13 respectively, we have

$$LS_2 = \left[-\frac{1}{2}\nabla^2_\rho + \frac{4}{r_1} - \frac{4}{r_2} - \frac{2}{r_{13}} + \frac{2}{r_{23}} - \frac{\kappa^2}{2}\right]$$
$$\times \frac{1}{\sqrt{4\pi}}\Phi_{He^+}(r_3)\Phi_{Ps}(r_{12})\sqrt{2\kappa}\frac{\sin \kappa\rho}{\kappa\rho}. \qquad (4.27)$$

and since $\sin \kappa\rho/\kappa\rho$ is an eigenfunction of $-\frac{1}{2}\nabla^2_\rho$ with eigenvalue $\kappa^2/2$, we have

$$LS_2 = \left[\frac{4}{r_1} - \frac{4}{r_2} - \frac{2}{r_{13}} + \frac{2}{r_{23}}\right]S_2. \qquad (4.28)$$

We note here that the potential terms in the bracket in equation 4.28 are anti-symmetric with respect to the permutation of the labels 1 and 2, while the functions S_2 and C_2 are symmetric with respect to that permutation. Therefore, as was the case for positron-hydrogen calculations, we have

$$(S_2, LS_2) = (C_2, LS_2) = 0. \tag{4.29}$$

But because of exchange, we need to evaluate $(\overline{S}_2, L\overline{S}_2)$ and $(\overline{C}_2, L\overline{S}_2)$ which contain cross terms between S_2 or C_2 and $P_{23}S_2$ or $P_{23}C_2$, and are not symmetric with respect to the $1 \leftrightarrow 2$ permutation. Using the notation, $P_{23}S_2 = S_2'$ and $P_{23}C_2 = C_2'$, the same analysis can be made for the S_2' and the C_2' terms with respect to the $1 \leftrightarrow 3$ permutation, and we have

$$(\overline{S}_2, L\overline{S}_2) = (2S_2', \left[\frac{4}{r_1} - \frac{4}{r_2} - \frac{2}{r_{13}} + \frac{2}{r_{23}}\right] S_2), \tag{4.30}$$

$$(\overline{C}_2, L\overline{S}_2) = (2C_2', \left[\frac{4}{r_1} - \frac{4}{r_2} - \frac{2}{r_{13}} + \frac{2}{r_{23}}\right] S_2), \tag{4.31}$$

where we have used $(S_2', LS_2 = (S_2, LS_2')$ and $(C_2', LS_2) = (C_2, LS_2')$ which can be shown using the properties of the P_{23} operator.

The terms involving LC_2 are more complicated due to the presence of the shielding function, but a similar analysis to that for LS_2 yields:

$$
\begin{aligned}
LC_2 &= \frac{1}{\sqrt{4\pi}}\Phi_{He^+}(r_3)\Phi_{Ps}(r_{12})\sqrt{2\kappa} \\
&\quad \times \left[\frac{\kappa\mu}{2}e^{-\mu\rho}(1 + \mu\rho)\frac{\sin\kappa\rho}{\kappa\rho} + \frac{\mu^3\rho}{2}e^{-\mu\rho}\frac{\cos\kappa\rho}{\kappa\rho}\right. \\
&\quad \left. - \left(\frac{4}{r_1} - \frac{4}{r_2} - \frac{2}{r_{13}} + \frac{2}{r_{23}}\right)\frac{\cos\kappa\rho}{\kappa\rho}\left(1 - e^{-\mu\rho}(1 + \frac{\mu\rho}{2})\right)\right] \\
&\quad + \frac{1}{\sqrt{4\pi}}\Phi_{He^+}(r_2)\Phi_{Ps}(r_{13})\sqrt{2\kappa} \\
&\quad \times \left[\frac{\kappa\mu}{2}e^{-\mu\rho'}(1 + \mu\rho')\frac{\sin\kappa\rho'}{\kappa\rho'} + \frac{\mu^3\rho'}{2}e^{-\mu\rho'}\frac{\cos\kappa\rho'}{\kappa\rho'}\right. \\
&\quad \left. - \left(\frac{4}{r_1} - \frac{4}{r_3} - \frac{2}{r_{12}} + \frac{2}{r_{23}}\right)\frac{\cos\kappa\rho'}{\kappa\rho'}\left(1 - e^{-\mu\rho'}(1 + \frac{\mu\rho'}{2})\right)\right],
\end{aligned} \tag{4.32}
$$

where ρ' is defined in equation 2.2.

The matrix elements $(\overline{S}_2, L\overline{C}_2)$ and $(\overline{C}_2, L\overline{C}_2)$ can then be found by premultiplying equation 4.32 by $\overline{S}_2$ or $\overline{C}_2$. For the matrix elements involving both channel 1

and 2 long-range terms we use the symmetry relations from equation 4.19 and the results for $L\overline{S}_2$ and $L\overline{C}_2$ to evaluate $(S_1, L\overline{S}_2)$, $(S_1, L\overline{C}_2)$, $(C_1, L\overline{S}_2)$ and $(C_1, L\overline{C}_2)$. The reason for this is that, because these matrix elements involve the product of the target and fragment wavefunctions, $\Phi_{He}(\mathbf{r_2}, \mathbf{r_3})$ and $\Phi_{He^+}(\mathbf{r_3})\Phi_{Ps}(\mathbf{r_{12}})$, we cannot replace E_{He} by the expectation value of $\Phi_{He}(\mathbf{r_2}, \mathbf{r_3})$, and use equation 2.6 as before. It is therefore easier to operate with L on the channel 2 terms, as these contain fragment functions which are eigenfunctions of part of the operator L.

The same symmetry properties which we have used for the long-range – long-range matrix elements can also be applied to the long-range - short-range elements, to show that

$$
\begin{aligned}
(\phi_i, LS_k) &= (S_k, L\phi_i) \\
(\phi_i, LC_k) &= (C_k, L\phi_i)
\end{aligned}
\tag{4.33}
$$

for $i = 1, \ldots, N$ and $k = 1, 2$ (see appendix A). As will become clear when we discuss the short-range - short-range matrix elements, the evaluation of the matrix element with $L\phi_i$ will be much more complicated than that with L operating on a long-range term. For the $(\phi_i L, \overline{S}_2)$ and $(\phi_i L, \overline{C}_2)$ elements we can use the results derived above in eqs. 4.28 and 4.32. When evaluating (ϕ_i, LS_1) and (ϕ_i, LC_1), we need to introduce $H_{He}\Phi_{He}(\mathbf{r_2}, \mathbf{r_3})$ explicitly into the expression for LS_1 and LC_1, because we do not have the product form total wavefunction. This leads to extra terms in the LS_1 and LC_1 formulae which are of the form, for LS_1 for instance,

$$
\frac{1}{\sqrt{4\pi}}\sqrt{k}\frac{\sin kr_1}{kr_1}\left[-\nabla_{r_2}^2 - \nabla_{r_3}^2 - \frac{4}{r_2} - \frac{4}{r_3} + \frac{2}{r_{23}} - 2E_{He}\right]\Phi_{He}(\mathbf{r_2}, \mathbf{r_3}).
\tag{4.34}
$$

The explicit form for this expression is simular as that used in the Rayleigh-Ritz calculation of E_{He} as discussed in chapter 3.

The general form of a short-range - short-range matrix element is

$$
\begin{aligned}
(\overline{\phi}_i, L\overline{\phi}_j) = \int_\tau \overline{\phi}_i &\left[-\nabla_{r_1}^2 - \nabla_{r_2}^2 - \nabla_{r_3}^2 + \frac{4}{r_1} - \frac{4}{r_2} - \frac{4}{r_3} \right. \\
&\left. - \frac{2}{r_{12}} - \frac{2}{r_{13}} + \frac{2}{r_{23}} - 2E_{He} - k^2\right]\overline{\phi}_j d\tau
\end{aligned}
\tag{4.35}
$$

where $\overline{\phi}_i = (1 + P_{23})\phi = \phi + \phi'$. The ∇^2 operators will need to be expressed in terms of all the interparticle distances, which makes their form very complicated. But by

using integration by parts and the short-range nature of $\overline{\phi}$, we can write

$$\int_\tau \overline{\phi}_i \left[-\nabla_{r_1}^2 - \nabla_{r_2}^2 - \nabla_{r_3}^2\right] \overline{\phi}_j d\tau =$$
$$\int_\tau \left[\nabla_{r_1}\overline{\phi}_i . \nabla_{r_1}\overline{\phi}_j + \nabla_{r_2}\overline{\phi}_i . \nabla_{r_2}\overline{\phi}_j + \nabla_{r_3}\overline{\phi}_i . \nabla_{r_3}\overline{\phi}_j\right] d\tau, \quad (4.36)$$

which is more convenient as the expression for $\nabla\phi_i$ is much less complicated than that for $\nabla^2\phi_i$. And, therefore, we have

$$(\overline{\phi}_i, L\overline{\phi}_j) = \int_\tau \left\{\sum_{k=1}^3 \nabla_k\overline{\phi}_i . \nabla_k\overline{\phi}_j + \left[\frac{4}{r_1} - \frac{4}{r_2} - \frac{4}{r_3}\right.\right.$$
$$\left.\left. - \frac{2}{r_{12}} - \frac{2}{r_{13}} + \frac{2}{r_{23}} - 2E_{He} - k^2\right] \overline{\phi}_i\overline{\phi}_j\right\} d\tau \quad (4.37)$$

with

$$\sum_{k=1}^3 \nabla_k\overline{\phi}_i . \nabla_k\overline{\phi}_j =$$
$$\sum_{k=1}^3 \left[\nabla_k\phi_i . \nabla_k\phi_j + \nabla_k\phi_i . \nabla_k\phi'_j + \nabla_k\phi'_i . \nabla_k\phi_j + \nabla_k\phi'_i . \nabla_k\phi'_j\right]. \quad (4.38)$$

The short-range correlation terms are given as

$$\phi_i = \exp\left(-(\alpha r_1 + \beta r_2 + \beta r_3)\right) r_1^{k_j} r_2^{l_j} r_{12}^{m_j} r_3^{n_j} r_{13}^{p_j} r_{23}^{q_j} \quad (4.39)$$

and the explicit form for the first term on the RHS of 4.38 is

$$\sum_{k=1}^3 \nabla_k\phi_i . \nabla_k\phi_j = \phi_i\phi_j \left\{(\alpha^2 + 2\beta^2) - \frac{\alpha}{r_1}(k_i + k_j) - \frac{\beta}{r_2}(l_i + l_j) - \frac{\beta}{r_3}(n_i + n_j)\right.$$
$$+ \frac{k_i k_j}{r_1^2} + \frac{l_i l_j}{r_2^2} + \frac{n_i n_j}{r_3^2} + \frac{2m_i m_j}{r_{12}^2} + \frac{2p_i p_j}{r_{13}^2} + \frac{2q_i q_j}{r_{23}^2}$$
$$+ \frac{(r_1^2 + r_{12}^2 - r_2^2)}{2r_1^2 r_{12}^2} \left[-\alpha r_1(m_i + m_j) + (k_i m_j + k_j m_i)\right]$$
$$+ \frac{(r_1^2 + r_{13}^2 - r_3^2)}{2r_1^2 r_{13}^2} \left[-\alpha r_1(p_i + p_j) + (k_i p_j + k_j p_i)\right]$$
$$+ \frac{(r_2^2 + r_{12}^2 - r_1^2)}{2r_2^2 r_{12}^2} \left[-\beta r_2(m_i + m_j) + (l_i m_j + l_j m_i)\right]$$
$$+ \frac{(r_2^2 + r_{23}^2 - r_3^2)}{2r_2^2 r_{23}^2} \left[-\beta r_2(q_i + q_j) + (l_i q_j + l_j q_i)\right]$$
$$+ \frac{(r_3^2 + r_{23}^2 - r_2^2)}{2r_3^2 r_{23}^2} \left[-\beta r_3(q_i + q_j) + (n_i q_j + n_j q_i)\right]$$
$$+ \frac{(r_3^2 + r_{13}^2 - r_1^2)}{2r_3^2 r_{13}^2} \left[-\beta r_3(p_i + p_j) + (n_i p_j + n_j p_i)\right]$$
$$+ \frac{(r_{12}^2 + r_{13}^2 - r_{23}^2)}{2r_{12}^2 r_{13}^2} \left[m_i p_j + m_j p_i\right]\right\}. \quad (4.40)$$

For the other terms in 4.38, for which we use

$$\phi'_i = \exp\left(-(\alpha r_1 + \beta r_2 + \beta r_3)\right) r_1^{k'_j} r_2^{l'_j} r_{12}^{m'_j} r_3^{n'_j} r_{13}^{p'_j} r_{23}^{q'_j} \tag{4.41}$$

(with $k_i = k'_i, l_i = n'_i, m_i = p'_i, n_i = l'_i, p_i = m'_i$ and $q_i = q'_i$), we will have a similar results as in eq. 4.40.

Chapter 5

The computation of the matrix elements

5.1 The numerical integration of the matrix elements

The evaluation of the various matrix elements needed in the Kohn variational method involves an integration over the whole space of the problem (see figure 2.1). From the previous chapter it is obvious that, because of the complexity of the matrix elements, it will not be possible to evaluate the six dimensional integration analytically, and that we will have to resort to various numerical methods.

The position vectors of both electrons and of the positron span the whole space and we have

$$d\tau = d\boldsymbol{r}_1 d\boldsymbol{r}_2 d\boldsymbol{r}_3. \tag{5.1}$$

After integration over the three external Euler angles (see appendix B) we can write

$$d\tau = 8\pi^2 dr_1 r_2 dr_2 r_3 dr_3 r_{12} dr_{12} r_{13} dr_{13} d\phi_{23} \tag{5.2}$$

where ϕ_{23} is the angle between the planes of the triangles (r_1, r_2, r_{12}) and (r_1, r_3, r_{13}) (see figure 5.1).
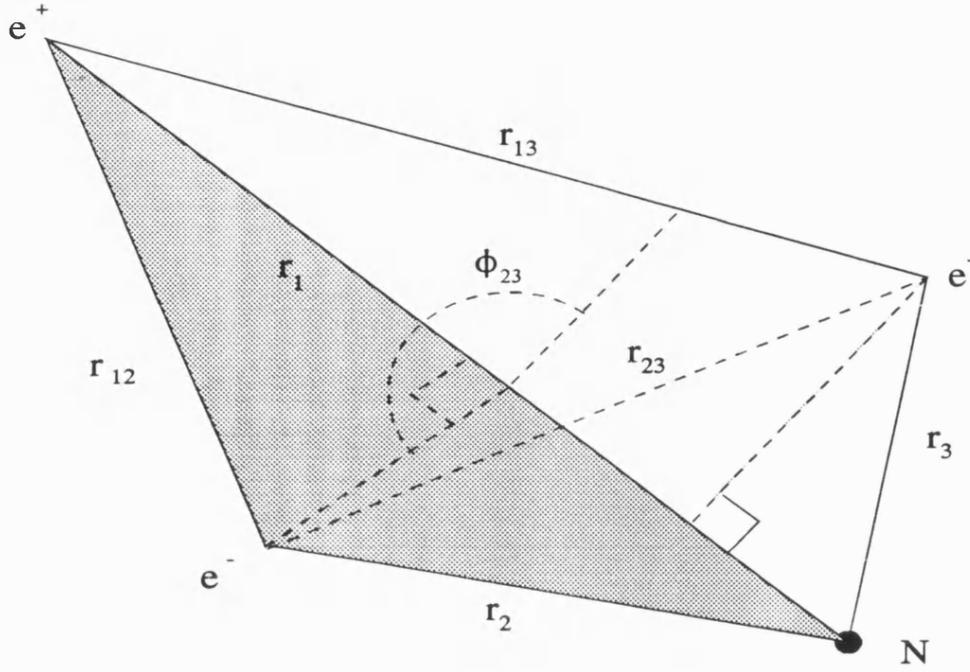
Figure 5.1: The positron-helium coordinate system and ϕ_{23}.

The angle ϕ_{23} is related to the variable r_{23} by

$$r_{23}^2 = r_2^2 + r_3^2 - 2r_2 r_3 \left[\sin\theta_{12} \sin\theta_{13} \cos\phi_{23} + \cos\theta_{12}\cos\theta_{13} \right] \qquad (5.3)$$

and can, therefore, be used for the r_{23} integration. In the work of Humberston (1973) and of Campeanu and Humberston (1977) the power of r_{23}, i.e. q, was restricted to be even only so that exact integration could be done over the variable ϕ_{23}. Indeed for even powers of r_{23}, the integrand for the ϕ_{23} integration will be of the form of a polynomial in $\cos\phi_{23}$, $D(\cos\phi_{23})$, which can be integrated numerically exactly using

$$\int_0^{2\pi} D(\cos\phi_{23})d\phi_{23} = \frac{2\pi}{n} \sum_{j=1}^{n} D\left[\cos\left(\frac{(2j-1)\pi}{2n} \right) \right]. \qquad (5.4)$$

This can be seen to be exact for a polynomial in $\cos\phi_{23}$ of degree $(2n - 1)$ or less. Because we have abandoned the method of models (and the product form of wavefunction), and instead will be using very elaborate target wavefunctions, the restriction on the powers of r_{23} needs to be lifted. This means that we do not expect to have exact numerical integration for the ϕ_{23} variable, but we have kept the same

numerical procedure, as in equation 5.4, increasing the number of points, n, until a sufficiently accurate result was obtained. The integration over ϕ_{23} is done within the integration over all the other variables, and this means that it is done at specific values of r_1, r_2, r_{12}, r_3 and r_{13}. Hence, the range of values of r_{23} is fixed between r_{23min} and r_{23max} by eq. 5.3 with $\phi_{23} = 0$ and $\phi_{23} = \pi$ respectively and

$$r_{23min}^2 = r_2^2 + r_3^2 - 2r_2r_3 \left[\sin\theta_{12}\sin\theta_{13} + \cos\theta_{12}\cos\theta_{12}\right] \tag{5.5}$$

$$r_{23max}^2 = r_2^2 + r_3^2 - 2r_2r_3 \left[-\sin\theta_{12}\sin\theta_{13} + \cos\theta_{12}\cos\theta_{12}\right].$$

When the ratio r_{23min}/r_{23max} is close to one, the variation of r_{23} with ϕ_{23} will be smooth and fewer integration points in the ϕ_{23} integration will be needed (see fig 5.2). On the other hand if the ratio is small , then r_{23} will be a more rapidly varying function of ϕ_{23} and we will need more integration points to achieve the required accuracy.
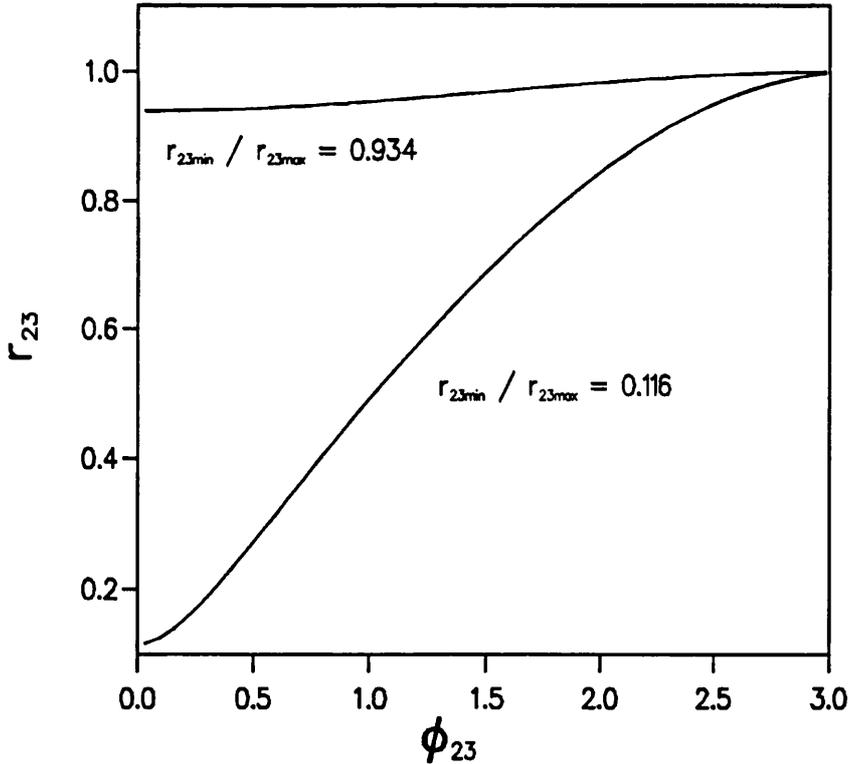

Figure 5.2: The variation of r_{23} as a function of ϕ_{23}.

Ideally one would then wish to find for various values of ratio r_{23min}/r_{23max} the

optimum number of integration points. The practical difficulty is that this would require within the innermost integration loop of the computer program a series of IF statement which would slow down the program dramatically. We have found that a significant gain in computer time could be achieved, while still obtaining accurate results, by considering only one value for the ratio, i.e. $r_{23min}/r_{23max} = 0.3$. For the ratio $r_{23min}/r_{23max} \leq 0.3$ we have taken a minimum of 15-25 integration points depending on the type of matrix element, and for ratio $r_{23min}/r_{23max} > 0.3$ between 6 and 8 points gave very good results for all matrix elements. A second drawback of the introduction of odd powers of r_{23} into the target and the trial wavefunction is that we do not have exact integration in the other variables anymore. Indeed from eq. 5.3 and noting that

$$\cos\theta_{ij} = \frac{r_i^2 + r_j^2 - r_{ij}^2}{2r_i r_j}, \tag{5.6}$$

we see that odd powers of r_{23} will introduce half integer powers of the other variables, which we will see makes their exact integration not possible. After having integrated over r_{23}, the integration which still needs to be done, in the case of a short-range - short-range matrix element, is

$$I = \int_0^\infty e^{-\alpha r_1} \int_0^\infty e^{-\beta r_2} \int_0^\infty e^{-\beta r_3} \int_{|r_1-r_2|}^{|r_1+r_2|} \int_{|r_1-r_3|}^{|r_1+r_3|} F(r_1, r_2, r_3, r_{12}, r_{13}) dr_1 dr_2 dr_3 dr_{12} dr_{13} \tag{5.7}$$

where F is a polynomial of finite degree for all variables only if we have previously integrated exactly over even powers of r_{23}. But even in this case, the limits of the r_{12} and r_{13} integration makes the integrand for r_2 and r_3 no longer a polynomial of finite degree. Humberston (Armour & Humberston 1979) has shown that this difficulty could be avoided by breaking up the integral I into several parts which could each be integrated exactly for even powers of r_{23}, but because we have not kept this restriction on the powers of r_{23} this method could no longer be used. We have kept the same integration quadratures as were used in the work of Campeanu and Humberston (1977), as they are very flexible and have achieved a good accuracy by increasing the number of integration points in each variable.

The integration over the variables r_1, r_2 and r_3 was done using the Gauss-

Laguerre quadrature,

$$\int_0^\infty e^{-x} f(x) dx = \sum_{i=1}^N w_i f(x_i), \tag{5.8}$$

where the weights and abscissae, w_i and x_i, can be calculated or found tabulated in books on numerical integration (Abramowitz & Stegun 1964). This method is exact if $f(x)$ is a polynomial of degree $n \leq 2N - 1$. For the integration over the r_{12} and r_{13} variables, as we do not have an exponential fall-off in these variables, we use the Gauss-Legendre quadrature

$$\int_a^b f(y) dy = \sum_{i=1}^N u_i f(y_i) \tag{5.9}$$

where u_i and y_i are the rescaled weights and abscissae obtained by mapping the range a to b onto the usual -1 to +1 range.

The limits of the integration of r_{12} and r_{13} will depend on the values of r_1, r_2 and r_3, and a similar analysis as that made for the r_{23} integration shows that for a given condition on the values of r_1, r_2 and r_3 the number of integration points can be greatly reduced and a very good accuracy achieved. The condition in this case is that $|r_1 - r_2|/(r_1 + r_2) \leq 0.3$ or $|r_1 - r_3|/(r_1 + r_3) \leq 0.3$. Also the presence of the modulus sign in the lower limits of the r_{12} and r_{13} integrations will create a significant problem in the r_2 and r_3 integrations and make accurate results impossible to achieve, if a single Gauss-Laguerre quadrature is used for these variables. To see how this comes about we can use the symmetry of the integrands in r_2 and r_3, and in r_{12} and r_{13}, and consider a form of integral with only r_1, r_2 and r_{12} variables. After the r_{23} integration we have an integral of the form

$$I_{12} = \int_0^\infty e^{-\alpha r_1} \int_0^\infty e^{-\beta r_2} \int_{|r_1-r_2|}^{|r_1+r_2|} f(r_1, r_2, r_{12},) dr_1 dr_2 dr_{12}. \tag{5.10}$$

Now the integrand for r_{12} will always be of the form r_{12}^n, so the r_{12} integration is simple and we have

$$I_2 = \int_0^\infty e^{-\alpha r_1} \int_0^\infty e^{-\beta r_2} \left[\frac{(r_1 + r_2)^{n+1}}{n+1} - \frac{|r_1 - r_2|^{n+1}}{n+1} \right] dr_1 dr_2. \tag{5.11}$$

But $|r_1 - r_2| = r_1 - r_2$ for $r_1 < r_2$ and $|r_1 - r_2| = r_2 - r_1$ for $r_2 < r_1$. Therefore I_2 will have different forms for $r_1 > r_2$ and for $r_2 > r_1$ if n is odd or half integer. For

instance, if $n = 0$, i.e. $f(r_1, r_2, r_{12}) = 1$ we have for $r_2 < r_1$

$$I_2 = 2 \int_0^\infty e^{-\alpha r_1} \int_0^\infty e^{-\beta r_2} r_2 dr_1 dr_2 \tag{5.12}$$

and for $r_2 > r_1$

$$I_2 = 2 \int_0^\infty e^{-\alpha r_1} \int_0^\infty e^{-\beta r_2} r_1 dr_1 dr_2 \tag{5.13}$$

Hence, the integrand for the r_2 integration has a discontinuity in its slope at $r_2 = r_1$, although it is continuous over the whole range of r_2. This gives rise to a cusp in the r_2 integrand (see figure 5.3) whose presence will prevent us from achieving accurate integration unless some alternative strategy is adopted.
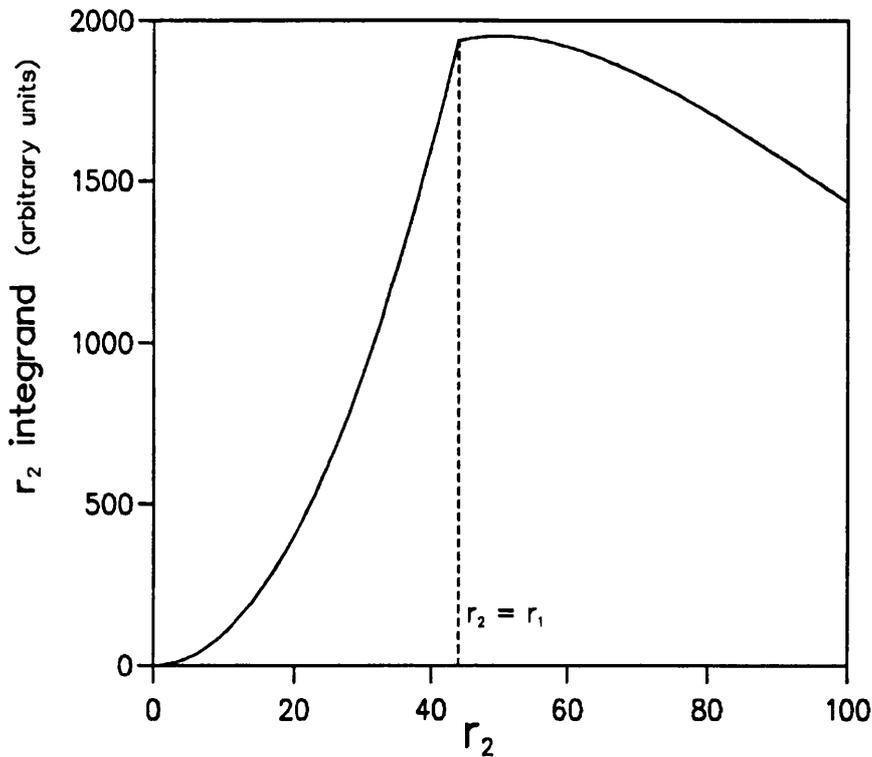

Figure 5.3: The cusp in the r_2 integrand.

The solution has been to split the r_2 integration at $r_2 = r_1$ using Gauss-Legendre quadrature for $r_2 < r_1$ and Gauss-Laguerre for $r_2 > r_1$. For large values of r_1, the exponential fall-off in r_2 will reduce the effect of the cusp and a single Gauss-Laguerre quadrature can be used over the whole range of r_2. By symmetry a similar analysis shows that the same method can be used for the r_3 integration.

The accuracy of the integration is very dependent on the type of matrix element one is considering. For instance the trigonometric functions in the long-range – long-range and long-range – short-range elements make exact integration impossible, but good accuracy can still be achieved with a reasonable number of integration points. The use of the Gauss-Laguerre quadrature is justified in these elements because there is in most of them an explicit or implicit exponential fall-off in r_1, r_2 and r_3. In the cases where no explicit exponential fall-off is present, we find that we can introduce it artificially by multiplying the integrand by $\exp(-Ar)\exp(Ar)$. This method was tested and found to give very good results over a wide range of values of A. Also, the use of helium target functions which contain odd powers of r_{23} makes exact integration over r_{12}, r_{13} and r_{23} not possible in the long-range - long-range and the long-range - short-range terms. For these matrix elements we have determined the number of integration points for each variable so as to achieve at least a 4-5 figure accuracy in each of them. We have also found that by reducing this accuracy significantly, i.e. having 30% to 50% less points in each variable, the final result was only affected to the order of one to two percent, and we are therefore confident to have achieved sufficient accuracy in our integration procedure. Furthermore, if we wished to achieve an accuracy of 6-7 figures in each elements, the increase in the number of integration points would be such that the time taken to compute the matrix elements would be much too long to make such a calculation feasible.

A significant gain in computer time can be achieved in the calculation of the short-range – short-range matrix elements by integrating separately the integrands with overall even powers of r_{23} and those with overall odd powers of r_{23} . As these matrix elements do not contain the target wavefunction, if we calculate the $2/r_{23}$ potential term separately, many matrix elements will contain only even powers of r_{23}, and therefore the r_{12}, r_{13} and r_{23} integrations can be done exactly using very few points. Table 5.1 gives the number of terms with only even or both even and odd powers of r_{23} in a short-range expansion for a given value of ω.

All short-range – short-range matrix elements which involve a product of two terms with even powers of r_{23} or those with both terms having odd powers of r_{23}

ω	1	2	3	4	5	6
n	5	18	50	120	256	502
n_{23}	4	14	30	84	172	330

Table 5.1: n:total number of short-range correlation terms in the trial function, n_{23}:number of terms with only even powers of r_{23}.

will have an overall even power of r_{23}. Also because $(\phi_i, L\phi_j) = (\phi_j, L\phi_i)$, we need to calculate only the upper or the lower triangle of the full $(\phi_i, L\phi_j)$ matrix. This means that the total number of elements that needs to be evaluated for $\omega = 6$ is $(502 \times 503)/2 = 126253$ and the total of "even type " matrix elements is $(330 \times 331)/2 + (172 \times 173)/2 = 69493$. Thus more than half of the short-range - short-range matrix elements can be evaluated exactly for the r_{12}, r_{13} and r_{23} integrations. This leads to a very significant gain in computer time, as typically one needs 3 to 4 times more points in each of these variables to achieve a reasonable accuracy in the inexact integrations than is required for exact integration.

As mentioned above, the evaluation of the $2/r_{23}$ potential term in the various matrix elements where it appears was done separately. The integration of an inverse power of r_{23} using the ϕ_{23} integration procedure and, in general, the integration of an inverse power in any variable, can never be done exactly, and a great number of integration points needs to be used to achieve reasonable accuracy. All potential terms other than $2/r_{23}$ could be easily integrated because of the implicit or explicit presence of at least a power one of the variables in the volume element which cancels out the inverse power. This is not the case for the $2/r_{23}$ term and a reasonable accuracy could only be achieved with a great number of points in all variables which is not required for the other terms in the matrix element. This problem can be overcome by noticing that the order in which one does the integration over the six variables is arbitrary. If we choose to take for instance the variable r_{12} as that to be integrated over first, and therefore integrate over the angle ϕ_{12}, i.e. the angle between the planes formed by the triangle r_1, r_3, r_{13} and r_2, r_3, r_{23}, then the volume

element $d\tau'$ is given by

$$d\tau' = 8\pi^2 r_1 dr_1 dr_2 r_3 dr_3 r_{23} dr_{23} r_{13} dr_{13} d\phi_{12} \qquad (5.14)$$

The potential term $2/r_{23}$ can now be integrated trivially on its own with very few points. We note that in this case, the terms with odd powers of r_{12} cannot be integrated exactly in the ϕ_{12} integration, but because of the restriction imposed by exchange on the various powers in the Hylleraas functions there will be fewer odd r_{12} type matrix elements than odd r_{23} elements. Also the change of the order of integration means there is no more a symmetry in r_2 and r_3 and, therefore, the cusp condition will change , giving a cusp in r_3 at $r_3 = r_1$ and in r_2 at $r_2 = r_3$.

5.2 The computer program

From the general formulation of the Kohn variational method developed in chapter 2 and from the specific form of the various matrix elements which need to be evaluated as given in chapter 4, it is clear that the main computational work in our calculations will be in the numerical evaluation of the different matrix elements. We have therefore broken up the general structure of the computer algorithm used for positron-hydrogen scattering (see Brown 1986) into three separate programs.

The first program calculates and stores the long-range - long-range and the short-range - long-range type of matrix elements, which are energy dependent. The second program evaluates the short-range - short-range elements, which are also energy dependent because of the $-k^2$ term in the operator L. But by calculating and storing the matrix elements $(\phi_i, L'\phi_j)$ and (ϕ_i, ϕ_j), where L' is the operator L without the $-k^2$ term, the energy dependence can be reintroduced trivially after the matrix evaluation using $(\phi_i, L\phi_j) = (\phi_i, L'\phi_j) - k^2(\phi_i, \phi_j)$. The third program reads in all the calculated matrix elements, reconstructs the $(\phi_i, L\phi_j)$ terms, builds up the matrices for equation 2.103, and evaluates the value of the linear parameters from which the optimized trial function, the variational K matrix elements and the cross sections can be calculated.

The first program contains two separate subroutines for the evaluation of the long-range – long-range and the short-range – long-range types of elements without the $2/r_{23}$ potential terms. These are referred to as subroutines SINGLE and COLUMN (see Brown 1986). Two similar SINGLE and COLUMN subroutines where the order of integration has been changed, as explained above, are then used for the evaluation of the $2/r_{23}$ potential term. In the second program, SQUARE, the short-range - short-range matrix elements are evaluated in the same manner with the $2/r_{23}$ potential term done separately. In this program, we only need to evaluate the upper or lower triangle of the $(\phi_i, L\phi_j)$ matrix, as by symmetry we have $(\phi_i, L\phi_j) = (\phi_j, L\phi_i)$, and this reduces the number of these types of element which need to be evaluated for a matrix of dimension N from N^2 to $N(N+1)/2$, i.e by nearly 50 percent. A flow chart of the computer program is given in figure 5.4. The subroutines CONST and CONSTHEL create the powers of the various variables in the short-range terms and in the helium target function respectively. The RMAT subroutine solves the set of non-linear equations (see equation 2.103) and calculates the cross sections.

The general structure of the matrix elements evaluation subroutines is that of six nested loops corresponding to the six dimensional integrations. One extra loop is added in the COLUMN subroutines to create the (ϕ_i, LS) and (ϕ_i, LC) types of terms, and the matrix elements $(\phi_i, L\phi_j)$ are created in two extra loops within the most inner integration loop in the SQUARE program. The length of each integration loop can be varied depending on the type of matrix element and also on the complexity of the integrand within the specific loop, for instance the presence of the cusp or the value of ratio r_{23} as explained above. Because of the symmetry in the r_2 and the r_3 variables, we can choose to integrate over only half the (r_2, r_3) space. Therefore, the r_3 integration loop needs to go up to the value of the r_2 loop if the order of integration is $r_1, r_2, r_3, \ldots$. This reduces the computation time by 50% but it cannot be used in the subroutines where the $2/r_{23}$ potential term is evaluated as the new order of integration gives rise to a volume element which is not symmetric in r_2 and r_3.
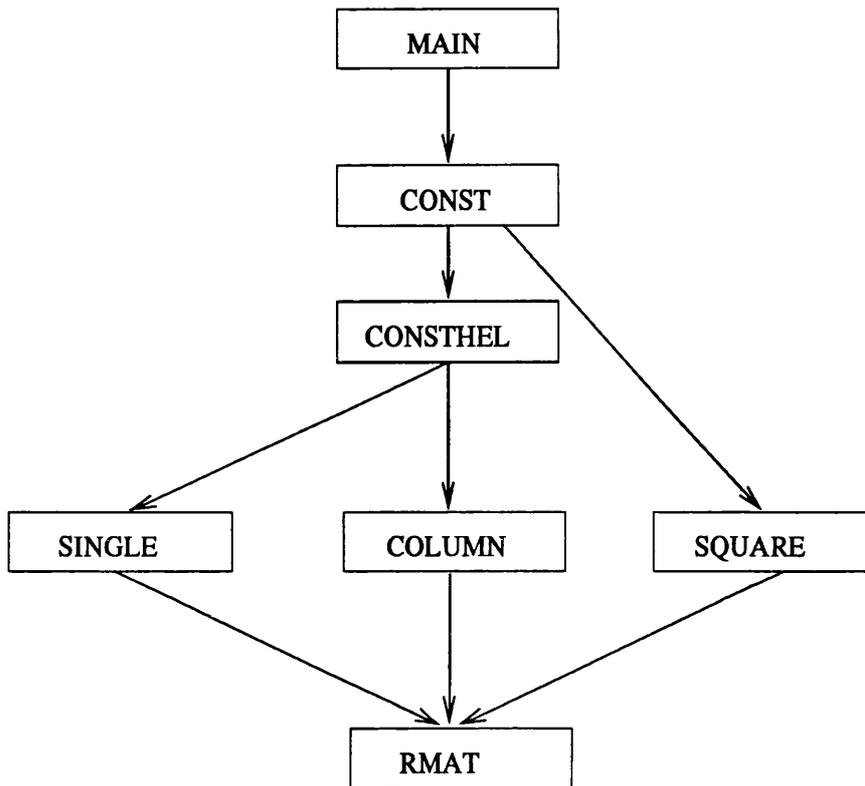
Figure 5.4: Flow chart of the computer program.

The evaluation of the weights and abscissae for the Gauss-Laguerre and the Gauss-Legendre quadratures was done using two subroutines written explicitly into the program. The main difference between the computational effort in this work and that for positron-hydrogen scattering (Brown 1986) and positron-lithium scattering (Watts 1994) is the increase of the computational time due to the six dimensional integration. This increase can be estimated by multiplying out the number of points for the r_{12}, r_{13} and r_{23} integration loops considering that the numbers used in the r_1, r_2 and r_3 are similar to those used in the hydrogen case. We find that if we have an integrand in r_{12}, r_{13} and r_{23} which can be integrated easily, the increase in time is of the order of $2^3 = 8$. But for more complex integrands we could readily have a factor $20^3 = 8000$. Fortunately, because of the various methods we have developed to deal with the r_{12}, r_{13} and r_{23} integrations, i.e. the ratio conditions explained above, the average increase is much more manageable and for the SQUARE program we have a factor 200. The actual time for the evaluation of an s-wave $(\phi_i, L\phi_j)$ matrix, for

$\omega = 5$ (256 terms), was of the order of 150 hours on a Digital DEC 300 workstation. The increase in computational time has meant that the various programs needed to be written in a very efficient manner but at the same time we have taken care to make them as readable as possible, so that they could be understood relatively easily by an outsider.

The SQUARE program is, by its nature, the one which is the most time consuming even though it is only run once for all energies. We have developed an algorithm for the s-wave calculation which makes it possible to reduce the time taken by SQUARE by a factor 2 to 3, but this has made the structure of the program much more complicated.

In this new method we use the relation

$$\int \phi_k \phi_m d\tau = \int \phi_l \phi_n d\tau \qquad (5.15)$$

even if $k \neq l$ and $m \neq n$, provided that the sum of the powers of each variable is the same in each case. For instance, for a one variable function we have

$$\int r^{p_k} r^{p_m} dr = \int r^{p_l} r^{p_n} dr, \qquad (5.16)$$

if $p_k + p_m = p_l + p_n$. Therefore, we find that when we integrate the matrix elements (ϕ_i, ϕ_j), for $i, j = 1, \ldots, N$, many elements will be exactly the same and need to be evaluated only once. Also, equation 4.40 can be written in a different form, as a sum of products of (ϕ_i, ϕ_j) type terms multipied by a polynomial function, $F(r_1, r_2, r_3, r_{12}, r_{13}, r_{23})$ which is independent of i and j, and a constant coefficient which depends only on i and j. As the polynomial is independent of i and j, we know that if 2 matrix elements, (ϕ_i, ϕ_j) and (ϕ_k, ϕ_l), are indentical the same will be true for the elements $(\phi_i, \phi_j)F(r_1, r_2, r_3, r_{12}, r_{13}, r_{23})$ and $(\phi_k, \phi_l)F(r_1, r_2, r_3, r_{12}, r_{13}, r_{23})$. So that, although no two elements of the upper triangle of the $(\phi_i, L\phi_j)$ matrix are identical, each of them is made up of various terms which are identical for different values of i and j. The integration structure of the program is the same as before, but now in the most inner loop various (ϕ_i, ϕ_j) and $(\phi_i, \phi_j)F(r_1, r_2, r_3, r_{12}, r_{13}, r_{23})$ types of terms are evaluated at specific values of i and j. The complete $(\phi_i, L\phi_j)$ matrix elements are rebuilt after the integration is done in a new set of loops which

ω	2	3	4	5	6
n_1	171	1275	7260	32896	126253
n_2	116	485	1561	4106	9468
n_3	133	653	2293	6414	15395

Table 5.2: n_1:total number of terms in upper triangle of $(\phi_i, L\phi_j)$ matrix, n_2:number of (ϕ_i, ϕ_j) terms which need to be evaluated, n_3:number of $(\phi_i, P_{23}\phi_j)$ terms which need to be evaluated.

run over all the values of i and j. To find which (ϕ_i, ϕ_j) matrix elements are identical we can use the prime number relation

$$1^{A_1} 3^{A_2} 5^{A_3} 7^{A_4} 11^{A_5} 13^{A_6} = 1^{B_1} 3^{B_2} 5^{B_3} 7^{B_4} 11^{B_5} 13^{B_6}, \qquad (5.17)$$

if, and only if, $A_1 = B_1, A_2 = B_2, \ldots$, etc. Table 5.2 shows how many (ϕ_i, ϕ_j) and $(\phi_i, P_{23}\phi_j)$ matrix elements need to be evaluated as compared to the total number of elements in the upper triangle of the $(\phi_i, L\phi_j)$ matrix for a given value of ω. As expected, the probability of matrix elements being identical increases as ω increases and, therefore, this technique becomes more efficient for high values of ω. This method has given a gain in computer time but, because the (ϕ_i, ϕ_j) and $(\phi_i, P_{23}\phi_j)$ types of terms need to be evaluated separately and the operations within the most inner integration loop are now much more complicated, the gain in computer time is not simply proportional to the reduction of matrix elements which need to be evaluated as given in table 5.2.

We have also rewritten the SQUARE program so that it could be run on the parallel supercomputer Intel iPSC/860 at the Daresbury Laboratory. Because of the loop structure of the program we have been able to implement the changes to our program in a straightforward manner as a first test. The main structure of our parallel program is the use of one node (i.e. one processor) to create the various parameters needed to evaluate the (ϕ_i, ϕ_j) and $(\phi_i, L\phi_j)$ matrix elements (i.e. the value of the powers for each i and j, the weights and abscissae, etc ...) and to send these parameters to the other nodes where the matrix elements are evaluated. On

the parallel computer at Daresbury, one must request a number of nodes equal to powers of 2 (i.e. 2,4,8,16,32,64(max)). Therefore, if 16 nodes have been requested we can use 15 to evaluate the matrix elements and the gain in time will come from the fact that each processor must only calculate a 15th of the full matrix. We have found that each processor on the Intel iPSC/860 is slower than the workstation we have used before, and we estimate the gain in computer time to be of a factor 4 when 15 nodes are used.

We have only adapted the 'old' SQUARE program to the parallel architecture and have not yet fully optimized it, for instance the first node could also be used to calculate the matrix elements. Also we believe that the transformation of the new method of evaluation of the $(\phi_i, L\phi_j)$ matrix will lead to a much greater gain in computational time.

Chapter 6

s-wave positron-helium scattering results

6.1 Introduction

Having established in chapter 4 the s-wave scattering wavefunction and the form of the matrix elements which need to be evaluated when using the Kohn variational method, we can now calculate, with the numerical techniques described in chapter 5, the variational K matrix and both the elastic scattering and positronium formation cross sections for s-wave positron-helium scattering.

Before any information can be inferred about the cross sections, the quality of the calculation must be considered. As described in chapter 2, when flexible trial functions (i.e. with high ω, see equation 2.87) are used, a reasonably good agreement between the Kohn and inverse Kohn results for all the K matrix elements is a necessary, but not a sufficient, condition which needs to be satisfied to ensure an accurate result. Also the monotonic convergence of the diagonal K matrix elements is an important feature of the Kohn method and any results which do not satisfy the empirical lower bound on the K_{11} and the K_{22} matrix elements must be treated with some suspicion. Furthermore, by investigating the energy region around the

threshold for positronium formation we will know if our variational results are consistent with the threshold behaviour of σ_{11} and σ_{12} predicted by Wigner's threshold theory. Therefore, before presenting and analyzing the results for the cross sections, we will investigate these various aspects of our calculations.

However, prior to undertaking a full variational calculation, i.e. an evaluation of the linear parameters for a large value of ω, we need to find the optimum values of the non-linear parameters in the trial wavefunction and this is the subject of the next section.

6.2   The choice of the non-linear parameters

The optimization of the non-linear parameters in the trial wavefunction is a very important first step in any variational calculation, because only when this is achieved in a satisfactory manner can the variational principle work efficiently. For instance, a clear convergence pattern of the diagonal K matrix elements with respect to increasing values of ω and a smaller probability of Schwartz singularities occurring, can only be obtained if the non-linear parameters have been correctly optimized.

In this work the optimized values of the non-linear parameters α, β, λ and μ in equations 4.2 and 4.3 are not determined by the variational principle itself but by a trial and error method. This method relies on the empirical lower bound on the diagonal K matrix elements. A small calculation (for instance $\omega = 3$) is repeated with a trial function in which the value of the non-linear parameter we wish to optimize is varied. The results for K_{11} and K_{22} are then analysed and the value of the non-linear parameter which gives rise to the most positive values of K_{11} and K_{22} is taken as the optimum value. The difficulty with this procedure is that the choice of non-linear parameters giving rise to the most positive value of K_{11} is unlikely to give the most positive value of K_{22}. This can be understood by considering the physical interpretation of the non-linear parameters. There are two types of these non-linear parameters, first λ and μ which are contained in the shielding functions

of $n_0(kr_1)$ and $n_0(\kappa\rho)$. and secondly α and β which control the exponential fall-off of the short-range terms. The values of λ and μ will determine the region over which the Neuman functions are effective. A shielding factor with too small a value of these non-linear parameters will cut off the C_1 and C_2 types of function too far from the origin (see figure 6.1 curve C) and, therefore, there will be a region of space in which the short-range terms will have to try and represent these asymptotic type functions.
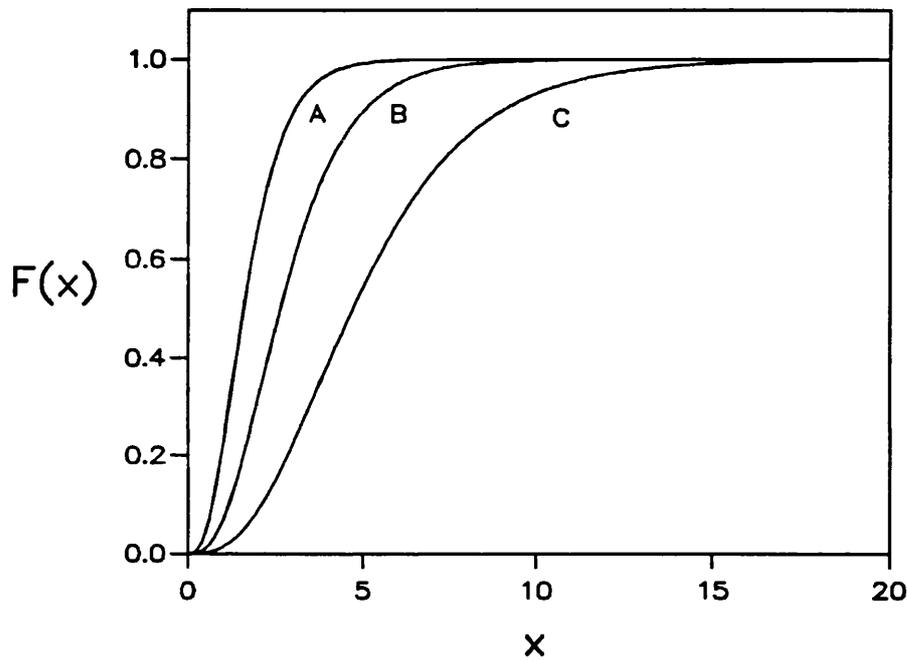
Figure 6.1: Variation of the shielding function $F(x) = (1 - \exp(-\mu x)(1 + 0.5\mu x))^3$ with respect to x. Curve A: $\mu = 1.5$; curve B: $\mu = 0.9$; curve C: $\mu = 0.5$.

The difficulty in this case is that the short-range terms are not well suited to represent this type of function and this will lead to less positive values of K_{11} and K_{22}. If λ and μ are too large (curve A in figure 6.1), then the shielding factor will become more effective close to the origin in a very rapid manner. This will lead to a very abrupt variation of the C type terms in the trial function close to the origin and would correspond to rapidly varying kinetic energy in this region, which is not a correct representation of the system under consideration. This is particularly so for the C_2 terms, which depend on ρ, as this variable relates to the center of mass

94

of the positronium atom and there is therefore no particile at the position $\rho = 0$. The choice of the values of α and β will determine the range over which the short-range terms are effective. Although the $\mathbf{K}$ matrix formulation implies the coupling of all the possible channels, one can loosely associate the K_{11} matrix element with e^+- He elastic scattering and K_{22} with Ps - He$^+$ elastic scattering. These are two very different processes; a point like particle, the positron, scattering on a relatively tightly bound He atom in one case and a very diffuse positronium atom scattering on a very tightly bound He$^+$ ion in the other. It is therefore clear that the optimization of α and β. which are closely related to how diffuse the e^+- He system is, that gives the most positive value of K_{11} is unlikely to give the most positive value for K_{22}. We have chosen the values of α and β which give the most positive value of K_{11} because it was recognized from the start of our investigations that the s-wave elastic scattering cross section would be a major component of the total elastic scattering cross section. while the s-wave positronium formation cross section was not expected to contribute much to the total positronium formation cross section in the Ore gap. It was therefore decided that the s-wave elastic scattering cross section should be calculated with the best accuracy (i.e. the best convergence) possible, to reduce the error in the total cross section.

The calculation to find the optimized value for a given non-linear parameter was undertaken with the other non-linear parameters not having their optimized values (for instance for the optimization of μ, the other non-linear parameters α, β and λ had the same values as in the trial function for elastic scattering below the positronium formation threshold). Once an optimized value was found in this manner for all the non-linear parameters, the calculation for each one was repeated with the other parameters now having there optimized values, to verify if the optimization was still correct. The results of this optimization procedure are presented in figure 6.2 to 6.6. Before analysing the results one must bear in mind that these calculations were done with a relatively low value of ω and therefore recognise that when a full calculation is done, the values of K_{11} and K_{22} will be less sensitive to the value of the non-linear parameter (for instance a maximum type of feature will flatten out in a similar manner as the minimum features in the bound state calculation did

when ω was increased (see figure 3.4)). Also, as discussed in chapter 2, we know that Schwartz singularities will become much narrower as ω increases and accurate results will be easier to infer.

In figure 6.2. we show the variation of K_{11} and K_{22} with respect to λ. One sees that there is a maximum in the K_{11} curve where both the Kohn and the inverse Kohn results are identical. The K_{22} curve shows very little variation with λ and a systematic difference between the Kohn and inverse Kohn results. The value of $\lambda = 0.75$ was taken because it is in the region of the maximum of the K_{11} curve and is identical to that found when optimizing for the s-wave phase shift below the positronium formation threshold. Figures 6.3 and 6.4 show the variation of K_{11} and K_{22} with respect to μ at two different energies (one close to the positronium formation threshold and another in the higher energy range of the Ore gap). Again, the optimum value is not the same for K_{11} and K_{22}, and one can see that it will not be the same for all energies. Although the best value at $k = 1.204(a.u)$ for the K_{11} curve is at $\mu = 0.6$. the fractional difference is very small and will become even smaller for higher values of ω, so we have chosen $\mu = 0.9$ as a compromise value.

The variation of K_{11} and K_{22} with respect to α shows in a more dramatic way the difficulty in optimizing the non-linear parameters. In figure 6.5 we see that there is a clear maximum in the K_{11} curve, but not in the K_{22} curve which contains many Schwartz singularities making the analysis even more complicated. We have chosen $\alpha = 1.05$ as the optimum value for α as this gives the most positive value for K_{11} and lies in a region where K_{22}. although far from its most positive value, does not vary very much and is not affected too dramatically by Schwartz singularities. In figure 6.6 a similar pattern can be seen in the variations of the diagonal K matrix elements with respect to β and the optimum value was taken to be $\beta = 1.6$, for the same reasons as indicated in the α optimization.

This analysis of the optimization of the non-linear parameters highlights the difficulty in obtaining a trial function perfectly optimized for all possible channels, but we believe the compromise set of values we have chosen, $\lambda = 0.75$, $\mu = 0.9$, $\alpha = 1.05$ and $\beta = 1.6$ gives reliable and accurate results.
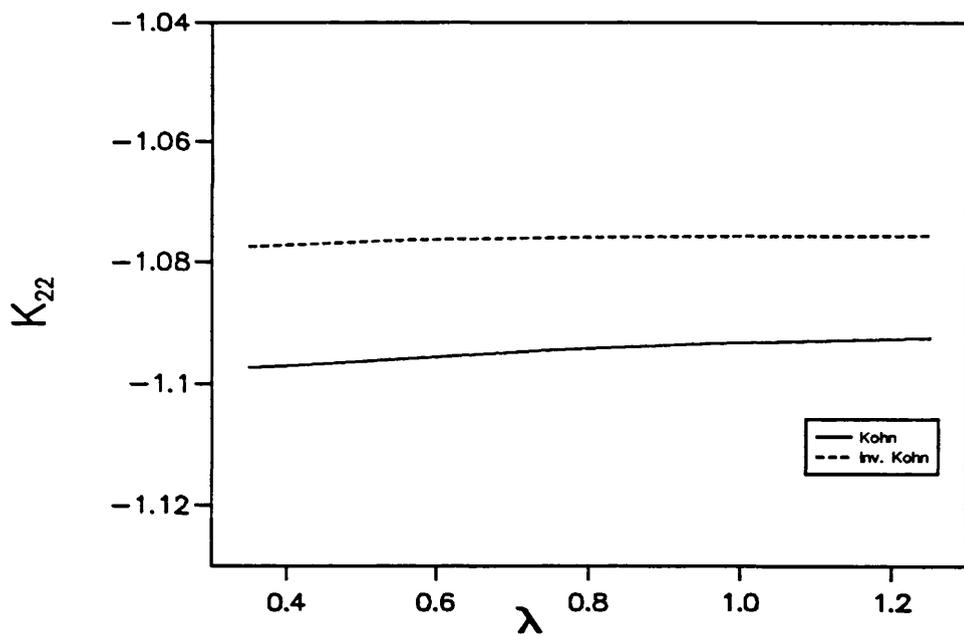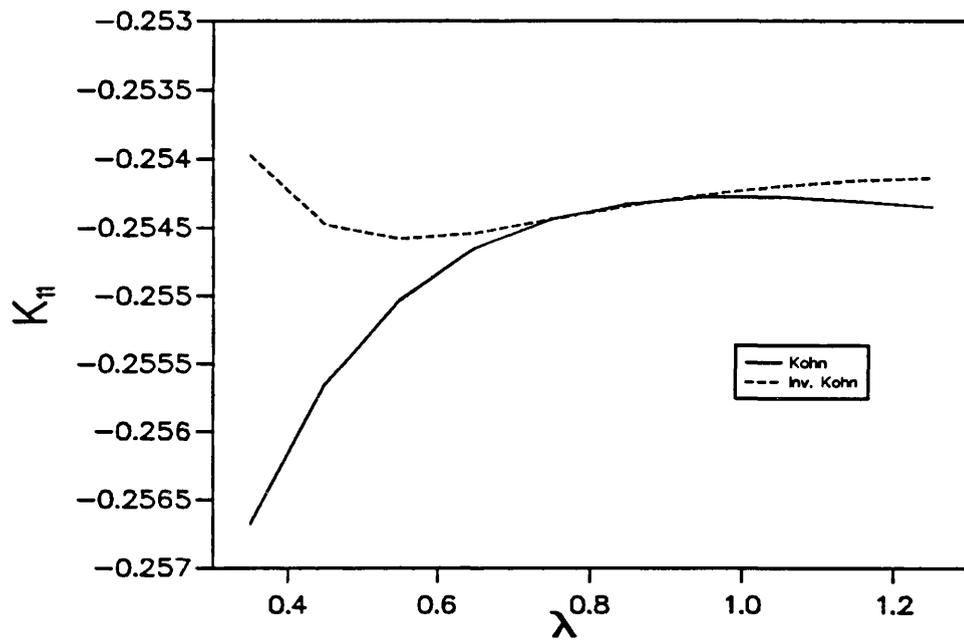
Figure 6.2: The variation of the K matrix elements K_{11} and K_{22} with λ for s-wave scattering at k= 1.169 (a.u.) and ω=3.
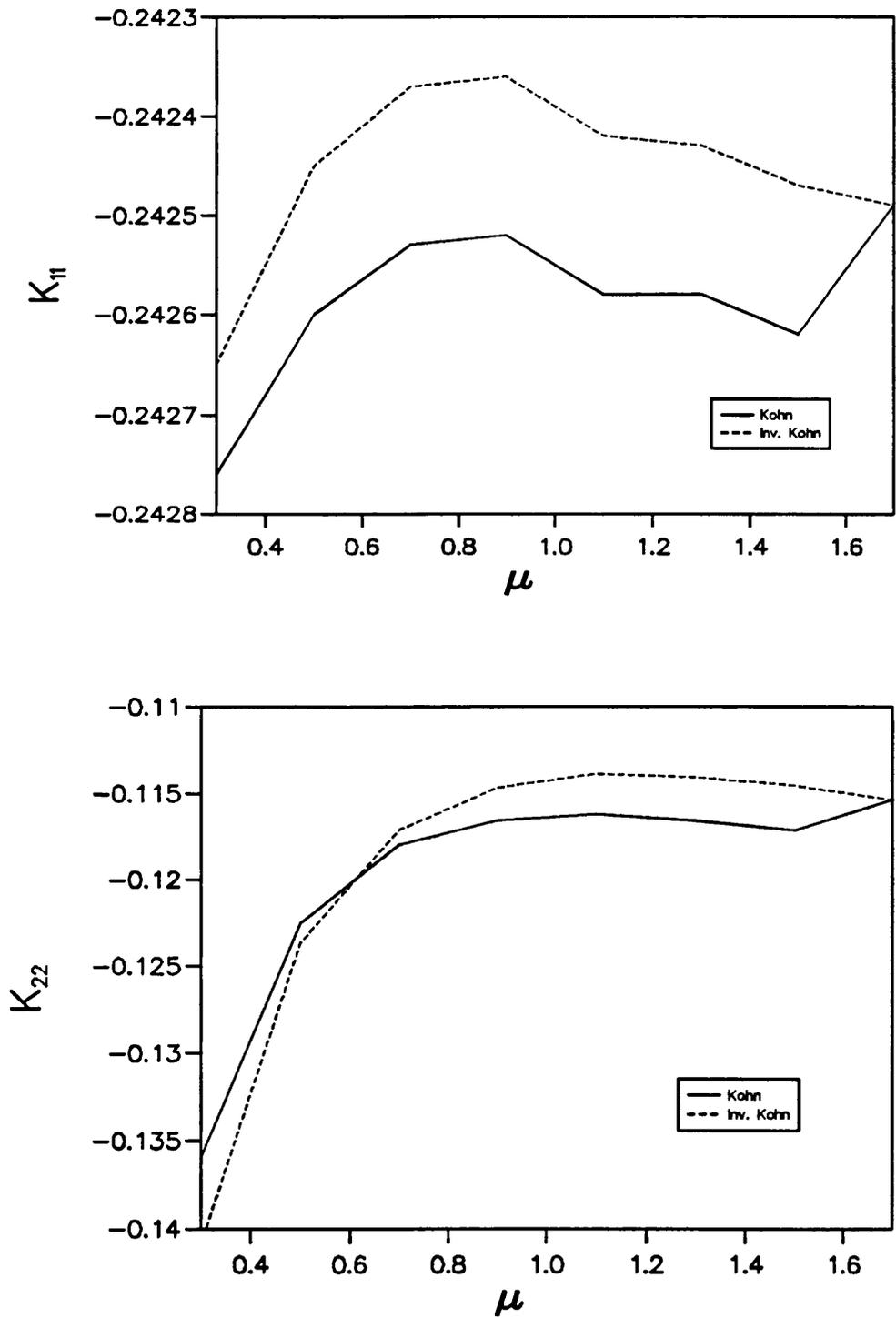
Figure 6.3: The variation of the K matrix elements K_{11} and K_{22} with μ for s-wave scattering at k= 1.144 (a.u) and ω=3.
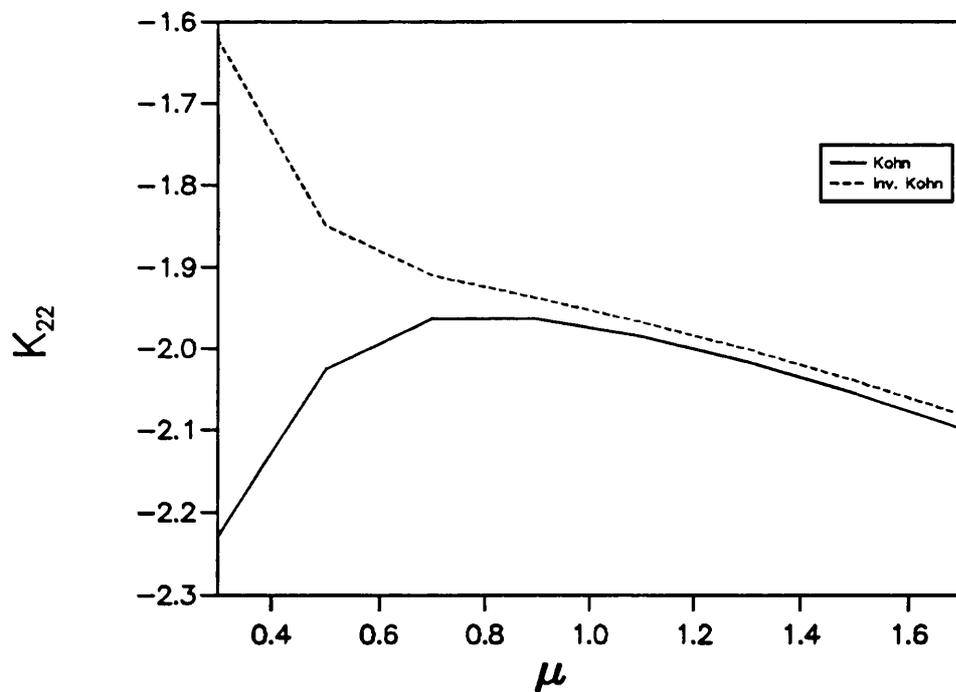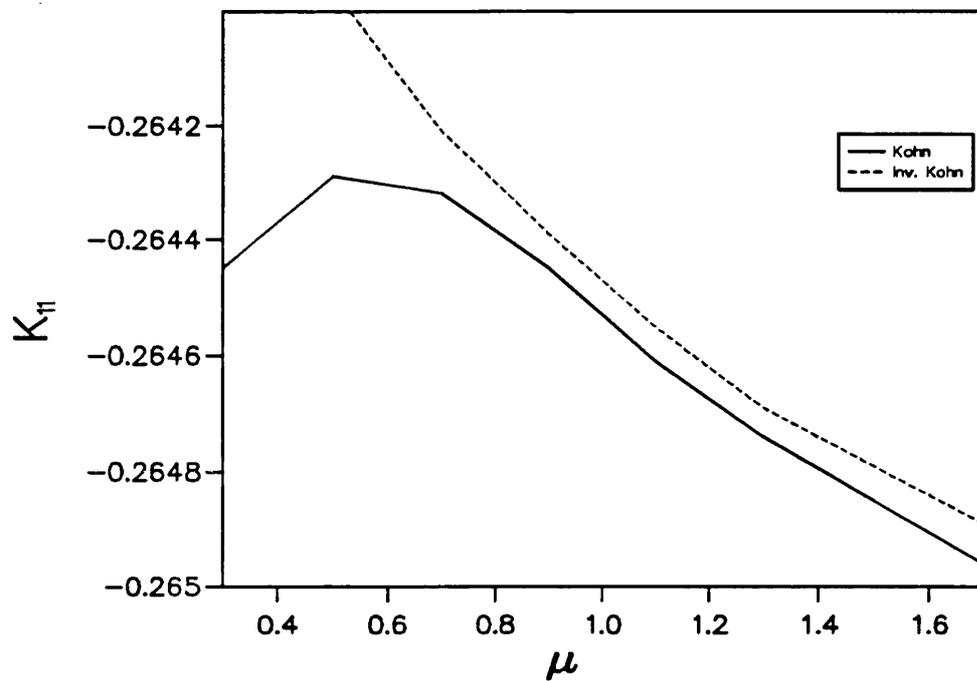
Figure 6.4: The variation of the K matrix elements K_{11} and K_{22} with μ for s-wave scattering at k= 1.204 (a.u) and ω=3.
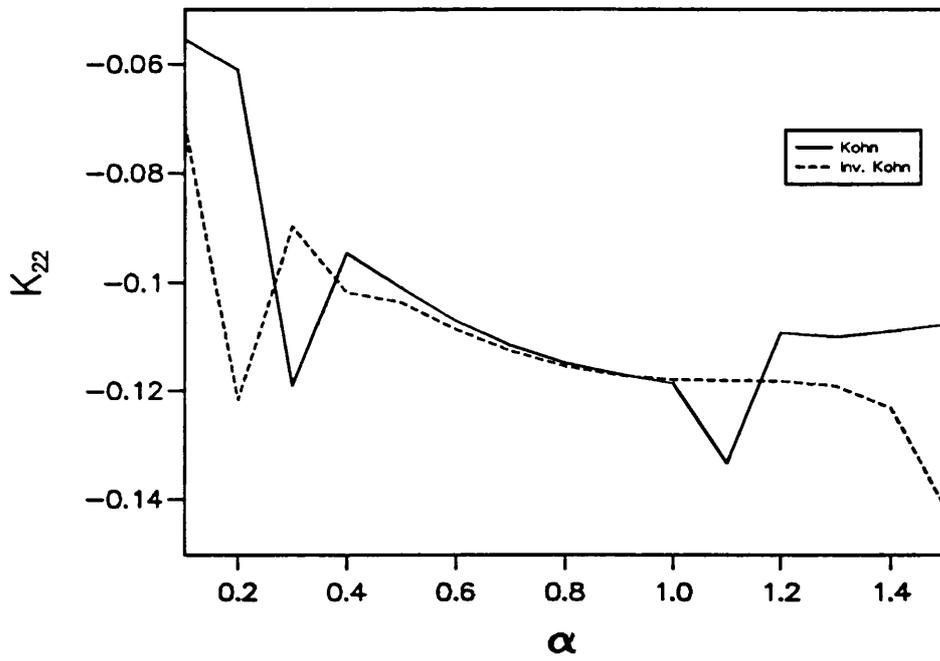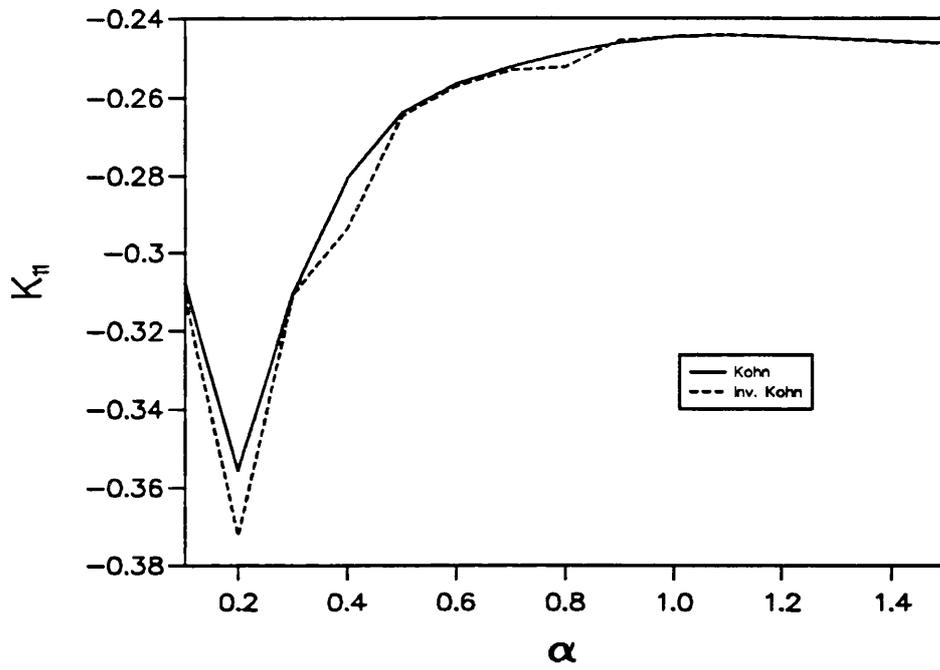
Figure 6.5: The variation of the K matrix elements K_{11} and K_{22} with α for s-wave scattering at k= 1.169 (a.u.) and ω=3.

100
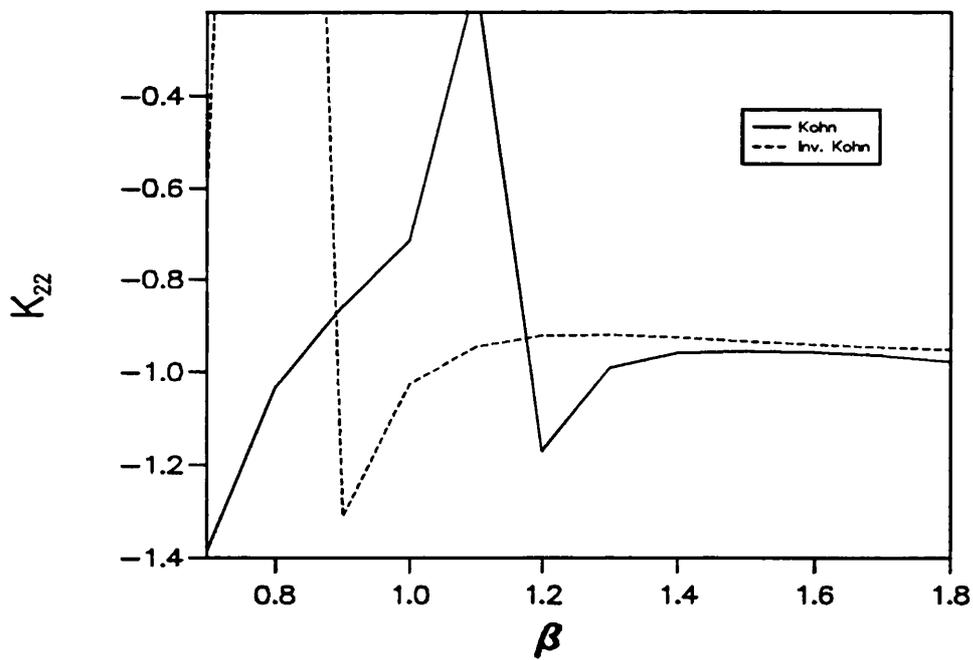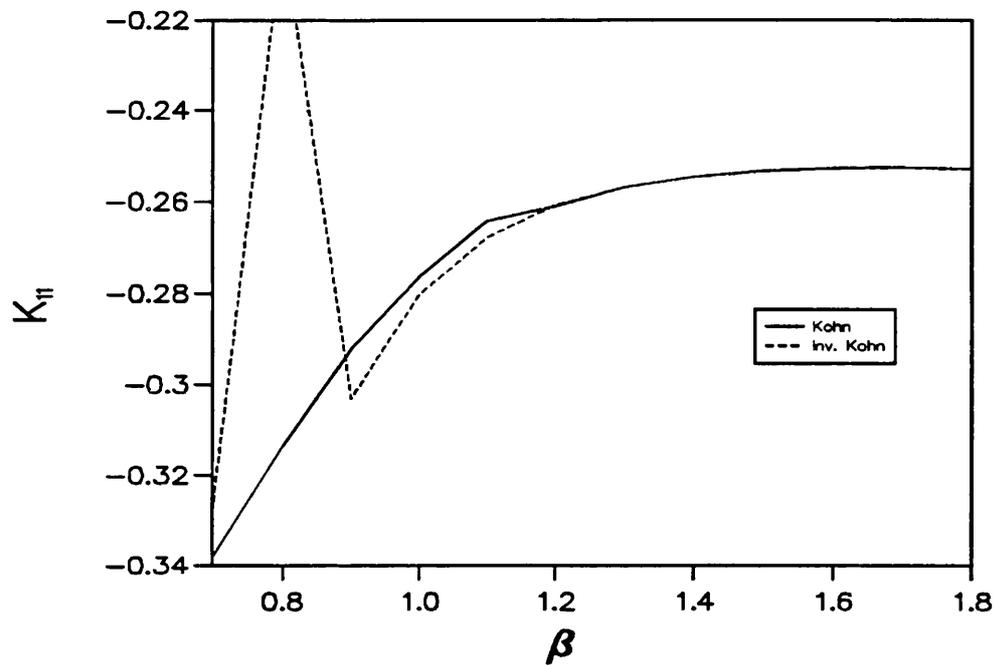
Figure 6.6: The variation of the K matrix elements K_{11} and K_{22} with β for s-wave scattering at k= 1.169 (a.u) and ω=3.

6.3 The convergence of the diagonal K matrix elements

As mentioned in the previous section and in chapter 3, there is no rigorous bound on the variational values of the K matrix elements, contrary to the case in a Raleigh-Ritz calculation of the ground state energy. The only bound that exists in a two channel variational calculation is an empirical one on the diagonal K matrix elements. This pseudo-bound translates into a monotonic convergence pattern for K_{11} and K_{22} with respect to increasing values of ω, which makes extrapolation to infinite ω possible. This is shown in figure 6.7 where we have plotted K_{11} versus k, for energies within the Ore gap, for $\omega = 2(1)6$. The monotonic convergence is very clear and is seen to hold for all energies.
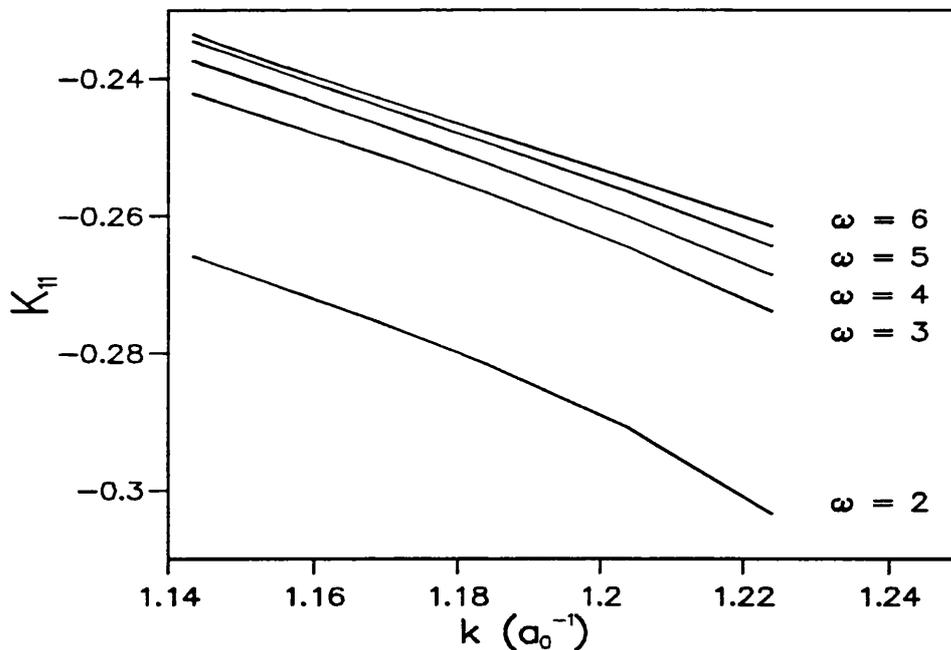
Figure 6.7: The convergence with respect to ω of the K matrix element K_{11} for s-wave positron-helium scattering plotted as a function of the positron wavenumber k.
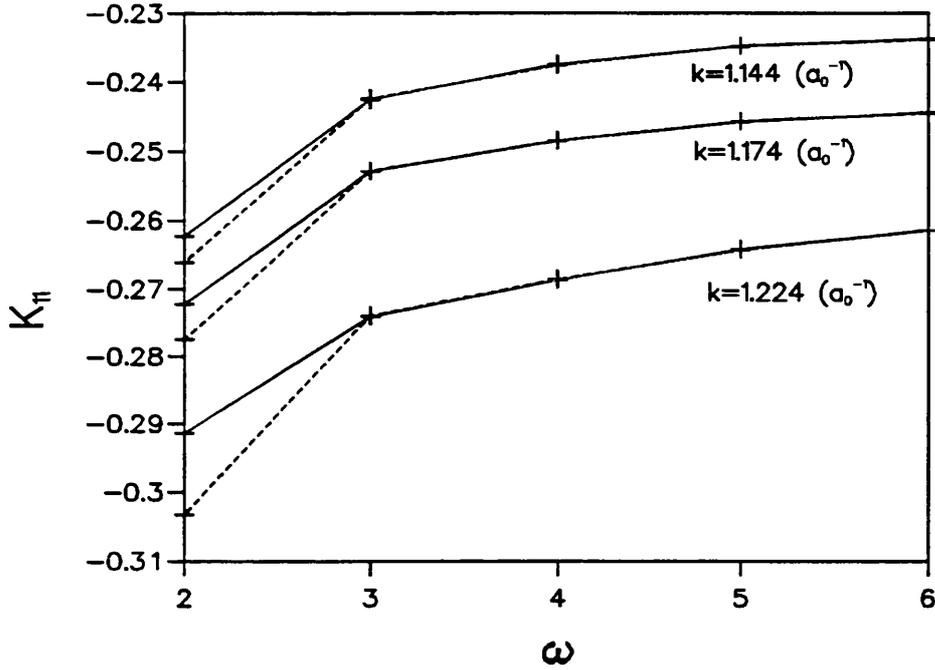
Figure 6.8: The convergence with respect to ω of the K matrix element K_{11} for s-wave positron-helium scattering. The solid and dashed lines correspond to the Kohn and inverse Kohn results respectively.

In figure 6.8 we have plotted the convergence of K_{11} with respect to ω for only 3 energies, and a rapid rise for low ω and small increase for large ω can be noticed. The extrapolation to infinite ω. i.e. the closest to an exact result one could get, can be obtained by using the extrapolation formula

$$K_{11}(\omega) = K_{11}(\omega = \infty) + \frac{D}{\omega^n} \tag{6.1}$$

where D and n are fitting parameters. A more empirical method has been used in this work: we have plotted K_{11} versus $1/\omega^n$ and varied n until all points lie on a straight line (see figure 6.9). The value of $K_{11}(\omega = \infty)$ is then the intercept of this line with the y axis. Because of the complexity of the positron-helium calculation we have not been able to go to as high values of ω as was done in the positron-hydrogen case (Watts 1994). Therefore, the extrapolation procedure is less precise and the uncertainty in the value of $K_{11}(\omega = \infty)$ is greater. Also, this procedure can only be used for K_{11} and K_{22}, and as the cross sections depend on all K matrix elements,

103
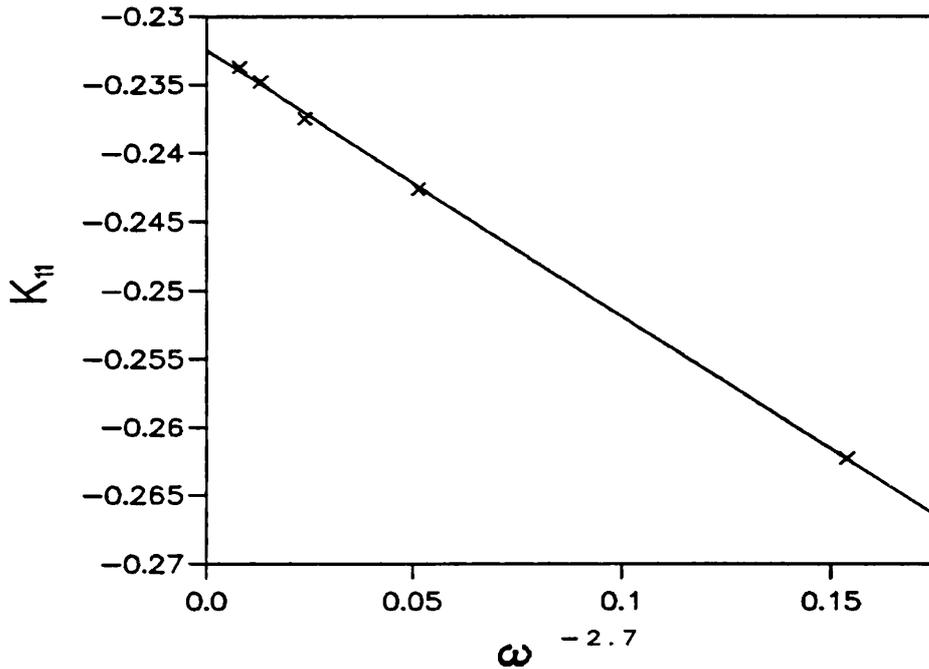
Figure 6.9: The convergence with respect to ω of the $\boldsymbol{K}$ matrix element K_{11} for s-wave positron-helium scattering according to equation 6.1. This is Kohn result for k=1.144 (a.u).

it is not possible to find extrapolated values for σ_{11} and σ_{12}.

In figure 6.10 we have plotted K_{22} versus κ, the positronium wavenumber, for $\omega = 2(1)6$. In this case K_{22} increases monotonically with ω, but convergence is only apparent at the higher energies. As explained in the previous section, the choice of non-linear parameters was made in such a manner as to optimize the results for K_{11} instead of K_{22} and, therefore, the poorer convergence of K_{22} with respect to ω is to be expected. At energies just above the positronium formation threshold, the slow incoming positronium atom is strongly distorted by the helium ion. This is of a long-range nature which is not very well reproduced by the choice of non-linear parameters we have made, and leads to a lack of convergence for K_{22} in this energy region (see figure 6.10).

The inclusion in the trial function of additional long-range polarization terms, similar to those included in calculations of the scattering length (Drachman 1971,
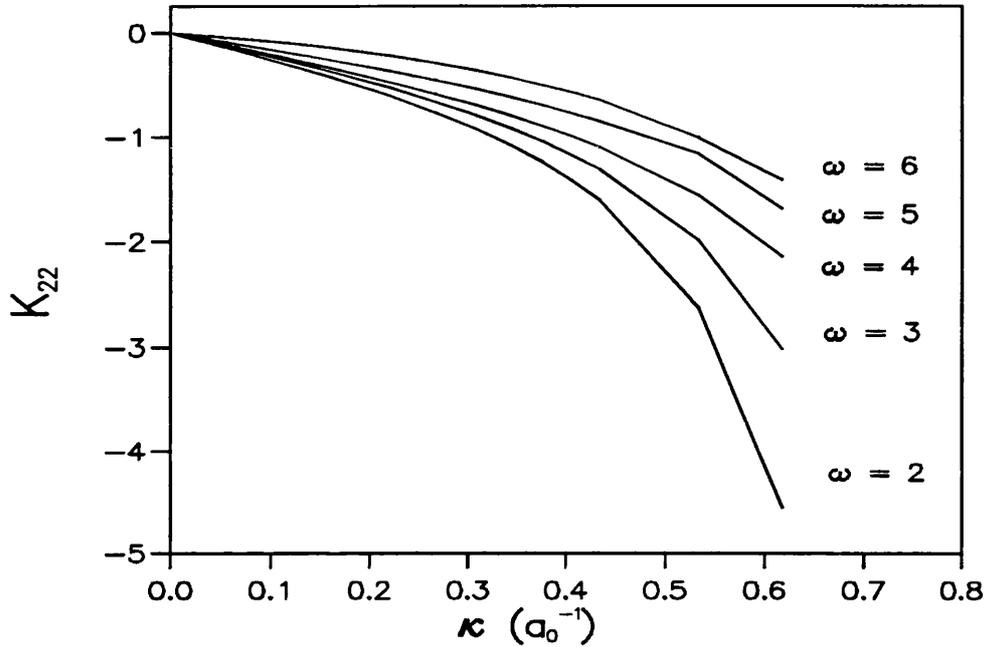
Figure 6.10: The convergence with respect to ω of the $\boldsymbol{K}$ matrix element K_{22} for s-wave positron-helium scattering plotted as a function of the positron wavenumber k.

Humberston and Wallace 1972 and Humberston 1973) is needed if an improvement in the rate of convergence is to be obtained. We have not included such a term in our calculation because we are not primarily investigating the positronium-helium-plus elastic scattering process as such, and we know that the lack of convergence of K_{22} in this energy region will not have a strong effect on the values of σ_{11} and σ_{12}, which are the main interest of this work. Figure 6.11 shows the convergence of K_{22} with respect to ω for two energies. We can see very well that the convergence is much more rapid for the higher energy, but for both cases it is too slow for the extrapolation procedure (equation 6.1) to be applied.
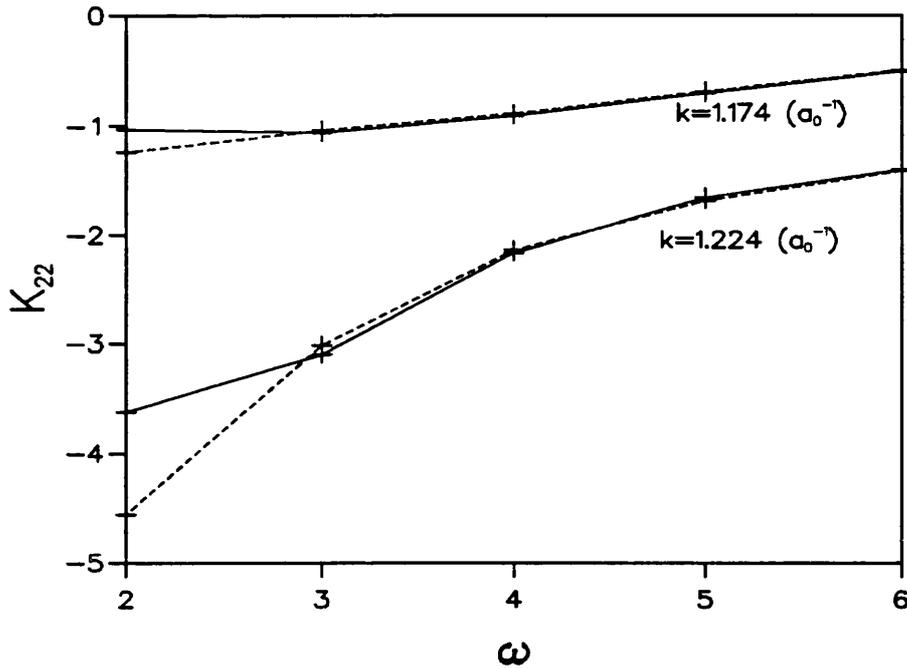
Figure 6.11: The convergence with respect to ω of the K matrix element K_{22} for s-wave positron-helium scattering. The solid and dashed lines correspond to the Kohn and inverse Kohn results respectively.

6.4 The positronium formation cross section.

The absence of a bound. whether rigorous or empirical, on the off-diagonal K matrix elements makes it very difficult to analyse the convergence of the K_{12} matrix element. A test on the reliability of K_{12} is the confirmation of the threshold behaviour with respect to energy of the positronium formation cross section as predicted by Wigner's threshold theory (Wigner 1948). However one should recognise that in general this energy dependence can also be reproduced by more approximate methods, such as the Born approximation. and that it is therefore not a very severe test on the quality of our calculation.

For a given partial wave, l, Wigner's threshold theory requires the positronium formation cross section to behave as

$$\sigma_{12}^l \propto \kappa^{2l+1} \tag{6.2}$$

106

and, as close to threshold $\sigma_{12}^l \propto K_{12}^2$, we expect

$$K_{12} \propto \kappa^{\frac{2l+1}{2}}.$$ (6.3)

Therefore, for s-wave scattering we expect to have $K_{12} \propto \kappa^{1/2}$ close to the positronium formation threshold. Our most converged results ($\omega = 6$), which are plotted in figure 6.12, reproduce this threshold behaviour, as can be seen by the linearity of the K_{12} versus $\kappa^{1/2}$ curve from the threshold up to a value of $\kappa^{1/2} = 0.4(a_0^{-1/2})$.
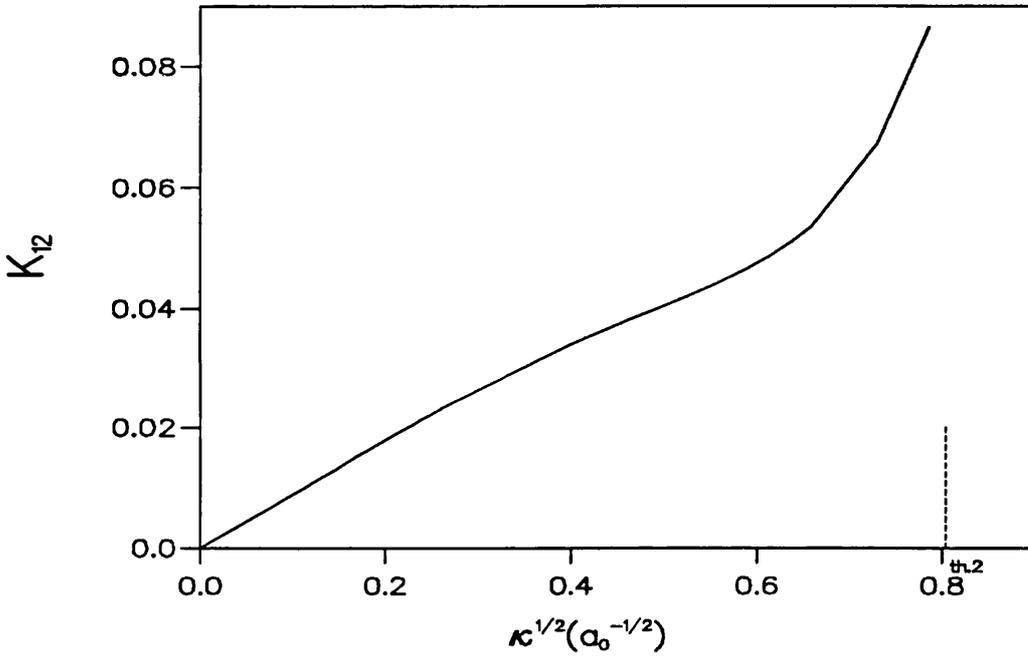

Figure 6.12: The variation of the K matrix element K_{12} with $\kappa^{1/2}$ for s-wave positron-helium scattering(th.2 is the $2\,^1S$ excitation threshold of He).

The s-wave positronium formation cross section is plotted as a function of positron energy in figure 6.13. There is a very rapid rise from threshold up to a value of $k^2 = 1.34(a_0^{-2})$ and then a much less rapid increase up to the $2\,^1S$ excitation threshold of He at 20.58eV. At the positronium formation threshold itself, the cross section has an infinite gradient, with respect to k^2, which is a consequence of equation 6.2. The gradient of the cross section with respect to k is (Watts 1994)

$$\frac{\partial \sigma_{12}^l}{\partial k} = 2k(2l+1)\kappa^{2l-1},$$ (6.4)

107

and, therefore, as $\kappa \rightarrow 0$, the s-wave cross section will have an infinite derivative with respect to k.
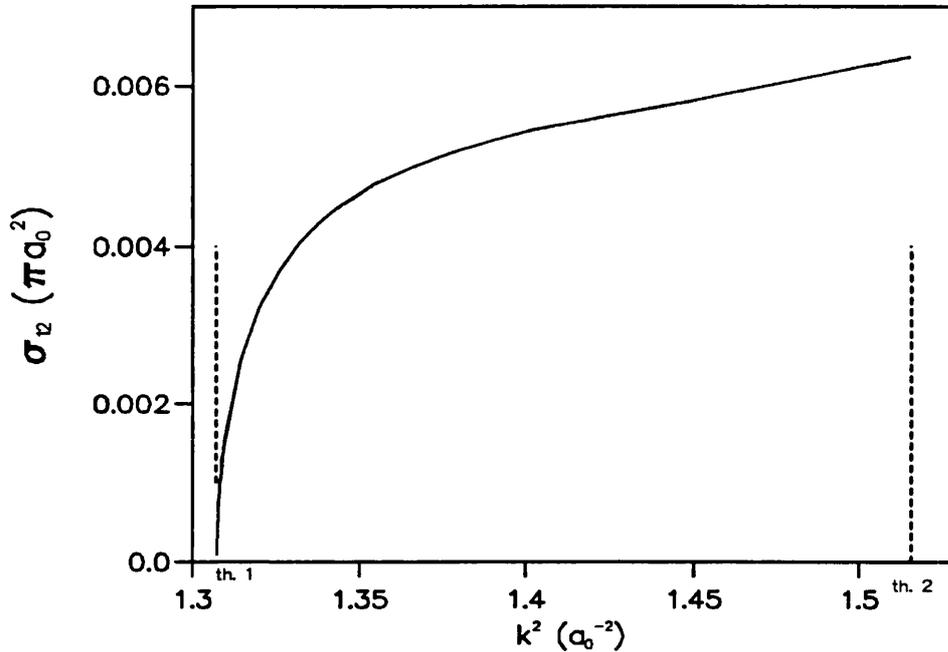

Figure 6.13: The variation of the s-wave positronium formation cross section ($\omega = 6$) with positron energy for positron-helium scattering (th.1 is the positronium formation threshold and th.2 is the $2\,^1S$ excitation threshold of He).

The general form of the s-wave positronium formation cross section for positron-helium scattering which is presented here, is very similar to that found in variational calculations of positronium formation in positron-hydrogen scattering (Humberston 1982, Watts 1994), although an even sharper rise from the threshold is found there and a clear plateau region is then reached (see figure 6.14). We believe that with a trial function better optimized for the threshold energy region and containing polarization terms, the fully converged results for the e^+- He positronium formation cross sections will be even more similar to those for e^+- H. Also, the magnitude of the cross section in the plateau region is very similar ($4 - 6 \times 10^{-3}\pi a_0^2$) for both hydrogen and helium, and as yet no explanation has been found as to why the s-wave partial wave contribution to the positronium formation cross section is much smaller than the elastic scattering cross section for both target atoms. In figure 6.15
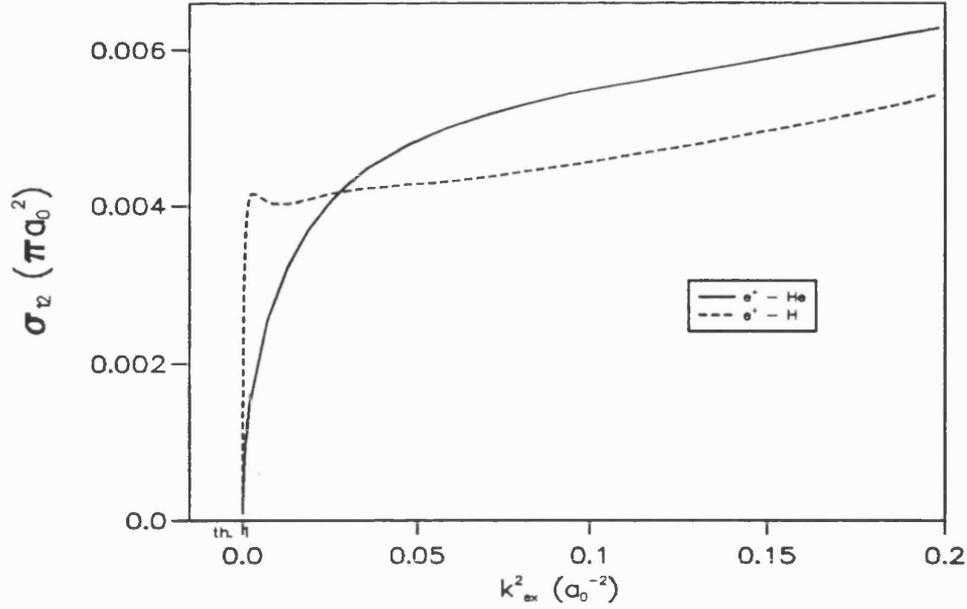
Figure 6.14: Comparison of variation the s-wave positronium formation cross section with excess positron energy ($k_{ex}^2 = k^2 - E_{th}(a_0^{-2})$) for s-wave positron-helium ($\omega = 6$) and positron-hydrogen ($\omega = 7$) scattering.

we have plotted σ_{12} with respect to ω for 3 different energies. One can easily see the non-monotonic convergence but we believe we can estimate the $\omega = 6$ results to be within 10% and 20% of the exact results. Also we note how the agreement between Kohn and the inverse Kohn improves as ω increases.

The s-wave positronium formation cross sections presented here are the first accurate values for energies within the Ore gap. Various workers have investigated positronium formation in positron-helium scattering; however, as they were mainly interested in collisions at positron energies greater than 30 eV, they used approximation methods which are more suitable for these higher energies. The first such calculation was by Massey and Moussa (1960) using the first Born approximation, and the total positronium formation cross sections they found were much larger than the experimental data. A coupled static approximation by Mandal et al (1975 & 1976) did not agree with experiment either. The s-wave contribution to the positronium formation cross section at 20 eV (the only energy they calculated within the Ore gap) given in the second paper is $\sigma_{12} = 0.00593(\pi a_0^2)$, which is close to our

109
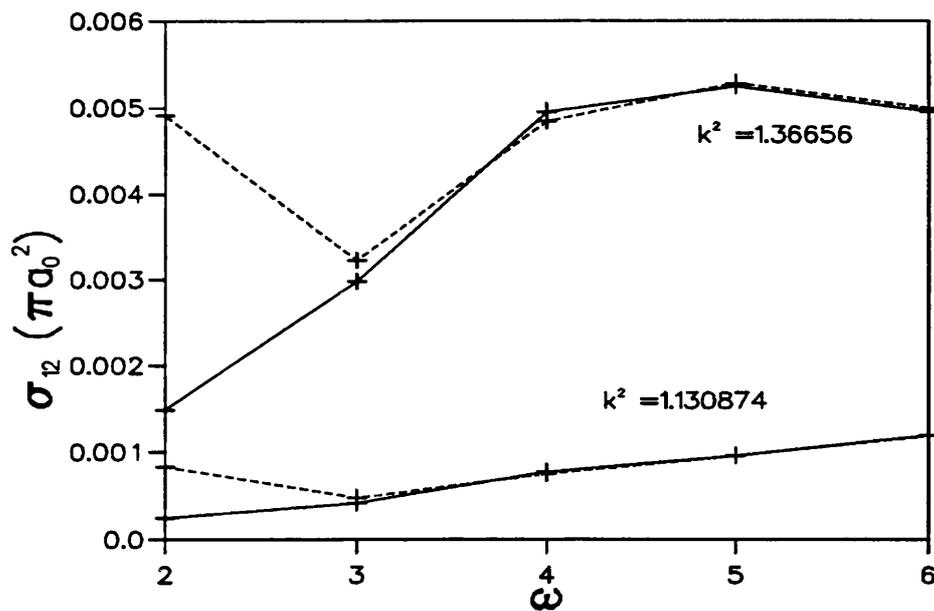
Figure 6.15: The convergence of the s-wave positronium formation cross section with respect to ω for two energies within the Ore gap. The solid and dashed lines correspond to the Kohn and Inverse Kohn results respectively.

result, but the total positronium formation cross section is wrong by a factor 4. The same group have investigated the energy region 20-100 eV using the distorted wave method and have calculated the positronium formation cross section for four partial waves (Mandal *et al* 1979). For the s-wave they found $\sigma_{12} = 0.00619(\pi a_0^2)$ at 20 eV, which is in reasonable agreement with our results, and their total cross section agrees well with experiment. However, as will be shown in the next chapter, there is a disagreement between their results for the p- and d-wave cross sections and the Kohn results of this work. More recent calculations by Hewitt *et al* (1992) and McAlinden and Walters (1992), using a close coupling approximation, concentrated only on the higher energy region were elastic scattering, positronium formation, excitation of either the helium or positronium atom and ionization of the helium atom can all occur. In figure 6.16 we present a comparison between the s-wave positronium formation cross section in the Ore gap calculated using the first Born approximation and the variational Kohn method. The first Born results were calculated by McAlinden (1996) as an extension to a calculation undertaken for the

110
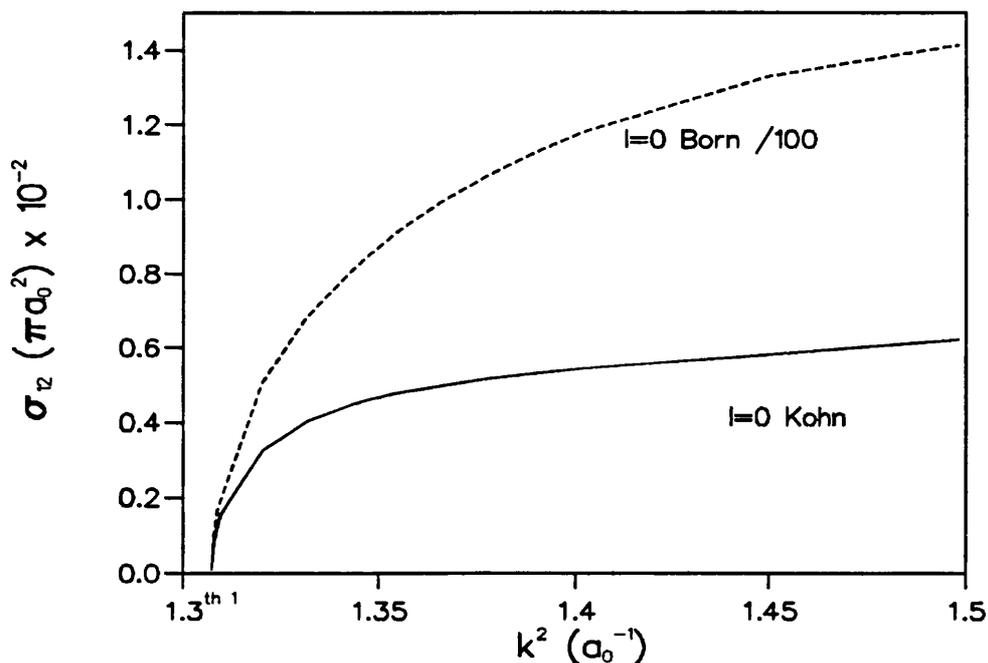
Figure 6.16: Comparison of the variation of the positronium formation cross section with positron energy for s-wave positron-helium scattering calculated with the first Born approximation and the Kohn variational method.

higher energy range. They are not expected to be in good agreement with the Kohn results, and we see that there is a factor 200 difference between both calculations, which is very similar to the ratio of the positronium formation cross sections for e^+-H calculated with the same two methods.

6.5 The elastic scattering cross section

We have calculated the elastic scattering cross section in the Ore gap using the two channel trial function and have extended our calculations to energies below the positronium formation threshold in order to find better converged phase shifts than the earlier results of Humberston (1973) and Campeanu and Humberston (1977), and also to investigate the threshold behaviour of σ_{11}.

111

k (a.u.)	H5	H22
0.1	0.031	0.0310
0.2	0.040	0.0404
0.3	0.030	0.0300
0.4	0.007	0.0081
0.5	–0.023	–0.0210
0.6	–0.057	–0.0542
0.7	–0.093	–0.0889
0.8	–0.128	–0.124
0.9	–0.163	–0.157
1.0	–0.195	–0.189

Table 6.1: The phase shifts for helium model H5 (Humberston (1973), $\omega = 4$) and H22 (this work, $\omega = 6$) for positron-helium s-wave elastic scattering.

Below the positronium formation threshold we have used a one channel trial function of the form

$$\Psi^t = S_1 + \tan \eta_0^t C_1 + \sum_{i=1}^{N} (1 + P_{23}) c_i \phi_i \tag{6.5}$$

where η_0 is the s-wave phase shift and S_1, C_1 and ϕ are defined as in 4.12, 4.14 and 4.16 respectively. We have chosen for consistency to use the same values of the non-linear parameters above and below the threshold so that the same calculation of the $(\phi_i, L\phi_j)$ matrix could be used in both cases.

In table 6.1 we compare the present phase shifts with $\omega = 6$ for helium model H22 to the results obtained with $\omega = 4$ for H5 by Humberston (1973). The H5 phase shifts were obtained with the method of models while for the H22 calculation the method of models was not used and, as mentioned in chapter 3, because there is no bound on the phase shift with respect to the helium target function used, we believe no direct comparison can be made between the H5 and H22 results presented in table 6.1. On the other hand, the reasonable agreement between the two sets of results indicates that there is no breakdown in the convergence, as discussed in chapter 3,

in the H22 phase shifts and that these can therefore be considered as accurate and reliable results.
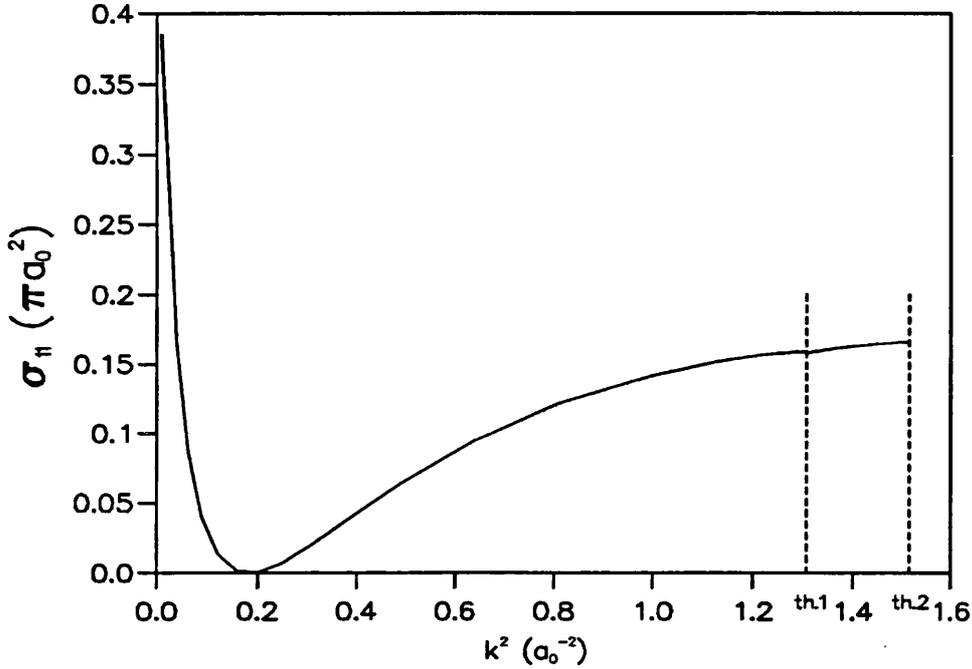

Figure 6.17: The variation of the s-wave positron-helium elastic scattering cross section with positron energy.

The general form of the elastic cross section below the positronium formation threshold as can be seen in figure 6.17 is similar to that of previous work, with a Ramsauer minimum due to the cancellation of the attractive dipole potential and the repulsive static potential, which make the s-wave phase shift go through zero close to $k = 0.4$ (a_0^{-1}). For energies greater than the positronium formation threshold energy the cross section is seen to vary only slowly with k^2 and a small discontinuity is noticed at the threshold itself. In figure 6.18, the enlarged plot of the elastic scattering cross section in the energy region just around the threshold shows this discontinuity more clearly. The curve A is that obtained with the trial function of equation 6.5 and the solid line just above the threshold is the elastic cross section obtained with the two channel trial function for energies greater than 17.78 eV.

This type of discontinuity has been noticed in previous variational calculations of

113
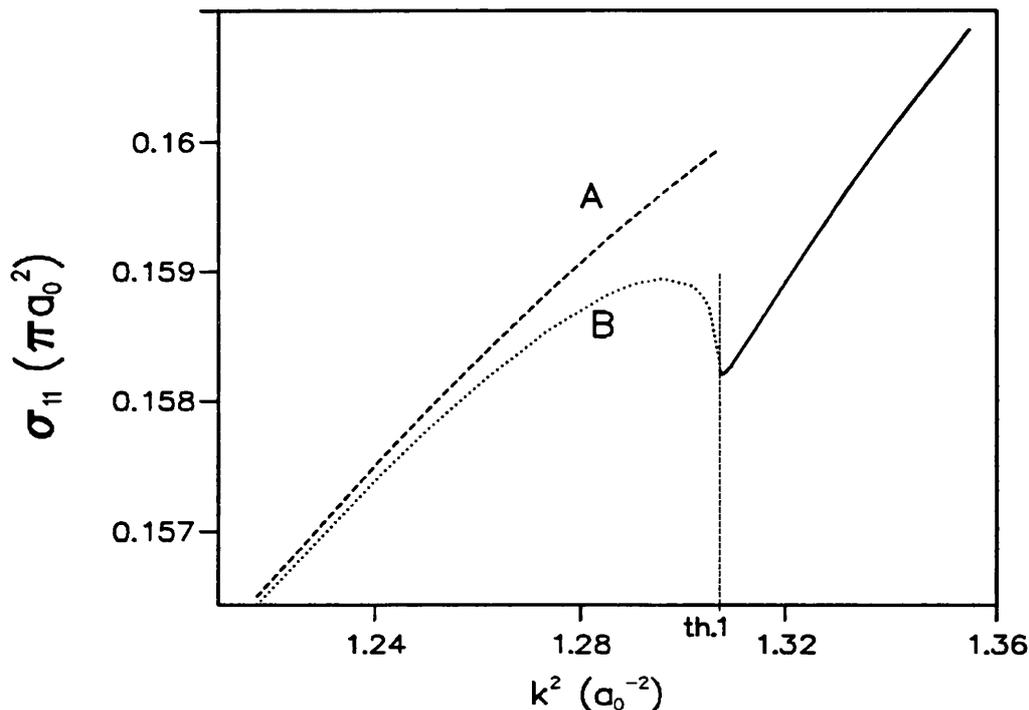
Figure 6.18: The variation of the s-wave positron-helium elastic scattering cross section with positron energy. Curve A gives the cross section obtained without the inclusion of the explicit virtual term 6.6 in the elastic scattering trial function. Curve B gives the cross section with the term included.

positron-hydrogen elastic scattering at the positronium formation threshold, most prominently in the d-wave cross section (Watts 1994). The main reason for this discontinuity was found to be the poorer convergence of the results just below the threshold, as compared to those just above, due to the absence of an explicit representation of virtual positronium formation in the elastic scattering trial function (equation 6.5). Just below the positronium formation threshold, virtual positronium can be formed but cannot escape as an open channel. One can imagine the positronium atom having been formed, trying to escape from the interaction region but not having enough energy to detach the electron from the helium atom. The possibility of virtual positronium formation is implicitly included in our calculation as we use the full Hamiltonian of the system and because the short-range terms are included in the trial function to describe whatever occurs in the interaction region. But the virtual positronium formation process is of somewhat longer range than

114

the short-range correlation terms and will therefore not be very well reproduced by the trial function. To ameliorate the convergence of the phase shifts just below the threshold, we have therefore included in the trial function (6.5) an extra term of the form

$$f = [1 + P_{23}] \Phi_{Ps}(r_{12}) \Phi_{He^+}(r_3) \frac{\exp(-\kappa\rho)}{\rho} [1 - \exp(-\delta\rho)]^5 \qquad (6.6)$$

which represents more explicitly virtual positronium formation. The virtual positronium "wavenumber", κ, is now defined by (see equation 2.14)

$$k^2 + 2E_{He} = -\frac{1}{2}\kappa^2 - 4.5. \qquad (6.7)$$

The $1/\rho$ term is shielded at the origin and the exponential fall-off in $\kappa\rho$ ensures that this term vanishes in the asymptotic region and does not affect the results for energies away from the threshold region. The optimization of the non-linear parameter δ was carried out in a similar manner to that explained above, but in this case the optimum value of $\delta = 0.75$ corresponded to that which gave the most positive value for the phase shift.

The elastic cross section just below the positronium formation threshold, calculated with the inclusion of this explicit virtual positronium term, is shown in figure 6.18, as curve B, and one sees that the cross section is now continuous at the threshold and displays a 'rounded step' type of feature. This behaviour of the elastic cross section at threshold is also predicted by R-matrix threshold theory (Meyerhof 1995). In the R-matrix analysis, described by Watts (1994), the effect on the elastic cross section of opening a new inelastic channel is investigated and threshold features just below and above the threshold are predicted.

The s-wave elastic cross section close to the threshold in this formalism is given as

$$\sigma_{el}^0 = \frac{4\pi}{k^2}(2l + 1)\sin^2\eta_0 - \sigma_{Ps}^0 \begin{cases} 2\sin^2\eta_0 & E \geq E_{thr} \\ \sin 2\eta_0 & E < E_{thr} \end{cases} \qquad (6.8)$$

where η_0 is defined within the R-matrix theory as the s-wave elastic phase shift uncoupled from either the real and virtual positronium formation channel above the threshold or from only the virtual positronium channel below (Meyerhof 1962, 1963 and Watts 1994). In the Kohn formalism it is not possible to uncouple completely
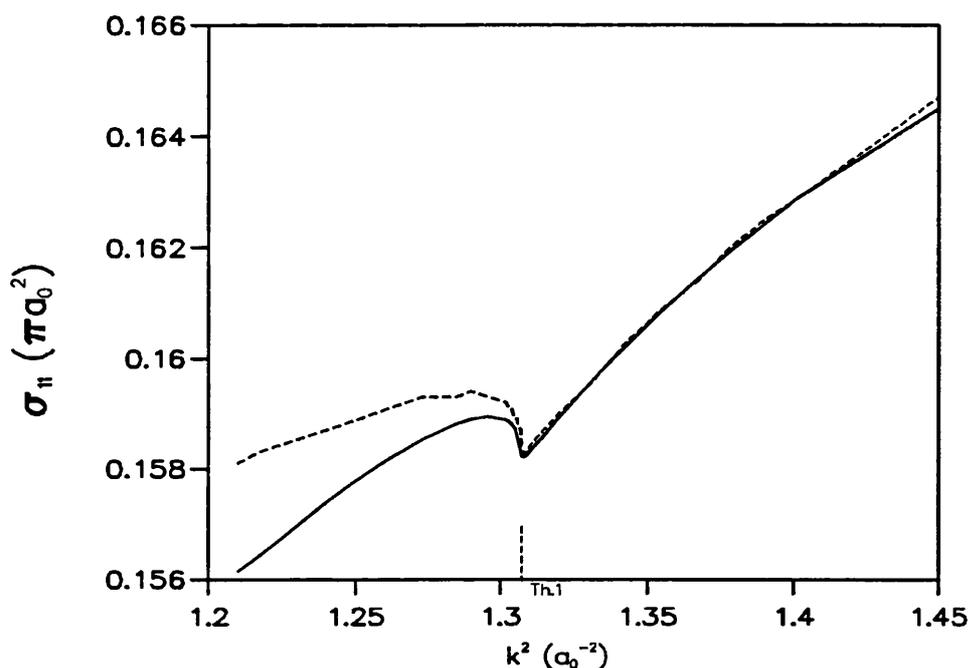
Figure 6.19: Comparisons of the Kohn calculation (solid line) and the R-matrix fit (dashed results) of the variation of the s-wave elastic cross section.

the two channels in the Ore gap or to totally suppress the virtual positronium channel as there is always an implicit reference to positronium formation in the use of both the exact total Hamiltonian of the system and the Hylleraas short-range functions. But as it is assumed that η_0 varies very little in the threshold region, it can be taken to have the value of the phase shift at the threshold itself. From 6.8, R-matrix theory predicts that the elastic cross section will fall immediately above the threshold as the positronium formation cross section rises with an infinite slope and η_0 does not vary much. Also, as the phase shift is between 0 and $-\pi/2$, just below the threshold region, we have $\sin 2\eta < 0$, and from equation 6.8 the elastic scattering cross section is expected to increase as we move away from the threshold. Both these predictions are confirmed by our calculations, and the full R-matrix evaluation of the threshold behaviour by Meyerhof (1995) based on the present values of the scattering parameters gives results very similar to ours (see figure 6.19).

We have also investigated the effect of uncoupling the elastic channel from the positronium formation channel on the elastic scattering cross section in the Ore gap. As indicated earlier, because we have included the full Hamiltonian in our calculations the short-range terms will always attempt to represent the virtual positronium channel. We have undertaken these uncoupled calculations both with and without the explicit virtual positronium term (6.5) and the results are plotted in figure 6.20. The uncoupled elastic cross section both with and without the virtual positronium
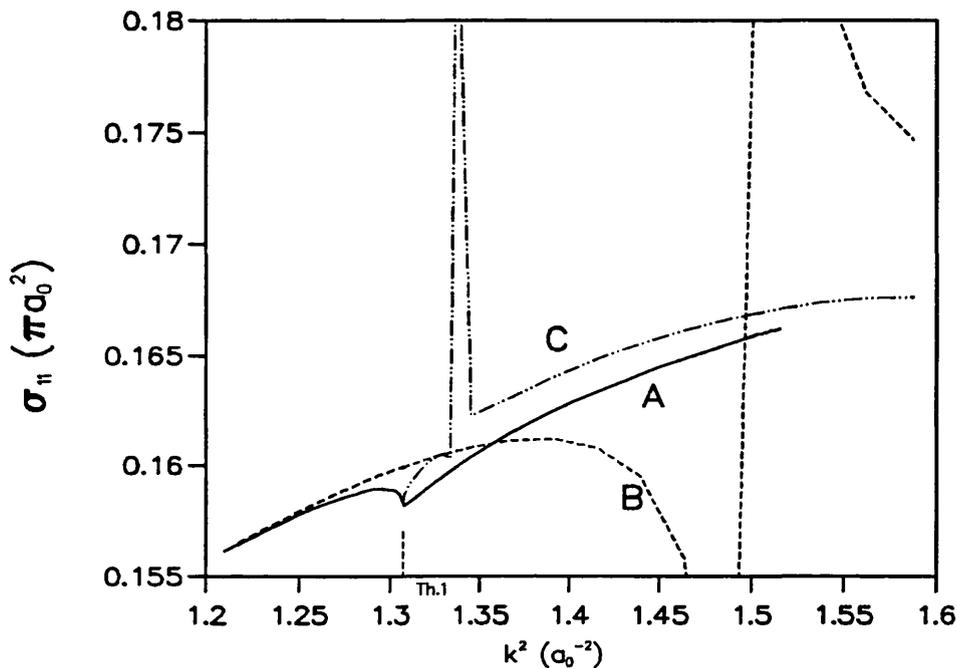
Figure 6.20: Comparison of the s-wave elastic scattering cross section obtained with and without the coupling of the positronium channel. Curve A: the coupled results; curve B: the uncoupled results with no explicit virtual positronium term in the trial function; curve C: the uncoupled results with the explicit virtual positronium term included.

term are seen to be inaccurate, especially close to the threshold, and a resonance-type feature is seen in both cases. This feature, which is known to be unphysical, arises from the uncoupling, and is very similar to features found in close-coupling calculations when open channels are neglected. An extreme example of this type of phenomenon, is the Higgins-Burke resonance (1991) in positron-hydrogen scat-

tering. In this close-coupling calculation a resonance feature was found above the ionization threshold, but its width and position were very dependent on the number of states and pseudo-states included in the calculation. There is no physical reason for a real resonance to occur in this energy region and there are theoretical grounds (Simon 1978) for believing that such resonances can not exist. It has been shown (Kernoghan et al 1995) that this resonance feature is due to the lack of complete representation of the continiuum of states which the pseudo-states try to represent, in the same manner as the non inclusion of the positronium channel affects the elastic channel in the Ore gap.
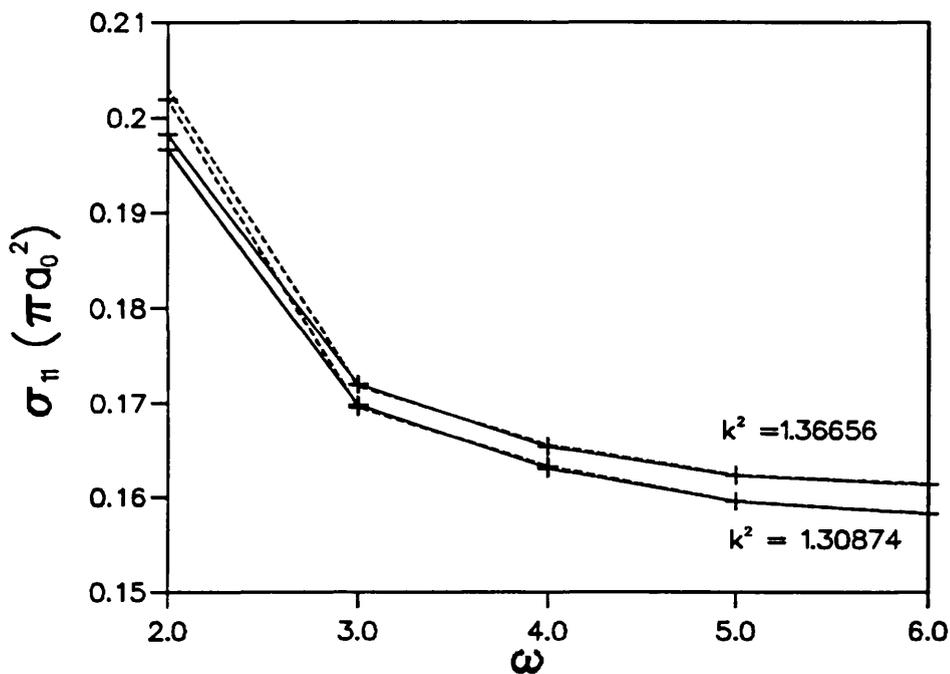
Figure 6.21: The convergence of the s-wave elastic scattering cross section with respect to ω for two energies within the Ore gap. The solid and dashed lines correspond to the Kohn and Inverse Kohn results respectively.

Figure 6.21 shows the convergence of the elastic cross section with respect to ω for two energies within the Ore gap. One can see that we have achieved reasonably well converged results, with good agreement between Kohn and inverse Kohn method, and we believe they can be estimated to be within less than 3% of the exact

results. As was the case for the positronium formation cross sections, the elastic scattering cross sections presented here are the first accurate ones calculated for energies within the Ore gap. Various workers have investigated the elastic phase shift below the positronium formation threshold using variational methods (Drachman 1968, Humberston 1973, Aulenkamp *et al* 1974) or other approximation methods (see Gosh *et al* 1982 and Campeanu 1977 for a review). McEachran *et al* (1977 and 1978) have used the polarized orbital method and have extended the calculation above the threshold (1996), without the positronium channel, and found elastic cross section 5-8% smaller than those presented in this work. The calculations which have explicitly investigated elastic scattering above the threshold have used approximation methods which are more suitable for the high energy range (>30eV), and give no information on the elastic scattering cross section in the Ore gap (Dewagan and Walters 1977, Hewitt *et al* 1992, and McAlinden 1993).

6.6 Conclusion

The complexity of the positron-helium system, and the difficulty of representing all the processes with the same trial function, have affected the quality of our results. Indeed, because of the computer time required to calculate the various matrix elements needed in the Kohn variational method, we have only been able to calculate the s-wave cross sections with trial functions corresponding to $\omega = 6$. In the latest positron-hydrogen calculations, Watts (1994) was able to go up to $\omega = 8$ and it is therefore to be expected that the helium results will not to be as well converged.

A positron-helium scattering trial function with $\omega = 6$ corresponds to 502 short-range terms, of which 330 have only even powers of the inter-electron coordinate r_{23}. As explained in chapter 3, the removal of the terms with odd powers of r_{23} affected very little the phase shifts calculated with the method of models. However, when the method was not used, this removal had a dramatic effect if the target function did not itself contain odd powers of r_{23} and was not very elaborate. In an effort to try to identify the short-range terms in the scattering wavefunction,

used in the two channel calculations, which do not contribute significantly to the value of the cross sections. we have investigated the effect of removing terms with odd powers of r_{23} from the two channel trial function. In table 6.2 we present the cross sections for $\omega = 6$ both with and without terms containing odd powers of r_{23}. We have also included a calculation in which the first 14 terms with odd powers of r_{23}, corresponding to this type of terms for $\omega = 2$, have been kept in the trial function. One can see that the elastic and positronium formation cross sections are not affected by the total or partial removal of terms with odd powers of r_{23}, the differences being less than one percent. Only the σ_{22} results, close to the positronium formation threshold, are affected to any extent and this could be due to the poor optimization of the trial function for K_{22} in this energy region. We believe that the good agreement between the results calculated with scattering trial function containing terms with and without odd powers of r_{23} for both σ_{11} and σ_{12} shows that there is no breakdown in the calculation as discussed in chapter 3, and is a further confirmation of the reliability of our results and of the quality of the H22 target function we have used in this calculation. We have also investigated the effect of the removal of terms with odd powers of r_{13} and, because of the P_{23} operator, odd powers of r_{12}, from the short-range terms in the trial function to see if this variable had the same behaviour as the r_{23} variable. In table 6.3 we present a comparison of the results with all terms included in the trial function and those obtained with the removal of either all or some of the terms containing odd powers of r_{13}. We see that the total removal of this type of terms strongly affects the results for all the cross sections, but that if only the terms with odd powers of r_{13} greater than one are removed, then the results are much closer to those of the full calculation. In this case also, the removal of terms with odd powers of r_{23} does not change the results significantly.

The removal from the trial function of terms containing odd powers of r_{13} reduces the number of short-range terms in the trial function for $\omega = 6$ from 502 to 440 only, and we have therefore not investigated further this reduction of the number of short-range terms because it seemed clear that any significant reduction in computational work would come from the removal of terms containing odd powers of r_{23}. Also,

k^2 (a.u)	σ_{11}	σ_{12}	σ_{21}	σ_{22}
1.30874	0.158191	0.001194	0.586010	2.153840
	0.158234	0.001188	0.582810	2.240170
1.40186	0.162841	0.005413	0.040167	6.361640
	0.162894	0.005446	0.040414	6.166550
1.49818	0.165799	0.006219	0.024417	6.914570
	0.165822	0.006223	0.024435	6.944030

case A

1.30874	0.158255	0.001185	0.581611	2.570080
	0.158318	0.001175	0.576566	2.722510
1.40186	0.162904	0.005513	0.040911	6.575650
	0.163013	0.005457	0.040496	6.156440
1.49818	0.165914	0.006298	0.024731	6.954820
	0.165974	0.006399	0.025125	7.014290

case B

1.30874	0.158710	0.001154	0.566015	2.761640
	0.158771	0.001147	0.562588	2.921490
1.40186	0.163294	0.005444	0.040398	6.677660
	0.163399	0.005374	0.039877	6.321120
1.49818	0.166289	0.006255	0.024559	7.003910
	0.166356	0.006352	0.024943	7.064120

case C

Table 6.2: Cross sections for positron-helium s-wave scattering in πa_0^2 ($\omega = 6$). Case A: all terms with powers of r_{23} even and odd included in the trial function; Case B: all terms with even powers of r_{23} and only first 14 terms with odd power of r_{23} included ; Case C: only terms with even powers of r_{23} included. The first entry is the Kohn result and the second entry is the inverse Kohn result.

k^2 (a.u)	σ_{11}	σ_{12}	σ_{21}	σ_{22}
1.30874	0.158191	0.001194	0.586010	2.153840
	0.158234	0.001188	0.582810	2.240170
1.40186	0.162841	0.005413	0.040167	6.361640
	0.162894	0.005446	0.040414	6.166550
1.49818	0.165799	0.006219	0.024417	6.914570
	0.165822	0.006223	0.024435	6.944030

case A

k^2 (a.u)	σ_{11}	σ_{12}	σ_{21}	σ_{22}
1.30874	0.182899	0.000721	0.353841	5.511030
	0.183061	0.000692	0.339632	5.740530
1.40186	0.187511	0.004087	0.030326	7.688330
	0.187246	0.004457	0.033077	7.379800
1.49818	0.190348	0.005684	0.022319	7.252920
	0.190333	0.005706	0.022405	7.347070

case B

k^2 (a.u)	σ_{11}	σ_{12}	σ_{21}	σ_{22}
1.30874	0.158745	0.001169	0.573396	2.575530
	0.158784	0.001166	0.572160	2.679890
1.40186	0.163367	0.005470	0.040594	6.535960
	0.163433	0.005424	0.040252	6.331280
1.49818	0.166379	0.006267	0.024609	6.957010
	0.166426	0.006332	0.024862	6.990900

case C

k^2 (a.u)	σ_{11}	σ_{12}	σ_{21}	σ_{22}
1.30874	0.159340	0.001132	0.555192	2.842280
	0.159395	0.001127	0.553131	2.958220
1.40186	0.163886	0.005410	0.040147	6.702320
	0.163971	0.005355	0.039735	6.468890
1.49818	0.166879	0.006239	0.024498	7.027270
	0.166946	0.006314	0.024793	7.070070

case D

Table 6.3: Cross sections for positron-helium s-wave scattering in πa_0^2 ($\omega = 6$). Case A: all terms included in the trial function; Case B: no terms with odd powers of r_{13} included; Case C: only the terms with odd power of r_{13} equal to one included; Case D: only the terms with odd power of r_{13} equal to one and no odd power of r_{23} included.

k (a.u)	K_{11}	K_{12}	K_{21}	K_{22}
1.144	-0.233740	0.020324	0.020324	-0.038030
	-0.233770	0.020269	0.020269	-0.038784
1.149	-0.235660	0.034155	0.034155	-0.135840
	-0.235700	0.033987	0.033987	-0.140150
1.159	-0.239310	0.041119	0.041119	-0.313680
	-0.239330	0.041594	0.041594	-0.289400
1.169	-0.242770	0.046351	0.046351	-0.440070
	-0.242800	0.046393	0.046393	-0.430780
1.184	-0.247830	0.053795	0.053795	-0.657790
	-0.247860	0.053608	0.053608	-0.643400
1.224	-0.261450	0.086084	0.086084	-1.403300
	-0.261490	0.086480	0.086480	-1.412200

Table 6.4: K matrix elements for positron-helium s-wave scattering ($\omega = 6$).

we believe that, as this is the first very accurate calculation of positron-helium scattering in the Ore gap, it is prudent to keep the same systematic increase in the number of short-range terms as given in chapter 4.

To conclude this chapter, we present two tables of the K matrix elements and the related cross sections at various energies in the Ore gap for $\omega = 6$. The results obtained by both the Kohn and inverse Kohn method are included and are seen to agree very well.

k^2 (a.u)	σ_{11}	σ_{12}	σ_{21}	σ_{22}
1.30874	0.158191	0.001194	0.586010	2.153840
	0.158234	0.001188	0.582810	2.240170
1.32020	0.158875	0.003281	0.169214	2.814660
	0.158920	0.003245	0.167359	2.993020
1.34328	0.160224	0.004324	0.080940	4.968030
	0.160259	0.004483	0.083929	4.284260
1.36656	0.161368	0.004960	0.057288	5.456150
	0.161411	0.005003	0.057781	5.263490
1.40186	0.162841	0.005413	0.040167	6.361640
	0.162894	0.005446	0.040414	6.166550
1.49818	0.165799	0.006219	0.024417	6.914570
	0.165822	0.006223	0.024435	6.944030

Table 6.5: Cross sections for positron-helium s-wave scattering in πa_0^2 ($\omega = 6$).

Chapter 7

Higher partial waves contributions and the total cross sections

7.1 Introduction

At the low energies being considered in this work, the positron does not have enough energy to provoke a change in the total angular momentum of the helium atom. Therefore, we require, by conservation of angular momentum, that the incoming positron and the outgoing positron or positronium atom, have the same orbital quantum number, l.

The asymptotic form of the scattering wavefunction for higher partial waves is then similar to the $l = 0$ case (see equations 4.2 and 4.3) but with the appropriate Bessel and Neumann functions and spherical harmonics. In the interaction region, where the short range terms are effective, the total angular momentum is not associated solely with either the positron or with one of the target electrons, but it is shared between all three particles. There is in theory an infinite number of ways in which the total angular momentum, l, can be constructed from the sum of the individual angular momenta, l_1 and l_2, of each particle. Schwartz (1961b) has shown that when the total Hamiltonian is used, the interparticle potential terms will in-

troduce a form of coupling between the individual momenta, and the sum over all possible couplings to produce the correct total angular momemtum can be greatly reduced.

This coupling is introduced by the use of the vector coupled state, $\psi(l_1, l_2, l, m)$, with specific values of the angular momentum on the particles, and an eigenstate of the total angular momentum can be expanded as

$$\Psi(\boldsymbol{r_1}, \boldsymbol{r_2}, \boldsymbol{r_3}, l, m) = \sum_{l_1, l_2} \psi(l_1, l_2, l, m) F_{l_1, l_2}(r_1, r_2, r_{12}, r_3, r_{13}, r_{23}). \qquad (7.1)$$

Schwartz showed that the summation is restricted by the constraint

$$l_1 + l_2 = l \qquad (7.2)$$

and, therefore. there are $l + 1$ types of short range terms, F_{l_1, l_2} of a given parity, which are referred to as symmetries. In the case of s-wave scattering the wavefunction was required to go as r^l as $r \rightarrow 0$. However, for the higher partial waves, as the angular momentum can be shared, we require that each type of short-range terms satisfy the boundary conditions and we find that the wavefunction must go as $r_1^{l_1}$ and $r_2^{l_2}$ as $r_1 \rightarrow 0$ and $r_2 \rightarrow 0$ respectively. One must note that because of the exchange between the two target electrons, the coupling is effectively between all three particles, but we have not included symmetries where the total angular momentum is shared between the two target electrons for the partial waves ≥ 2.

7.2 The p-wave trial function and matrix elements

In the case of p-wave positron-helium scattering we find that, as $l=1$, we need to include two symmetries in our trial function, i.e. two types of short range term are required, one of which can be associated with the one unit of angular momentum as being mainly on the positron and the other with the angular momentum being mainly on one of the target electrons. The function ψ in equation 7.1 is now given by

$$\psi(l_1, l_2, l, m) = \sum_{m_1, m_2} Y_{l_1 m_1}(\theta_1, \phi_1) Y_{l_2 m_2}(\theta_2, \phi_2) < l_1, m_1, l_2, m_2 \mid lm > \qquad (7.3)$$

126

where the summation is subject to the constraints

$$m_1 + m_2 = m \qquad (7.4)$$

and

$$-l_i \leq m_i \leq l_i \qquad (7.5)$$

and the term $< l_1, m_1, l_2, m_2 \mid l, m >$ is the Clebsch-Gordan coefficient. Because of the axial symmetry of the scattering system, we can choose to work with the z component of the total angular momentum set to zero, i.e. $m=0$ and as $l = l_1 + l_2 = 1$ we have $m_1 = m_2 = 0$. Therefore we have,

$$\psi(1,0,1,0) = Y_{10}(\theta_1, \phi_1) Y_{00}(\theta_2, \phi_2) < 1, 0, 0, 0 \mid 1 0 > \qquad (7.6)$$

and

$$\psi(0,1,1,0) = Y_{00}(\theta_1, \phi_1) Y_{10}(\theta_2, \phi_2) < 0, 0, 1, 0 \mid 1 0 > \qquad (7.7)$$

One must bear in mind that because all the interparticle distances are included in the short-range terms in the trial wave function, there is automatically a coupling of the angular momentum between the positron and the target electrons, and therefore in a given symmetry the unit of angular momentum cannot, strictly speaking, be considered to be solely on a given particle. Also, because of the boundary conditions discussed above, we need to multiply the short-range terms of the first symmetry (that associated with the positron) by r_1 and those of the second symmetry (associated with one of the target electrons) by r_2 (or r_3 for the exchanged form).

The p-wave trial function therefore has the form,

$$
\begin{aligned}
\Psi_1 = & \; Y_{10}(\theta_1) \Phi_{He}(\boldsymbol{r_2}, \boldsymbol{r_3}) \sqrt{k} \left\{ j_1(kr_1) - K_{11}^t n_1(kr_1) \left[1 - \exp(-\lambda r_1) \right]^3 \right\} \\
& - \frac{1}{\sqrt{2}} \left[1 + P_{23} \right] Y_{10}(\theta_\rho) \Phi_{Ps}(r_{12}) \Phi_{He^+}(r_3) \\
& \times \sqrt{2\kappa} K_{21}^t \left\{ n_1(\kappa\rho) \left[1 - \exp(-\mu\rho)(1 + \frac{\mu}{2}\rho) \right]^5 \right\} \\
& + \left[1 + P_{23} \right] Y_{10}(\theta_1) \exp\left(-\alpha r_1 - \beta(r_2 + r_3) \right) r_1 \sum_{i=1}^{N} a_i r_1^{k_i} r_2^{l_i} r_{12}^{m_i} r_3^{n_i} r_{13}^{p_i} r_{23}^{q_i} \\
& + \left[1 + P_{23} \right] Y_{10}(\theta_2) \exp\left(-\alpha r_1 - \beta(r_2 + r_3) \right) r_2 \sum_{j=1}^{N} b_j r_1^{k_j} r_2^{l_j} r_{12}^{m_j} r_3^{n_j} r_{13}^{p_j} r_{23}^{q_j} \qquad (7.8)
\end{aligned}
$$

127

$$\Psi_2 = \frac{[1+P_{23}]}{\sqrt{2}} Y_{10}(\theta_\rho)\Phi_{Ps}(r_{12})\Phi_{He^+}(r_3)$$

$$\times \sqrt{2\kappa}\left\{ j_1(\kappa\rho) - K_{22}^t n_1(\kappa\rho)\left[1 - \exp(-\mu\rho)(1 + \frac{\mu}{2}\rho)\right]^5\right\}$$

$$-Y_{10}(\theta_1)\Phi_{He}(\boldsymbol{r_2},\boldsymbol{r_3})\sqrt{k}K_{12}^t\{n_1(kr_1)\left[1 - \exp(-\lambda r_1)\right]^3\}$$

$$+[1+P_{23}]Y_{10}(\theta_1)\exp\left(-\alpha r_1 - \beta(r_2+r_3)\right)r_1 \sum_{i=1}^{N} c_i r_1^{k_i} r_2^{l_i} r_{12}^{m_i} r_3^{n_i} r_{13}^{p_i} r_{23}^{q_i}$$

$$+[1+P_{23}]Y_{10}(\theta_2)\exp\left(-\alpha r_1 - \beta(r_2+r_3)\right)r_2 \sum_{j=1}^{N} d_j r_1^{k_j} r_2^{l_j} r_{12}^{m_j} r_3^{n_j} r_{13}^{p_j} r_{23}^{q_j} \quad (7.9)$$

where we have absorbed the Clebsch-Gordan coefficients into the variational linear parameters and $Y_{10}(\theta)$ is the p-wave spherical harmonic given by

$$Y_{10}(\theta) = \sqrt{\frac{3}{4\pi}}\cos\theta. \quad (7.10)$$

The first order spherical Bessel and Neumann function are

$$j_1(kr) = \frac{\sin(kr)}{(kr)^2} - \frac{\cos(kr)}{kr} \quad (7.11)$$

$$n_1(kr) = -\frac{\cos(kr)}{(kr)^2} - \frac{\sin(kr)}{kr}. \quad (7.12)$$

As was the case in the s-wave trial function, the singularity in the Neuman function is removed by an appropriate shielding function, subject to the condition of equations 4.8 and 4.10. Using a similar notation to that in the s-wave case, we can write the two componant p-wave trial function as,

$$\Psi_1^t = Y_{10}(\theta_1)S_1 + Y_{10}(\theta_1)K_{11}^t C_1 + \frac{(1+P_{23})}{\sqrt{2}}Y_{10}(\theta_\rho)K_{21}^t C_2$$

$$+Y_{10}(\theta_1)(1+P_{23})\sum_{i=1}^{N} r_1 a_i\phi_i + (1+P_{23})\left[Y_{10}(\theta_2)\sum_{j=1}^{N} r_2 b_j\phi_j\right] \quad (7.13)$$

$$\Psi_2^t = \frac{(1+P_{23})}{\sqrt{2}}Y_{10}(\theta_\rho)S_2 + \frac{(1+P_{23})}{\sqrt{2}}Y_{10}(\theta_\rho)K_{22}^t C_2 + Y_{10}(\theta_1)K_{12}^t C_1$$

$$+Y_{10}(\theta_1)(1+P_{23})\sum_{i=1}^{N} r_1 c_i\phi_i + (1+P_{23})\left[Y_{10}(\theta_2)\sum_{j=1}^{N} r_2 d_j\phi_j\right]. \quad (7.14)$$

The various matrix elements of $(\boldsymbol{\Psi^t}, \boldsymbol{L\Psi^t})$ can now be evaluated in a similar manner to that used in the s-wave calculation, except that now the angular part of the wavefunction is not a constant but is a function of the external angles θ_1, θ_2, θ_3, θ_{ρ_2}

and θ_{ρ_3} on which L will operate. The method used for the angular integration of the external angle dependent terms of the p-wave trial function is given in appendix B together with the results for various combinations of p-wave spherical harmonics.

The matrix elements which contain LS_1 or $\overline{LS_2}$ terms (with $\overline{LS_2} = (1+P_{23})S_2/\sqrt{2} = S_2+S_2'$) are of a similar form as those for s-wave scattering, and we find, for instance, that

$$S_1 LS_1 = S_1 \left[\frac{4}{r_1} - \frac{2}{r_{12}} - \frac{2}{r_{13}}\right] S_1 \tag{7.15}$$

and

$$\overline{S_2}L\overline{S_2} = 2S_2 \left[\frac{4}{r_1} - \frac{4}{r_2} - \frac{2}{r_{13}} + \frac{2}{r_{23}}\right] S_2'. \tag{7.16}$$

The elements containing LC_1 or $\overline{LC_2}$ are more complicated than in s-wave scattering because of the more complex form of the Neuman and related shielding functions.

We find, for instance, that

$$
\begin{aligned}
C_1 LC_1 = \ & \Phi_{He}^2(\boldsymbol{r_2},\boldsymbol{r_3})k n_1(kr_1)\left(1 - e^{-\lambda r_1}\right)^3 \\
& \times \left[2\left(-\frac{n_1(kr_1)}{r_1} - \frac{\cos(kr_1)}{r_1}\right)3\lambda e^{-\lambda r_1}\left(1 - e^{-\lambda r_1}\right)^2 \right. \\
& \left. + n_1(kr_1)3\lambda^2\left(4e^{-\lambda r_1} - 3e^{-2\lambda r_1} - 1\right)\right] \\
& + \Phi_{He}^2(\boldsymbol{r_2},\boldsymbol{r_3})k n_1^2(kr_1)\left(1 - e^{-\lambda r_1}\right)^6\left[\frac{4}{r_1} - \frac{2}{r_{12}} - \frac{2}{r_{13}}\right]
\end{aligned} \tag{7.17}
$$

and

$$
\begin{aligned}
C_1 LC_2 = \ & \Phi_{He}(\boldsymbol{r_2},\boldsymbol{r_3})\Phi_{He^+}(r_3)\Phi_{Ps}(r_{12})\sqrt{2k\kappa}\, n_1(kr_1)\left(1 - e^{-\lambda r_1}\right)^3 \\
& \times \left\{\frac{5}{2}\left(1 - e^{-\mu\rho}(1 + \frac{\mu\rho}{2})\right)^3 e^{-\mu\rho} \right. \\
& \times \left[n_1(\kappa\rho)\left[-\mu\left(1 - e^{-\mu\rho}(1 + \frac{\mu\rho}{2})\right)(\frac{1}{\rho} + \mu + \frac{\mu^2}{2}\rho) + e^{-\mu\rho}(\mu + \mu^2\rho)^2\right]\right. \\
& \left. - \frac{\cos(\kappa\rho)}{\rho}(\mu + \mu^2\rho)\left(1 - e^{-\mu\rho}(1 + \frac{\mu\rho}{2})\right)\right] \\
& \left. - n_1(\kappa\rho)\left(1 - e^{-\mu\rho}(1 + \frac{\mu\rho}{2})\right)^5\left[\frac{4}{r_1} - \frac{4}{r_2} - \frac{2}{r_{13}} + \frac{2}{r_{23}}\right]\right\}
\end{aligned} \tag{7.18}
$$

from which $(C_1 L\overline{C_2})$ can be found. Note that, for clarity, the above matrix elements have been given without the appropriate factor from the external angle integration which can be found in appendix B (for instance for $C_1 LC_2$ we will have to integrate $Y_{10}(\theta_1)Y_{10}(\theta_\rho)$). Again, the long-range - short-range matrix elements can be

formulated in a similar manner as in the s-wave case, using the results above and including the two types of short-range term.

The main difference between the p-wave and s-wave short-range - short-range matrix elements, is that in the p-wave case we need to include the action of the kinetic energy operator from the Hamiltonian on the spherical harmonics. For the matrix elements which involve only short-range terms of the same symmetry this will give rise to a centrifugal term of the form $l(l+1)/r^2$. This repulsive centrifugal term, becomes even more significant for the higher values of l, and its effect is to keep the positron away from the atomic region, therefore making the short-range terms less needed for the higher partial waves. Also, there are extra terms, with respect to equation 4.40, which arise from the cross terms of the form $\nabla_k \theta_k . \nabla_k \phi_j$ in the matrix elements containing either only second symmetry terms and those containing both first and second symmetry terms. For instance, before the external angle integration, the terms involving the kinetic energy operator (see 4.38) in the matrix elements containing both symmetries can be written, excluding exchange for clarity, as

$$\int I_{12} d\tau = \int \sum_{k=1}^{3} \left[\nabla_k (\cos \theta_1 \phi_i) . \nabla_k (\cos \theta_2 \phi_j) \right] d\tau \qquad (7.19)$$

where we have absorbed the r_1 and r_2 factors into the ϕ_i and ϕ_j terms. Expanding, we have

$$\int I_{12} d\tau = \int \sum_{k=1}^{3} \left[\cos \theta_1 cos\theta_2 \nabla_k (\phi_i) . \nabla_k (\phi_j) + \nabla_k (\cos \theta_1) \phi_i . cos\theta_2 \nabla_k (\phi_j) \right.$$
$$\left. + \cos \theta_1 \nabla_k (\phi_i) . \nabla_k (cos\theta_2) \phi_j + \phi_i \phi_j \nabla_k (\cos \theta_1) . \nabla_k (cos\theta_2) \right] d\tau \; (7.20)$$

which after integration over external angles becomes,

$$I_{12} = 2\pi \left\{ \sum_{k=1}^{3} \cos \theta_{12} \nabla_k \phi_i . \nabla_k \phi_j \right.$$

$$+ \phi_i \phi_j \left[\frac{-m_i r_1}{r_{12}^2 r_2} \sin^2 \theta_{12} - \frac{q_i r_3}{r_{23}^2 r_2} \left(\cos \theta_{13} - \cos \theta_{12} \cos \theta_{23} \right) \right.$$

$$\left. \left. \frac{-m_j r_2}{r_{12}^2 r_1} \sin^2 \theta_{12} - \frac{q_j r_3}{r_{13}^2 r_1} \left(\cos \theta_{23} - \cos \theta_{12} \cos \theta_{13} \right) \right] \right\} \quad (7.21)$$

where $\nabla_k \phi_i . \nabla_k \phi_j$ is given by equation 4.40. For the matrix elements containing only second symmetry terms, we find that, including exchange and after external angle

integration,

$$I_{\overline{22}} = 2\pi \left\{ \sum_{k=1}^{3} \left[\nabla_k o_i \cdot \nabla_k \phi_j + \nabla_k \phi'_i \cdot \nabla_k \phi'_j \right. \right.$$

$$\left. + \cos\theta_{23} \left(\nabla_k \phi_i \cdot \nabla_k \phi'_j + \nabla_k \phi'_i \cdot \nabla_k \phi_j \right) + \left(\frac{2}{r_2^2} + \frac{2}{r_3^2} \right) \phi_i \phi_j \right]$$

$$- \phi_i \phi'_j \left[\frac{p_i r_1}{r_{13}^2 r_3} \left(\cos\theta_{12} - \cos\theta_{13} \cos\theta_{23} \right) + \sin^2\theta_{23} \left(\frac{q_i r_2}{r_{23}^2 r_3} + \frac{q'_j r_3}{r_{23}^2 r_2} \right) \right.$$

$$\left. + \frac{m'_j r_1}{r_{12}^2 r_2} \left(\cos\theta_{13} - \cos\theta_{12} \cos\theta_{23} \right) \right]$$

$$- o'_i o_j \left[\frac{p'_i r_1}{r_{13}^2 r_3} \left(\cos\theta_{12} - \cos\theta_{13} \cos\theta_{23} \right) + \sin^2\theta_{23} \left(\frac{q'_i r_2}{r_{23}^2 r_3} + \frac{q_j r_3}{r_{23}^2 r_2} \right) \right]$$

$$\left. \left. + \frac{m_j r_1}{r_{12}^2 r_2} \left(\cos\theta_{13} - \cos\theta_{12} \cos\theta_{23} \right) \right] \right\} \qquad (7.22)$$

7.3   The p-wave results

The non-linear parameters α, β, μ and λ have been optimized in a similar manner as in the s-wave calculation. using a p-wave trial function with only first symmetry terms ($\omega = 3$), and we have found that the values of α, β and λ which gave the best compromise between the optimization for K_{11} and K_{22} were the same in both the s-wave and p-wave trial functions. The new value of the non-linear parameter μ was $\mu = 1.5$ and again. as in s-wave scattering, it was not possible to obtain a value which gave the most positive values for both K_{11} and K_{22}. We have found that the poorer representation of the positronium - He$^+$ system is more pronounced in our p-wave calculation and this has lead to a greater difference between the Kohn and inverse Kohn results for K_{22}.

The first results we obtained for p-wave scattering above and below the positronium formation threshold highlighted a problem in our calculation and we have therefore investigated in detail the convergence of the diagonal K matrix elements to verify the accuracy of our results. The phase shifts below the positronium formation threshold with $\omega=4$ in both symmetries agreed very well with those obtained by Campeanu (1977) and a clear convergence pattern with ω could be seen. Above the positronium formation threshold the convergence pattern of the K_{11} and K_{22}

matrix elements did not correspond to that obtained in the s-wave scattering calculation. We found that when the value of ω was increased simultaneously in both symmetries, the values of the diagonal K matrix elements at first became more positive and then, for larger values of ω, behaved erratically. By increasing first the value of ω in the first symmetry, and then adding in the second symmetry, we found that the problem was mainly due to the first symmetry terms. To investigate this phenomenon in more detail, we decided to consider the convergence of the diagonal K matrix elements not with respect to ω but with respect to the number of terms in the trial function.

The choice of parameter with respect to which the convergence of K_{11} and K_{22} is considered is arbitrary as long as the parameter represents, in some sense, the quality of the trial function, i.e. the variation of the parameter can be linked to how close the trial function tends to the exact wavefunction. In the analysis of the s-wave results and of the previous Kohn variational calculations of positron-hydrogen scattering, the convergence was always considered with respect to ω, as this parameter represents the improvement of the trial function in a systematic way. Indeed, from the definition of ω, i.e. $k_i + l_i + m_i + n_i + p_i + q_i \leq \omega$, one can see that an increase in ω corresponds to adding a specific set of terms to the trial function and therefore making it more flexible and closer to the exact wavefunction. On the other hand, for a given value of ω, the order in which the terms are added individually to the trial function is completely arbitrary and while the inclusion of some terms may play an important role, it is known that some terms do not contribute much to the improvement of the trial function.

In fig 7.1 and 7.2 we have plotted the variations of the diagonal K matrix elements with respect to the number of terms in the trial function, for two different energies. The total number of terms corresponds to $\omega = 6$ in both symmetries (with only even powers of r_{23}) and we have chosen to start with the first symmetry up to 330 terms (in steps of 5) and then add the second symmetry. One can see in the graphs for K_{11} that there is a rapid rise when the first symmetry starts, up to $\approx$ 80-120 terms, at which point a plateau region is reached. Between 200-330 terms,
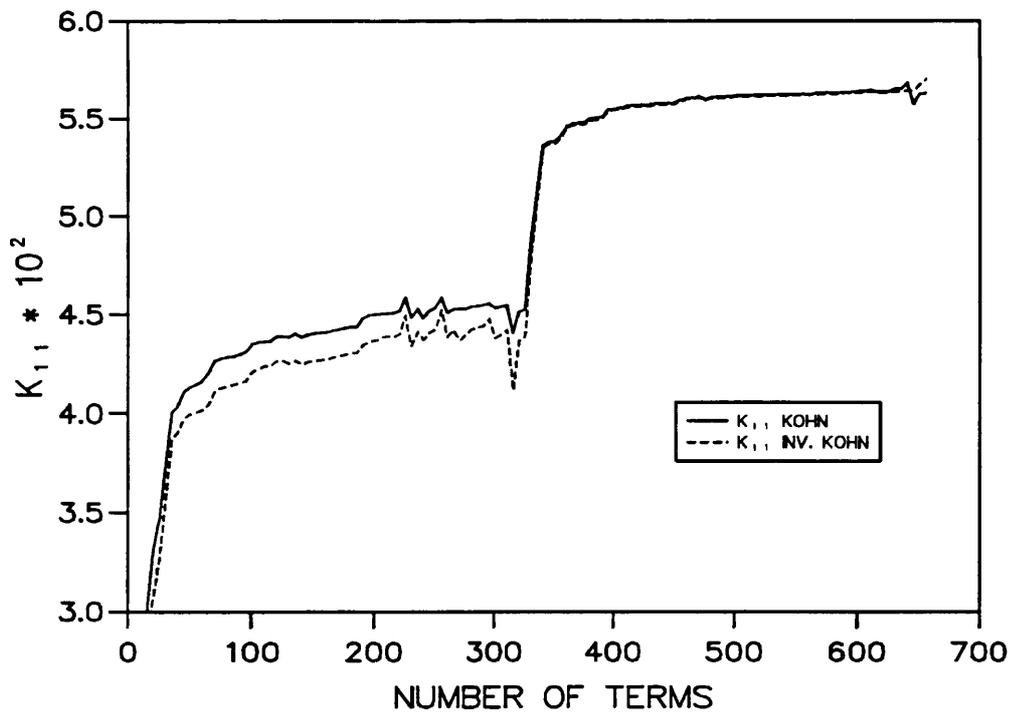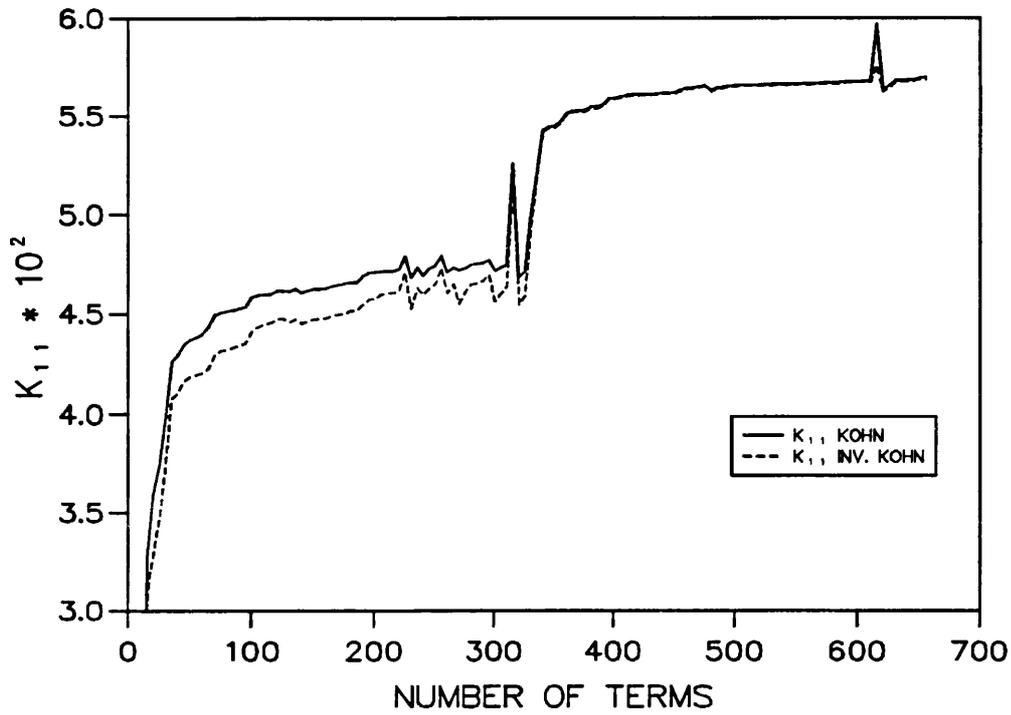
Figure 7.1: The variation of the K matrix element K_{11} with the number of terms in the trial function for p-wave scattering at k= 1.144 (a.u.) and k= 1.174 (a.u.) with ω=6 in both symmetries.

Figure 7.2: The variation of the K matrix element K_{22} with the number of terms in the trial function for p-wave scattering at k= 1.144 (a.u.) and k= 1.174 (a.u.) with $\omega=6$ in both symmetries.

134
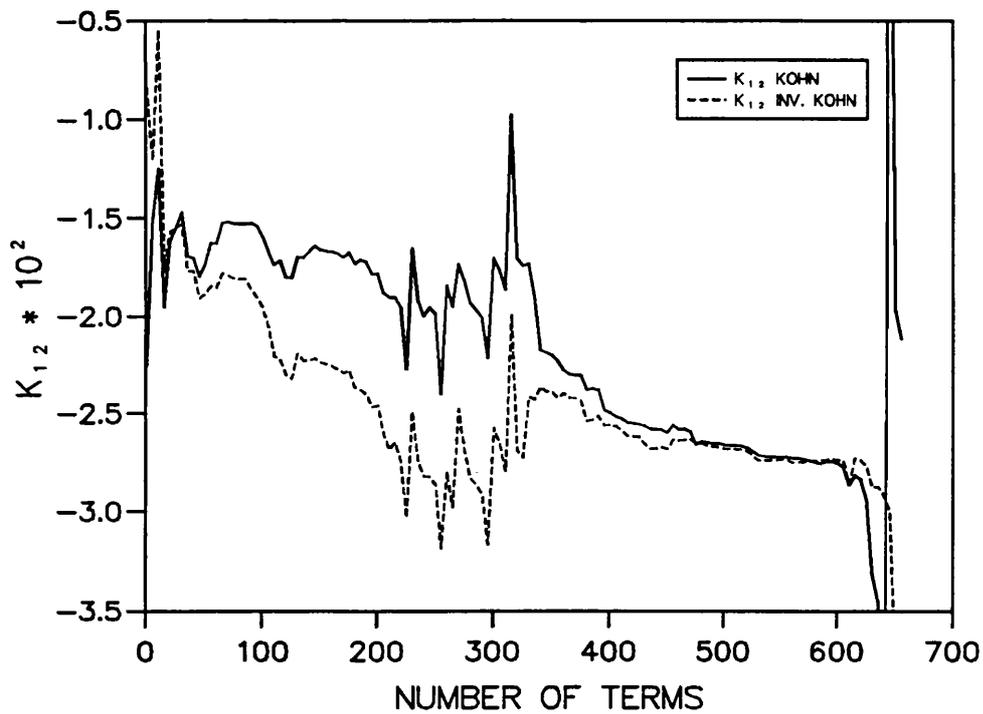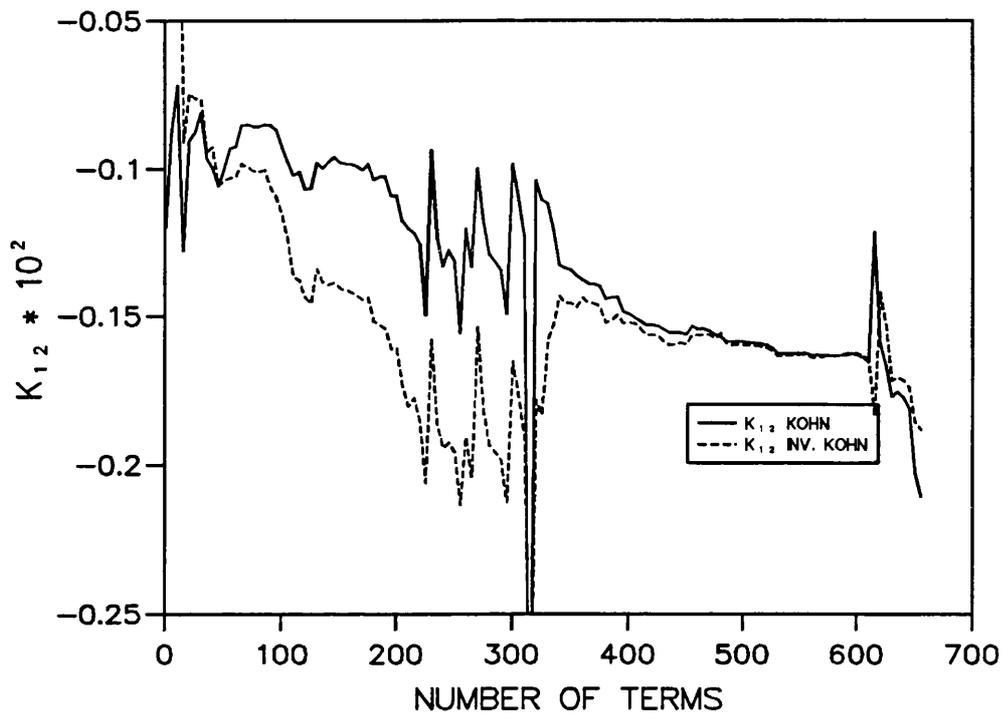
Figure 7.3: The variation of the K matrix element K_{12} with the number of terms in the trial function for p-wave scattering at k= 1.144 (a.u.) and k= 1.174 (a.u.) with ω=6 in both symmetries.

there is some resonance-type structure, which clearly violates the empirical lower bound which we have assumed to hold for the diagonal K matrix elements. When the second symmetry terms are included, at 330 terms, there is again a very rapid rise in the value of K_{11} up to a plateau region where K_{11} varies very little. One can see that, although some resonance-like structure appears when more than 600 terms are included, on the whole the results are much smoother than when only the first symmetry was included. There is a clear disagreement between the Kohn and inverse Kohn results when only the first symmetry is included, but it is important to note that the resonance-type structure appears in both results at the same place (note that the number of terms in the graph have been increased in steps of 5) and that they are therefore not identical to the Schwartz singularities discussed in chapter 2. When the second symmetry terms are included, both the Kohn and the inverse Kohn results agree well and the small resonance structure around 600 - 630 terms appears in both methods.

The variation of K_{22} with respect to the number of terms in the trial function (see figure 7.2) shows a similar pattern to that of K_{11} but, because the optimization of the trial function for K_{22} is less good as that for K_{11}, we do not have the same rapid rises and plateau regions. Again, at around 200 terms in the first symmetry, there is a resonance-type structure, in both the Kohn and inverse Kohn results, which disappears when the second symmetry is included but reappears when around 600 terms in total are included. In this case, the inclusion of the second symmetry did not make the Kohn and inverse Kohn results agree better in terms of magnitude, and this we believe can be explained by the poorer optimization of the non-linear parameters for K_{22}. In figure 7.3 we present the variation of K_{12} with respect to the number of terms in the trial function, and a similar pattern to that described above is found. In this case there is no empirical bound on the K matrix element, but again we see a resonance-type structure appearing in the first symmetry, followed by smoother results when the second symmetry is included and some structure around 600 terms in the trial function. We have also calculated trial functions which included both even and odd powers of r_{23} in the short-range terms but, as in s-wave scattering (see table 6.2), the inclusion of odd powers of r_{23} did not improve

the results. We found that including terms containing odd powers of r_{23} in the first symmetry introduced many resonance features when the second symmetry terms were included and destroyed completely the convergence pattern for all K matrix elements.

From the results presented above, we can clearly see that there is a new type of breakdown in the convergence pattern of the diagonal K matrix elements, which makes the analysis of the results more complicated than in the s-wave calculation. We believe that there are various reasons which combine to create the partial breakdown of our calculations. If we first consider the case of the K_{11} matrix element, we see that the resonance-type features in the first symmetry appear in the plateau region where the value of K_{11} does not increase significantly. In this region, we find that adding new terms to the trial function does not make the value of K_{11} much more positive. This is consistent with the fact that for the higher partial waves, the inclusion of the centrifugal barrier reduces the importance of the short-range terms. Also, we know that when two identical terms are included in the trial function, the linear independence is removed in equation 2.103 and the matrix A becomes ill-conditioned. giving values of K_{11} which lie between $-\infty$ and $+\infty$. It seems, therefore, that the resonance-type structure could be explained by the fact that, in this plateau region, the addition of more and more first symmetry terms to the trial function, is not very effective in making K_{11} more positive. This would then be very much like adding two identical terms, making the matrix A numerically ill conditioned. We have also found this type of phenomenon in the d-wave positron-hydrogen scattering results, but there the breakdown was much less dramatic. This indicates that the breakdown is not due to the inexact integration of the $(\phi_i, L\phi_j)$ matrix elements in the positron-helium p-wave scattering results, as these elements are integrated exactly in the positron-hydrogen case. Also, the fact that the resonance features seem to be mainly due to the addition of short-range terms could explain why they appear in nearly exactly the same place for both the Kohn and inverse Kohn methods.

It is important to notice that the ill-contidionong of A is due to the combination

of all matrix elements and not just of one element on its own. Therefore, if a resonance feature appears at a given term in the trial function, it may disappear completely if some other term is removed. Hence, it is not possible to identify a specific element which creates the problem, but from the analysis of the variation of K_{11} with the number of terms in the trial function, it is clear that it is in the set of terms between 150 and 330 in the first symmetry that the problem first arises. In the case of the K_{22} matrix element, the same phenomenon occurs with the additional problem of the poor optimization of the non-linear parameters, which explains why the Kohn and inverse Kohn results do not agree very well in magnitude. Again, here, and also in the K_{12} case (see figure 7.3), the resonance structure starts when at least 150 terms of the first symmetry have been added to the trial function.

We have, therefore, repeated the K matrix evaluation for p-wave scattering with a trial function containing 150 terms of the first symmetry and 330 terms of the second symmetry. The results, presented in figures 7.4, 7.5 and 7.6 show that in general we have a much better convergence pattern in all K matrix elements and that the resonance-type features have nearly completely disappeared. The removal of these first symmetry terms has not affected the most converged values of K_{11} and K_{12} by more than a few percent, but it has dramatically reduced the magnitude of K_{22}, which can be explained by the poor optimization of the non-linear parameters for K_{22}. We believe that we can accept these poorer results for the K_{22} matrix element, because we have found that, although all K matrix elements are involved in the evaluation of the elastic scattering and positronium formation cross sections, the effect of the K_{22} element is minimal except if K_{22} goes to $\pm\infty$. To verify this, we have calculated the p-wave cross sections with the calculated K_{22} matrix element and also with $K_{22}=0$, and have found that the difference was less than 0.1%.

In figures 7.7, 7.8 and 7.9 we show the energy dependence of the K matrix elements. As predicted by Wigner's threshold theory, the K_{12} matrix element has a linear dependence on $\kappa^{3/2}$ close to the threshold, and we see that the Kohn and inverse Kohn results agree very well for both K_{11} and K_{12} while, as expected, they do not for the K_{22} matrix element. The p-wave positronium formation cross section
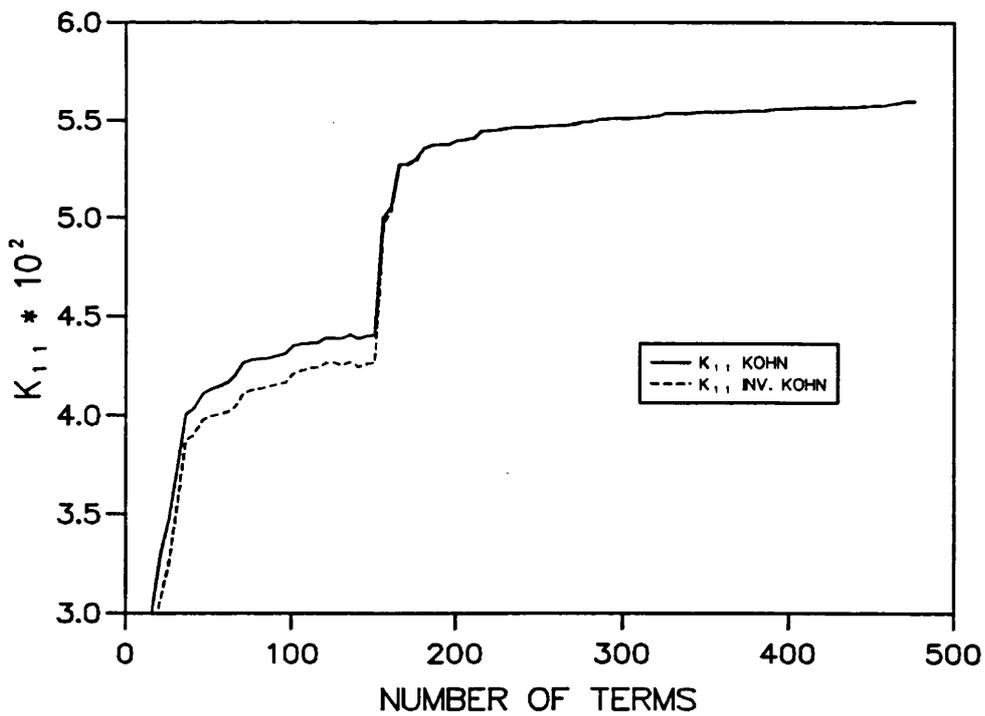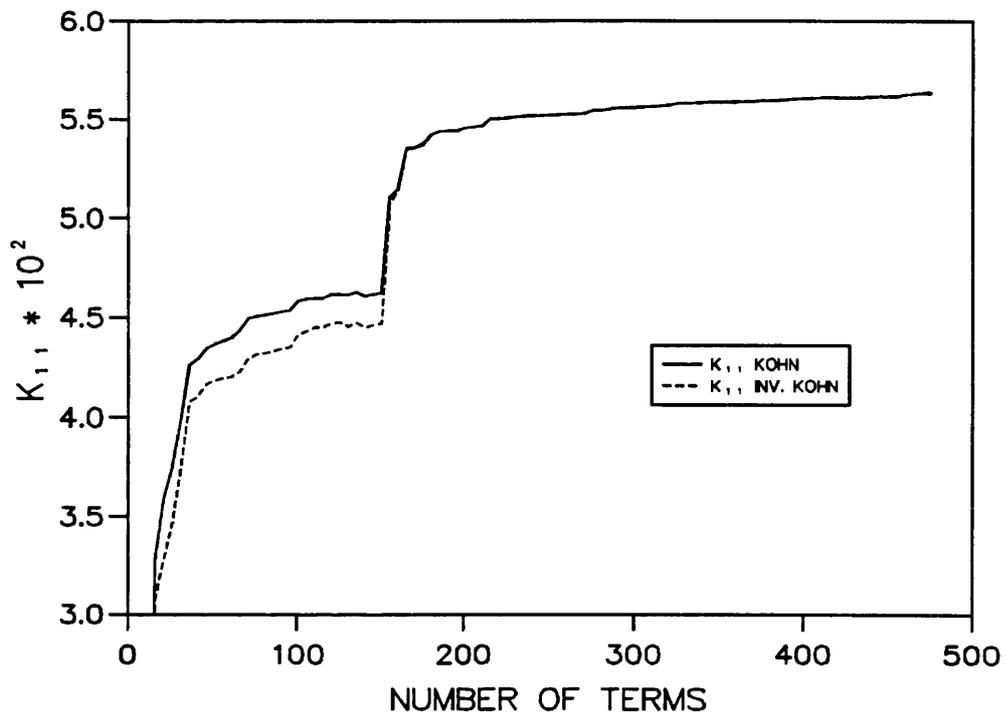
Figure 7.4: The variation of the K matrix element K_{11} with the number of terms in the trial function for p-wave scattering at k= 1.144 (a.u.) and k= 1.174 (a.u.) with up to 150 terms in the first symmetry and up to 330 terms in the second.
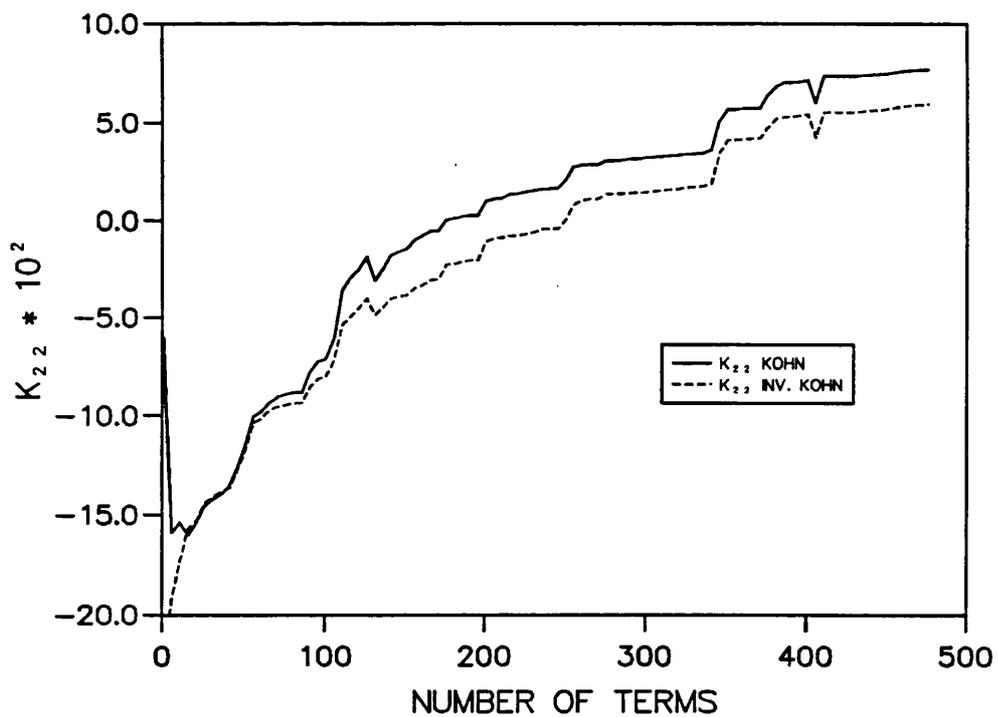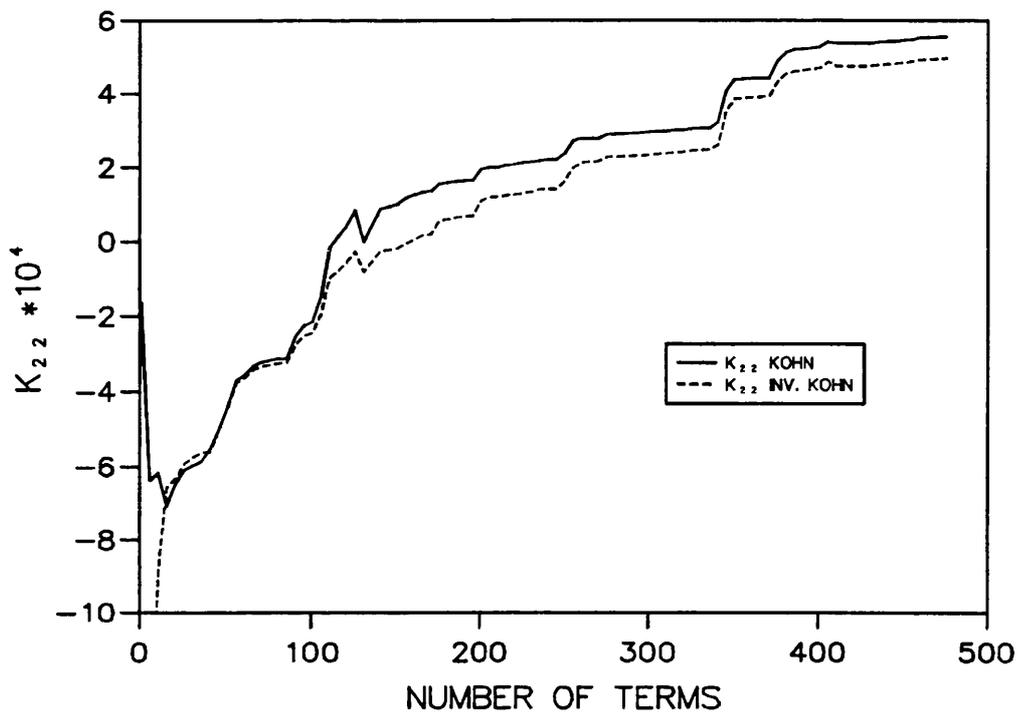
Figure 7.5: The variation of the K matrix element K_{22} with the number of terms in the trial function for p-wave scattering at k= 1.144 (a.u.) and k= 1.174 (a.u.) with up to 150 terms in the first symmetry and up to 330 terms in the second.
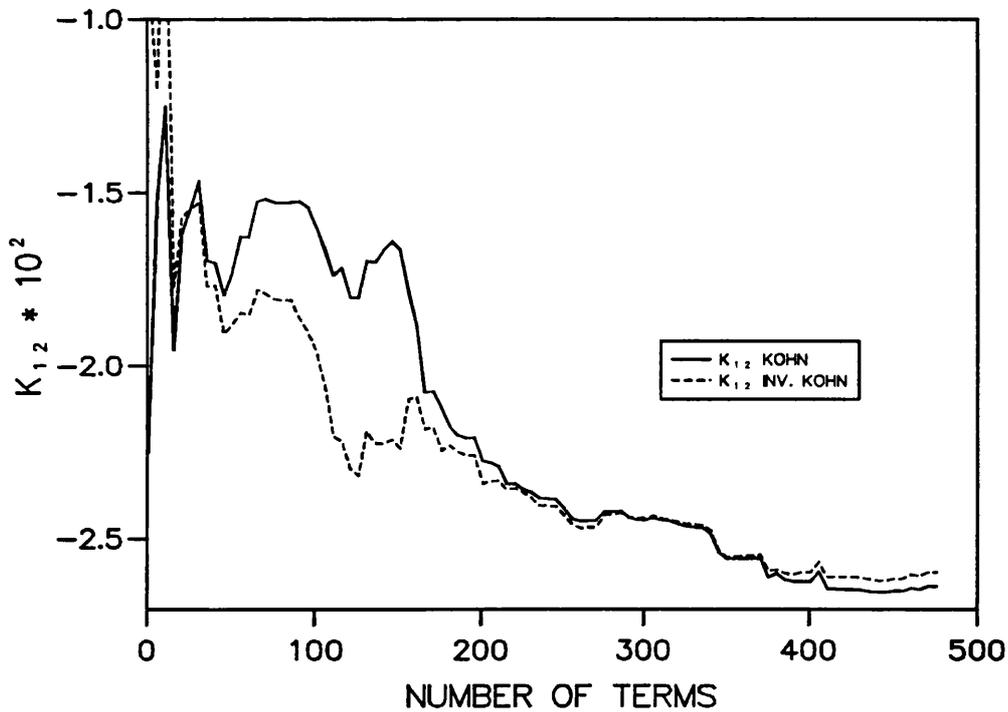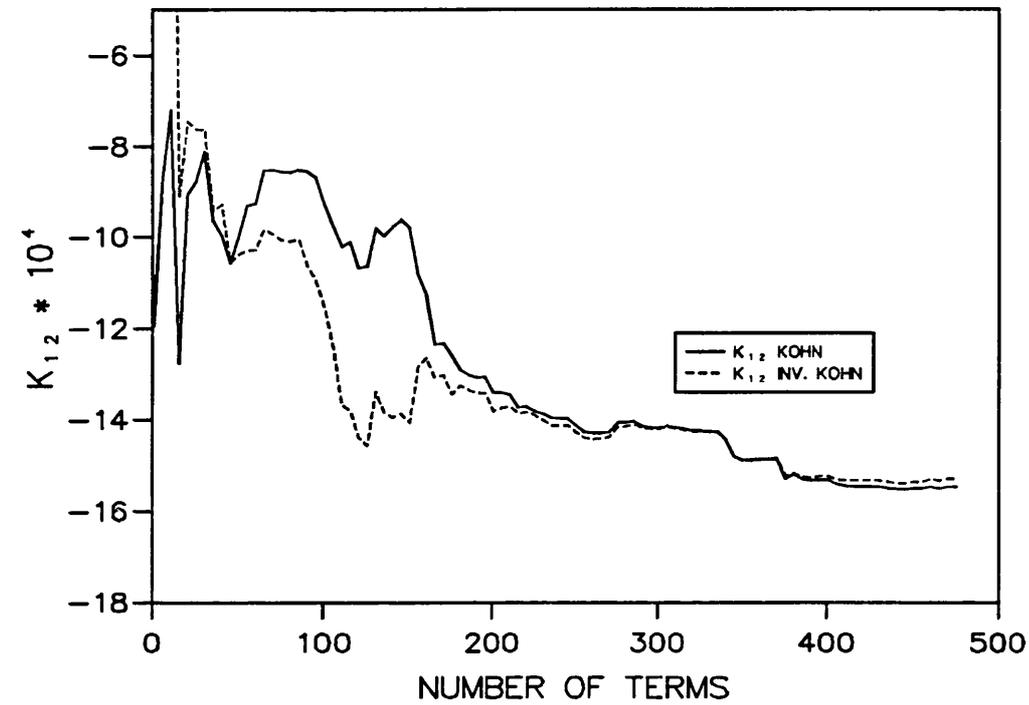
Figure 7.6: The variation of the K matrix element K_{12} with the number of terms in the trial function for p-wave scattering at k= 1.144 (a.u.) and k= 1.174 (a.u.) with up to 150 terms in the first symmetry and up to 330 terms in the second.

141
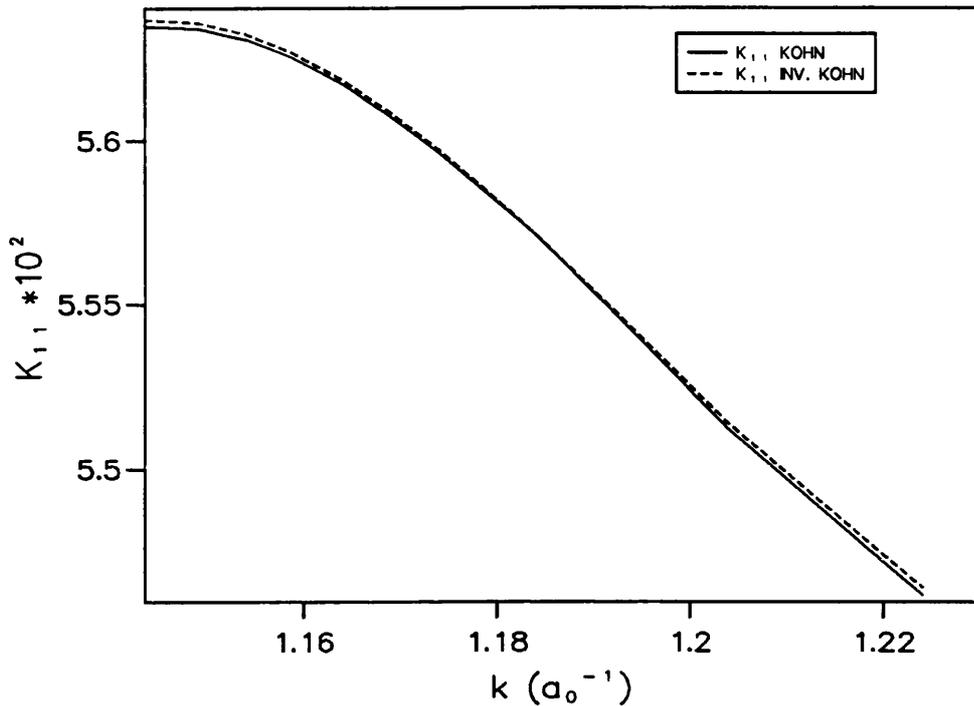
Figure 7.7: The variation of the K matrix element K_{11} with positron wave number for p-wave positron-helium scattering with up to 150 terms in the first symmetry and up to 330 terms in the second.

is plotted as a function of positron energy in figure 7.10. There is not such a rapid rise from the threshold as in the s-wave positronium formation cross section, and one sees that there is a nearly linear dependence of σ_{12} on k^2. The magnitude of the p-wave positronium formation cross section is relatively small, reaching only twice the value of the s-wave cross section for the higher energies in the Ore gap. In figure 7.11 we present a comparison of the variational Kohn results and the results of the first Born approximation of McAlinden (1996). We see that, for the higher energy region, the ratio of the two cross sections is approximately three, very similar to that found in hydrogen (Humberston 1996). As was the case in s-wave positron-helium scattering, there has been no previous detailed investigation of the p-wave scattering within the Ore gap, and the only results with which comparisons can be made are those of Mandal et al. (1979). They quote a p-wave positronium formation cross section of 0.0583 πa_0^2 at 20 eV which is approximately five times larger than that found in this work. As there are no other energies in the Ore gap
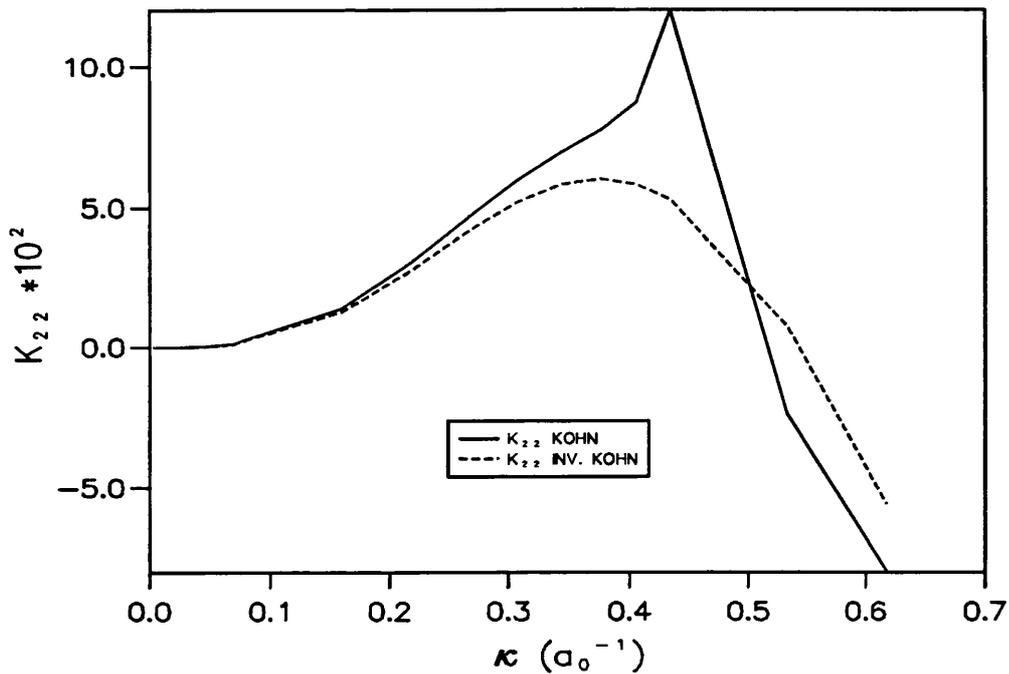
Figure 7.8: The variation of the K matrix element K_{22} with positronium wave number for p-wave positron-helium scattering with up to 150 terms in the first symmetry and up to 330 terms in the second.
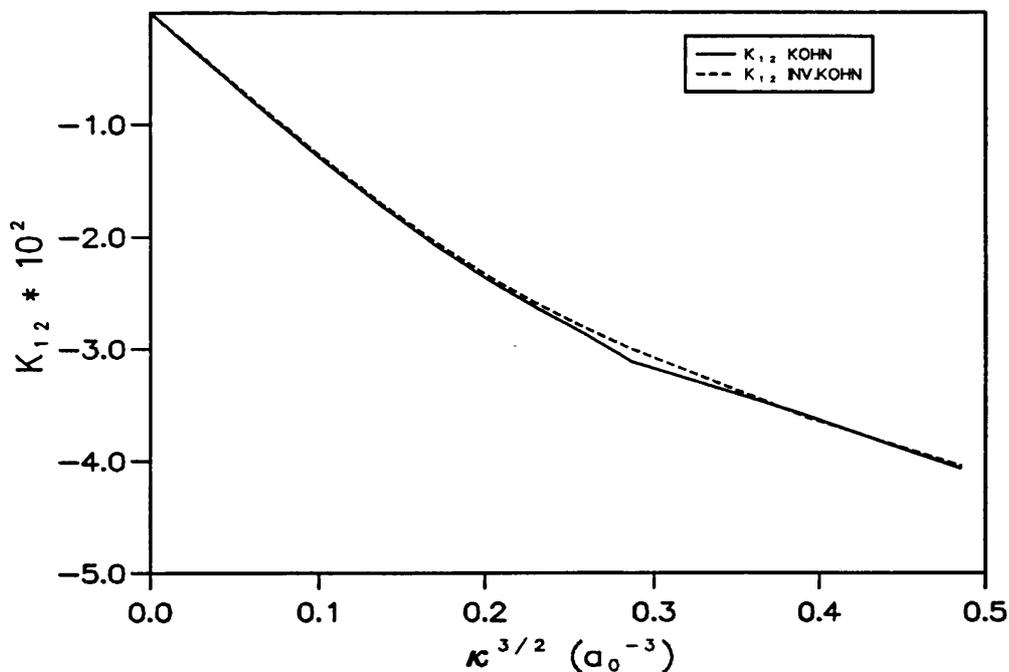

Figure 7.9: The variation of the K matrix element K_{12} with positronium wave number for p-wave positron-helium scattering with 150 terms in the first symmetry and 330 terms in the second.
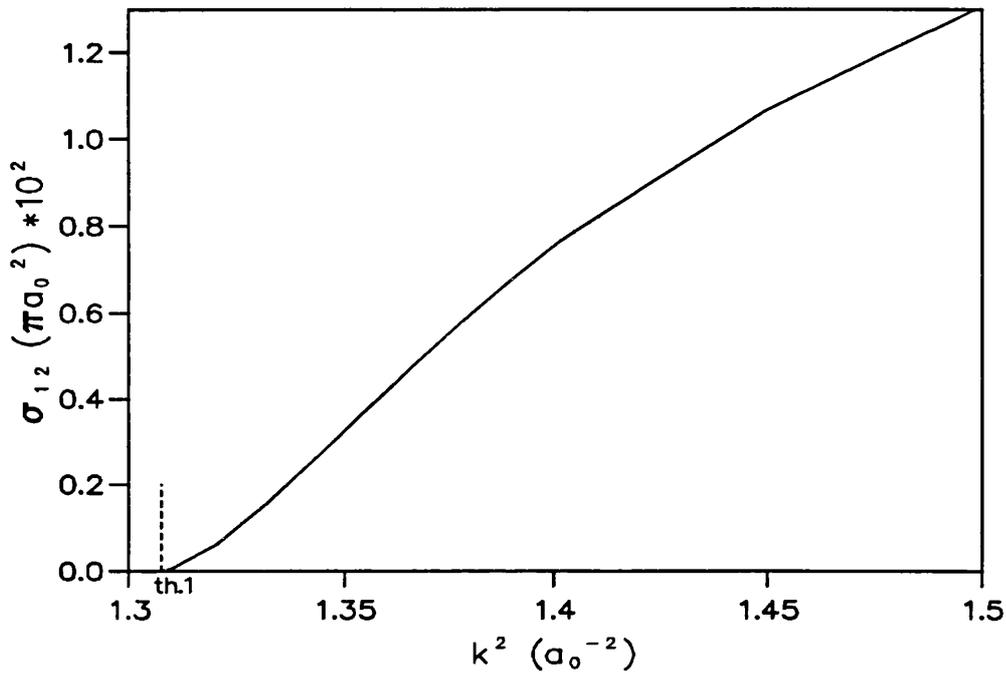
Figure 7.10: The variation of the p-wave positronium formation cross section with positron energy for positron-helium scattering.
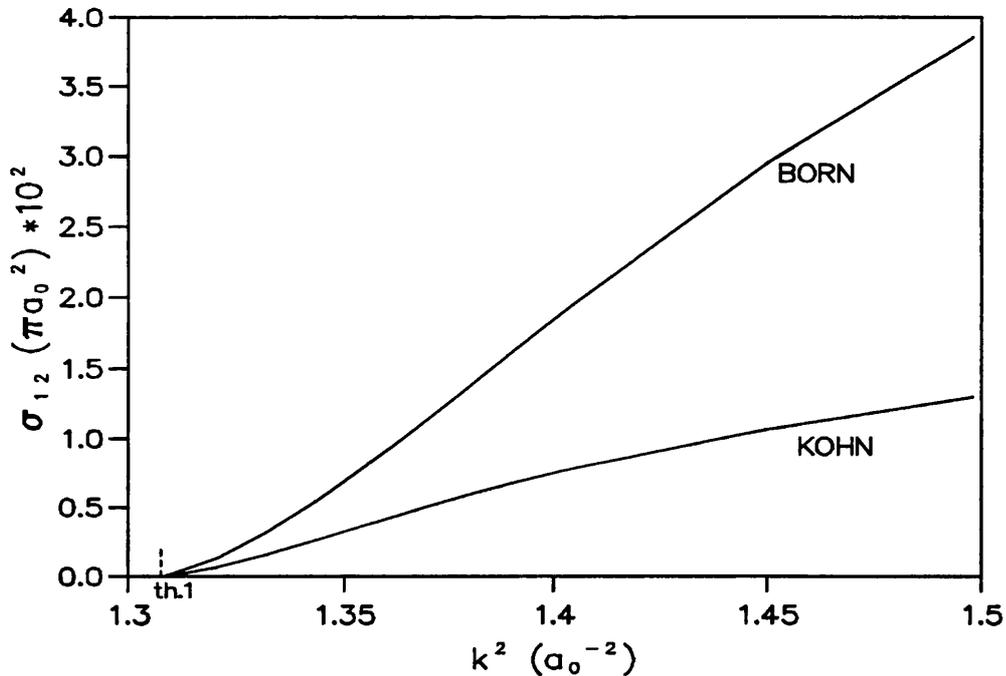

Figure 7.11: Comparison of the variation of the p-wave positronium formation cross section with positron energy for p-wave positron-helium calculated with the first Born approximation and the Kohn variational method.

at which these authors have calculated the positronium formation cross section, it is very difficult to make a meaningful comparison. The only information which may indicate a weakness in the results of Mandal et $al.$, is that their results for positron-hydrogen scattering, which is a much simpler system, do not agree with the various very accurate results.
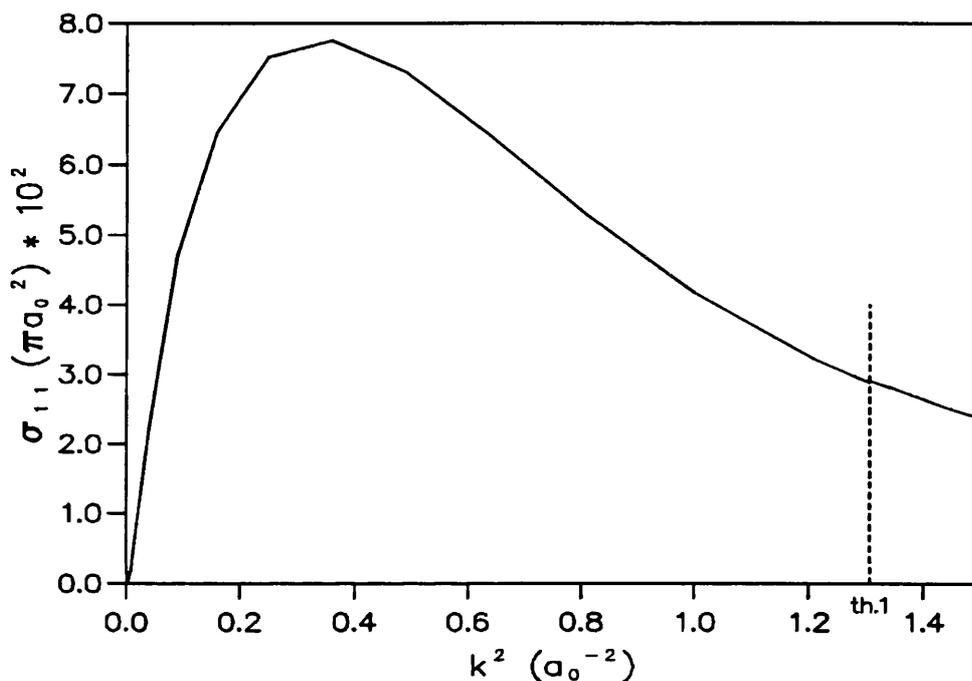

Figure 7.12: The variation of the p-wave elastic scattering cross section with positron energy for positron-helium scattering.

In figure 7.12 we present the p-wave elastic scattering cross section above and below the positronium formation threshold. The results below the threshold have been calculated using a p-wave scattering trial function similar to that used in the s-wave calculation (see equation 6.5), including both types of short-range terms. These results did not display the same behaviour as those above the threshold, but for consistency we have included the same number of terms in each symmetry for all energies. In the Ore gap, the p-wave elastic scattering cross section is found to be $\approx 20\%$ of the s-wave and again at the threshold a slight discontinuity in the cross section can be noted. We have not investigated this discontinuity because the magnitude of the p-wave cross section at threshold would make any effect very

145

small. Also, as the uncertainty in σ_{11}, due to various problems described above, is significantly greater above the threshold than below, it is very unlikely that exact matching of the cross sections at the threshold could be achieved.

7.4 The d-wave wavefunction and matrix elements

The d-wave trial function and matrix elements are derived using the same formalism as the one developed for p-wave scattering, but now, as $l=2$, there are three different symmetries of short-range correlation terms, one of which represents the total angular momentum shared between the positron and one of the target electrons.

The three combinations which give the correct total angular momentum are: $(l_1 = 2, l_2 = 0)$, $(l_1 = 1, l_2 = 1)$ and $(l_1 = 0, l_2 = 2)$. The first and third cases, referred to as first and third symmetries, can only have $m_1 = m_2 = 0$, and we have

$$\psi(2,0,2,0) = Y_{20}(\theta_1, \phi_1) Y_{00}(\theta_2, \phi_2) < 2,0,0,0 \mid 2,0 > \qquad (7.23)$$

and

$$\psi(0,2,2,0) = Y_{00}(\theta_1, \phi_1) Y_{20}(\theta_2, \phi_2) < 0,0,2,0 \mid 2,0 > . \qquad (7.24)$$

Again, as in the p-wave calculation, both the Clebsch-Gordan coefficients and the first order spherical harmonics. $Y_{00}(\theta, \phi)$, will be absorbed into the variational parameters of the short-range terms and we only need to consider the second order spherical harmonics which are of the form

$$Y_{20}(\theta, \phi) = \sqrt{\frac{5}{4\pi}} \left(\frac{3}{2} \cos^2 \theta - \frac{1}{2} \right) . \qquad (7.25)$$

The main difference in the formulation as compared to the p-wave scattering formulation is the second symmetry case with $(l_1 = 1, l_2 = 1)$. From equations 7.4 and 7.5, we see that there are now three sets of values of m which need to be considered, and we have

$$
\begin{aligned}
\psi(1,1,2,0) = {} & Y_{1,-1}(\theta_1, \phi_1) Y_{1,+1}(\theta_2, \phi_2) < 1,-1,1,+1 \mid 2,0 > \\
& + Y_{1,0}(\theta_1, \phi_1) Y_{1,0}(\theta_2, \phi_2) < 1,0,1,0 \mid 20 > \\
& + Y_{1,+1}(\theta_1, \phi_1) Y_{1,-1}(\theta_2, \phi_2) < 1,+1,1,-1 \mid 2,0 > \qquad (7.26)
\end{aligned}
$$

Using the first order spherical harmonics, $l = 1$, for $m = 0$ given in equation 7.10 and those for $m = \pm 1$ which are

$$Y_{1,+1}(\theta, \phi) = -\sqrt{\frac{3}{8\pi}} \sin\theta e^{i\phi} \tag{7.27}$$

$$Y_{1,-1}(\theta, \phi) = +\sqrt{\frac{3}{8\pi}} \sin\theta e^{-i\phi}, \tag{7.28}$$

we find that, including the appropriate Clebsch-Gordan coefficients,

$$\psi(1,1,2,0) = \frac{3}{4\pi}\left[\frac{1}{\sqrt{6}}\right](3\cos\theta_1\cos\theta_2 - \cos_{12}). \tag{7.29}$$

The form of the two component d-wave scattering trial function is then

$$
\begin{aligned}
\Psi_1^t &= Y_{20}(\theta_1)S_1 + Y_{2,0}(\theta_1)K_{11}^t C_1 + \frac{(1+P_{23})}{\sqrt{2}}Y_{20}(\theta_\rho)K_{21}^t C_2 \\
&\quad + Y_{20}(\theta_1)(1+P_{23})\sum_{i=1}^{N} r_1^2 a_i \phi_i + (1+P_{23})\left[\psi_{(1,1,2,0)}(\theta_1,\theta_2)\sum_{i=1}^{N} r_1 r_2 b_i \phi_i\right] \\
&\quad + (1+P_{23})\left[Y_{20}(\theta_2)\sum_{i=1}^{N} r_2^2 c_i \phi_i\right]
\end{aligned}
\tag{7.30}
$$

$$
\begin{aligned}
\Psi_2^t &= \frac{(1+P_{23})}{\sqrt{2}}Y_{20}(\theta_\rho)S_2 + \frac{(1+P_{23})}{\sqrt{2}}Y_{20}(\theta_\rho)K_{22}^t C_2 + Y_{20}(\theta_1)K_{12}^t C_1 \\
&\quad + Y_{20}(\theta_1)(1+P_{23})\sum_{j=1}^{N} r_1^2 d_j \phi_j + (1+P_{23})\left[\psi_{(1,1,2,0)}(\theta_1,\theta_2)\sum_{j=1}^{N} r_1 r_2 f_j \phi_j\right] \\
&\quad + (1+P_{23})\left[Y_{20}(\theta_2)\sum_{j=1}^{N} r_2^2 g_j \phi_j\right],
\end{aligned}
\tag{7.31}
$$

where we have used a similar notation to that in the s-wave and p-wave calculations.

The second order Bessel and Neumann functions for d-wave scattering are

$$j_2(kr) = \left[\frac{3}{k^3 r^3} - \frac{1}{kr}\right]\sin(kr) - \frac{3}{k^2 r^2}\cos(kr) \tag{7.32}$$

and

$$n_2(kr) = -\left[\frac{3}{k^3 r^3} - \frac{1}{kr}\right]\cos(kr) - \frac{3}{k^2 r^2}\sin(kr) \tag{7.33}$$

respectively, and the shielding function which removes the singularity in the Neumann function, subject to the conditions of equations 4.8 and 4.10, is, for $n_2(kr_1)$

$$f_{sh}(r_1) = (1 - e^{-\lambda r_1})^5, \tag{7.34}$$

and for $n_2(\kappa\rho)$

$$f_{sh}(\rho) = \left[1 - e^{-\mu\rho}(1 + \frac{\mu}{2}\rho)\right]^7. \tag{7.35}$$

147

The specific forms of the various matrix elements which are required for a d-wave scattering calculation are similar to those of the p-wave scattering matrix elements and, therefore, we will only give a brief description of them, and not their explicit form. The long-range – long-range and long-range – short-range matrix elements are more complex because of the more complicated form of the Bessel and Neumann functions and the associated shielding functions for $l = 2$. The short-range – short-range matrix elements involving first and third symmetry terms are very similar to those found in p-wave scattering, but a more complex external angle integration has to be performed. The elements which involve either only second symmetry, or cross terms between second symmetry and either first or third symmetry terms, are more complicated in both the formulation of the explicit form of the matrix element and also in the external angle integration, mainly because in the second symmetry terms the angular function depends on two external angles. In appendix B, we give the results of the various external angle integrations which are required for a d-wave scattering calculation.

7.5   The d-wave results

We have included in the d-wave trial function only short-range terms of the first and third symmetries because, although most of the formulation for the second symmetry terms has been done, there has not been sufficient time to complete it and to write a reliable computer program to perform the calculations. It is not possible to estimate in a rigorous manner how strongly the omission of the second symmetry terms affects both the convergence of the K matrix elements and the magnitude of the cross sections. The only guide that we have is the calculation of the d-wave positron-hydrogen K matrix elements (Watts 1994), from which we have found that the removal of the second symmetry terms does not change the values of the K matrix elements significantly (see table 7.1). We see that the removal of the third symmetry affects the K_{22} and K_{12} matrix elements strongly, while the removal of the first symmetry affects mostly K_{11} and less K_{22}.

148

	K_{11}	K_{12}	K_{21}	K_{22}
all three symmetries	0.10806E+00	0.97455E-01	0.97455E-01	0.18033E+00
only first and third	0.10676E+00	0.97374E-01	0.97374E-01	0.17678E+00
only first and second	0.10217E+00	0.90257E-01	0.90257E-01	0.11683E+00
only second and third	0.63984E-01	0.96995E-01	0.96995E-01	0.14018E+00
only first	0.99390E-01	0.88997E-01	0.88997E-01	0.10929E+00

Table 7.1: Analysis of the removal of a symmetry in the calculation of the d-wave K matrix elements for positron-hydrogen scattering. $\omega = 6$ in each symmetry and k=0.75 (a.u.).

We believe that, although this analysis of positron-hydrogen d-wave scattering can only serve as a guide, we can estimate that our positron-helium d-wave K matrix elements are not affected by more than a few percent because of the omission of the second symmetry terms. On the other hand, we must recognise that, as both systems are very different, there may be physical factors, such as the inclusion of exchange in the positron-helium case, which make the effect of the second symmetry less important for positron-hydrogen scattering than for positron-helium scattering.

The non-linear parameters α, β, μ and λ have been optimized in a similar manner to that used in the s-wave and p-wave calculations, and the same values as in the p-wave trial function were found to give the best compromise between the optimization of K_{11} and K_{22}. As was seen in the p-wave calculation, the poorer representation of the positronium - He$^+$ system has lead to a greater difference between the Kohn and inverse Kohn results for K_{22} than for K_{11}.

We have calculated the K matrix elements for positron-helium scattering in the Ore gap, with a trial function containing 84 short-range terms ($\omega = 4$) of the first symmetry and 172 terms ($\omega = 5$) of the third symmetry (with the power of r_{23} even only), and we have found a similar behaviour for the variation of the K matrix elements with respect to the number of short-range terms in the trial function as that described in the analysis of the p-wave results. We believe that the resonance-
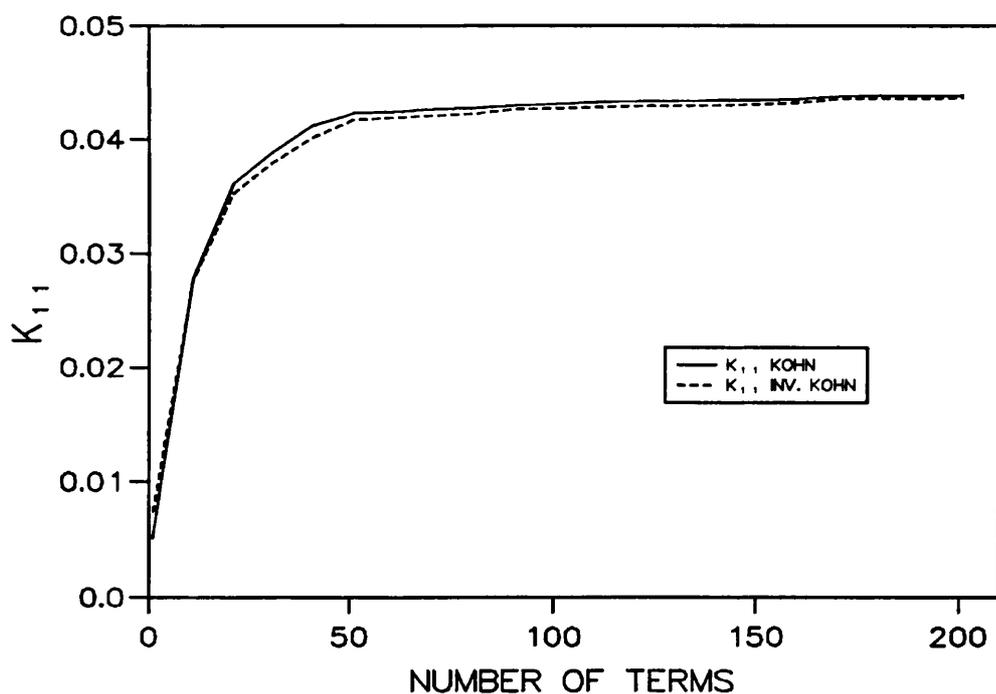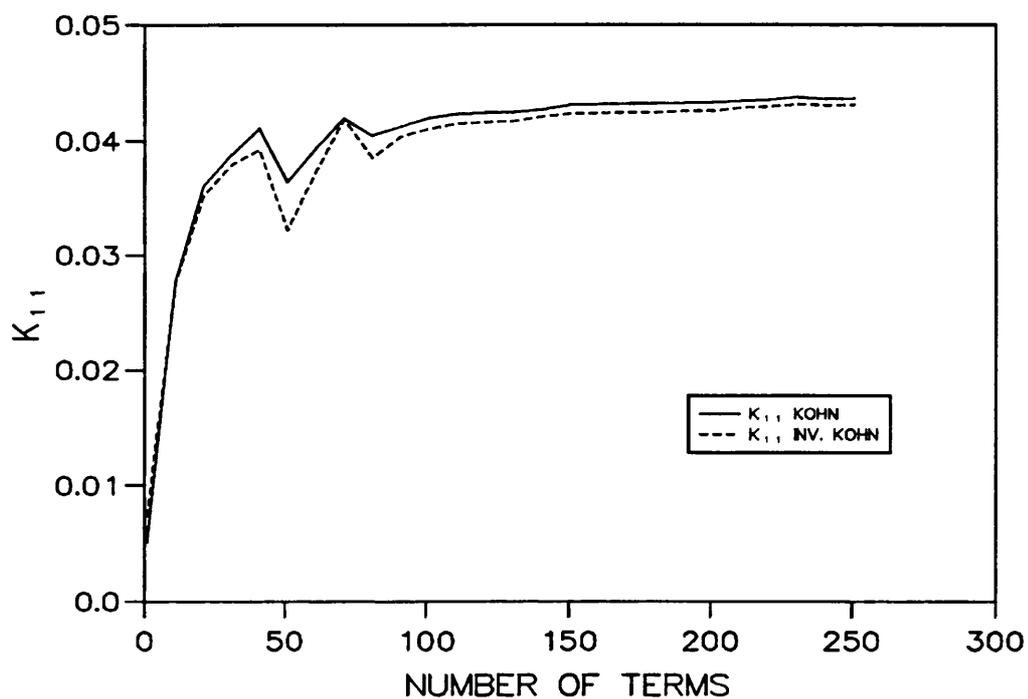
Figure 7.13: The variation of the K matrix element K_{11} with the number of terms in the trial function for d-wave scattering at k= 1.144 (a.u.). Top figure: up to 84 short-range terms ($\omega = 4$) in the first symmetry and up to 172 terms ($\omega = 5$) in the third symmetry. Bottom figure: up to 36 short-range terms ($\omega = 3$) in the first symmetry and up to 172 terms ($\omega = 5$) in the third symmetry.

150
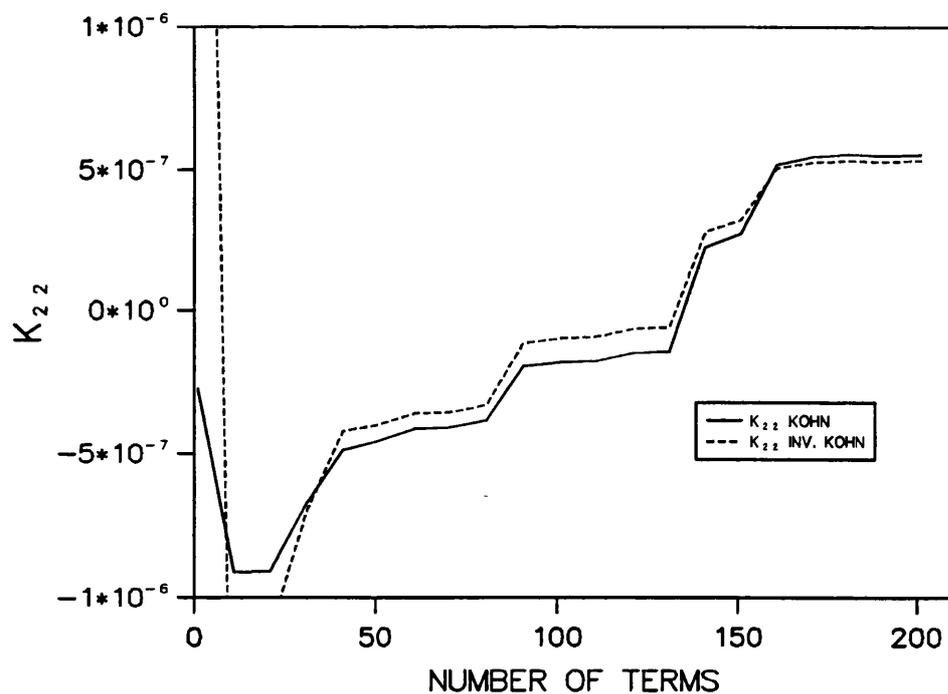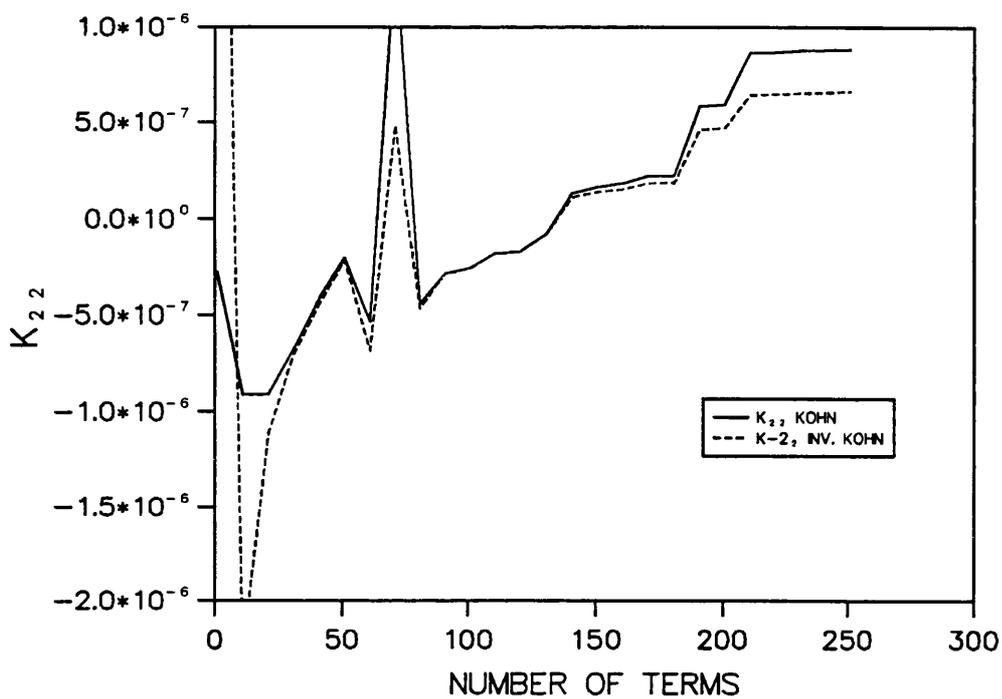
Figure 7.14: The variation of the K matrix element K_{22} with the number of terms in the trial function for d-wave scattering at k= 1.144 (a.u.). Top figure: up to 84 short-range terms ($\omega = 4$) in the first symmetry and up to 172 terms ($\omega = 5$) in the third symmetry. Bottom figure: up to 36 short-range terms ($\omega = 3$) in the first symmetry and up to 172 terms ($\omega = 5$) in the third symmetry.

151
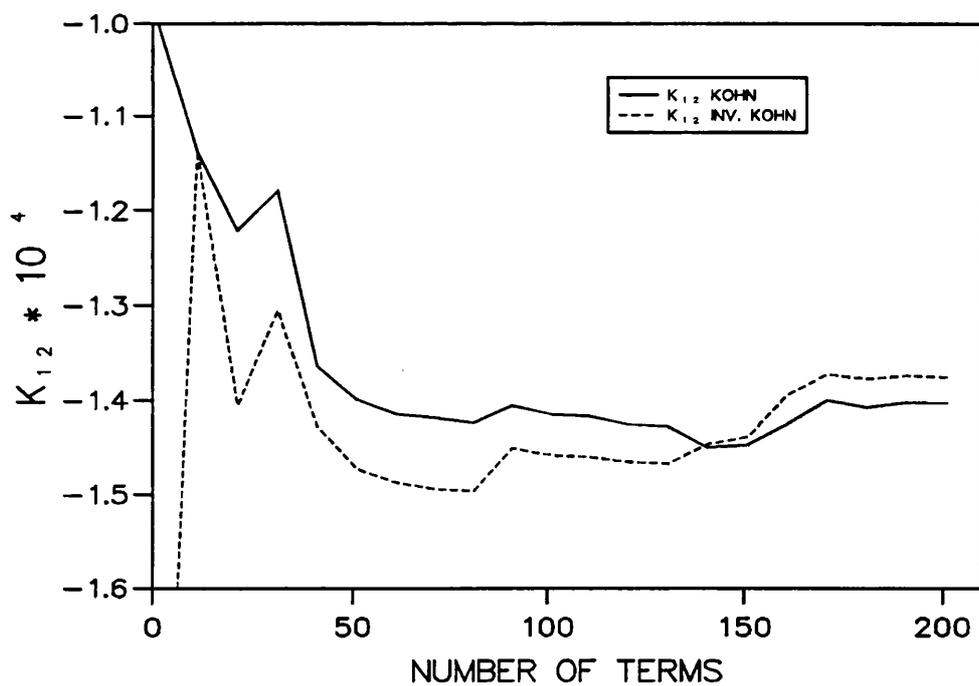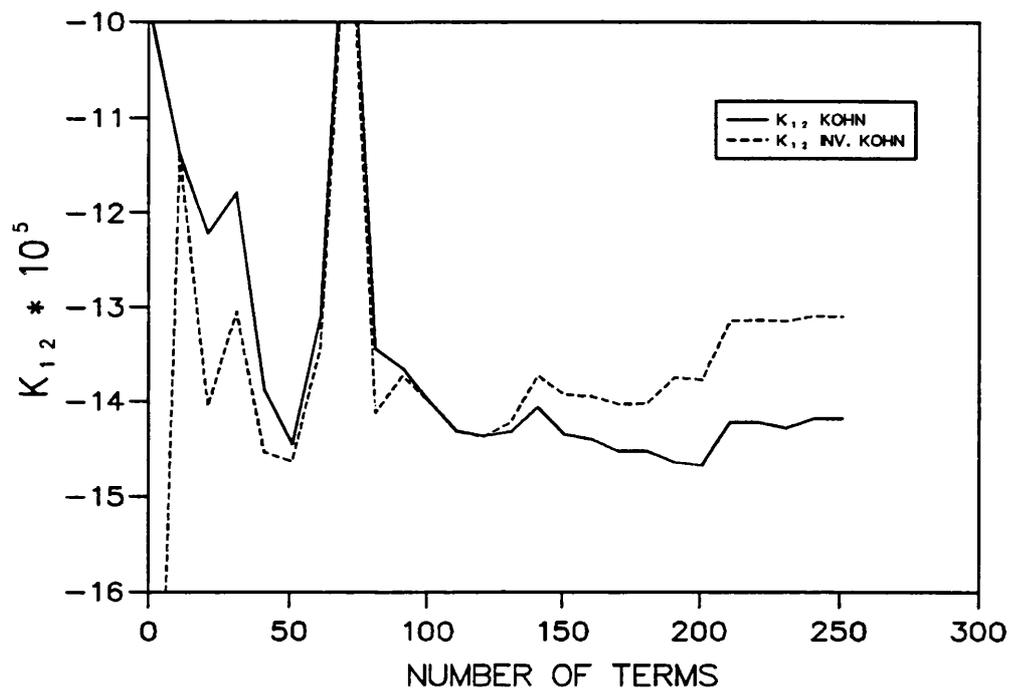
Figure 7.15: The variation of the K matrix element K_{12} with the number of terms in the trial function for d-wave scattering at k= 1.144 (a.u.). Top figure: up to 84 short-range terms ($\omega = 4$) in the first symmetry and up to 172 terms ($\omega = 5$) in the third symmetry. Bottom figure: up to 36 short-range terms ($\omega = 3$) in the first symmetry and up to 172 terms ($\omega = 5$) in the third symmetry.

152

type features which are found in the d-wave results have the same origin as those in the p-wave calculations and,we have, therefore, used the same technique to reduce their effects. i.e. we have included only 36 short-range terms ($\omega = 3$) of the first symmetry and 172 terms ($\omega = 5$) of the third symmetry. In figure 7.13, 7.14 and 7.15 we compare the results obtained with all the matrix elements and those obtained with the reduced first symmetry, and we can see that there is a great amelioration of both the convergence and the agreement between the Kohn and inverse Kohn results. In figure 7.16 we present the variation of K_{12} with respect to $\kappa^{5/2}$, and
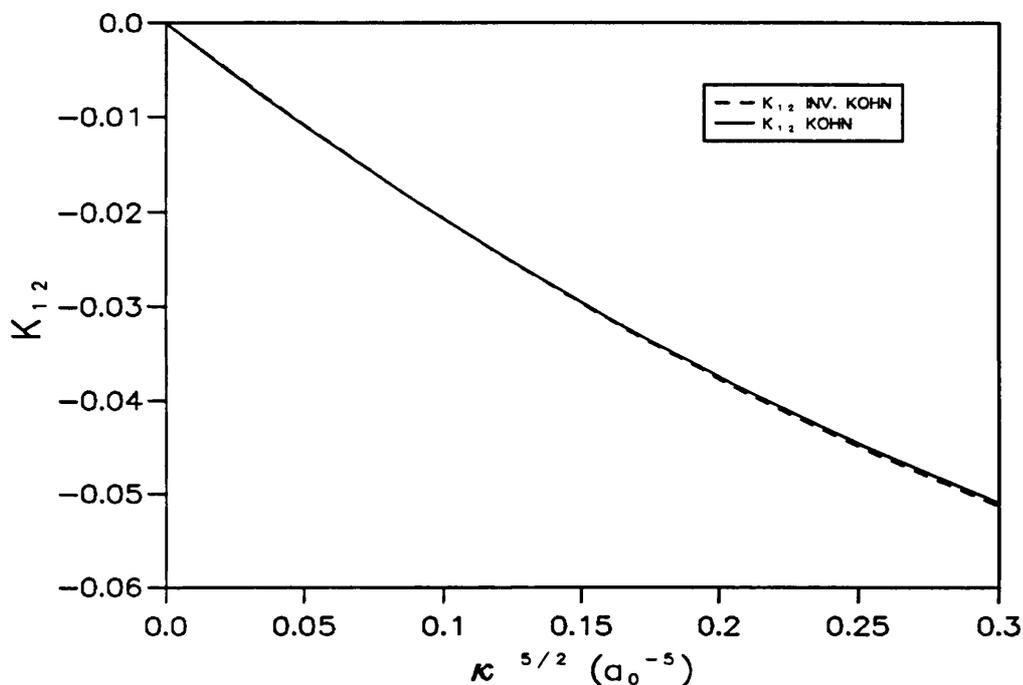
Figure 7.16: The variation of the K matrix elements K_{12} with respect to the positronium wavenumber.

we find that Wigner's threshold law (equation 6.2) is indeed confirmed up to more than 1eV above the positronium formation threshold. As mentioned previously, this is not a very constraining check on our calculation as such, but we believe that the confirmation of the threshold behaviour of the K_{12} matrix element indicates that there is no fundamental error in our calculation which would have given rise to the resonance features we have discussed above.
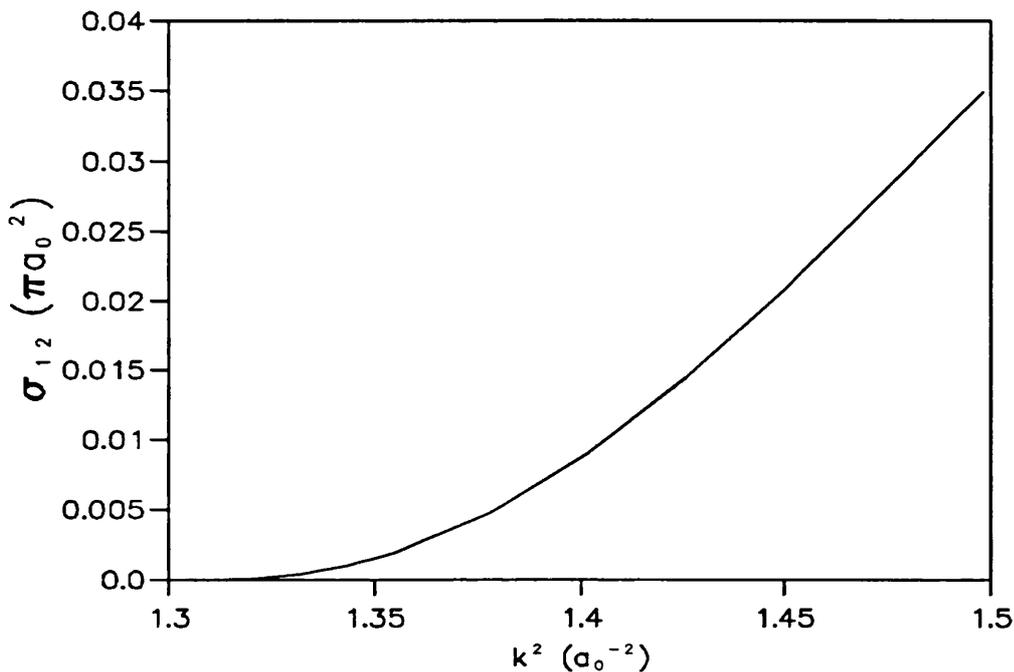
Figure 7.17: The variation of the d-wave positronium formation cross section with positron energy for positron-helium scattering.

The positronium formation cross section for d-wave positron-helium scattering within the Ore gap is presented in figure 7.17. There is a slow rise from threshold, as is expected from the energy dependence of $\sigma_{12}(l = 2)$, and we find that the d-wave positronium formation cross section becomes dominant for energies 1 eV above the threshold (i.e. at $k^2 \approx 1.41(a.u.)$), reaching a value three times that of the p-wave at the highest energy in the Ore gap. Our results do not agree very well with those of Mandal et al. (1979) who found $\sigma_{12}(l = 2) = 0.0237$ (πa_0^{-2}) at 20 eV, which is $\approx 25\%$ less than the value we have found. In figure 7.18, we present a comparison of our variational results with the Born results of McAlinden (1996) and we find that, as was the case in positron-hydrogen scattering (see Humberston 1986), the Kohn results are now greater than the Born results. Both cross sections are now of comparable magnitude which confirms that the first Born approximation gives more reliable results for the higher partial waves than for the lower ones.

We have calculated the d-wave elastic scattering cross section above and below the positronium formation threshold in a similar manner to that described in the

154
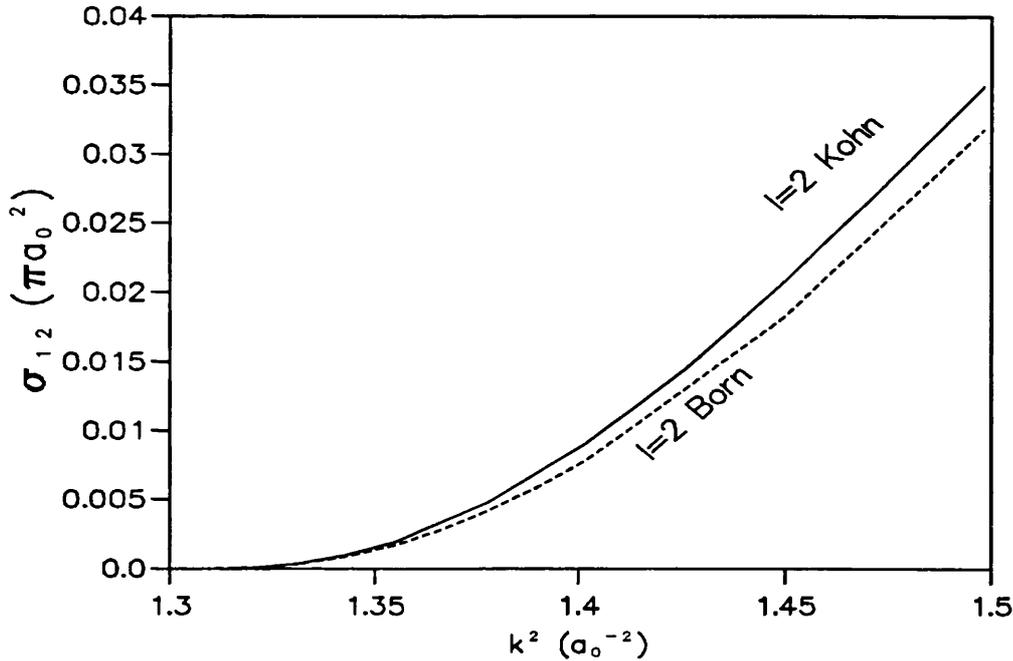
Figure 7.18: Comparison of variation the positronium formation cross section with positron energy for d-wave positron-helium scattering calculated with the first Born approximation and the Kohn variational method.

section on the p-wave elastic scattering cross section. The results are plotted in figure 7.19, and one can see that there is a significant difference between the results just above and just below the threshold. This gap at the threshold is much larger than was the case in the s-wave and the p-wave elastic cross sections, and it is very similar in relative magnitude to that found in positron-hydrogen d-wave elastic scattering (Watts 1994). Again, as discussed in the section on the s-wave elastic scattering cross sections, we believe that this phenomenon is due to the poorer convergence below the threshold and that the inclusion in the elastic scattering trial function of a virtual positronium term is needed to ensure the continuity of the cross section at the threshold. There was not sufficient time to include such a term in our calculation and it is not expected that any threshold features will be found in the d-wave elastic scattering cross section similar to that found in the s-wave case. The elastic phaseshifts of this work below the threshold agree very well with those of Campeanu (1977) for $k \geq 0.6$ ($a.u.$) and the difference at the lower energy is mainly

155
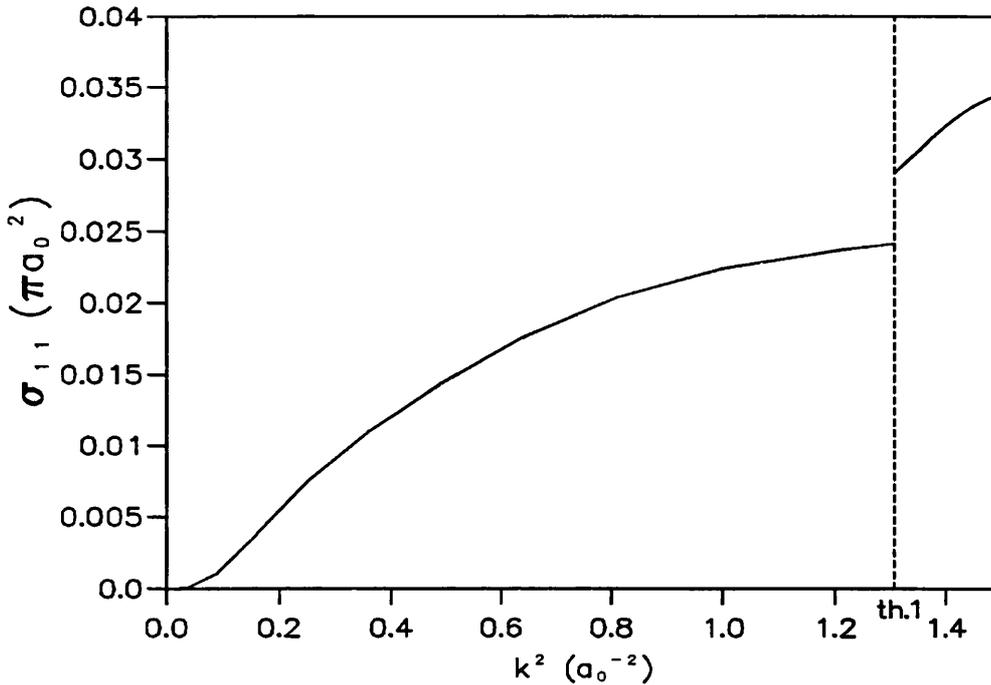
Figure 7.19: The variation of the d-wave elastic scattering cross section with positron energy for positron-helium scattering (th.1 is the threshold for positronium formation).

due to the fact that the trial function in this work has been optimized for the higher energies. The results we obtain for the d-wave elastic scattering cross section in the Ore gap are seen to increase smoothly with energy, and they are found to be $\approx 50\%$ greater than those of McEachran et $al.$(1996).

7.6 The total cross sections and the comparison with experiment.

We have not used the Kohn variational method to evaluate the scattering parameters of positron-helium scattering for partial waves with $l > 2$ because of the complexity of both the formulation and the numerical evaluation. Indeed, as can be seen from the formulation for d-wave scattering, an increase in l not only involves an increase

in the number of symmetries which need to be included into the trial function, but it also involves much more complex external angular functions for which the analytical integration becomes more difficult.

Fortunately, it is well established that because the centrifugal term, $l(l+1)/r^2$, becomes more effective at keeping the positron away from the nucleus as l increases, the role of the short-range terms becomes less significant for the higher partial waves. Hence, the results obtained with more approximate methods than the Kohn variational method (for instance the first Born approximation, where no attempt is made to include short-range interactions) are expected to be sufficiently reliable. Also, we find that, as was the case in positron-hydrogen scattering, for both positronium formation and elastic scattering, the contribution from the sum of all the partial waves with $l > 2$ is much smaller than the sum of the s-, p- and d-wave contribution. Therefore, the errors in the cross sections for the higher partial waves are not expected to contribute very significantly to the error in the total positronium formation and elastic scattering cross sections.

We have chosen to evaluate the partial wave elastic scattering cross sections for $l > 2$, below the positronium formation threshold. with the approximation formula for the elastic phaseshift of O'Malley et al (1962).

$$\eta_l = \frac{\pi \alpha k^2}{(2l-1)(2l+1)(2l+3)}, \tag{7.36}$$

where α is the dipole polarizability of the helium atom. We have also used the same formula above the threshold for these higher partial waves, even though it does not take into account the coupling of the positronium formation channel. We believe this choice to be reasonable because for these higher partial waves the coupling is expected to be very small and, as their contribution is also small, the error introduced into the total elastic cross section will be relatively small. From figure 7.20 we can see from the $l > 2$ curve that the smooth continuation of the cross section through the threshold confirms the validity of our choice. In figure 7.20 we present the total elastic scattering cross section for positron-helium scattering above and below the positronium formation threshold, together with the individual contributions of the first three partial waves. The sum up to $l = 60$ of all partial waves with
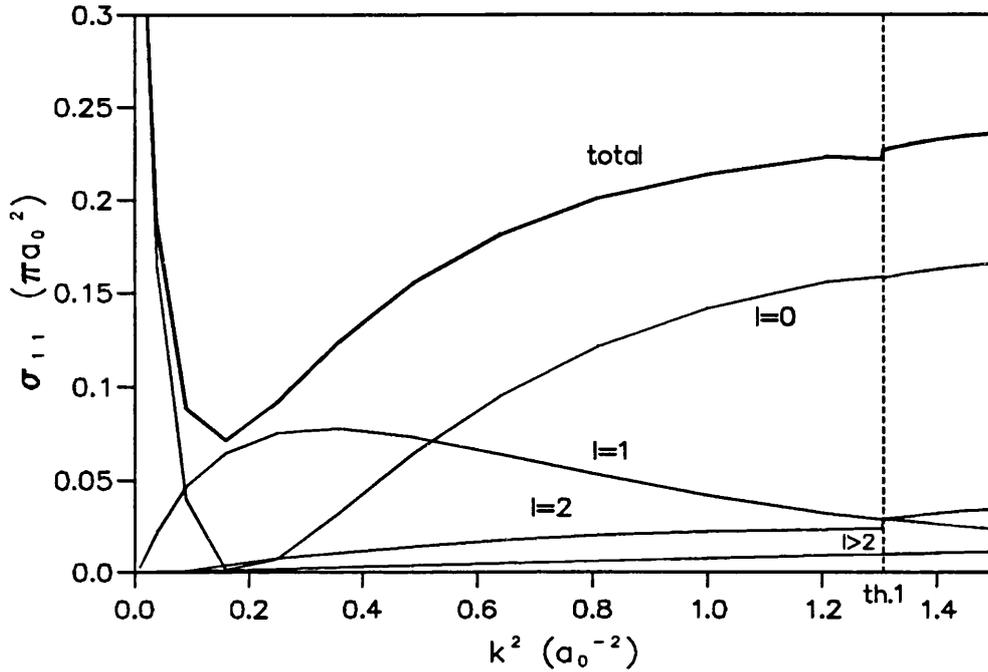
Figure 7.20: The variation of the elastic scattering cross section with positron energy for positron-helium scattering. The $l = 0$, $l = 1$ and $l = 2$ results were obtained with the Kohn variational method. The $l > 2$ results were obtained using equation 7.36.

$l > 2$, calculated using 7.36, is plotted as curve labelled $l > 2$, and it is found to contribute $\approx 5\%$ to the total elastic cross section in the Ore gap. One can see that the discontinuity at the positronium formation threshold due to the d-wave component is significant and that within the Ore gap the elastic scattering cross section increases only very slightly with positron energy.

The contribution to the total positronium formation cross section from all partial waves with $l > 2$ has been evaluated using the total positronium formation cross section calculated in the first Born approximation by McAlinden (1996), and subtracting the contributions from s-, p- and d-wave scattering calculated by the same author. In figure 7.21, we plot the resulting total positronium formation cross section for positron-helium scattering within the Ore gap together with plots of each component separately up to $l=2$ and the sum of all $l > 2$.
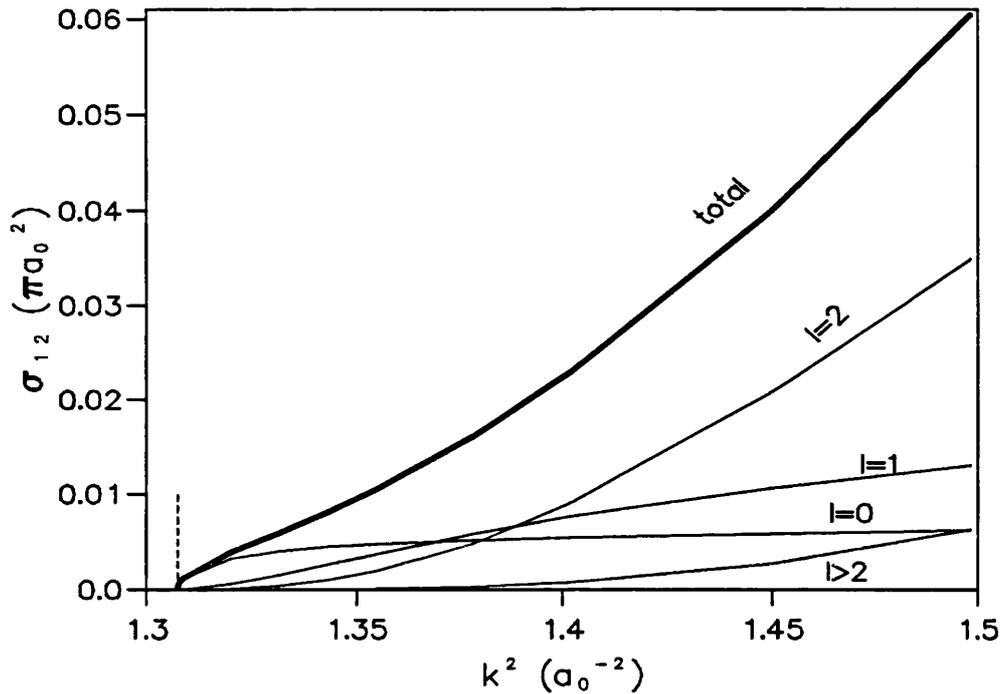
Figure 7.21: The variation of the positronium formation cross section with positron energy for positron-helium scattering. The $l = 0$, $l = 1$ and $l = 2$ results were obtained with the Kohn variational method. The $l > 2$ results were obtained using the first Born approximation by McAlinden (1996).

Again, the threshold behaviour of σ_{12} is clearly seen with the initial rapid rise due solely to the s-wave component. Also, the d-wave component is confirmed as becoming the dominant component for positron energies greater than 1eV above the threshold, rising to more than 50% of the total cross section at the highest energy calculated. The contribution of partial waves with $l > 2$ is found to be $\approx 10\%$ of the total cross section for the highest energy, approximately equal to the s-wave component. We believe it is possible that the Born approximation may underestimate the contribution of the $l > 2$ cross sections and that there are two main reasons for this. First, as can be seen from the comparison of the Kohn results with the first Born results for s-, p- and d-wave positron-helium scattering (see figures 6.16,7.11 and 7.18), when l increases not only does the agreement between the Born and the Kohn improve, going from a ratio of ≈ 200 for s-wave to nearly 1 for the d-wave, but we also notice that for the d-wave the Born results of McAlinden

159

are lower than the Kohn results of this work. A similar pattern was found in the ratio of the Born and Kohn results for positron-hydrogen scattering (Humberstom 1986) and this seems to indicate that the Born results for $l > 2$ are likely to be too low. The second reason which makes us estimate the higher partial waves contributions to the total cross section should be larger is the fact that as the d-wave component is the main contributor at the higher energies, it is likely that the f-wave and g-wave components will also be contributing significantly at these energies to the total positronium formation cross section.
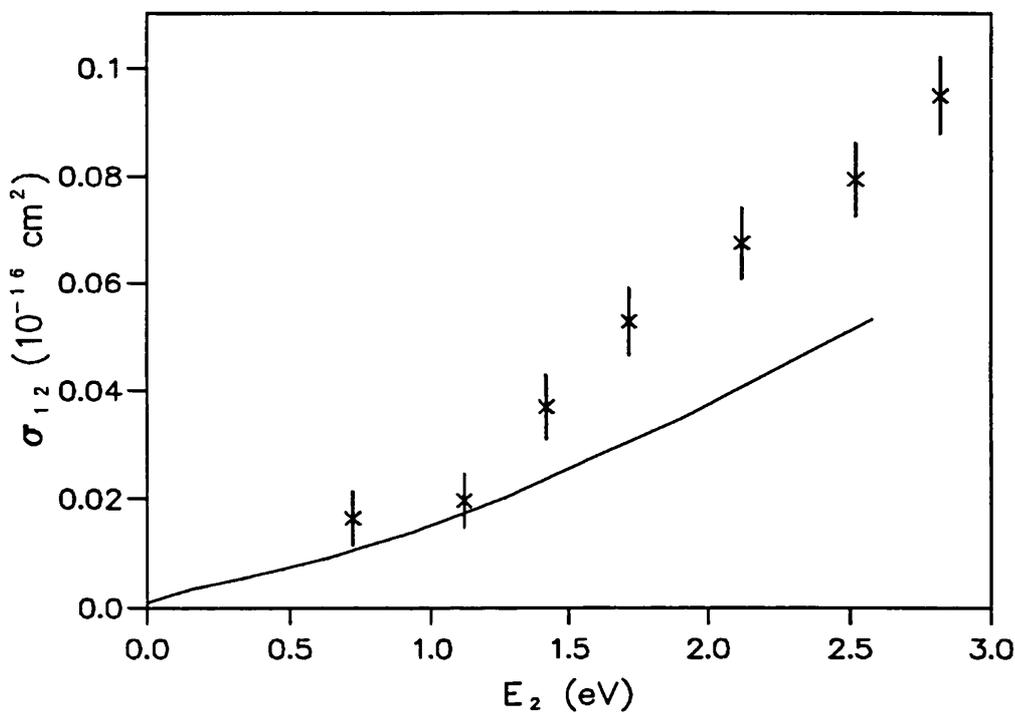
Figure 7.22: Comparison of theoretical and experimental total positronium formation cross section for positron-helium scattering. E_2 is the excess energy of the positron, i.e. $E_2 = E_{e+} - E_{Th}$. The experimental data ($\times$) are those of Moxom *et al.* (1994)

In figure 7.22 we present a comparison of the theoretical positronium formation cross section within the Ore gap with the experimental results of Moxom *et al.* which agree well with other experimental data (see figure 1.3). We find that our results are on average 30% lower than the experimental data and display a less pronounced

slope. There are both theoretical and experimental considerations which we believe can explain the discrepancy between our results and experiment. First, we recognise that there is still a possibility that some formulation or computational error is present in our calculation. We have checked thoroughly all the computer programs as well as the formulations and believe that both the reasonable convergence pattern we obtain for K_{11} and for K_{12} and the good agreement between the Kohn and inverse Kohn results are proofs of the reliabilty of our calculations. On the other hand, the presence of the non-physical resonances in the p- and d-wave calculations which we have attributed to an over representation from the first symmetry terms, could still be attributed either to a formulation or computational error. We believe that such an error is very unlikely because of the various checks we have made and also because the smooth behaviour of the variation of the K matrix elements with respect to the increase in the number of short range terms is reestablished when second symmetry (or third symmetry for d-wave scattering) terms are introduced. Therefore, it is more likely that part of the disagreement between theory and experiment is due to the fact that the Kohn results for s-, p- and d-wave cross sections are not yet fully converged and also that the Born estimate for the $l > 2$ contribution is too low. The uncertainty in the contribution of the $l > 2$ partial components has been discussed above and can unfortunately not be estimated. Furthermore, it is not possible to extrapolate the results for the positronium formation cross section to find fully converged results as there is no bound on the K_{12} matrix element. However, we believe that, from the behaviour of the convergence patterns for K_{12} we have shown for the s-, p- and d-waves, we can estimate the error in the positronium formation cross section to be in the range 10% to 20%, even though we must recognise that, as there is no bound on K_{12}, fully converged partial cross sections may be lower than those presented here. Also, the omission of second symmetry terms in the d-wave calculation may have a greater effect than we have estimated.

Experimentally, the uncertainties are mainly due to the normalization of the data and the estimate of the positronium formation threshold. The positron data presented here were normalized at very high energy to the total ionization cross sections for electrons and positrons (where $\sigma_I^{tot} = \sigma_I + \sigma_{Ps}$) and the absolute values

are estimated to be accurate $\pm20\%$. Note that this normalization procedure is different to that given in Moxom et $al.$ (1994) and confirms the results of that work (Laricchia, private communication). The positron energy scale, which determines the positronium formation threshold, was calibrated to ±0.1eV by linearizing a plot of the ion yield as a function of energy (see Moxom et $al.$ 1994). In this paper the authors have made an analysis of the threshold behaviour of the experimental results for σ_{12}. From their analysis, they concluded that the main contribution to the positronium formation cross section close to the threshold came from p-wave scattering and they have used this result for the calibration of the positron energy scale. From the theoretical results which we present here, we believe that, even by taking into account the lack of convergence of our results, the p-wave component is not dominant in the Ore gap, but the d-wave is, although not overwhelmingly so. Therefore, there is still an uncertainty in the calibration of the experimental data but we do not expect the error to be such as to explain all the differences between theory and experiment.

In figure 7.23, we present a comparison of the theoretical total cross section, i.e σ_{11} below the threshold and $\sigma_{11} + \sigma_{12}$ above, and the experimental results of Stein et $al.$ (1978) and Mizogawa et $al.$ (1985). We see that the relative difference between theory and experiment is now much smaller, $\approx 10\%$ for the results of Mizogawa et $al.$ and $\approx 5\%$ for those of Stein et $al.$ (for both sets of experiments the uncertanties are estimated to be $\pm5\%$). Again, at the threshold itself the discontinuity in the total theoretical cross section due to the d-wave elastic cross section can be seen, but one can notice that there is a disagreement between theory and experiment as to the value of σ_{tot} at the threshold. If one neglects the unreliable experimental result at the threshold itself, and takes the theoretical value of σ_{tot} just above the threshold (which is mainly σ_{11} and can be considered to be very accurate), there is a difference of nearly 3% between theory and the experiment of Mizogawa et $al.$. Again, this difference is not sufficient to totally resolve the disagreement between theory and experiment but it seems to indicate that the normalization of the data at the threshold and the calibration of the positron energy scale could be an important factor in explaining the differences between theory and experiment.
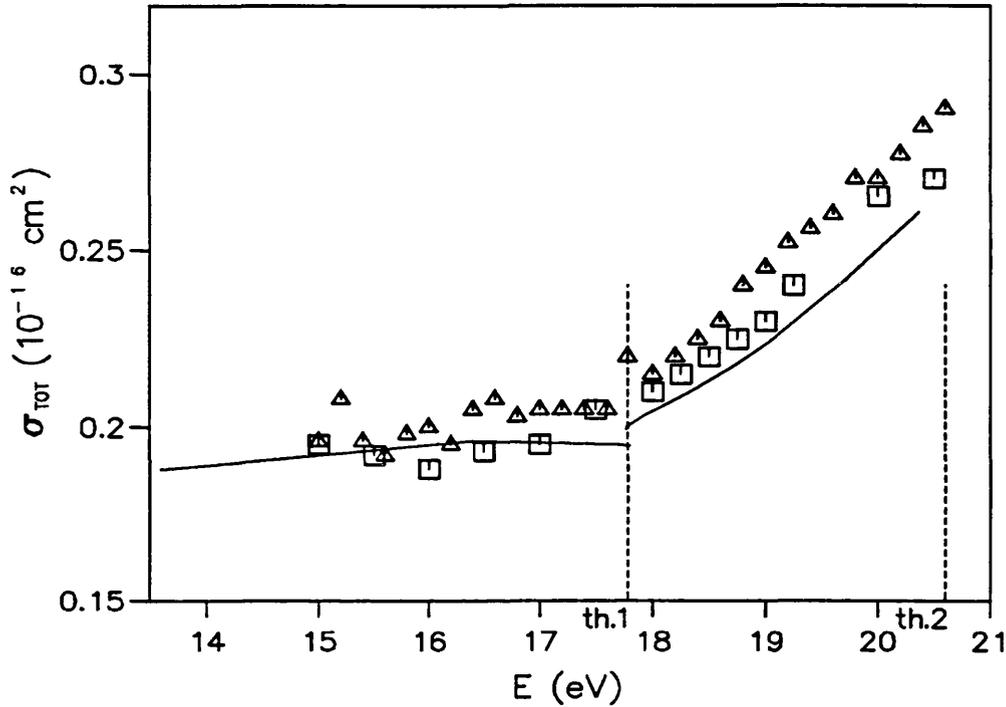
Figure 7.23: Comparison of theoretical and experimental total cross section for positron-helium scattering. The experimental data are those of Stein et al.(1978) ($\square$) and Mizogawa et al. (1985) ($\triangle$).

In figure 7.24 we have plotted the positronium formation cross sections of Moxom et al. (1994) for positron-helium scattering within the Ore gap with respect to the excess positron energy, $E_2 = E_{e^+} - E_{Th}$. We have also included the difference between the total cross section of Mizogawa et al. and the theoretical elastic cross section within the Ore gap, referred to as σ_{12}^A. The theoretical elastic cross section are expected to be correct to within 1-2% and will not affect the uncertainty in σ_{12}^A. Therefore, we believe that, as both experimental data sets have been measured under completely different conditions, we have here two independent measurements of the positronium formation cross section. We can see that there is a reasonable agreement between both sets of data in terms of the magnitude but the slope is slightly different, which may be related to the positron energy calibration procedure of Moxom et al. (1994) (note that, because of the beam resolution, the data points close to the threshold have a larger uncertainty and comparisons there are less reliable).
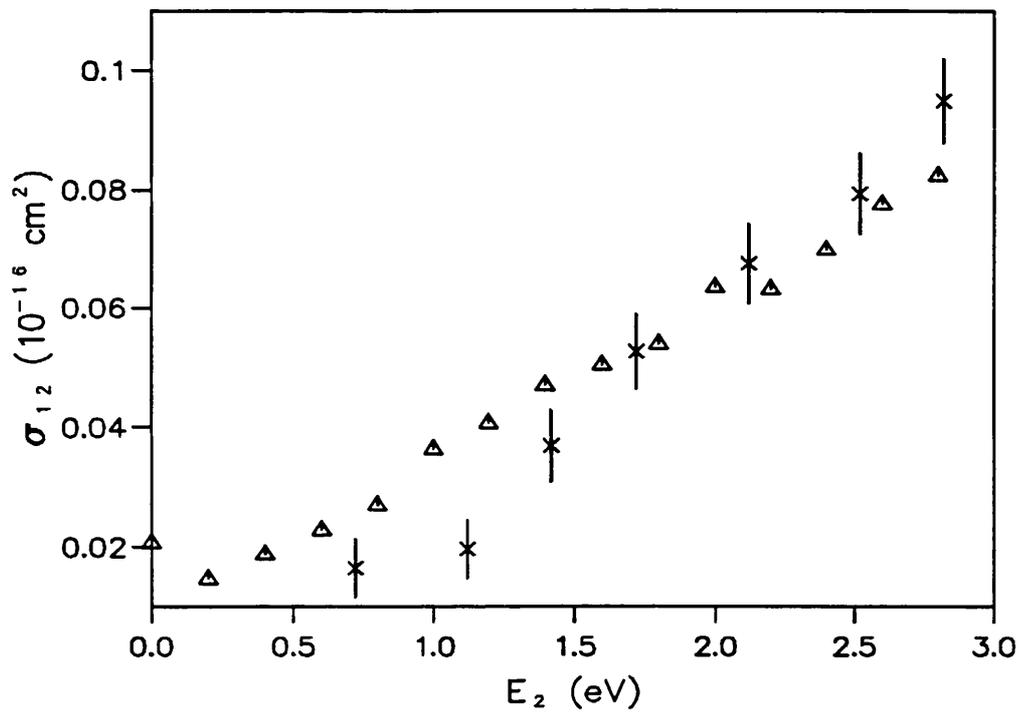
Figure 7.24: Comparison of the positronium formation cross section of Moxom *et al.* (1994) ($\times$) and the difference between the experimental total cross section of Mizogawa *et al.* (1985) ($\triangle$) and the theoretical elastic cross section.

Chapter 8

Annihilation in low energy positron-helium scattering

8.1 Introduction

One of the major differences between electron-atom and positron-atom scattering, is the possibility of annihilation of the low energy incoming positron with one of the electrons of the target atom. At the low energies we are considering in this work, the cross section for electron-positron annihilation is negligible compared to that for elastic scattering or positronium formation, except in the limit of zero incident energy when it tends to infinity. However, the investigation of this process gives very useful information on the nature of positron-atom interactions, on the atoms themselves and on the quality of the scattering wavefunction we have used in this work.

A free electron-positron pair will decay mainly into two or three γ-rays as the one γ-ray decay is not possible, since energy and momentum cannot be conserved, and because the higher order processes, although possible, are highly improbable. In an experiment with an unpolarized positron beam, which is in general the case, the two γ-ray decay comes from the 25% of electron-positron pairs which are in a singlet

spin state. while the three γ-ray decay arises from the annihilation of the other 75% of electron-positron pairs which are in a triplet spin state. The annihilation rate for three γ-ray decay is found to be only 1/370 of that for two γ-ray decay (see Bransden 1969) and. therefore, only the annihilation into two γ-rays needs to be considered. For low energy incoming positrons, the total energy of the electron-positron pair is essentially equal to the rest energy, $2mc^2$, where m is the mass of the electron, and in the reference frame of the centre of mass of the electron-positron pair the two γ-rays are emitted in opposite directions, each with the same energy of $mc^2 = 511keV$.

In this chapter we will investigate the two γ-ray annihilation rate in positron-helium scattering and also calculate the angular correlation function of the two γ-rays which arises because, in the laboratory frame of reference, the two γ-rays are not observed to be emitted in exactly opposite directions. The analysis of this angular correlation function is of interest as it gives information about the momentum distribution of the annihilating electron-positron pairs.

8.2   The annihilation rate and Z_{eff}

The annihilation rate into two γ-rays of a singlet spin state electron-positron pair is

$$\lambda = \pi r_0^2 cn, \tag{8.1}$$

where $r_0 = \epsilon^2/(mc^2)$ is the classical radius of the electron, c is the speed of light and n is the electron density in the vicinity of the positron where annihilation occurs.

We can rewrite equation 8.1 as

$$\lambda = \pi r_0^2 cNZ_{\text{eff}}, \tag{8.2}$$

where N is the number density of atoms in the vicinity of the annihilating positron and Z_{eff}, which is velocity dependent, is the effective number of electrons per atom. In terms of the annihilation rate, the annihilation cross section, σ_a, is given by

$$\sigma_a = \frac{\lambda}{Nv} = \frac{1}{v}\pi r_0^2 cZ_{\text{eff}}, \tag{8.3}$$

where v is the velocity of the incoming positron.

The effective number of electrons per atom, Z_{eff}, can be thought of as the number of electrons with which the positron can annihilate, and this is greater than the real number of electrons in the atom because the positron polarizes the atom and distorts the electron cloud. For annihilation to take place, the positron and the electron must be at the same position in space, or at least within r_0 of each other, and therefore, Z_{eff} is a measure of the probability of the positron being at the same position as one of the target electrons. This can readily be calculated from the elastic scattering wavefunction, Ψ_{el}, described in chapter 6 for s-wave scattering, using

$$Z_{\text{eff}} = 2 \int \mid \Psi_{el}(r_1 = r_2, r_2, r_3) \mid^2 dr_2 dr_3 \qquad (8.4)$$

where Ψ_{el} is normalized to unit positron density as $r_1 \to \infty$ and the factor 2 comes from the fact that both electrons are equally likely to annihilate with the positron. Because equation 8.4 does not constitute a variational principle, the error in Z_{eff} is of first order in the error in the trial function and not of second order as was the case in the evaluation of the phaseshift. Therefore, the accuracy of Z_{eff} will be a sensitive test of the quality of the trial function we have used in our elastic scattering calculations, although one must bear in mind that the evaluation of Z_{eff} involves the trial function in a very restricted region of space, i.e. $r_1 = r_2$.

Before annihilation, the positrons, which we assume to have thermalized in the helium gas, have a mean energy of $(3/2)k_B T$, where T is the absolute temperature of the gas, k_B is Boltzmann's constant, and therefore at $T = 300K$ we have an average energy $\overline{E} = 0.04eV$. In this energy region, the dominant contribution to Z_{eff} is from s-wave scattering and the only other significant contribution comes from the p-wave. We have evaluated Z_{eff} at different energies below the positronium formation threshold using the s-wave elastic scattering wavefunction (equation 6.5) with $\omega = 6$ for helium model H22, as well as a similar p-wave elastic scattering trial function with $\omega = 4$ in each symmetry. The polynomial fits to the dependence of $Z_{\text{eff}}(l = 0)$ and $Z_{\text{eff}}(l = 1)$ on k, the positron momentum, are given by

$$Z_{\text{eff}}(l = 0) = 3.9321 + 0.18584k - 19.563k^2 + 46.670k^3 - 38.212k^4 \qquad (8.5)$$

$$Z_{\text{eff}}(l=1) \quad = \quad 3.8741k^2 - 1.6910k^3 - 0.64117k^4, \tag{8.6}$$

which are plotted in figure 8.1. We have restricted the polynomial fit for $Z_{\text{eff}}(l=1)$ to have no constant and linear terms because the expansion of $Z_{\text{eff}}(l=1)$ around $k=0$ should not contain these terms.
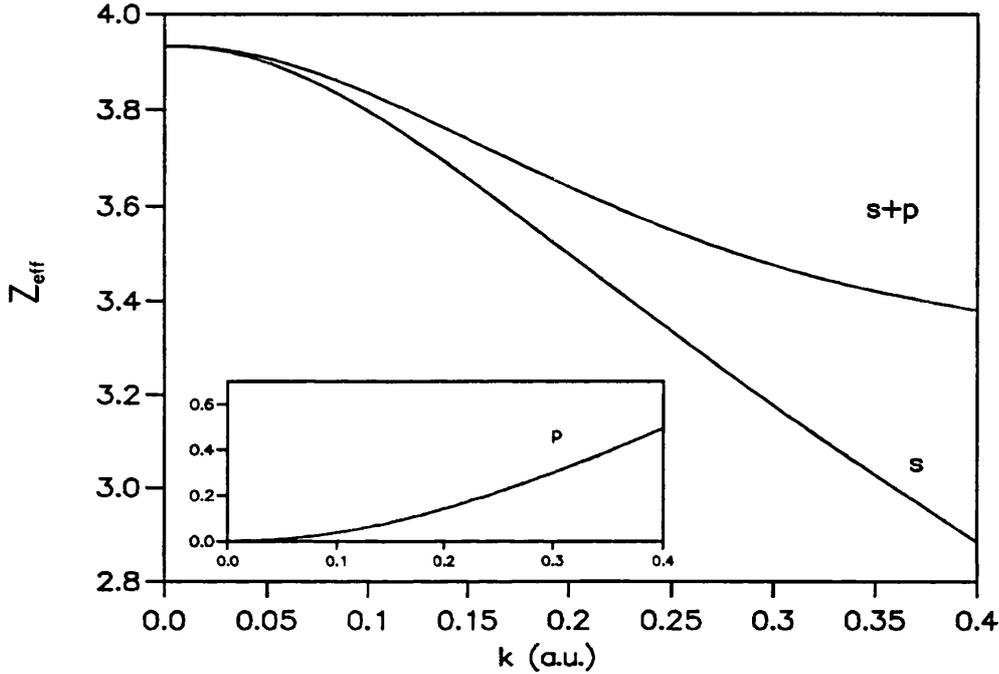
Figure 8.1: The theoretical dependence of Z_{eff} on the positron momentum.

The value of Z_{eff} measured experimentally is an average over the Maxwell-Boltzman distribution of the positrons in the gas. We have therefore convoluted the sum of the fits for the s-wave and the p-wave contributions to Z_{eff} with this speed distribution using

$$\overline{Z}_{\text{eff}} = \frac{\int_0^\infty Z_{\text{eff}}(k)k^2 e^{\frac{-k^2}{2k_B T}} dk}{\int_0^\infty k^2 e^{\frac{-k^2}{2k_B T}} dk}. \tag{8.7}$$

The variation of $\overline{Z}_{\text{eff}}$ with gas temperature is plotted in figure 8.2, and at $T = 293K$ we obtained $\overline{Z}_{\text{eff}} = 3.88 \pm 0.01$ (one should note that at the higher temperature ($> 5000K$) the contributions of higher partial wave ($l > 1$), which are not included here, will become more significant).

There has not yet been any accurate experimental investigation of the variation of $\overline{Z}_{eff}$ with gas temperature for helium, and the most accurate result for $\overline{Z}_{eff}$ at room temperature is that of Coleman *et al.* (1975) who found $\overline{Z}_{eff} = 3.94 \pm 0.02$ at $T = 293K$. which is in reasonable agreement with the present theoretical results. Although the scattering wavefunction we have used for the evaluation of $\overline{Z}_{eff}$ was not fully optimized for the low values of k considered here, we believe that we have obtained a well converged value of $\overline{Z}_{eff}$, and that the agreement with experiment indicates that the trial function we have used is of a high quality.
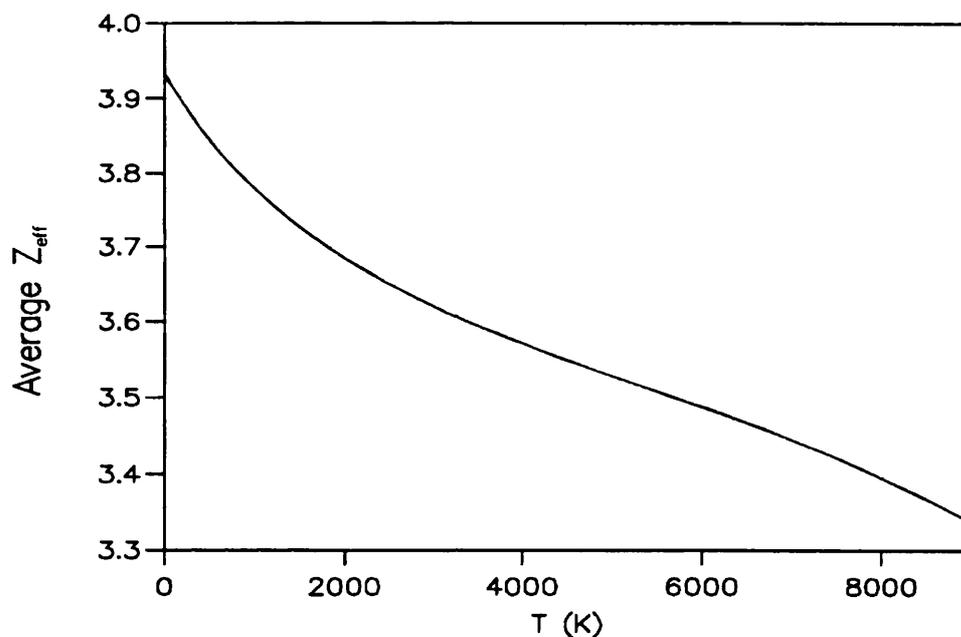
Figure 8.2: The theoretical dependence of $\overline{Z}_{eff}$ on the temperature of the helium gas.

8.3 Angular correlations from positron annihilation in helium

As mentioned in the introduction of this chapter, the most probable outcome of the annihilation of an electron-positron pair is the production of two γ-rays, each of which, in the frame of reference of the centre of mass of the electron-positron pair, has an energy $E_0 = h\nu_0 = mc^2 = 511$ keV. These two γ-rays emerge in exactly opposite directions, i.e. the angle between them is π.

However, because of the motion of the centre of mass of the electron-positron pair, the angle between the two γ-rays as observed in the laboratory frame of reference is not π but $(\pi - \theta)$ (see figure 8.3 in which one should note that θ $(=\theta_1 + \theta_2)$ is greatly exaggerated as in reality it is of the order of a few milli-radians). Also, in the
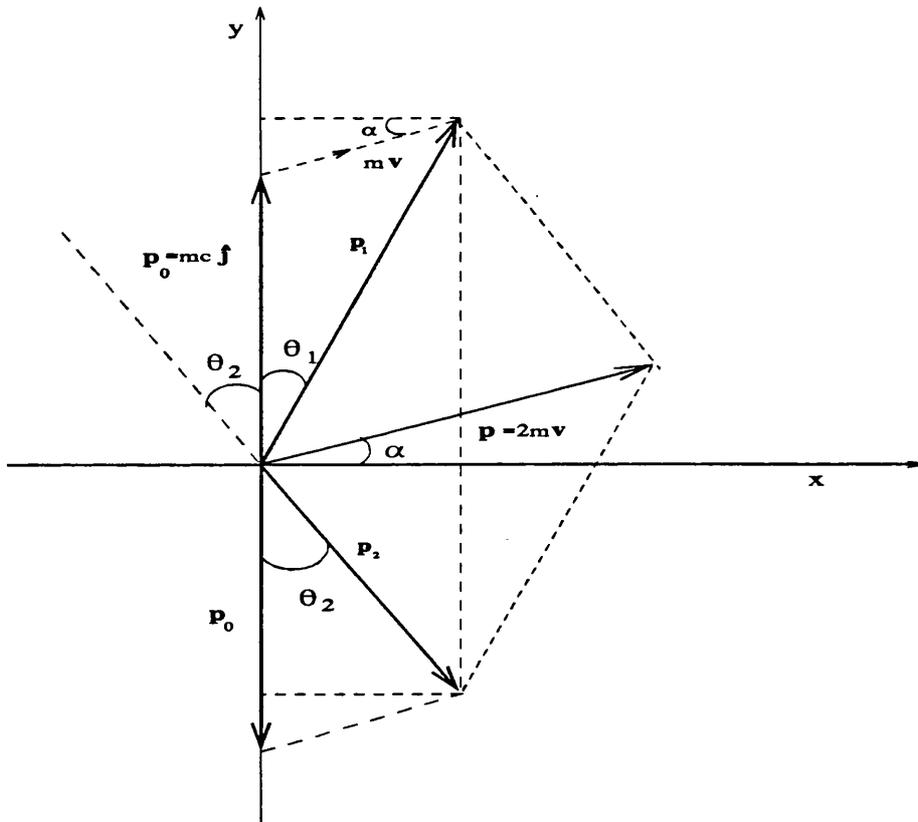
Figure 8.3: Illustration of the relationships between the momenta of the annihilation γ-rays in the centre of mass coordinate system and in the laboratory system.

laboratory frame of reference, the pair has a velocity v and a momentum $p = 2mv$, and the two γ-rays are therefore Doppler shifted to other energies $E_1 = h\nu_1$ and $E_2 = h\nu_2$. The measurement of this energy shift, and the angle θ, are related to the momentum distribution of the annihilating electron-positron pair just before the annihilation, and can be used to infer the momentum distribution of the electrons in the atom. This type of analyis forms the basis of a technique widely used to study the momentum distribution of electrons in solids and liquids.

The angular shift between the two γ-rays of the annihilating pair is measured using the angular correlation of annihilation radiation (ACAR) technique in which both γ-rays are detected in coincidence through two narrow slits, and therefore only the projection of the angle between them onto one particular plane is measured (Stewart et al. 1990. Coleman et al. 1994). The energy shift measurement involves recording the Doppler shift in the energy of only one of the γ-rays from 511keV, i.e. its value in the centre of mass reference frame (Shizuma et al. 1978, Tang et al.1992). This technique makes it possible to have large count rates and therefore much more accurate results. Theoretically, the angular and the energy aspects of the annihilation process can be related by considering the transformation from the centre of mass reference frame to that of the laboratory. Because of the isotropy of the system, we can choose without any loss of generality a set of axes which makes the transformation simpler to implement and clearer to visualize. For instance, we can consider that in the centre of mass reference frame the momenta of the two annihilation γ-rays, $\pm p_0$ (both of magnitude $E_0/c = mc$), lie along the positive and negative y-axis (see figure 8.3). Also the velocity of the centre of mass in the laboratory frame may be chosen to lie in the $x - y$ plane, making an angle α with the positive x-axis. The momenta of the two γ-rays in the laboratory reference frame, p_1 and p_2, add up to the momentum of the electron-positron pair, $p = p_1 + p_2$, and as $p = 2mv$, p also makes an angle α with the positive x-axis. Because the velocity of the electron-positron pair is much less than the speed of light, the transformation of the momenta of the two γ-rays from the centre of mass reference frame to that of the laboratory can be done non-relativistically.

From figure 8.3 we have

$$\boldsymbol{p_1} = mc\hat{\jmath} + m\boldsymbol{v} \qquad \text{and} \qquad \boldsymbol{p_2} = -mc\hat{\jmath} + m\boldsymbol{v}, \qquad (8.8)$$

where $\hat{\jmath}$ is a unit vector along the y-axis. To first order in v/c, and noting that the angles θ_1 and θ_2 are of the order of milli-radians. we have

$$p_1 = mc + mv\sin\alpha = mc + \frac{1}{2}p_y \qquad (8.9)$$

$$p_2 = mc - mv\sin\alpha = mc - \frac{1}{2}p_y, \qquad (8.10)$$

where $p_y = 2mv\sin\alpha$ is the y-component of the momentum of the electron-positron pair. The Doppler shift from the centre of mass energy of the γ-rays is

$$\Delta E_1 = (E_1 - E_o) = c(p_1 - mc) = (1/2)cp_y$$

$$\Delta E_2 = (E_2 - E_o) = c(p_2 - mc) = -(1/2)cp_y. \qquad (8.11)$$

We see that it is the same in magnitude for both γ-rays and it is sufficient to detect only one γ-ray to make a Doppler shift measurement.

In the laboratory frame of reference the angle between the two γ-rays is $\pi - \theta$ and from figure 8.3 we get

$$\begin{aligned} \theta &= \theta_1 + \theta_2 \\ &= \frac{mv\cos\alpha}{mc + mv\sin\alpha} + \frac{mv\cos\alpha}{mc - mv\sin\alpha} \\ &= \frac{2m^2vc\cos\alpha}{m^2c^2 - m^2v^2\sin^2\alpha} \end{aligned} \qquad (8.12)$$

which to first order in v/c reduces to

$$\theta \simeq \frac{2mv\cos\alpha}{mc}. \qquad (8.13)$$

As $2mv\cos\alpha$ is the x-component of the momentum of the electron-positron pair, we have

$$\theta = \frac{p_x}{mc}. \qquad (8.14)$$

However, because of the isotropy of the positron-atom system, all directions of $\boldsymbol{p}$, the total momentum of the annihilating pair, are equally likely, and therefore p_x and p_y will have the same distribution function. Hence, we can use either the distribution

172

function for δE (equation 8.11) or the angular correlation function for the angle $(\pi - \theta)$ (equation 8.14), and from both these equations we find

$$\frac{1}{2}cp_y = \delta E = mc^2\frac{\theta}{2}. \tag{8.15}$$

We have calculated the angular correlation function in a similar manner to that of Humberston (1979) and transformed the results to an energy shift function using equation 8.15. The probability of the two γ-rays emerging with the angle between them in the range $(\pi - \theta)$ to $(\pi - (\theta + d\theta))$ is $F(\theta)d\theta$, where $F(\theta)$ is the angular correlation function given by

$$F(\theta) \propto \int_{-\infty}^{\infty} \int_{-\infty}^{\infty} \Gamma(p_x = mc\theta, p_y, p_z)dp_y dp_z. \tag{8.16}$$

The function $\Gamma(\boldsymbol{p})$ is the momentum distribution function of the annihilating electron-positron pair, which for the positron-helium system has the form

$$\Gamma(\boldsymbol{p}) = \int d\boldsymbol{r_3} \left| \int \exp(i\boldsymbol{p}.\boldsymbol{r_2})\Psi(\boldsymbol{r_1} = \boldsymbol{r_2}, \boldsymbol{r_2}, \boldsymbol{r_3})d\boldsymbol{r_2} \right|^2, \tag{8.17}$$

i.e. the overlap of the momentum eigenstate, $\exp(i\boldsymbol{p}.\boldsymbol{r_2})$, with the scattering wavefunction, Ψ, evaluated at $\boldsymbol{r_1} = \boldsymbol{r_2}$.

By fixing p_x in equation 8.16 we have restricted ourselves to the p_y - p_z plane and we can easily change to plane polar coordinates to evaluate the double integral.

So we have

$$p_y, p_z \rightarrow p', \beta \tag{8.18}$$

and

$$dp_y dp_z = p'dp'd\beta \tag{8.19}$$

with $p' = \sqrt{p_y^2 + p_z^2}$.

Hence

$$F(\theta) \propto \int_0^{\infty} \int_0^{2\pi} \Gamma(p')p'dp'd\beta \tag{8.20}$$

and using $p^2 = p_x^2 + p_y^2 + p_z^2 = p_x^2 + p'^2$, remembering that $p_x = mc\theta$ =const, we get,

$$d(p')^2 = d(p)^2 \tag{8.21}$$

173

and

$$p'dp' = pdp. \tag{8.22}$$

Integrating over β gives a factor 2π so that,

$$F(\theta) \propto 2\pi \int_{p_x}^{\infty} \Gamma(p)pdp. \tag{8.23}$$

The momentum distribution function, $\Gamma(p)$, is a function of the magnitude of p only as we are dealing with a spherically symmetric system, and we can therefore choose for the r_2 integration in equation 8.17 to put the vector p along r_3 for instance, if we take the case of the positron annihilating with electron 2. Now using $dr_2 dr_3 = r_2 dr_2 r_3 dr_3 r_{23} dr_{23} \sin \theta_2 d\theta_2 d\phi_2$ and performing the external angle integration, we have

$$\Gamma(p) = 4\pi \int_0^{\infty} \left| \int_0^{\infty} \int_{|r_2-r_3|}^{r_2+r_3} \exp(-ipr_2 \cos \theta_{23}) \Psi(r_1 = r_2, r_2, r_3) r_2 dr_2 r_{23} dr_{23} \right|^2 r_3 dr_3. \tag{8.24}$$

The evaluation of $F(\theta)$ can be done using the variational scattering function for elastic scattering, and the value of $F(\theta)$ for a given θ now corresponds to a different range of integration in equation 8.23, as we integrate from p_x to ∞ with $p_x = mc\theta$.

In figure 8.4 we present the angular correlation function, $F(\theta)$, normalized to unity at $\theta = 0$, for four different s-wave scattering wavefunctions (with either only the S_1 type of terms or with $\omega = 2$, 4 and 6 respectively) and the previous results obtained by Humberston (1979) for H5 using the method of models. At the time, Humberston's results were in disagreement with the most accurate experimental data of Briscoe et al. (1968) and it was proposed that this could be due to the fact that the theoretical results corresponded to annihilation in a gas while the experimental data referred to measurements in liquid helium. In figure 8.4 we see that the calculation with a wavefunction containing only S_1 type of function, which is essentially a Born approximation and corresponds to scattering from an undistorted helium target, gives a much wider spectrum than that obtained when the full wavefunction, including short-range terms, is used. This Born approximation spectrum represents the momentum distribution of the electrons in the undistorted target, as opposed to that of the electron-positron pair, and the broadening of the spectrum is

174
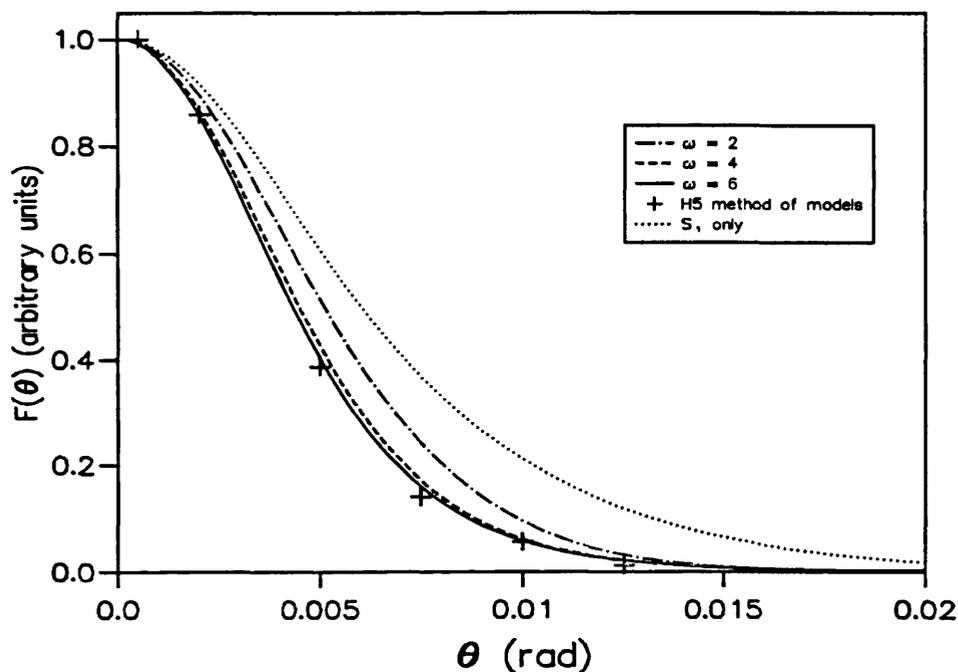
Figure 8.4: Angular correlation function calculated with an elastic scattering wavefunction containing only S_1 type of terms or with the full wavefunction and ω=2,4 and 6 respectively. Also included are the previous H5 results from Humberston (1979).

due to the fact that the electrons in the undistorted target have higher momentum than is the case when the positron distorts the atom, pulling the electrons away from the nucleus and slowing them down. Furthermore, one can notice that the $\omega = 6$ results can be considered to be well converged, although there is no rigorous bound on the value of $F(\theta)$ and that, as was the case in the calculation of Z_{eff}, the error is of first order in the error in the trial function.

The new theoretical results of this work were also found not to agree with the experimental results of Briscoe *et al.*, but recently new measurements of the Doppler-broadened annihilation γ-ray spectrum for positrons annihilating in helium have been made by the San Diego group, and more accurate results have been obtained with which our theoretical data can be compared. A Penning trap was used in which a large number of positrons with characterized energies can be stored, and

175

great accuracy was achieved in these measurements because of the increased count rate and improved signal-to-noise ratio (Tang *et al.* 1992 and Iwata *et al.* 1995).
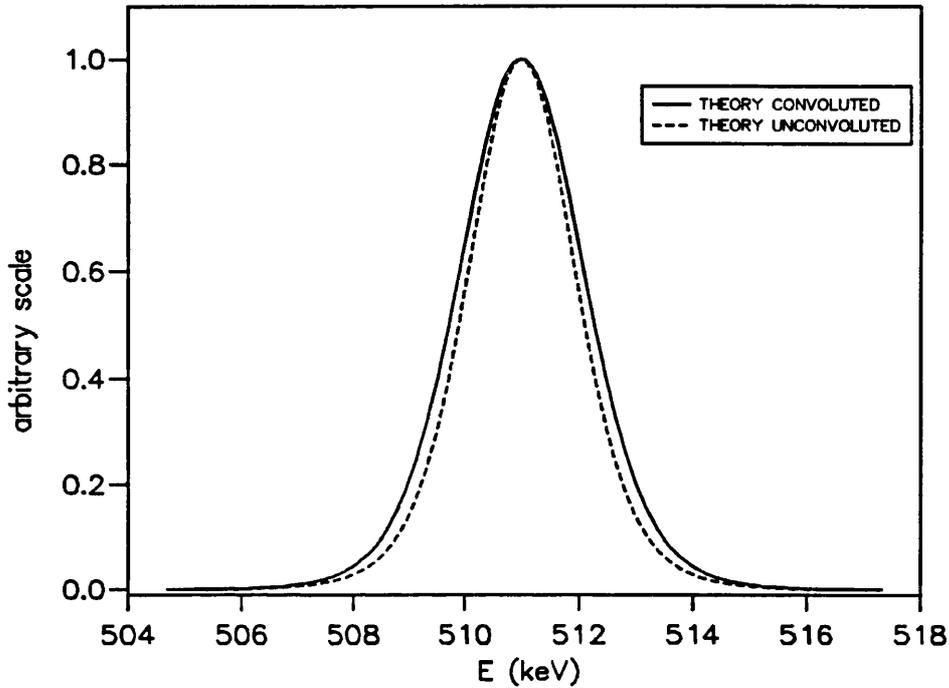
Figure 8.5: Theoretical annihilation spectrum with and without the convolution by the experimental detector response function.

The observed spectrum also contains the detector response, which is accurately approximated with a combination of a Gaussian with FWHM of 1.16 keV and a step function due to Compton scattering in the Ge crystal of the detector. To compare these results with theory the detector reponse needs to be extracted from the data, and while the substraction of the step function does not create any difficulty, the deconvolution of the data with the Gaussian function is found to be numerically very unstable. Therefore, instead, the theoretical results of this work, transformed into an energy spectrum using equation 8.15, have been convoluted with the Gaussian detector response, and we can see in figure 8.5 that this leads to a broadening of the spectrum. In figure 8.6(a) we present the convoluted theoretical energy spectrum calculated at a positron energy of 0.04 eV together with the experimental data from

the San Diego group (Van Reeth *et al.* 1996).

The agreement between the convoluted theory and experiment extends over three orders of magnitude without using fitting parameters and we find the value of $\chi^2/$(degrees of freedom) $= 1.2$ (see figure 8.6 c for residuals). In the analysis of previous experimental data (Stewart *et al.* 1990, Coleman *et al.* 1994) it was assumed, but with no theoretical justification, that the spectrum had a Gaussian form, but as indicated by the residuals in figure 8.6 b, the Gaussian does not give a very good fit, with $\chi^2/$(degrees of freedom) $= 4.7$ instead of approximately unity if the model of the Gaussian fit were correct.

8.4 Conclusion

The excellent agreement between the theoretical calculation and the experimental measurements of the γ-ray annihilation spectrum shows that we have achieved a very high degree of accuracy in the elastic scattering trial function, Ψ_{el}, used in our scattering calculations. One must emphasize that this does not constitute an exhaustive test of Ψ_{el}, as this calculation, as well as that for Z_{eff}, involves the scattering wavefunction only in a restricted region of space. Nevertheless, the agreement for the annihilation spectrum is such that we believe that both the theoretical and the experimental results can be considered to be very close to the exact results. Also, we expect that better agreement between theory and experiment could be achieved for the value of Z_{eff} if a scattering wavefunction including polarization terms was used and if a similar experimental technique to that employed for the annihilation spectrum measurement was used, i.e. a trap to confine the positrons with a well defined energy.
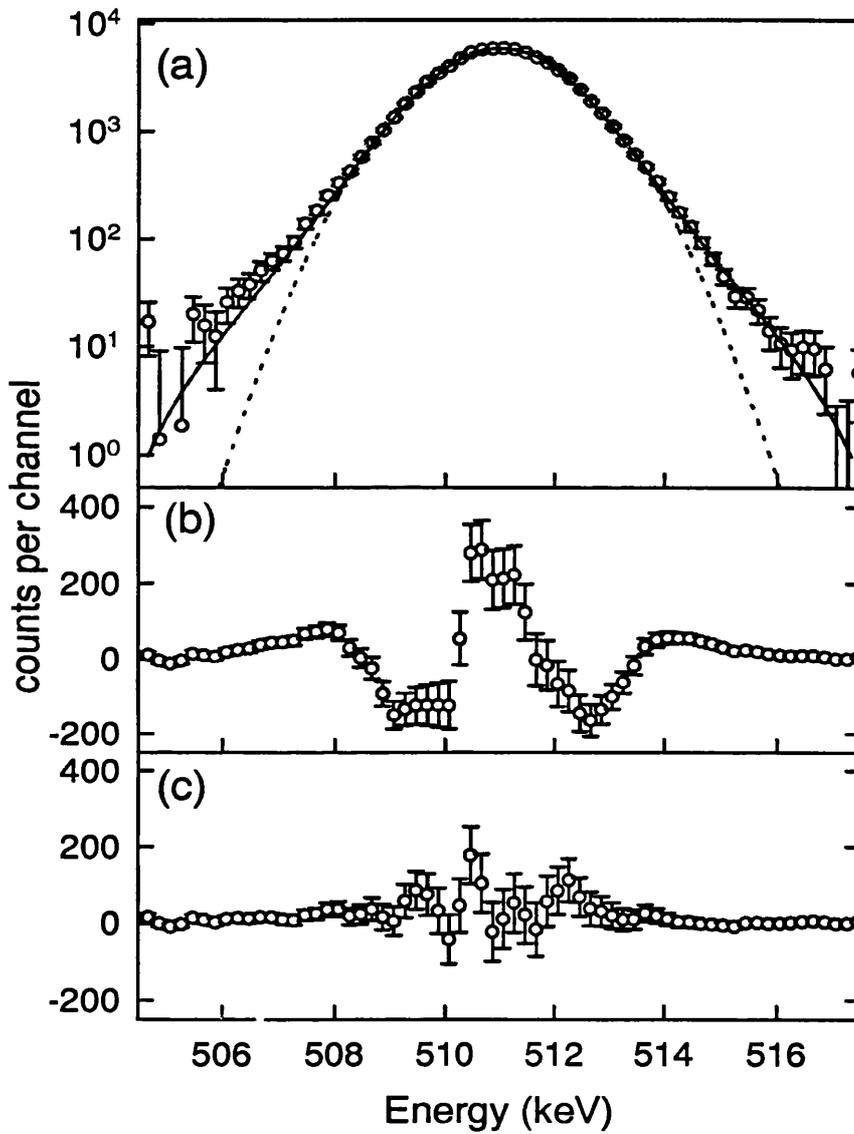
Figure 8.6: (a) Annihilation γ-ray spectrum for positrons interacting with helium atoms, as measured in the laboratory frame of reference. Solid line: theoretical prediction convolved with the response of the Ge detector; dashed line: Gaussian function fitted to the experimental data; o, experimental measurements. (b) Residuals from the Gaussian fit. (c) Residuals from the theoretical calculation.

Chapter 9

Conclusions

In this work, we have presented the results of a very elaborate variational calculation of the scattering parameters for low energy positron-helium scattering. The Kohn variational method has been used with multi-channel trial wavefunctions, and we have made a detailed investigation of the effect of using non-exact helium target wavefunctions in this type of variational calculation. The outcome of this investigation is that accurate and reliable results can be obtained when the method of models is not used, but only if very elaborate helium target wavefunction are used in the scattering calculation (see also Van Reeth and Humberston 1995a). We have created a very accurate helium wavefunction, refered to as H22, which contains 22 Hylleraas-type short-range terms, and gives very good results for both the ground state energy and the dipole polarizability of the helium atom. The results we have obtained for s-wave scattering below the positronium formation threshold without the method of model and using the helium target function H22, agree very well with those of Humberston (1973) and Campeanu and Humberston (1977) which were obtained with the method of models.

The main difficulty in the formulation and the computational work in these investigations have been concerned with the setting up of the four-body two channel Kohn variational method and the evaluation of the various matrix elements. The general formulation of the problem was found to be somewhat similar to that for

179

positron-hydrogen scattering, but both the inexactness of the target wavefunction and the inclusion of exchange between the two electrons in the target, as well as the increased number of interparticle coordinates, have made the formulation for positron-helium much more complicated. Because the method of models is not appropriate for the two channel problem, we have had to include new types of terms in several matrix elements, terms which contain the operation of H_{He} on the target wavefunction explicitly, and which were not present in the positron-hydrogen case. Moreover, the exchange between the electrons in the target has meant that more complicated angular functions occurred, and that some of the matrix elements which could be shown, using symmetry arguments, to be zero in the hydrogen case, are now non-zero and therefore need to be evaluated.

In terms of the evaluation of the matrix elements, the main difficulty was to create a six dimensional numerical integration procedure which was at the same time reliable, flexible, accurate and could also be performed in a reasonable amount of time. We believe that the various numerical methods and computational techniques we have developed have made it possible to get reasonably accurate results for the integration of all types of matrix elements. We recognize that we will never achieve excellent accuracy in the integration of most matrix elements, but the accuracy which we have achieved, 4-5 figure in the worst case, was found to be sufficient. We have investigated the sensitivity of the accuracy of the final results, i.e. the K matrix elements and the cross sections, by comparing our results with those obtained by reducing the accuracy of the integration in all matrix elements significantly, for instance to 3-4 figures in the worst case. We have found that there was less than 1% difference in K_{11} and only a few percents in K_{12} and K_{22}, and we are therefore satisfied that we have achieved sufficient numerical accuracy. We have also made great efforts in the optimization of the computer programs to reduce significantly the computational time, so that the matrix elements for trial functions with large ω could be evaluated. This was done by developing both the parallelization of the computer code and the new method we have used in the s-wave scattering calculations to evaluate the $(\phi_i, L\phi_j)$ matrix elements, both of which are described in chapter 5.

An important feature of the s-wave calculation we have presented in chapter 6, and which is also present in the p-wave and d-wave calculations, is the impossibility of a perfect optimization of the non-linear parameters in the two channel trial functions for both K_{11} and K_{22}. As explained in the analysis of the various partial waves diagonal K matrix elements, the reason why one set of non-linear parameters will not optimize the trial function for both K_{11} and K_{22} is that these K matrix elements are related to physical processes which do not have the same interaction region. Therefore, as the nonlinear parameters α and β, for instance, effectively define the region of space where the short-range correlation terms are effective, it is to be expected that one given set of α and β will not be correct for both K_{11} and K_{22}. We have chosen a set of non-linear parameters which optimizes the value of K_{11}, because this K matrix element is directly linked to the elastic scattering cross section for positron-helium scattering, while K_{22} is linked to the elastic scattering of positronium from the helium-plus ion, which is not the primary interest of our work. In addition, we have found that, although the definition of the cross sections in terms of the K matrix elements (equation 2.25) couples all K matrix elements together, there seems to be very little coupling of the K_{22} element in the evaluation of both σ_{11} and σ_{12}.

A further difficulty in the optimization of the non-linear parameters is that, as there is no bound on the K_{12} matrix element, which is closely related to the positronium formation channel, it is not possible to investigate precisely the optimization for K_{12} and to determine with rigour the accuracy of σ_{12}. The formation of positronium is a longer range process than the elastic scattering of positrons from helium, so one would expect that a set of non-linear parameters which optimizes the values of K_{22} would be suitable for the optimization of K_{12}. The analysis of the optimization of the non-linear parameters did not indicate that this was the case and, futhermore, the optimization of the non-linear parameters (see figures 6.2 to 6.6 for s-wave scattering) clearly shows that the optimized values for K_{22} would gave poor values for K_{11}. Therefore, we propose as a next step in this type of investigation, to include two short-range expansions into the trial function, each with a different set of non-linear parameters. It is expected that, if such a scheme were to be used,

less terms would be needed in each expansion to achieve good convergence for both K_{11} and K_{22} than is the case when only one type of short-range expansion is used. Unfortunately, this would make the formulation more complicated and require more computational work, and the main difficulty would be the integration of the matrix elements involving the non-linear parameters chosen to optimize K_{22}. Indeed, the best set of non-linear parameters for K_{22} is one which creates a more diffuse interaction region so as to represent the polarization of the positronium atom by the helium-plus ion more effectively. This means that the short-range terms with this set of non-linear parameters have a longer range behaviour than those which we have been considering in this work and that, therefore, difficulties could emerge in the integrations of the matrix elements containing such terms. We expect that a substantial increase in the number of integration points and computational time would be required to achieve the accuracy we have obtained in this work.

The s-wave positronium formation and elastic scattering cross sections have been calculated using trial functions containing 502 short-range terms ($\omega=6$). The elastic scattering cross section for s-wave scattering was found to be dominant within the Ore gap, and a small discontinuity was noted at the positronium formation threshold. This discontinuity was removed by introducing an explicit virtual positronium term in the elastic scattering trial function below the threshold and a Wigner 'rounded step' feature was found. The s-wave positronium formation cross section was found to be relatively small and very similar in both magnitude and energy dependence to the s-wave positronium formation cross section in positron-hydrogen scattering. We believe that the results presented in this work for s-wave scattering are within 2-3% for σ_{11} and 10-20% for σ_{12} from the exact ones.

The calculation of the p- and d-wave scattering parameters was more complex than that for s-wave scattering and the results we have obtained do not display the same clear convergence pattern as found previously. For both partial waves, there seemed to be a breakdown in the convergence pattern of the K matrix elements with respect to the increase in the number of first symmetry terms, with the appearance of resonance-type features which disappeared when higher symme-

try terms were included. We have not been able to determine exactly the reason why this occurred, but we have managed to reduce the effects of this breakdown on the convergence of K matrix elements by reducing the number of first symmetry short-range terms. Reasonably accurate p- and d-wave elastic scattering and positronium formation cross sections have been obtained within the Ore gap with p-wave trial function containing 150 short-range terms in the first symmetry and 330 in the second symmetry, and d-wave trial function containing 36 first symmetry terms and 172 third symmetry terms. We estimate σ_{11} to be within 5% of the exact result and σ_{12} to be within 10-20% for both p-wave and d-wave scattering. We find that the d-wave positronium formation cross section is dominant in the Ore gap for energies 1eV higher than the threshold, reaching $\approx$ 50% of the total cross section at the highest energy at which we have calculated. In both the p- and d-wave elastic cross sections a discontinuity was found at the threshold itself, and there was not sufficient time to include an explicit virtual positronium term in the calculation as was done for s-wave scattering to achieve continuity. This discontinuity was seen to be very pronounced in the d-wave scattering, which is very similar to the case for positron-hydrogen d-wave elastic scattering , and, therefore, we expect the inclusion of a virtual positronium term in the trial function to be very important for this partial wave. On the other hand, we do not expect to find any threshold features in the elastic scattering cross sections for p- and d-wave scattering similar to that found in s-wave scattering. An account of the s-wave and p-wave results has also been published (Van Reeth and Humberston (1995b) and Humberston and Van Reeth (1996)).

Total elastic scattering and positronium formation cross sections have been obtained using the sum of the s-, p- and d-wave components calculated in this work and adding an estimate of the higher partial waves contribution calculated with more approximate methods. The formula of O'Malley et al. (1962) (equation 7.36) was used, both below and above the positronium formation threshold, for the evaluation of the elastic scattering cross sections for $l > 2$, and the sum of these was found to contribute $\approx$ 5% to the total elastic cross section. The positronium formation cross sections for $l > 2$ calculated by McAlinden (1996), using a first Born approxima-

tion, are believed to be underestimates, but it was not possible to determine exactly by what amount. The total positronium formation cross sections calculated in this work are $\approx 30\%$ lower than the experimental results of Moxom *et al.* (1994) and the total cross sections, i.e. $\sigma_{11}+\sigma_{12}$, are $\approx 5-10\%$ lower than the experimental total cross section of Mizogawa *et al.* (1985) and Stein *et al.* (1978). The difference
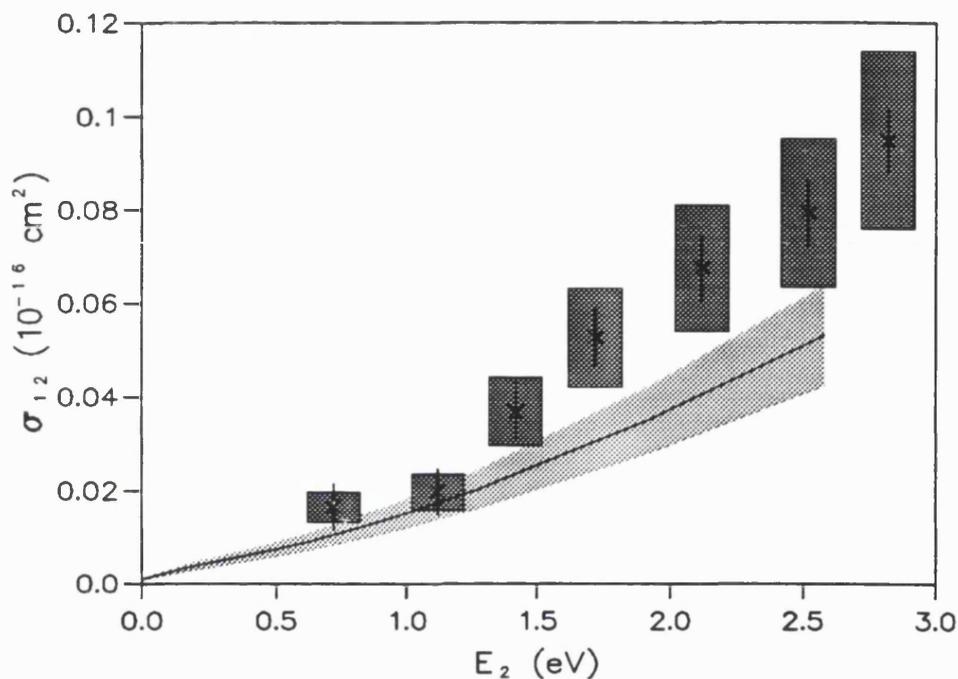

Figure 9.1: Comparison of theoretical and experimental total positronium formation cross sections for positron-helium scattering. E_2 is the excess energy of the positron beyond the positronium formation threshold, i.e. $E_2 = E_{e^+}$ - E_{Th}. The experimental data ($\times$) are those of Moxom *et al.* (1994). The boxes and the shaded area are the compound uncertainties of the experiment and the theory respectively (see text below).

between theory and experiment is believed to come from the uncertainties in both sets of results. Those in the theoretical calculation are mainly due to the lack of convergence of the Kohn variational results for σ_{12}, the underestimate of the Born results for the higher partial waves contributions, and the omission of the second symmetry short-range terms in the d-wave calculation. Experimentally, the uncertainties are due to the normalization of the data as well as to the calibration of the

184

positron energy scale. In figure 9.1 we present a comparison of the theoretical and experimental results for the positronium formation cross section, with an estimate of the compound uncertainties. The height of the boxes around the experimental data represent the 20% uncertainty in the magnitude of σ_{12} and the width is a measure of the ± 0.1eV uncertainty in the positron energy scale. The uncertainty in the theoretical results due to lack of convergence ($\pm 20\%$) is represented by the grey area surrounding the theoretical curve for σ_{12}. The difference between theory and experiment is now found to be nearly compatible with the uncertainties in both sets of results and this shows that, although there is still a disagreement on the exact energy dependence of σ_{12}, the magnitude of the positronium formation cross section in positron-helium scattering within the Ore gap is now reasonably well established both experimentally and theoretically.

Low energy positron-electron annihilation in helium has been investigated using elaborate s- and p-wave elastic scattering trial functions. The annihilation parameter Z_{eff}, which can be thought of as the number of electrons with which the positron can annihilate, was calculated and the thermally averaged value of $Z_{eff} = 3.88 \pm 0.01$ was found to be in good agreement with experiment. We have also calculated the annihilation energy spectrum which is related to the momentum distribution of the electron-positron pair before the annihilation, and the results we have obtained are in excellent agreement with the recent experimental data from the San Diego group (Van Reeth *et al.* (1996). As the calculation of these annihilation parameters is not based on a variational principle, the error in the results will be of first order in the error in the trial function and not of second order as was the case in the evaluation of the scattering parameters. Therefore, we believe that the quality of our results for Z_{eff} and for the annihilation energy spectrum indicates that we have developed very accurate and flexible trial scattering functions.

Appendix A

Symmetry arguments

The number of matrix elements which need to be evaluated to solve equation 2.103 can be reduced by symmetry arguments leading to a significant gain in computational time.

The general form of a matrix element is (g, Lf), where g and f are any of the short-range or long-range terms in the trial function and $L = 2(H - E)$ with H being the total Hamiltonian. Hence,

$$(g, Lf) = (g, [-\nabla_{r_1}^2 - \nabla_{r_2}^2 - \nabla_{r_3}^2 + \frac{4}{r_1} - \frac{4}{r_2} - \frac{4}{r_3} - \frac{2}{r_{12}} - \frac{2}{r_{13}} + \frac{2}{r_{23}} - 2E]f). \quad (A.1)$$

If we consider the functional $F = (g, Lf) - (f, Lg)$ we have

$$F = (-g, \nabla_{r_1}^2 f) + (f, \nabla_{r_1}^2 g) + (-g, \nabla_{r_2}^2 f) + (f, \nabla_{r_2}^2 g) + (-g, \nabla_{r_3}^2 f) + (f, \nabla_{r_3}^2 g), \quad (A.2)$$

which using Green's theorem (equation 2.52) can be written as

$$F = \int_{V_1} \int_{A_1} [g \nabla_{r_1} f - f \nabla_{r_1} g] . d\sigma_1 d\tau_1 \int_{V_2} \int_{A_2} [g \nabla_{r_2} f - f \nabla_{r_2} g] . d\sigma_2 d\tau_2$$
$$+ \int_{V_3} \int_{A_3} [g \nabla_{r_3} f - f \nabla_{r_3} g] . d\sigma_3 d\tau_3 \quad (A.3)$$

where A_i is the surface which encloses the volume V_i for $i = 1, 2$ or 3. These surfaces can be taken to be spheres of infinite radius (i.e. $r_i \rightarrow \infty$) and the surface element is then $d\sigma_i = r_i^2 \sin\theta_i d\theta_i d\phi_1 \hat{r}_i$. Therefore, if each integrand in equation A.3 tends to zero faster than r_i^{-2} the surface integrals will vanish as $r_i \rightarrow \infty$. This will be

the case if either f or g is a short-range term, as these contain an exponentially decreasing dependence on r_1, r_2 and r_3 and we therefore have

$$
\begin{aligned}
(\overline{\phi_i}, L\overline{\phi_j}) &= (\overline{\phi_j}, L\overline{\phi_i}) \\
(\overline{\phi_i}, LS_1) &= (S_1, L\overline{\phi_i}) \\
(\overline{\phi_i}, LC_1) &= (C_1, L\overline{\phi_i}) \\
(\overline{\phi_i}, L\overline{S_2}) &= (\overline{S_2}, L\overline{\phi_i}) \\
(\overline{\phi_i}, L\overline{C_2}) &= (\overline{C_2}, L\overline{\phi_i})
\end{aligned}
\tag{A.4}
$$

where $\overline{\phi_i} = (1 + P_{23})\phi_i = (\phi_i + \phi_i')$, $\overline{S_2} = 1/\sqrt{2}(1 + P_{23})S_2 = 1/\sqrt{2}(S_2 + S_2')$, etc.

For the long-range – long-range matrix elements, we first consider those which involve cross-terms between channel one and channel two type of terms, i.e. $(S_1, L\overline{S_2})$, etc. In this case also, the exponential dependence of the helium target function on r_2 and r_3 in the S_1 and C_1 terms ensures that the two last surface integrals in equation A.3 vanish as r_2 or r_3 go to infinity. For the first term in equation A.3 we see that, if we keep r_2 and r_3 fixed, the exponential fall-off in r_{12} or r_{13} of the positronium fragment function in the S_2 and C_2 type of term also ensures that this surface integral vanishes as $r_1 \rightarrow \infty$. Hence we have,

$$
\begin{aligned}
(S_1, L\overline{S_2}) &= (\overline{S_2}, LS_1) \\
(S_1, L\overline{C_2}) &= (\overline{C_2}, LS_1) \\
(C_1, L\overline{S_2}) &= (\overline{S_2}, LC_1) \\
(C_1, L\overline{C_2}) &= (\overline{C_2}, LC_1)
\end{aligned}
\tag{A.5}
$$

For matrix elements with terms of the same channel we only need to consider those which involve the cross product between the S and C types of term. We first consider the $(\overline{S_2}, L\overline{C_2})$ matrix element for which we can rewrite the functional $F = (\overline{S_2}, L\overline{C_2}) - (\overline{C_2}, L\overline{S_2})$, using the properties of the P_{23} operator, as

$$
\begin{aligned}
F &= (\frac{1}{\sqrt{2}}[S_2 + S_2'], L\frac{1}{\sqrt{2}}[C_2 + C_2']) - (\frac{1}{\sqrt{2}}[C_2 + C_2'], L\frac{1}{\sqrt{2}}[S_2 + S_2']) \\
&= [(S_2, LC_2) - (C_2, LS_2)] + [(S_2, LC_2') - (C_2', LS_2)] \\
&= F_2 + F_2'
\end{aligned}
\tag{A.6}
$$

We can, using equation 2.11, write equation A.3 for the F_2' functional as,

$$F_2' = \int_{V_1} \int_{A_{\rho_2}} \left[S_2 \frac{\boldsymbol{\nabla}_{\rho_2}}{2} C_2' - C_2' \frac{\boldsymbol{\nabla}_{\rho_2}}{2} S_2 \right] . d\boldsymbol{\sigma}_{\rho_2} d\tau_1 \qquad (A.7)$$

$$+ \int_{V_2} \int_{A_3} \left[S_2 \boldsymbol{\nabla}_{r_3} C_2' - C_2' \boldsymbol{\nabla}_{r_3} S_2 \right] . d\boldsymbol{\sigma}_3 d\tau_2$$

$$+ \int_{V_3} \int_{A_{12}} \left[S_2 2 \boldsymbol{\nabla}_{r_{12}} C_2' - C_2' 2 \boldsymbol{\nabla}_{r_{12}} S_2 \right] . d\boldsymbol{\sigma}_{12} d\tau_3.$$

The S_2 term contains an exponential fall-off in r_3 and r_{12} from the $He^+(r_3)$ and the $Ps(r_{12})$ wavefunctions, and therefore the two surface integrals on A_3 and A_{12} will vanish as $r_3 \to \infty$ and $r_{12} \to \infty$ respectively. Also the C_2' term has an exponential dependence on r_2 from the $He^+(r_2)$ wavefunction (which comes from $P_{23}He^+(r_3)$); therefore as $\rho_2 \to \infty$, with r_{12} and r_3 fixed, the surface integral on A_{ρ_2} will vanish too and we have

$$F_2' = (S_2, LC_2') - (C_2', LS_2) = 0 \qquad (A.8)$$

For the F_2 functional we have

$$F_2 = \int_{V_1} \int_{A_{\rho_2}} \left[S_2 \frac{\boldsymbol{\nabla}_{\rho_2}}{2} C_2 - C_2 \frac{\boldsymbol{\nabla}_{\rho_2}}{2} S_2 \right] . d\boldsymbol{\sigma}_{\rho_2} d\tau_1 \qquad (A.9)$$

$$+ \int_{V_2} \int_{A_3} \left[S_2 \boldsymbol{\nabla}_{r_3} C_2 - C_2 \boldsymbol{\nabla}_{r_3} S_2 \right] . d\boldsymbol{\sigma}_3 d\tau_2$$

$$+ \int_{V_3} \int_{A_{12}} \left[S_2 2 \boldsymbol{\nabla}_{r_{12}} C_2 - C_2 2 \boldsymbol{\nabla}_{r_{12}} S_2 \right] . d\boldsymbol{\sigma}_{12} d\tau_3.$$

Here also, because of the exponential fall-off from the positronium and the helium-plus wavefunctions, the two last surface integrals vanish, but as we do not have an implicit fall-off in ρ_2 the first term will not go to zero. Also, as we are considering surface elements which are normal to $\hat{\rho}$, we can ignore the angular dependence in $\boldsymbol{\nabla}_{\rho_2}$ and equation A.10 reduces to

$$F_2 = \int_{V_1} \frac{1}{2} \left[\int_{A_{\rho_2}} \left(C_2 \frac{\partial S_2}{\partial \rho_2} - S_2 \frac{\partial C_2}{\partial \rho_2} \right) \rho_2^2 \sin \theta_{\rho_2} d\theta_{\rho_2} d\phi_{\rho_2} \right] d\tau_1 \qquad (A.10)$$

On the surface A_{ρ_2}, using the asymptotic form of C_2 and S_2 for s-wave scattering, we have

$$\frac{\partial S_2}{\partial \rho_2} \underset{\rho_2 \to \infty}{\sim} \Phi_{He^+}(\boldsymbol{r}_3) \Phi_{Ps}(\boldsymbol{r}_{12}) \frac{\sqrt{2\kappa}}{\sqrt{4\pi}} \left[\frac{\kappa \rho_2 \cos \kappa \rho_2 - \sin \kappa \rho_2}{\kappa \rho_2^2} \right]$$

$$\frac{\partial C_2}{\partial \rho_2} \underset{\rho_2 \to \infty}{\sim} \Phi_{He^+}(\boldsymbol{r}_3) \Phi_{Ps}(\boldsymbol{r}_{12}) \frac{\sqrt{2\kappa}}{\sqrt{4\pi}} \left[\frac{-\kappa \rho_2 \sin \kappa \rho_2 - \cos \kappa \rho_2}{\kappa \rho_2^2} \right]. \qquad (A.11)$$

Hence,

$$F_2 = \int_{V_1} \frac{1}{2} \Phi_{He^+}(\boldsymbol{r_3}) \Phi_{Ps}(\boldsymbol{r_{12}}) \tag{A.12}$$

$$\times \left[\int_{A_{\rho_2}} \frac{2}{4\pi} \left[\frac{\sin \kappa \rho_2{}^2}{\rho_2^2} + \frac{\cos \kappa \rho_2{}^2}{\rho_2^2} \right] \rho_2^2 \sin \theta_{\rho_2} d\theta_{\rho_2} d\phi_{\rho_2} \right] d\tau_1$$

which using the normalization properties of $\Phi_{He^+}(\boldsymbol{r_3}) \Phi_{Ps}(\boldsymbol{r_{12}})$ gives

$$(S_2, LC_2) = (C_2, LS_2) + 1 \tag{A.13}$$

and therefore

$$(\overline{S_2}, L\overline{C_2}) = (\overline{C_2}, L\overline{S_2}) + 1. \tag{A.14}$$

Using similar arguments we can also show that

$$(S_1, LC_1) = (C_1, LS_1) + 1. \tag{A.15}$$

189

Appendix B

Angular integration

For s-wave scattering the spherical harmonic, $Y_{0,0}(\theta, \phi)$, has no azimuthal or polar dependence, and the external angular integration is relatively simple.

The volume element

$$d\tau = d\mathbf{r}_1 d\mathbf{r}_2 d\mathbf{r}_3 \tag{B.1}$$

can be rewritten as

$$d\tau = r_1^2 dr_1 \sin\theta_1 d\theta_1 d\phi_1 r_2^2 dr_2 \sin\theta_2 d\theta_2 d\phi_2 r_3^2 dr_3 \sin\theta_3 d\theta_3 d\phi_3, \tag{B.2}$$

where r_i, θ_i and o_i (i=1,2) are defined in figure B.1. Because of the spherical symmetry of the s-wave wavefunction, we can choose to rotate the whole four-body system in such a way as to facilitate the integration over a given external angle. For instance, when we do the $\mathbf{r}_2$ or $\mathbf{r}_3$ angular integration, we can choose to rotate the coordinate system so that the z-axis lies along the vector $\mathbf{r}_1$. Furthermore, when the $\mathbf{r}_3$ angular integration is performed, we can choose to rotate the coordinate system so that the vector $\mathbf{r}_2$ now lies in the x', z' plane (see figure B.2). Hence , we have

$$d\tau = r_1^2 dr_1 \sin\theta_1 d\theta_1 d\phi_1 r_2^2 dr_2 \sin\theta_{12} d\theta_{12} d\phi_2' r_3^2 dr_3 \sin\theta_{13} d\theta_{13} d\phi_{23}, \tag{B.3}$$

where ϕ_{23} is the angle between the planes of the triangles (r_1, r_2, r_{12}) and (r_1, r_3, r_{13}) and is an internal angle. The angle ϕ_2' is the azimuthal angle of $\mathbf{r}_2$ with the x'-axis before the rotation of $\mathbf{r}_2$ into the $x' - z'$ plane.
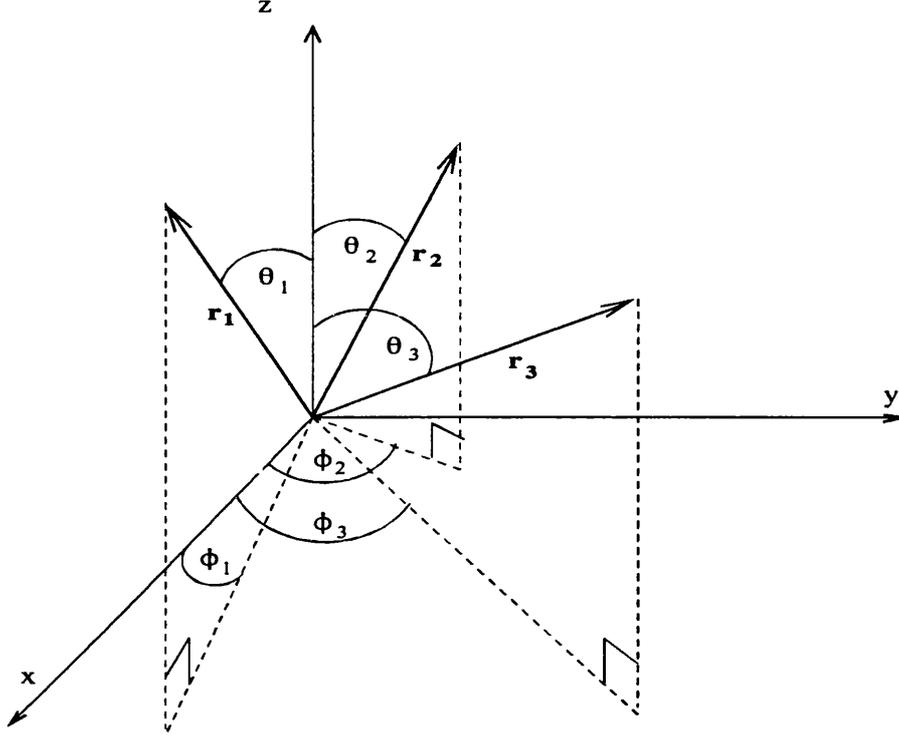
Figure B.1: The positron-helium atom coordinate system in an arbitrary (x, y, z) coordinate system.

Therefore, for s-wave scattering, after the external angle integration, the volume element becomes

$$d\tau = 8\pi^2 r_1^2 dr_1 r_2^2 dr_2 \sin\theta_{12} d\theta_{12} r_3^2 dr_3 \sin\theta_{13} d\theta_{13} d\phi_{23}, \qquad (B.4)$$

and using the relation $r_{kl}^2 = r_k^2 + r_l^2 - 2r_k r_l \cos\theta_{kl}$, we have

$$d\tau = 8\pi^2 dr_1 r_2 dr_2 r_3 dr_3 r_{12} dr_{12} r_{13} dr_{13} d\phi_{23} \qquad (B.5)$$

For the higher partial wave calculations, the absence of spherical symmetry in the $Y_{l,0}(\theta, \phi)$ functions makes the external angle integration more difficult, but a similar method as for the s-wave calculation can be used (i.e. rotation of the cooordinate system with the new z-axis along one of the position vectors) if one takes care to transform the various angular functions in the appropriate manner.

For p-wave scattering, the spherical harmonic is $Y_{1,0}(\theta, \phi) = \sqrt{3/4\pi} \cos\theta$ and a typical angular function which will need to be integrated will be of the form
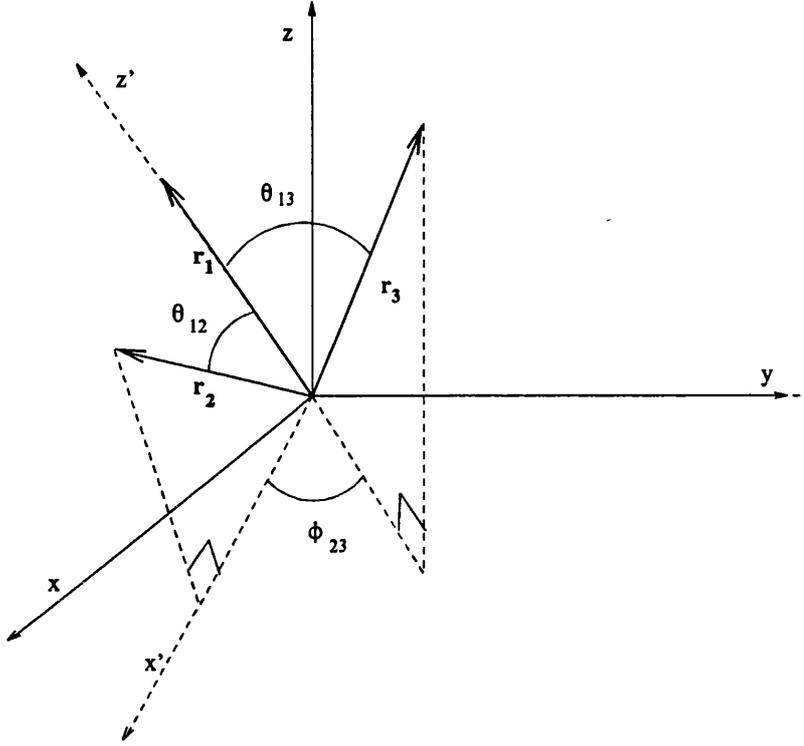
Figure B.2: The positron-helium atom coordinate system. in the transformed (x', y', z') coordinate system.

$\cos \theta_k \cos \theta_l$ with $k, l = 1, 2, 3$. Here again, we can choose the vector $\boldsymbol{r_k}$ as z-axis to do the angular integration over the vector $\boldsymbol{r_l}$. For this we rotate the coordinate system about the z-axis so that the vector $\boldsymbol{r_k}$ lies in the $x - z$ plane, and then rotate about the y-axis so that the z-axis lies along the vector $\boldsymbol{r_k}$. In this new coordinate system, the angle $\cos \theta_l$ is given by $\cos \theta_l = \hat{z}.\hat{r}_l$ where $\hat{z}$ is the unit vector of the original z axis in the new coordinate system. Using

$$\hat{z} = (-\sin \theta_k, 0, \cos \theta_k)$$

$$\hat{r}_l = (\sin \theta_{kl} \cos \phi'_l, \sin \theta_{kl} \sin \phi'_l, \cos \theta_{kl}), \qquad (B.6)$$

where θ_{kl} is an internal angle and ϕ'_l is the azimuthal angle of the vector $\boldsymbol{r_l}$ in the new coordinate system, we have

$$\cos \theta_l = \cos \theta_k \cos \theta_{kl} - \sin \theta_k \sin \theta_{kl} \cos \phi'_l. \qquad (B.7)$$

If we now consider a specific case, for instance

$$I = \int_{\tau_{ext}} \cos \theta_1 \cos \theta_2 d\tau_{ext} \qquad (B.8)$$

192

where $d\tau_{ext}$ implies that we are only considering the external angular integrations, we have

$$I = \int_0^\pi \cos\theta_1 \sin\theta_1 d\theta_1 \int_0^{2\pi} d\phi_1 \int_0^\pi \cos\theta_2 \sin\theta_2 d\theta_2 \int_0^{2\pi} d\phi_2 \int_0^\pi \sin\theta_3 d\theta_3 \int_0^{2\pi} d\phi_3 \tag{B.9}$$

The θ_3 and ϕ_3 integrations can be performed in a similar manner to that used in the s-wave calculation and they will be transformed into internal angular integrations, with respect to θ_{13} and ϕ_{23} respectively. The r_2 angular integration can now be done using the transformation outlined above and we have

$$I = \int_0^\pi \int_0^{2\pi} \int_0^{2\pi} \cos\theta_1 (\cos\theta_1 \cos\theta_{12} - \sin\theta_1 \sin\theta_{12} \cos\phi_2') \sin\theta_1 d\theta_1 d\phi_1 d\phi_2' \tag{B.10}$$

which, after integration over ϕ_1 and ϕ_2', gives

$$\begin{aligned} I &= 4\pi^2 \int_0^\pi \cos^2\theta_1 \cos\theta_{12} \sin\theta_1 d\theta_1 \\ &= \frac{8\pi^2}{3} \cos\theta_{12} \end{aligned} \tag{B.11}$$

Using the same method we can establish the following relation

$$\int_{\tau_{ext}} \cos\theta_k \cos\theta_l d\tau_{ext} = \frac{8\pi^2}{3} \cos\theta_{kl} \tag{B.12}$$

for k,l=1,2,3. One can also show that for the case $k = l$ we have

$$\int_{\tau_{ext}} \cos^2\theta_k d\tau_{ext} = \frac{8\pi^2}{3}. \tag{B.13}$$

In the evaluation of the long-range – long-range matrix elements, the spherical harmonics in the C_2 and S_2 terms depend on θ_{ρ_2} and θ_{ρ_3}. To perform the integration with respect to the external angles for such functions we use the relation

$$\cos\theta_{\rho_k} = \frac{r_1 \cos\theta_1 + r_k \cos\theta_k}{2\rho_k} \tag{B.14}$$

to transform the angular integration into one involving only the angles θ_1, θ_2, and θ_3 which can be done using the technique described above.

The various angular integrations which need to be evaluated for a p-wave calcu-

lation, and their solutions, are

$$\int_{\tau_{ext}} Y_{1,0}(\theta_k, \phi_k) Y_{1,0}(\theta_k, \phi_k) d\tau_{ext} \quad = \quad 2\pi \qquad\qquad k = 1, 2, 3.$$

$$\int_{\tau_{ext}} Y_{1,0}(\theta_k, \phi_k) Y_{1,0}(\theta_l, \phi_l) d\tau_{ext} \quad = \quad 2\pi \cos\theta_{kl} \qquad\qquad k, l = 1, 2, 3.$$

$$\int_{\tau_{ext}} Y_{1,0}(\theta_1, \phi_1) Y_{1,0}(\theta_{\rho_k}, \phi_{\rho_k}) d\tau_{ext} \quad = \quad \frac{2\pi}{2\rho_k}(r_1 + r_k \cos\theta_{1k}) \qquad k = 2, 3.$$

$$\int_{\tau_{ext}} Y_{1,0}(\theta_{\rho_k}, \phi_{\rho_k}) Y_{1,0}(\theta_{\rho_k}, \phi_{\rho_k}) d\tau_{ext} \quad = \quad 2\pi \qquad\qquad k = 2, 3.$$

$$\int_{\tau_{ext}} Y_{1,0}(\theta_{\rho_k}, \phi_{\rho_k}) Y_{1,0}(\theta_{\rho_l}, \phi_{\rho_l}) d\tau_{ext} \quad =$$

$$\frac{2\pi}{4\rho_k\rho_l}(r_1^2 + r_1 r_k \cos\theta_{1k} + r_1 r_l \cos\theta_{1l} + r_k r_l \cos\theta_{kl}) \quad k = 2, 3.$$

For a d-wave calculation we have,

$$\int_{\tau_{ext}} Y_{2,0}(\theta_k, \phi_k) Y_{2,0}(\theta_k, \phi_k) d\tau_{ext} \quad = \quad 2\pi \qquad\qquad k = 1, 2, 3.$$

$$\int_{\tau_{ext}} Y_{2,0}(\theta_k, \phi_k) Y_{2,0}(\theta_l, \phi_l) d\tau_{ext} \quad = \quad 2\pi \left(1 - \frac{3}{2}\sin^2\theta_{kl}\right) \qquad k, l = 1, 2, 3.$$

$$\int_{\tau_{ext}} Y_{2,0}(\theta_{\rho_k}, \phi_{\rho_k}) Y_{2,0}(\theta_{\rho_k}, \phi_{\rho_k}) d\tau_{ext} \quad = \quad 2\pi \qquad\qquad k = 2, 3.$$

$$\int_{\tau_{ext}} Y_{2,0}(\theta_1, \phi_1) Y_{2,0}(\theta_{\rho_k}, \phi_{\rho_k}) d\tau_{ext} \quad = \quad 2\pi \left(1 - \frac{3r_k^2 \sin^2\theta_{1k}}{8\rho_k^2}\right) \qquad k = 2, 3.$$

$$\int_{\tau_{ext}} Y_{2,0}(\theta_k, \phi_k) Y_{2,0}(\theta_{\rho_l}, \phi_{\rho_l}) d\tau_{ext} \quad = \quad 2\pi \left(\frac{3(r_1 \cos\theta_{1k} + r_l \cos\theta_{kl})^2}{8\rho_l^2} - \frac{1}{2}\right) \qquad k, l = 2, 3.$$

$$\int_{\tau_{ext}} Y_{2,0}(\theta_{\rho_k}, \phi_{\rho_k}) Y_{2,0}(\theta_{\rho_l}, \phi_{\rho_l}) d\tau_{ext} \quad = \quad 2\pi \left[\frac{3}{8}\frac{(4\rho_2^2 + 4\rho_3^2 - r_{23}^2)^2}{16\rho_2^2\rho_3^2} - \frac{1}{2}\right] \qquad k = 2, 3.$$

$$\int_{\tau_{ext}} \psi_{(1,1,2,0)}(\theta_1, \theta_k) Y_{2,0}(\theta_1, \phi_1) d\tau_{ext} \quad = \quad 6\sqrt{\frac{\pi}{5}}\cos\theta_{1k} \quad k = 2, 3$$

$$\int_{\tau_{ext}} \psi_{(1,1,2,0)}(\theta_1, \theta_k) Y_{2,0}(\theta_{\rho_k}, \phi_{\rho_k}) d\tau_{ext} \quad = \quad \frac{3}{4}\sqrt{\frac{\pi}{5}}\left[8\cos\theta_{1k} + \frac{3r_1 r_k \sin^2\theta_{1k}}{\rho_k^2}\right] \quad k = 2, 3$$

$$\int_{\tau_{ext}} \psi_{(1,1,2,0)}(\theta_1, \theta_k) Y_{2,0}(\theta_{\rho_l}, \phi_{\rho_l}) d\tau_{ext} \quad =$$

$$\frac{3}{4}\sqrt{\frac{\pi}{5}}\left[3\frac{\left[\cos\theta_{1k}(r_1^2 + r_1 r_l \cos\theta_{1l}) + \cos\theta_{kl}(r_1 r_l + r_l^2 \cos\theta_{1l})\right]}{\rho_l^2} - 4\cos\theta_{ik}\right] \quad k = 2, 3$$

References

Abramowitz M and Stegun I A 1964 Handbook of Mathematical Functions *Dover Publications*, New York

Anderson C D *Science* 1932 **76** 238

Aulenkamp H, Heiss P, Wichmann E 1974 *Z. Phys.* **268** 213

Armour E A G and Humberston J W 1991 *Phys. Reports* **204** 165

Bishop D M and Lam M 1988 *Phys. Rev. A* **37** 464

Blackett P M S and Occhialini G P S 1933 *Proc. Roy. Soc A* **139** 699

Bransden B H 1969 Case Studies in Atomic Physics edited by McDaniel and McDowell *North Holland*

Bransden B H 1983 Atomic Collision Theory *Benjamin & Cummings Publishing Company. Reading Massachusetts*

Briscoe C V, Choi S-I and Stewart A T 1968 *Phys. Rev. Lett.* **20** 493

Brown C J and Humberston J W 1984 *J.Phys. B* **17** L423

Brown C J and Humberston J W 1985 *J.Phys. B* **18** L401

Brown C J 1986 *Ph. D. Thesis, Univ. London*

Burciaga J R, Coleman P G, Diana L M and McNutt J D 1977 *J.Phys. B* **10** 569

Callaway J 1978 *Phys. Reports* **45** 89

Campeanu R I and Humberston J W 1975 *J.Phys. B* **8** L244

Campeanu R I and Humberston J W 1977 *J.Phys. B* **10** L153

Campeanu R I 1977 *Ph. D. Thesis, Univ. London*

Canter K F, Coleman P G, Griffith T C and Heyland G R 1973 *J.Phys. B* **6** L201

Charlton M and Larrichia G 1990 *J. Phys. B* **23** 1045

Coleman P G, Griffith T C, Heyland G R, and Killeen T L 1975 *J. Phys. B* **8** 1734

Coleman P G, Rayner S, Jacobsen F M, Charlton M and West R N 1994 *J. Phys. B* **27** 981

Dewangan D P and Walters H R J 1977 *J.Phys. B* **10** 637

Dirac P A M 1928 *Proc. Roy. Soc. A* **117** 610

Drachman R J 1968 *Phys. Rev.* **173** 190

Drachman R J 1971 *Phys.Letter* **37A** 187

Drachman R J 1972 *J.Phys. B* **5** L30

Fornari L S, Diana L M and Coleman P G 1983 *Phys. Rev. Lett.* **51** 2276

Gosh A S, Sil N C and Mandal P 1982 *Phys. Reports* **87** 313

Hartree D R 1928 *Proc. Cambridge. Phyl. Soc.* **24** 89

Hewitt R N, Noble C J and Bransden B H 1992 *J.Phys. B* **25** 557

Higgins K and Burke P G 1991 *J.Phys. B* **24** L343

Houston S K J 1973 *J.Phys. B* **5** 136

Humberston J W and Wallace J B G 1972 *J. Phys. B* **5** 1138

Humberston J W 1973 *J. Phys. B.* **6** L305

Humberston J W 1979 *Adv. At. Mol. Phys.* **15** 101

Humberston J W 1982 *Can. J. Phys.* **60** 591

Humberston J W 1986 *Adv. At. Mol. Phys.* **22** 1

Humberston J W 1994 *Adv. At. Mol. Phys.* **32** 205

Humberston J W and Van Reeth P 1996 *Can. J. Phys.* To be published.

Hylleraas 1929 *Z. f. Physik* **54** 347

Iwata K, Greaves R G, Murphy T J, Tinkle M D and Surko C M 1995 *Phys. Rev. A* **51** 473

Kahn P and Gosh A 1983 *Phys. Rev. A* **28** 2181

Kauppila W E, Stein T S, Smart J H, Dababneh M S, HO Y K, Downing J P and Pol V 1981 *Phys. Rev. A* **24** 725

Kauppila W E and Stein T S 1982 *Can. J. Phys.* **60** 471

Kauppila W E and Stein T S 1990 *Adv. At. Mol. Phys.* **26** 1

Kernogan A A, McAlinden M T and Walters H R J 1995 *J. Phys. B.* **28** 1079

Kohn W *Phys. Rev.* **74** 1763

Mandal P, Ghosh A S and Sil N C 1975 *J. Phys. B.* **8** 2377

Mandal P, Basu D and Ghosh A S 1976 *J. Phys. B.* **9** 2633

Mandal P, Guha S and Sil N C 1979 *J. Phys. B.* **12** 2913

Massey H S W and Moussa A H A 1960 *Proc. Phys. Soc.* **77** 811

Massey H S W 1976 *Physics Today* **29** No. 3

McAlinden M T and Walters H R J 1992 *Hyp. Int.* **73** 65

McAlinden 1993 *Ph. D. Thesis, Belfast*

McAlinden 1996 *Private Communication*

McEachran R P, Morgan D L, Ryman A G and Stauffer A D 1977 *J. Phys. B: Atom. Molec.* **10** 663

McEachran R P, Morgan D L, Ryman A G and Stauffer A D 1978 *J. Phys. B:*

Atom. Molec. **11** 951

McEachran R P and Stauffer A D 1996 *Private Communication*

Meyerhof W E 1962 *Phys. Rev.* **128** 2312

Meyerhof W E 1963 *Phys. Rev.* **129** 692

Meyerhof W E 1995 *Private Communication*

Mizogawa T, Nakayama Y, Kawaratmi T and Tosaki M 1985 *Phys. Rev. A* **31** 2171

Moxom J, Laricchia G, Charlton M , Kovar A and Meyerhof W E 1994 *Phys. Rev. A* **50**, 3129

Nesbet R K 1980 Variational Methods in Electron-Atom Scattering *Plenum, New York*

O'Malley T F, Rosenberg L and Spruch L 1962 *Phys. Rev.* **125** 1300

Ore A 1949 *Naturvidenskap Rikke* No 9 Univ. of. Bergen, Årbok

Page B A 1975 *J.Phys. B* **8** 2486

Peterkop R and Rabik L 1971 *J.Phys. B* **4** 1440

Schwartz C 1961a *Phys. Rev.* **124** 1468

Schwartz C 1961b *Phys. Rev.* **123** 1700

Shizuma K, Nishi M, Fujita T, and Yoshizawa Y 1978 *J. Phys. Soc. Japan Letters* **44** 1757

Simon B 1978 *Int. J. Quantum Chem.* **14** 529

Spruch L and Rosenberg L 1960 *Nucl. Phys.* **17** 30

Stein T S, Kauppila W E, Pol V, Smart J H and Jesion G 1978 *Phys. Rev. A* **17** 1600

Stein T S, Kauppila W E, Kwan C K, Lukaszew R A, Parikh S P, Wan Y J, Zou S and Dababneh M S 1990 In: *Annihililtaion in Gases and Galaxies* NASA Conferences Publication 3058 p.13.

Stewart A T, Briscoe C V and Steinbacher J J 1990 *Can. J. Phys.* **68** 1362

Sueoka O, Jin B and Hamada A 1994 *Atomic Collision Research in Japan* **20** 3

Tang S, Tinkle M D, Greaves R G and Surko C M 1992 *Phys. Review Lett.* **68** 3793

Thomas M A and Humberston J W 1972 *J.Phys.* B **5** L229

Thruhlar D G, Abdallah J and Smith R L *Adv. Chem. Phys.* **25** 211

Unsöld A 1927 *Ann. d. Phys.* **82** 355

Van Reeth P and Humberston J W 1995a *J.Phys.* B **28** L23

Van Reeth P and Humberston J W 1995b *J.Phys.* B **28** L511

Van Reeth P, Humberston J W, Iwata K, Greaves R G and Surko C M 1996 *J.Phys.* B **29** L465

Watts M S T and Humberston J W H 1992 *J.Phys.* B **25** L491

Watts M S T 1994 *Ph. D. Thesis, Univ. London*

Watts M S T and Humberston J W H 1994 *Hyp. Int.* **89** 47

Wigner E P 1948 *Phys. Rev.* **73** 1002